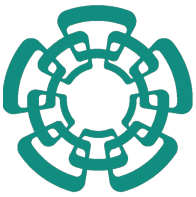

CENTRO DE INVESTIGACIÓN Y DE ESTUDIOS AVANZADOS DEL INSTITUTO POLITÉCNICO NACIONAL

UNIDAD ZACATENCO
DEPARTAMENTO DE QUÍMICA

Teoría del Funcional de la Densidad Auxiliar Adaptada por Simetría

T E S I S

Que presenta

Adrián Amor Martínez Carranza

Para obtener el grado de

Doctor en Ciencias

En la especialidad de

Ciencias Químicas

Director de Tesis: **Dr. Andreas M. Köster**

Ciudad de México Julio, 2021

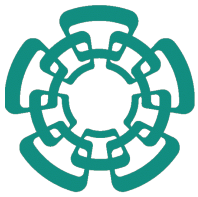

CENTER FOR RESEARCH AND ADVANCED STUDIES
OF THE NATIONAL POLYTECHNIC INSTITUTE

ZACATENCO CAMPUS
CHEMISTRY DEPARTMENT

Symmetry Adapted Auxiliary Density Functional Theory

T H E S I S

Submitted by

Adrián Amor Martínez Carranza

In order to obtain the

Doctor in Science

Degree, in the specialty of

Chemistry Sciences

Thesis Director: **Dr. Andreas M. Köster**

Mexico City July, 2021

A mi familia, amigos y compañeros.

The universe is an enormous direct product
of representations of symmetry groups.
— Steven Weinberg [1]

ACKNOWLEDGMENTS

I gratefully acknowledge the following people.

To the professors in the commission for their very valuable suggestions and corrections:

Dr. Tzonka Mineva
Dr. Lars G. M. Pettersson
Dr. Liliana Quintanar Vera
Dr. María de Jesús Rosales Hoz
Dr. Alberto Vela Amieva

To my assessor by its guide and keen observations:

Dr. Andreas M. Köster

To the present head of the Cinvestav chemistry department, Dr. Aaron Rojas Aguilar, the academic coordinator, Dr. Patrizia Calaminici, and the professors who have kindly supported me to present this thesis at Cinvestav.

To the doctors who have shared with me a bit of their deep knowledge (and I have not mentioned already): Dr. Gerald Geudtner, Dr. Héctor Hugo García Compean, Dr. José Luis Morales, and Dr. Luis G. Cota.

To my earlier companions of the theoretical chemistry laboratory, who bestowed me their wide help and knowledge anytime I asked them, without its help, my path would have been much more difficult: Dr. Aurelio Álvarez Ibarra, Dr. Bernardo Zuñiga Gutierrez, and Dr. Daniel Mejía Rodríguez.

To my companions and friends who have been very helpful and contributed to the development of this work: Dr. Sarah Elizabeth Pérez Figueroa, Dr. Nain Pedroza Montero, and Lic. Luis Ignacio Hernández Segura.

To my other companions and friends at the theoretical chemistry laboratory for their insight, discussion, and help: Dr. Rogelio Isaac Delgado Venegas, Dr. Francisco Antonio Delezma Díaz, Dr. Raúl Amaury Quintero Monsebaiz, Lic. Juan Diego Samaniego Rojas, Lic. Luis Lopez Sosa, and Lic. Jorge Luis Torres Moreno.

A todos mis amigos, compañeros y más allegados con quien he pasado parte de mi vida mientras hacía el doctorado: Filiberto H. C., Oscar X. G. G., Mónica H. L., Jhoely M. M. R., Jorge A. V. S., Alejandra E. V. L., Brenda R. C., María J. C. S., Vania C. T. G., Cleo P. B., Edan A. S. G., Hotaru F., y los compañeros del laboratorio. A ustedes, gracias a su compañía muy peculiar y única, les debo una importante parte de mi tranquilidad y salud mental, ingredientes indispensables para encontrar el ímpetu e inspiración para el desarrollo de este trabajo doctoral.

Y principalmente agradezco a mi querida familia que me apoya en todo momento: José Eutimio Martínez Murillo, Edith Carranza Novoa, José Erick Martínez Carranza, Edith Olimpia Martínez Carranza y sus familias.

Finalmente quiero agradecer al apoyo recibido por parte de las secretarias del departamento de química, al personal de la biblioteca de química, técnicos, a la comunidad de deMon2k, al Cinvestav por el uso de sus instalaciones, facilidades de cómputo y apoyo financiero, al equipo de cultura de Cinvestav por permitirme usar regularmente el piano, y al CONACyT por el apoyo financiero por parte de la beca de doctorado No. (559721/301383).

I hope this thesis (and related work) is useful to the reader and I put to your disposal my electronic contacts for further discussion:

a.amor.martinez.c@gmail.com
amartinezcar@cinvestav.mx
https://sites.google.com/site/aamartinezcarranzaqt/

This thesis was done at the theoretical chemistry laboratory in the chemistry department of Cinvestav, with address: Av. Instituto Politécnico Nacional 2508, Col. San Pedro Zacatenco, Delegación Gustavo A. Madero, Ciudad de México, México.

Resumen

El tema de esta tesis doctoral es la adaptación por simetría del ajuste variacional del potencial de Coulomb y de Fock en el marco de referencia de la teoría del funcional de la densidad auxiliar (ADFT por sus siglas en inglés) y de Kohn-Sham. Para este fin, las ecuaciones de trabajo para el ajuste variacional de la densidad ajustado por simetría se han desarrollado e implementado en el programa de química cuántica deMon2k junto con las ya consolidadas ecuaciones de Kohn-Sham adaptadas por simetría.

Los beneficios de usar la simetría en el marco de referencia de la ADFT es doble. Primero, la adaptación por simetría permite el etiquetamiento por simetría de orbitales moleculares, funciones de base y operadores matemáticos de acuerdo a representaciones irreducibles. Esto simplifica el análisis de cálculos de estructura electrónica y la asignación por simetría de estados electrónicos. Segundo, el uso de la simetría introduce una estructura de bloques dentro del álgebra lineal que surge de las ecuaciones de trabajo de la ADFT. Como resultado, la solución de un sistema de ecuaciones grande, puede ser sustituido por la solución de varios sistemas de ecuaciones más pequeños. El grado del bloqueo matricial se incrementa con el orden del grupo puntual. Desde un punto de vista computacional, la reducción de demanda de memoria de acceso aleatorio (RAM por sus siglas en inglés) asociada, permite cálculos adaptados por simetría de tamaños de sistemas que son de otra manera inaccesibles. Una simplificación adicional surge en las ecuaciones de ajuste adaptadas por simetría para densidades totalmente simétricas, para este caso, sólo la parte totalmente simétrica de las ecuaciones de ajuste necesitan ser resueltas, lo cual implica una dramática reducción en consumo de RAM.

El formalismo matemático usado para la adaptación por simetría de las ecuaciones de ajuste y las de Kohn-Sham se basa en la teoría de grupos. En ésta tesis sólo grupos puntuales se estudian, es decir, sólo la simetría rotacional se aprovecha. Las ecuaciones de Kohn-Sham y de ajuste adaptadas por simetría, se obtienen por la transformación de orbitales atómicos a una base orbital ajustada por simetría.

Las matrices de simetrización necesarias para este cambio de base se construyen mediante operadores de proyección proporcionados por la teoría de grupos. Estos operadores de proyección se construyen a partir de tablas de grupos puntuales las cuales que se agregaron al código de deMon2k. Las tablas de grupos puntuales se tomaron de la literatura o bien han sido recién generadas. Para ser consistente con el cálculo de integrales moleculares en demon2k, se desarrolló e implementó la construcción de matrices de simetrización para índices de momento angular arbitrarios. Para mejorar la eficiencia computacional, los orbitales atómicos y las funciones auxiliares se dividieron en conjuntos mínimos de funciones que se transforman entre sí por medio de operaciones de simetría. Nombramos a estos conjuntos, invariantes. Cada invariante se divide en dos espacios abstractos separados, el espacio de permutación atómica y el espacio de funciones centradas en el origen. La simplificación de las ecuaciones de trabajo de la ADFT debido a su representación adaptada por simetría derivada aquí, surge del teorema fundamental de la simetría, el cual establece que las integrales sobre funciones y operadores adaptados por simetría son diferentes de cero, únicamente, cuando su producto directo contiene a la representación totalmente simétrica.

Para dar ejemplos ilustrativos de aplicaciones del recién implementado enfoque de estructura electrónica adaptado por simetría en deMon2k, presentamos el análisis de orbitales moleculares del dímero de uranio, cálculos de energía adaptados por simetría de fullerenos gigantes y el etiquetado con representaciones irreducibles de estados excitados para varios sistemas.

La tesis se organiza de la siguiente manera. Los primeros dos capítulos dan una descripción básica de la teoría del funcional de la densidad y de la ADFT respectivamente. En el siguiente capítulo, se deriva la recién desarrollada ADFT adaptada por simetría. En el capítulo 4, se describe la construcción de matrices de simetrización para funciones de base y funciones auxiliares de momentos angulares arbitrarios. Se discute la implementación del algoritmo correspondiente en deMon2k. En el capítulo 5, se describe la construcción de las recién implementadas tablas de grupos puntuales en deMon2k. La validación del enfoque de la ADFT en el campo auto consistente (SCF por sus siglas en inglés) adaptada por simetría, se discute en el capítulo que le sigue. En el capítulo 7 se presentan aplicaciones seleccionadas. La tesis finaliza con conclusiones y perspectivas.

Abstract

The topic of this Ph.D. thesis is the symmetry adaptation of the variational fitting of the Coulomb and Fock potential in the framework of Kohn-Sham and auxiliary density functional theory (ADFT). To this end, the working equations for the symmetry-adapted variational density fittings are developed and implemented in the quantum chemistry program deMon2k along with the well-established symmetry-adapted Kohn-Sham equations.

The benefits of using symmetry in the ADFT framework are twofold. First, symmetry adaptation permits symmetry labeling of molecular orbitals, basis functions and mathematical operators according to irreducible representations. This simplifies the analysis of electronic structure calculations and the symmetry assignment of electronic states. Second, the use of symmetry introduces a block structure into the linear algebra that arises from the ADFT working equations. As a result, the solution of one large equation system can be substituted by the solutions of several smaller equation systems. The degree of this matrix blocking increases with the point group order. From a computational point of view, the associated reduction in random-access memory (RAM) demand permits symmetry-adapted calculations of system sizes that are otherwise inaccessible. A further simplification arises in the symmetry-adapted fitting equations for totally symmetric densities. For this case, only the totally symmetric part of the fitting equations needs to be solved which implies a dramatic reduction in RAM demand.

The mathematical formalism used for the symmetry adaptation of the fitting and Kohn-Sham equations is based on group theory. In this thesis only point groups are studied, i.e., only rotational symmetry is exploited. The symmetry-adapted Kohn-Sham and fitting equations are obtained by the transformation of the atomic orbital basis into a symmetry-adapted orbital basis.

The symmetrization matrices needed for this change of basis are built by means of projection operators provided by group theory. These projection operators are constructed from point group tables that are added to the deMon2k source. The point group tables were taken either from the literature or newly generated. To be consistent with the molecular integral calculation in deMon2k the construction of symmetrization matrices for arbitrary angular momentum indices was developed and implemented. To improve computational efficiency, the atomic orbitals and auxiliary functions are split into minimal sets of functions that transform between themselves by means of symmetry operations. We name these function sets invariants. Each invariant is split into two separated abstract spaces, the atom permutation space and the origin-centered function space. The simplification of the ADFT working equations due to the here derived symmetry-adapted representation arises from the fundamental theorem of symmetry, namely that integrals over symmetry-adapted functions and operators are only different from zero when their direct product contains the totally symmetric representation.

In order to give illustrative application examples of the newly implemented symmetry-adapted electronic structure approach in deMon2k, we present the molecular orbital analysis of the uranium dimer, the symmetry-adapted energy calculations of giant fullerenes and the irreducible representation labeling of excited states of several systems.

The thesis is organized in the following form. The first two chapters give basic descriptions of density functional theory and ADFT, respectively. In the following chapter, the newly developed symmetry-adapted ADFT is derived. In Chapter 4 the construction of symmetrization matrices for arbitrary angular momenta of basis and auxiliary functions is outlined. The implementation of the corresponding algorithm in deMon2k is discussed. The construction of the newly implemented point group tables in deMon2k is described in Chapter 5. The validation of the symmetry-adapted ADFT self-consistent field (SCF) approach is discussed in the next chapter. In Chapter 7 selected applications are presented. The thesis finishes with conclusions and perspectives.

CONTENTS

LIST OF FIGURES

LIST OF TABLES

ACRONYMS

AO Atomic Orbital

ADFT Auxiliary Density Functional Theory

CPU Central Processing Unit

DFT Density Functional Theory

DF-DFT Density Fitted - Density Functional Theory

DIIS Direct Inversion of the Iterative Space

ERI Electron Repulsion Integral

LCAO Linear Combination of Atomic Orbitals

LCGTO Linear Combination of Gaussian Type Orbitals

LDA Local Density Approximation

GGA Generalized Gradient Approximation

MO Molecular Orbital

RI Resolution of the Identity

RAM Random Access Memory

SAO Symmetry-Adapted Orbital

SCF Self Consistent Field

TD-ADFT Time Dependent Auxiliary Density Functional Theory

TED Truncated Eigenvalue Decomposition

1

DENSITY FUNCTIONAL THEORY

1.1 The electronic Schrödinger equation

Within the adiabatic Born-Oppenheimer approximation [2–4], the non-relativistic, time-independent electronic Schrödinger equation for a molecular system with N electrons (3N independent variables) and M fixed nuclei (3M parameters for the nuclear coordinates) is:

$$\hat{H}\Psi(\mathbf{r}, \mathbf{r}_2, ..., \mathbf{r}_N) = E\Psi(\mathbf{r}, \mathbf{r}_2, ..., \mathbf{r}_N) \tag{1.1}$$

To avoid cluttering of notation the parametric dependency from all nuclear coordinates is being neglected. The expression of the (electronic) Hamiltonian in atomic units is:

$$\hat{H} = -\frac{1}{2}\sum_{i=1}^{N}\nabla_i^2 + \sum_{i=1}^{N}\sum_{j>i}^{N}\frac{1}{|\mathbf{r}_i - \mathbf{r}_j|} + \sum_{i=1}^{N} v(\mathbf{r}_i) \tag{1.2}$$

The first term

$$\hat{T}_e = -\frac{1}{2}\sum_{i=1}^{N}\nabla_i^2 \tag{1.3}$$

is the electronic kinetic energy operator, the second term

$$\hat{V}_{ee} = \sum_{i=1}^{N}\sum_{j>i}^{N}\frac{1}{|\mathbf{r}_i - \mathbf{r}_j|} \tag{1.4}$$

is the Coulomb repulsion between the electrons and the last term is the potential operator

for the nuclear-electron attraction:

$$\hat{V}_{en} = \sum_{i=1}^{N} v(\mathbf{r}_i), \qquad \text{with} \qquad v(\mathbf{r}_i) = -\sum_{A=1}^{M} \frac{Z_A}{|\mathbf{r}_i - \mathbf{R}_A|} \tag{1.5}$$

If no other interactions are considered, the one-electron function $v(\mathbf{r}_i)$ is called the external potential. It has the parameters of the molecular geometry $\{\mathbf{R}_1, \mathbf{R}_2, ..., \mathbf{R}_M\}$ and the nuclear charges $\{Z_1, Z_2, ..., Z_M\}$. It is called "external" because in the Born-Oppenheimer approximation the quantum calculations are only on the electrons since the electronic degrees of freedom are the main variables. Therefore, the nuclei are "external" fixed objects which exert their Coulomb potential to the electrons. In a general situation, such an external potential could be provided not only by the nuclei configuration but also from a non-molecular source like an external electromagnetic field. Although, we will not consider that case here. Compactly the Hamiltonian can be written as:

$$\hat{H} = \hat{F} + \hat{V}_{en}, \qquad \text{with} \qquad \hat{F} = \hat{T}_e + \hat{V}_{ee} \tag{1.6}$$

Thus, the Hamiltonian is determined by the number of electrons, N, and the external potential. The expectation value of $\hat{V}_{en}$ with the wave function is [5, p. 33]

$$\langle \Psi | \hat{V}_{en} | \Psi \rangle = \int v(\mathbf{r}) \rho(\mathbf{r}) \, d\mathbf{r} \tag{1.7}$$

where $\rho(\mathbf{r})$ is the electron density:

$$\rho(\mathbf{r}) = N \int \cdots \int \Psi^*(\mathbf{r}, \mathbf{r}_2, ..., \mathbf{r}_N) \, \Psi(\mathbf{r}, \mathbf{r}_2, ..., \mathbf{r}_N) \, d\mathbf{r}_2 \, d\mathbf{r}_3 ... d\mathbf{r}_N \tag{1.8}$$

For simplicity, we neglect spin dependency. The here used short-hand integration notation is in Cartesian coordinates defined as:

$$\int d\mathbf{r}_i \equiv \int_{-\infty}^{\infty} \int_{-\infty}^{\infty} \int_{-\infty}^{\infty} dx_i \, dy_i \, dz_i \tag{1.9}$$

The electron density has the property that its integral yields the number of electrons, i.e.

$$\int \rho(\mathbf{r})\,\mathrm{d}\mathbf{r} = N \tag{1.10}$$

The energy of the system is given by the expectation value of the Hamiltonian:

$$\begin{aligned} E &= \langle \Psi | \hat{H} | \Psi \rangle \\ &= \langle \Psi | \hat{F} | \Psi \rangle + \langle \Psi | \hat{V}_{en} | \Psi \rangle \\ &= F + \int v(\mathbf{r}) \rho(\mathbf{r})\,\mathrm{d}\mathbf{r} \end{aligned} \tag{1.11}$$

Where $F = \langle \Psi | \hat{F} | \Psi \rangle$. Eq. (1.11) defines the energy of a system in terms of expectation values. Now, we can apply the variational principle to obtain the energy of a (non-degenerate) molecular ground state as:

$$E_0 = \langle \Psi_0 | \hat{H} | \Psi_0 \rangle < \langle \Psi | \hat{H} | \Psi \rangle \tag{1.12}$$

Here Ψ_0 is the true ground state wave function, E_0 its corresponding energy and Ψ a quantum mechanically valid trial wave function. Since (1.1) is a many-body problem, only approximate numerical solutions are feasible. Therefore, the development of computationally efficient methods for the approximate solution of the electronic Schrödinger equation is a very active research field. In particular, for the calculation of ground state energies the development of Density Functional Theory (DFT) provides computationally efficient and reliable approximations for the solution of the electronic Schrödinger equation. The exact formalism of DFT is based on the Hohenberg-Kohn [6] theorems that establishes an unique mapping from the ground state density, $\rho_0(\mathbf{r})$, to the corresponding energy, i.e.

$$\rho_0(\mathbf{r}) \rightarrow E[\rho_0] \equiv E_0 \tag{1.13}$$

This allows the formulation of electronic structure methods on the basis of the electronic density instead of the wave function. The advantage of having as basic variable the density instead of the wave function is that the density is simpler since it only depends on three spatial coordinates and not on 3N variables as the wave function. Furthermore, the density is an observable and can be measured. Therefore, within DFT the construction of the complicated many-body wave function can be avoided.

1.2 Hohenberg-Kohn theorems

DFT is based on the two Hohenberg-Kohn theorems. The first states: *The external potential* $v(\mathbf{r})$ *of a (non-degenerate) ground state is determined, within a trivial additive constant, by the electron density* $\rho(\mathbf{r})$. Therefore, the density can be used as the basic variable for the calculation of the ground state energy. The proof uses the minimum energy principle for the ground state as outlined in the following [5]: If there were two external potentials v and v' differing by more than a constant, yielding the same density ρ_0, we would have two Hamiltonians $\hat{H}$ and $\hat{H}'$ whose ground state densities are the same, although their wave functions Ψ and Ψ' would be different. Due to the minimum energy principle for the ground state, Eq. (1.12), we find:

$$E_0 < \langle \Psi' | \hat{H} | \Psi' \rangle = \langle \Psi' | \hat{H}' - \hat{H}' + \hat{H} | \Psi' \rangle \tag{1.14}$$

$$= \langle \Psi' | \hat{H}' | \Psi' \rangle + \langle \Psi' | \hat{H} - \hat{H}' | \Psi' \rangle \tag{1.15}$$

$$= E_0' + \langle \Psi' | \hat{V}_{en} - \hat{V}_{en}' | \Psi' \rangle \tag{1.16}$$

Eq. (1.16) can be rewritten as:

$$E_0 < E_0' + \int \rho'(\mathbf{r}) v(\mathbf{r}) \, d\mathbf{r} - \int \rho'(\mathbf{r}) v'(\mathbf{r}) \, d\mathbf{r} \tag{1.17}$$

$$= E_0' + \int \rho'(\mathbf{r}) \left[v(\mathbf{r}) - v'(\mathbf{r}) \right] d\mathbf{r} \tag{1.18}$$

Because $\rho'(\mathbf{r}) = \rho(\mathbf{r})$ by construction, we finally obtain:

$$E_0 < E_0' + \int \rho(\mathbf{r}) \left[v(\mathbf{r}) - v'(\mathbf{r}) \right] d\mathbf{r} \tag{1.19}$$

Here E_0 and E_0' are the ground state energies obtained with $\hat{H}$ and $\hat{H}'$, respectively. In the same way we can take Ψ as trial wave function for the Hamiltonian H':

$$E_0' < \langle \Psi | \hat{H}' | \Psi \rangle \tag{1.20}$$

$$E_0' < \langle \Psi | \hat{H} | \Psi \rangle + \langle \Psi | \hat{H}' - \hat{H} | \Psi \rangle \tag{1.21}$$

$$E_0' < E_0 - \int \rho(\mathbf{r}) [v(\mathbf{r}) - v'(\mathbf{r})] d\mathbf{r} \tag{1.22}$$

Adding Eq. (1.19) and (1.22) we obtain $E_0 + E_0' < E_0' + E_0$, which is a contradiction. Therefore, there cannot be two different external potentials that give the same ground state density. As a result, the functional dependency on the electron density of the energy is established:

$$E[\rho(\mathbf{r})] = \int \rho(\mathbf{r}) v(\mathbf{r}) d\mathbf{r} + F[\rho(\mathbf{r})] \tag{1.23}$$

In Eq. (1.23) the system-dependent part is the external potential $v(\mathbf{r})$ and $F[\rho(\mathbf{r})]$ is called the universal functional, meaning that it is system independent.

On the basis of the variational principle, and taking as basic variable the density instead of the wave function, the second Hohenberg-Kohn theorem provides a route for the calculation of the ground state density and energy. It states: *For a trial density* $\rho'(\mathbf{r})$ *such that* $\rho'(\mathbf{r}) \geqslant 0 \, \forall \, \mathbf{r}$ *and* $\int \rho'(\mathbf{r}) d\mathbf{r} = N$ *holds:*

$$E_0 = E[\rho_0] \leqslant E[\rho'(\mathbf{r})] \tag{1.24}$$

Here $E[\rho'(\mathbf{r})]$ *is the energy functional of Eq.* (1.23) *evaluated with* $\rho'(\mathbf{r})$. This is the variational principle for the ground state energy as functional of the electron density. The proof makes use of the previous theorem; since a trial density ρ' determines its own potential

v' and therefore its own wave function Ψ', which can be taken as trial wave function for the ground state Hamiltonian with potential $v(\mathbf{r})$, it follows:

$$\langle \Psi' | \hat{H} | \Psi' \rangle = \int \rho'(\mathbf{r}) v(\mathbf{r}) \, d\mathbf{r} + F[\rho'(\mathbf{r})] = E[\rho'(\mathbf{r})] \geqslant E[\rho_0(\mathbf{r})] \tag{1.25}$$

Only when ρ' equals ρ_0 the energies would be the same. This implies that the variation of the energy with respect of the densities $\{\rho\}$ that integrate to N electrons must satisfy the stationary principle. So if we would know the form of the universal functional $F[\rho]$ then we could use the variational principle using trial densities until the energy is minimized. However, the exact form of the universal functional remains unknown.

1.3 Kohn-Sham method

In order to evaluate $F[\rho]$ one has to resort to approximations since its actual exact form is currently unknown. Traditionally, it is split into kinetic, $T[\rho]$, and potential energy, $V_{ee}[\rho]$, containing all the electron-electron interaction energy contributions:

$$F[\rho] = T[\rho] + V_{ee}[\rho] \tag{1.26}$$

Of course, also the exact form of these functionals is unknown. There are several approximations for the kinetic and potential energy functionals such as the ones based on the Thomas-Fermi model [5, 7, 8]. In general, their accuracy is not sufficient for chemical applications [9]. To overcome this drawback, Kohn and Sham reintroduced orbitals for the total energy calculation in DFT [10]. To this end, they split the kinetic energy functional into a one-particle contribution, $T_s[\rho]$, and a remaining correlation correction, $T_c[\rho]$:

$$T[\rho] = T_s[\rho] + T_c[\rho] \tag{1.27}$$

Following this route, they introduced a fictitious non-interacting system with an effective local potential, $v_s(\mathbf{r})$, that gives rise to the following eigenvalue equations:

$$\left[-\frac{1}{2}\nabla^2 + v_s(\mathbf{r})\right]\psi_i(\mathbf{r}) = \varepsilon_i\psi_i(\mathbf{r}) \tag{1.28}$$

with eigenfunctions $\{\psi_i\}$ called Kohn-Sham orbitals. By construction, these orbitals of the non-interacting system must yield a density, $\rho_s(\mathbf{r})$, that matches the one of the real system, $\rho(\mathbf{r})$. Because the fictitious system is non-interacting, its exact wave function is given by a single Slater determinant built with the Kohn-Sham orbitals, which we request to be orthonormal:

$$\langle\psi_i|\psi_j\rangle = \delta_{ij} \tag{1.29}$$

The density, $\rho_s(\mathbf{r})$, and kinetic energy, T_s, of the non-interacting system are given by:

$$\rho_s(\mathbf{r}) = \sum_i^{occ} |\psi_i(\mathbf{r})|^2 \tag{1.30}$$

$$T_s[\rho_s] = -\frac{1}{2}\sum_i^{occ}\langle\psi_i[\rho_s]|\nabla^2|\psi_i[\rho_s]\rangle \tag{1.31}$$

Here, the one-particle kinetic energy is written as a functional of the density since it has been shown that the Kohn-Sham orbitals are functionals of the density [11–13]. To connect the fictitious with the real system the variation of the energy is used. To this end, we write the energy of the real system as:

$$E[\rho] = T_s[\rho] + J[\rho] + E_{xc}[\rho] + V[\rho] \tag{1.32}$$

$$\text{with} \quad E_{xc}[\rho] = T_c[\rho] + V_{ee}[\rho] - J[\rho], \quad \text{and} \quad V[\rho] = \int v(\mathbf{r})\rho(\mathbf{r})\,d\mathbf{r} \tag{1.33}$$

Here, $J[\rho]$, is known as the classical electrostatic or direct or Coulomb or Hartree energy, which is coming from the electron density interacting with itself via the Coulomb's law:

$$J[\rho] = \frac{1}{2}\iint \frac{\rho(\mathbf{r}_1)\rho(\mathbf{r}_2)}{|\mathbf{r}_1 - \mathbf{r}_2|}\,d\mathbf{r}_1\,d\mathbf{r}_2 \tag{1.34}$$

Also, in Eq. (1.32), $E_{xc}[\rho]$ is known as the Kohn-Sham exchange-correlation functional. It contains the kinetic energy correlation correction, $T_c[\rho]$, to the kinetic energy of the non-interacting system, $T_s[\rho]$, and the electron-electron exchange and correlation corrections to the Hartree energy $J[\rho]$ [14]. The functional derivative of the energy,

$$\frac{\delta E[\rho]}{\delta\rho(\mathbf{r})} = \frac{\delta T_s[\rho]}{\delta\rho(\mathbf{r})} + \frac{\delta J[\rho]}{\delta\rho(\mathbf{r})} + \frac{\delta E_{xc}[\rho]}{\delta\rho(\mathbf{r})} + \frac{\delta V[\rho]}{\delta\rho(\mathbf{r})} \tag{1.35}$$

and that of the fictitious system,

$$\frac{\delta E_s[\rho]}{\delta\rho(\mathbf{r})} = \frac{\delta T_s[\rho]}{\delta\rho(\mathbf{r})} + \frac{\delta V_s[\rho]}{\delta\rho(\mathbf{r})} \tag{1.36}$$

are identical if the effective potential, $v_s(\mathbf{r}) = \frac{\delta V_s[\rho]}{\delta\rho(\mathbf{r})}$, is given by:

$$v_s(\mathbf{r}) = \frac{\delta J[\rho]}{\delta\rho(\mathbf{r})} + \frac{\delta E_{xc}[\rho]}{\delta\rho(\mathbf{r})} + \frac{\delta V[\rho]}{\delta\rho(\mathbf{r})} \tag{1.37}$$

$$= \int \frac{\rho(\mathbf{r}')}{|\mathbf{r} - \mathbf{r}'|}\,d\mathbf{r}' + v_{xc}[\rho(\mathbf{r})] + v(\mathbf{r}) \tag{1.38}$$

In Eq. (1.38) the exchange-correlation potential is introduced and is defined as:

$$v_{xc}[\rho(\mathbf{r})] = \frac{\delta E_{xc}[\rho]}{\delta\rho(\mathbf{r})} \tag{1.39}$$

Therefore, one can calculate the density of the interacting system by solving the equations of a non-interacting system with effective potential $v_s(\mathbf{r})$. Since $v_s(\mathbf{r})$ depends on $\rho(\mathbf{r})$, the problem of solving Eqs. (1.28), known as Kohn-Sham equations, is a non-linear one. Expanding $v_s[\rho(\mathbf{r})]$ yields the explicit form of the Kohn-Sham equations:

$$\left(-\frac{1}{2}\nabla^2 + v(\mathbf{r}) + \int \frac{\rho(\mathbf{r}')}{|\mathbf{r} - \mathbf{r}'|}\,d\mathbf{r}' + v_{xc}[\rho](\mathbf{r})\right)\psi_i(\mathbf{r}) = \varepsilon_i(\mathbf{r})\psi_i(\mathbf{r}) \quad \forall \quad i \tag{1.40}$$

From this discussion follows that the Kohn-Sham method yields exact electronic energies if the exact form of $E_{xc}[\rho]$ is used. Therefore, the Kohn-Sham approach is in principle

exact, unlike the Hartree-Fock method, despite the use of a single determinant for the expansion of the wave function. The approximation only enters when we have to decide on an explicit form for the unknown functional of the exchange-correlation energy $E_{xc}[\rho]$. Because the Kohn-Sham effective potential $v_s[\rho](\mathbf{r})$ is local, in the sense that it is a function of only the spatial variable $\mathbf{r}$ and independent from other points in space, and also, is multiplicative and is the same for all electrons, it provides simpler expressions than the Hartree-Fock method with its non-local exchange operator. On the other hand the Kohn-Sham effective potential will probably have a very complex dependence on the density [13, 15]. The central goal of modern DFT is, therefore, to find better and better approximations to the exchange-correlation energy and potential. Once an approximation for the exchange-correlation energy has been chosen, an iteration procedure is the usual way of solving the Kohn-Sham equations. The quality of any DFT calculation that uses the Kohn-Sham method is, therefore, determined by the approximation used for $E_{xc}[\rho]$. Different types of approximations have been established over the years such as the Local Density Approximation (LDA) [16, 17], the Generalized Gradient Approximation (GGA) [18, 19] in form of BLYP [20–23] and PBE [24] functionals or the hybrid functionals [25] like B3LYP and PBE0 [26, 27]. Given that the Kohn-Sham method is very similar to the Hartree-Fock method, many ideas and technical knowledge can be inherited from it and other ab initio methods. Some programs like ADF [28, 29] use Slater type orbitals for the expansion of the Kohn-Sham orbitals, others like DMol [30] use numerical basis sets and many other programs, like deMon2k [31], use the Linear Combination of Gaussian Type Orbitals (LCGTO) approximation. In any case, the Kohn-Sham equations are recast in matrix form yielding Roothaan-Hall type equation systems [32, 33]. Details of the LCGTO approximation are given in the next section.

1.4 THE KOHN-SHAM LCGTO-DFT METHOD

In the Linear Combination of Atomic Orbitals (LCAO) approximation a (real) Molecular Orbital (MO) is given by:

$$\psi_i(\mathbf{r}) = \sum_\mu c_{\mu i}\mu(\mathbf{r}) \tag{1.41}$$

Here $\mu(\mathbf{r})$ denotes a real basis function centered at an atom and $c_{\mu i}$ is the corresponding MO coefficient. In the LCGTO approximation, the atomic orbitals, $\mu(\mathbf{r})$, are expressed as contracted Cartesian Gaussian type orbitals. The unnormalized form of them is:

$$\mu(\mathbf{r}) = (x - A_x)^{a_x}(y - A_y)^{a_y}(z - A_z)^{a_z}\sum_k^{K_\mu} d_k e^{-\zeta_k(\mathbf{r}-\mathbf{A})^2} \tag{1.42}$$

This function is defined completely by its atomic center $\mathbf{A}$, its angular momentum vector index $\mathbf{a} = (a_x, a_y, a_z)$, its contraction degree K_μ, the contraction coefficients d_k and the orbital exponents ζ_k. The contraction coefficients remain constant during the electronic structure calculation. The closed-shell LCGTO density is then given by:

$$\rho(\mathbf{r}) = 2\sum_i^{occ}\psi_i(\mathbf{r})\psi_i(\mathbf{r}) = 2\sum_i^{occ}\sum_{\mu,\nu} c_{\mu i}c_{\nu i}\mu(\mathbf{r})\nu(\mathbf{r}) = \sum_{\mu,\nu} P_{\mu\nu}\mu(\mathbf{r})\nu(\mathbf{r}) \tag{1.43}$$

In Eq. (1.43), $P_{\mu\nu}$ denotes an element of the (closed-shell) density matrix:

$$P_{\mu\nu} = 2\sum_i^{occ} c_{\mu i}c_{\nu i} \tag{1.44}$$

The extension to the open-shell case is described in [34–36]. Using the above-mentioned expansions for the MOs and the density, the expression for the Kohn-Sham energy can be written in the form:

$$E = \sum_{\mu,\nu} P_{\mu\nu}H_{\mu\nu} + \frac{1}{2}\sum_{\mu,\nu}\sum_{\sigma,\tau} P_{\mu\nu}P_{\sigma\tau}\langle\mu\nu||\sigma\tau\rangle + E_{xc}[\rho] \tag{1.45}$$

The elements of the mono-electronic core Hamiltonian, $H_{\mu\nu}$, are given by:

$$H_{\mu\nu} = -\frac{1}{2}\langle\mu|\nabla^2|\nu\rangle - \sum_A \langle\mu|\frac{Z_A}{|\mathbf{r}-\mathbf{R}_A|}|\nu\rangle \tag{1.46}$$

The core Hamiltonian matrix elements contain the kinetic energy and nuclear attraction of the electrons. Modifications of the external potential are usually added to these matrix elements. The second term in (1.45), corresponding to the Hartree energy (see Eq. 1.34), represents the Coulomb repulsion energy of the electrons. It contains four-center Electron Repulsion Integrals (ERIs) for which we use the following short-hand notation:

$$\langle\mu\nu||\sigma\tau\rangle = \iint \frac{\mu(\mathbf{r}_1)\nu(\mathbf{r}_1)\sigma(\mathbf{r}_2)\tau(\mathbf{r}_2)}{\mathbf{r}_1-\mathbf{r}_2}\,d\mathbf{r}_1\,d\mathbf{r}_2 \tag{1.47}$$

In (1.47), the double bar is the Coulomb operator $\frac{1}{|\mathbf{r}_1-\mathbf{r}_2|}$. The functions in the bra depend on $\mathbf{r}_1$ while the functions in the ket depend on $\mathbf{r}_2$. The same notation is used for two- and three-center ERIs that will appear later in the text.

In order to derive the Kohn-Sham equations in the LCGTO approximation we minimize the energy expression in equation (1.45) with respect to the molecular orbital coefficients, imposing MO orthonormality:

$$\langle\psi_i \mid \psi_j\rangle = \sum_{\mu,\nu} c_{\mu i} S_{\mu\nu} c_{\nu j} = \mathbf{c}_i^T \mathbf{S}\mathbf{c}_j = \delta_{ij} \tag{1.48}$$

In Eq. (1.48), $\mathbf{S}$ is the atomic orbital overlap matrix with elements $S_{\mu,\nu} = \langle\mu|\nu\rangle$. Introducing the Lagrangian

$$L_{KS} \equiv E - 2\sum_{i,j}\lambda_{ij}\left(\mathbf{c}_i^T\mathbf{S}\mathbf{c}_j - \delta_{ij}\right) \tag{1.49}$$

The partial derivative of the Lagrangian with respect to a given molecular orbital coefficient is given by:

$$\frac{1}{4}\frac{\partial L_{KS}}{\partial c_{\mu i}} = \sum_\nu \left[\left(H_{\mu\nu} + \sum_{\sigma,\tau} P_{\sigma\tau}\langle\sigma\tau||\mu\nu\rangle + \langle\mu\,|v_{xc}|\,\nu\rangle\right)c_{\nu i} - S_{\mu\nu}\sum_j c_{\nu j}\lambda_{ji}\right] \tag{1.50}$$

At this point it is convenient to introduce the Kohn-Sham matrix, $\mathbf{K}$, which is defined by the differentiation of the electronic energy with respect to density matrix elements:

$$K_{\mu\nu} \equiv \frac{\partial E}{\partial P_{\mu\nu}} = H_{\mu\nu} + \sum_{\sigma,\tau} P_{\sigma\tau}\langle\sigma\tau\|\mu\nu\rangle + \langle\mu|v_{xc}|\nu\rangle \tag{1.51}$$

The last term arises from the differentiation of the exchange-correlation energy with respect to density matrix elements, which is obtained as follows:

$$\frac{\partial E_{xc}[\rho]}{\partial P_{\mu\nu}} = \int \frac{\delta E_{xc}[\rho]}{\delta\rho(\mathbf{r})}\frac{\partial\rho(\mathbf{r})}{\partial P_{\mu\nu}}d\mathbf{r} = \int v_{xc}(\mathbf{r})\mu(\mathbf{r})\nu(\mathbf{r})d\mathbf{r} \tag{1.52}$$

This contribution usually has to be calculated numerically. The minimization of the Lagrangian,

$$\frac{\partial L_{KS}}{\partial c_{\mu i}} = 0 \quad \forall \quad c_{\mu i}$$

then yields:

$$\sum_{\nu} K_{\mu\nu}c_{\nu i} = \sum_{j}\sum_{\nu} S_{\mu\nu}c_{\nu j}\lambda_{ji} \quad \forall \quad \mu, i$$

This system of generalized eigenvalue equations reads in matrix notation:

$$\mathbf{Kc} = \mathbf{Sc\lambda} \tag{1.53}$$

The electronic density is invariant under orthogonal transformations of the occupied MOs. Therefore, it is convenient to choose a set of MOs for which the off-diagonal undetermined Lagrange multipliers are zero. These MOs are called canonical MOs [37] and are solutions of the canonical Kohn-Sham equations:

$$\mathbf{Kc} = \mathbf{Sc\varepsilon} \tag{1.54}$$

Eq. (1.54) is a generalized eigenvalue equation which can be transformed into a special eigenvalue equation by a Löwdin orthogonalization [38, 39] as follows:

$$\mathbf{S}^{-\frac{1}{2}}\mathbf{K}\mathbf{S}^{-\frac{1}{2}}\mathbf{S}^{\frac{1}{2}}\mathbf{c} = \mathbf{S}^{-\frac{1}{2}}\mathbf{S}\mathbf{c}\boldsymbol{\epsilon} \tag{1.55}$$

$$\mathbf{K}^{\lambda}\mathbf{c}^{\lambda} = \mathbf{c}^{\lambda}\boldsymbol{\epsilon} \tag{1.56}$$

Upon diagonalization of $\mathbf{K}^{\lambda}$ the coefficients $\mathbf{c}^{\lambda}$ and MO energies $\boldsymbol{\epsilon}$ are obtained. Afterwards, the inverse transformation:

$$\mathbf{c} = \mathbf{S}^{-\frac{1}{2}}\mathbf{c}^{\lambda} \tag{1.57}$$

is needed to obtain the MO coefficients in the original non-orthogonal Atomic Orbital (AO) representation, which is needed for the evaluation of the energy according to Eq. (1.45). Note that Eq. (1.54) is a Roothaan-Hall type equation system and since it is non-linear ($\mathbf{K}$ depends on $\mathbf{c}$) it has to be solved by a Self Consistent Field (SCF) procedure. In brief, the SCF involves calculation of the energy from an initial density guess, building the Kohn-Sham matrix, solving Eq. (1.54) for $\mathbf{c}$ as well as ε and building a new density according to the Aufbau principle. With this density a new energy is calculated and the SCF convergence is checked by comparing to the previous energy. These steps are repeated until the SCF convergence criteria is reached.

To estimate the computational complexity of the here outlined Kohn-Sham SCF, we analyze the scaling for the computation of the Kohn-Sham matrix elements, Eq. (1.51), and energy, Eq. (1.45). The computation of $H_{\mu\nu}$ scales formally N_{bas}^2, where N_{bas} is the number of basis functions. The Coulomb term introduces a formal N_{bas}^4 scaling. For the calculation of the exchange-correlation energy a numerical integration has to be performed. This integration scales as $N_{bas}^2 \times G$, where G is the number of grid points used for the numerical integration. It follows that the calculation of the Coulomb repulsion energy represents the computationally most demanding task. To overcome this problem the variational fitting of the Coulomb potential is used for reducing the formal scaling from N_{bas}^4 by the introduction of an auxiliary function set to approximately $3N_{bas}^3$. Next,

we present the variational fitting of the Coulomb potential, which greatly reduces the computation effort for ERI calculations.

2

AUXILIARY DENSITY FUNCTIONAL THEORY

2.1 Variational fitting of the Coulomb potential

The variational fitting of the Coulomb potential [40–43] is a technique that nowadays is used in almost all LCGTO-DFT programs to accelerate the calculations of two-electron Coulomb repulsion integrals. These calculations are computationally expensive because they involve the evaluation of four-center integrals. In the variational fitting of the Coulomb potential, this is avoided and instead three- and two-center integrals along with linear algebra tasks have to be calculated. This technique was widespread available for use since its introduction into the deMon-KS [44] and DGAUSS [45] programs, and is implemented in deMon2k. In practice, the variational fitting of the Coulomb potential is equivalent to the so-called Resolution of the Identity (RI) [46] used in other programs like TURBOMOLE [47] or Gaussian [48]. A more extended discussion about the RI approach and the variational fitting of the Coulomb potential can be found in [49, 50].

The variational fitting of the Coulomb potential is based on the minimization of the following error functional:

$$\varepsilon_2 = \frac{1}{2}\iint \frac{[\rho(\mathbf{r}_1) - \tilde{\rho}(\mathbf{r}_1)][\rho(\mathbf{r}_2) - \tilde{\rho}(\mathbf{r}_2)]}{|\mathbf{r}_1 - \mathbf{r}_2|} d\mathbf{r}_1 d\mathbf{r}_2 \geqslant 0 \tag{2.1}$$

The approximated auxiliary density $\tilde{\rho}(\mathbf{r})$ is expanded in a linear combination of auxiliary functions

$$\tilde{\rho}(\mathbf{r}) = \sum_{\bar{k}} x_{\bar{k}} \bar{k}(\mathbf{r}) \tag{2.2}$$

In deMon2k the auxiliary functions $\bar{k}(\mathbf{r})$ are primitive Hermite Gaussian functions that are indicated by a bar [43]. The unnormalized form of an auxiliary function localized in atom A with exponent $\zeta_{\bar{k}}$ is given by:

$$\bar{k}(\mathbf{r}) = \left(\frac{\partial}{\partial A_x}\right)^{\bar{k}_x} \left(\frac{\partial}{\partial A_y}\right)^{\bar{k}_y} \left(\frac{\partial}{\partial A_z}\right)^{\bar{k}_z} e^{-\zeta_{\bar{k}}(\mathbf{r}-\mathbf{A})^2} \tag{2.3}$$

The auxiliary functions are normalized with respect to the Coulomb norm. In deMon2k the auxiliary functions are grouped in `s`, `spd`, `spdfg` and `spdfghi` sets . The exponents within these sets are shared [51, 52]. For the so-called GEN auxiliary function sets in deMon2k the exponents are generated automatically via an almost well-tempered expansion. The range of values taken for the exponents is determined by the smallest, $\zeta_{\min}$, and largest, $\zeta_{\max}$, exponent of the primitive Gaussian of the used basis set. Specially developed integral recurrence relations [43, 53] ensure maximum performance in the analytic molecular integral calculations with these auxiliary function sets. The LCGTO expansion of $\rho(\mathbf{r})$ and $\tilde{\rho}(\mathbf{r})$ yields for ε_2:

$$\begin{aligned}\varepsilon_2 &= \frac{1}{2}\langle \rho - \tilde{\rho} || \rho - \tilde{\rho}\rangle = \frac{1}{2}\langle \rho||\rho\rangle - \langle \rho||\tilde{\rho}\rangle + \frac{1}{2}\langle\tilde{\rho}||\tilde{\rho}\rangle \\ &= \frac{1}{2}\sum_{\mu,\nu}\sum_{\sigma,\tau} P_{\mu\nu}P_{\sigma\tau}\langle\mu\nu||\sigma\tau\rangle - \sum_{\mu,\nu}\sum_{\bar{k}} P_{\mu\nu}\langle\mu\nu||\bar{k}\rangle x_{\bar{k}} + \frac{1}{2}\sum_{\bar{k},\bar{l}} x_{\bar{k}}x_{\bar{l}}\langle\bar{k}||\bar{l}\rangle\end{aligned} \tag{2.4}$$

As ε_2 is semi-positive definite, the following inequality holds:

$$\frac{1}{2}\sum_{\mu,\nu}\sum_{\sigma,\tau} P_{\mu\nu}P_{\sigma\tau}\langle\mu\nu||\sigma\tau\rangle \geqslant \sum_{\mu,\nu}\sum_{\bar{k}} P_{\mu\nu}\langle\mu\nu||\bar{k}\rangle x_{\bar{k}} - \frac{1}{2}\sum_{\bar{k},\bar{l}} x_{\bar{k}}x_{\bar{l}}\langle\bar{k}||\bar{l}\rangle \tag{2.5}$$

The fitting coefficients $x_{\bar{k}}$ are obtained by minimizing ε_2 with respect to them:

$$\frac{\partial\varepsilon_2}{\partial x_{\bar{k}}} = -\sum_{\mu,\nu} P_{\mu\nu}\langle\mu\nu||\bar{k}\rangle + \sum_{\bar{l}} x_{\bar{l}}\langle\bar{l}||\bar{k}\rangle = 0 \quad \forall \quad \bar{k} \tag{2.6}$$

At this point it is convenient to define the Coulomb matrix,

$$\mathbf{G} = \begin{pmatrix} \langle 1||\bar{1}\rangle & \langle 1||\bar{2}\rangle & \cdots & \langle 1||\bar{m}\rangle \\ \langle 2||\bar{1}\rangle & \langle 2||\bar{2}\rangle & \cdots & \langle 2||\bar{m}\rangle \\ \vdots & \vdots & \ddots & \vdots \\ \langle \bar{m}||\bar{1}\rangle & \langle \bar{m}||\bar{2}\rangle & \cdots & \langle \bar{m}||\bar{m}\rangle \end{pmatrix} \tag{2.7}$$

and Coulomb vector,

$$\mathbf{J} = \begin{pmatrix} \sum_{\mu,\nu} P_{\mu\nu} \langle \mu\nu||\bar{1}\rangle \\ \sum_{\mu,\nu} P_{\mu\nu} \langle \mu\nu||\bar{2}\rangle \\ \vdots \\ \sum_{\mu,\nu} P_{\mu\nu} \langle \mu\nu||\bar{m}\rangle \end{pmatrix} = \begin{pmatrix} \langle \rho||\bar{1}\rangle \\ \langle \rho||\bar{2}\rangle \\ \vdots \\ \langle \rho||\bar{m}\rangle \end{pmatrix} \tag{2.8}$$

Then the fitting coefficients gathered in the vector $\mathbf{x}$ are obtained by solving the inhomogeneous equation system:

$$\mathbf{G}\mathbf{x} = \mathbf{J} \tag{2.9}$$

A straightforward solution is given by the inversion of the Coulomb matrix $\mathbf{G}$:

$$\mathbf{x} = \mathbf{G}^{-1}\mathbf{J} \tag{2.10}$$

The normalization of the auxiliary functions with respect to the Coulomb norm ensures that $G_{\bar{k}\,\bar{l}} \leqslant 1$ for any matrix element. This gives certain numerical control over $\mathbf{G}$. Nevertheless the inversion of $\mathbf{G}$ is a delicate numerical process, especially if large auxiliary function sets are chosen. In this case, the matrix can become easily ill-conditioned. In practice, in deMon2k, in order to reduce numerical problems, a Truncated Eigenvalue Decomposition (TED) is often used for obtaining the inverse of $\mathbf{G}$. To perform this decomposition the $\mathbf{G}$ matrix is diagonalized,

$$\mathbf{D} = \tilde{\mathbf{M}}\mathbf{G}\mathbf{M} \tag{2.11}$$

where the $\mathbf{D}$ matrix is the Coulomb matrix in diagonal representation and its entries are the eigenvalues of $\mathbf{G}$. In the following step all eigenvalues below a certain threshold ϵ are quenched, i.e. set to zero. Accordingly, the dimensionality of the active space (number of non-vanishing columns in $\mathbf{M}$) is reduced to a smaller dimension d,

$$\mathbf{D}^{d} = \tilde{\mathbf{M}}^{d}\mathbf{G}\mathbf{M}^{d} \tag{2.12}$$

Transformation of Eq. (2.9) into the diagonal representation leads to:

$$\begin{aligned} \mathbf{D}^{d}\tilde{\mathbf{M}}^{d}\mathbf{x} &= \tilde{\mathbf{M}}^{d}\mathbf{J} \\ \mathbf{D}^{d}\mathbf{x}^{d} &= \mathbf{J}^{d} \end{aligned} \tag{2.13}$$

The fitting coefficients $\mathbf{x}^{d}$ are calculated first in the diagonal representation and then transformed back by:

$$\mathbf{x} = \mathbf{M}^{d}\mathbf{x}^{d} \tag{2.14}$$

This increases the numerical stability compared to the direct calculation of the fitting coefficients in the non-diagonal representation Eq. (2.10). Although, the TED is performed only one time at the beginning of a calculation, the involved diagonalization of the $\mathbf{G}$ matrix can become a critical computational bottleneck if more than a hundred thousand auxiliary functions are used. This is due to that the diagonalization scales approximately as the third power of the number of auxiliary functions. To overcome this computational bottleneck the iterative density fitting with the Krylov subspace method MINRES [54] has been recently implemented in deMon2k.

The expression for the energy which includes the variational fitting of the Coulomb potential can be derived using the energy expression in Eq. (1.45) and the inequality given by Eq. (2.5):

$$E = \sum_{\mu,\nu} P_{\mu\nu} H_{\mu\nu} + \sum_{\mu,\nu} \sum_{\bar{k}} P_{\mu\nu} \langle \mu\nu || \bar{k} \rangle x_{\bar{k}} - \frac{1}{2} \sum_{\bar{k},\bar{l}} x_{\bar{k}} x_{\bar{l}} \langle \bar{k} || \bar{l} \rangle + E_{xc}[\rho] \tag{2.15}$$

In deMon2k this formulation is triggered by the BASIS option of the VXCTYPE keyword [55] because the density $\rho(\mathbf{r})$, which is expanded in terms of the basis set functions according to Eq. (1.43), is used for the calculation of the exchange-correlation energy. In the literature this approach is often named Density Fitted - Density Functional Theory (DF-DFT). Once the fitting coefficients are obtained for a given Coulomb vector by solving Eq. (2.9), we can obtain the DF-DFT Kohn-Sham matrix elements by the variation of Eq. (2.15) with respect to the elements of the density matrix as:

$$K_{\mu\nu} = H_{\mu\nu} + \sum_{\bar{k}} \langle \mu\nu || \bar{k} \rangle x_{\bar{k}} + \langle \mu | \nu_{xc}[\rho] | \nu \rangle \tag{2.16}$$

The accuracy of the variational approximation of the Coulomb potential is within the intrinsic accuracy of the LCGTO approximation [56]. It has to be noticed that since the auxiliary function density is adjusted to the orbital density which changes in each SCF step, the fitting must be performed in each SCF step. Nevertheless, the variational fitting of the Coulomb potential eliminates the four-center ERI calculation from the SCF. Instead, three-center ERIs are needed for the building of the Kohn-Sham matrix and the Coulomb vector. In deMon2k, even in the direct SCF method, where the three-center ERIs are calculated two times in each SCF step, this approximation is much faster than the traditional SCF procedure which involves the calculation of four-center ERIs. Thus, the scaling for the ERI calculation has been reduced from N_{bas}^4 to $N_{bas}^2 \times N_{aux}$. Here N_{aux} is the number of auxiliary functions which is usually two to three times N_{bas}. The scaling of ERI calculation can be further reduced if the symmetry of matrices is exploited and screening techniques are used. As a result, the computationally most demanding task in DF-DFT approaches is usually the calculation of the exchange-correlation contributions since it scales as $N_{bas}^2 \times G$, with G being the number of grid points, which can become quite large. In conclusion, we have exchanged the calculation of four-center integrals by the calculation of three- and two-center integrals and an additional linear algebra

task for solving Eq. (2.9). Next, an additional approximation for dealing with the exchange-correlation terms is described.

2.2 AUXILIARY DENSITY EXCHANGE-CORRELATION POTENTIAL

In general, the integrals involved in the exchange-correlation terms for the energy and Kohn-Sham matrix elements are too complicated for analytic solutions. Therefore, the exchange-correlation integrals are computed numerically using three-dimensional grids in Euclidean space. A point to note is that this problem does not arise in LCGTO Hartree-Fock methods because the Fock exchange integrals can be evaluated in closed form [57]. In order to reduce the computational demand for the numerical integration, it is possible to use the linear scaling auxiliary function density, $\tilde{\rho}(\mathbf{r})$, obtained from the variational fitting of the Coulomb potential [49, 58–60], for the calculation of the exchange-correlation energy. This yields the following energy expression:

$$E = \sum_{\mu,\nu} H_{\mu\nu} + \sum_{\mu,\nu} \sum_{\tilde{k}} P_{\mu\nu} \langle \mu\nu || \tilde{k} \rangle x_{\tilde{k}} - \frac{1}{2} \sum_{\tilde{k},\tilde{l}} x_{\tilde{k}} x_{\tilde{l}} \langle \tilde{k} || \tilde{l} \rangle + E_{xc}[\tilde{\rho}] \tag{2.17}$$

The resulting approximation has been named Auxiliary Density Functional Theory (ADFT). In deMon2k, this approach is triggered by the AUXIS option of the VXCTYPE keyword. It is the default method for calculating the exchange-correlation contributions. In ADFT it is essential that $\tilde{\rho}(\mathbf{r})$ inherits some properties of $\rho(\mathbf{r})$, specifically, that $\tilde{\rho}(\mathbf{r}) \geqslant 0$ and $\int \tilde{\rho}(\mathbf{r}) d\mathbf{r} = N$. The normalization constraint of the density to the number of electrons, N, can be included into the variational density fitting but even without this constraint the number of electrons is conserved to high accuracy. Also the situation of $\tilde{\rho}(\mathbf{r}) < 0$ happens usually only in small regions where $\rho(\mathbf{r}) \approx 0$. These regions can be eliminated by enlarging the auxiliary function set. As most exchange-correlation functionals are undefined for negative values of the density, the sporadic negative auxiliary density values are handled adequately simply by setting them to zero without sacrificing the

accuracy of the numerically integrated electron number [59]. This screening is equivalent to defining the exchange-correlation functional to be identically zero for negative values of the density. This maintains continuity in the exchange-correlation functional and its first derivatives and thus there will be no problems with SCF convergence caused by this treatment, as verified in practice [61].

The corresponding ADFT Kohn-Sham matrix elements are given by:

$$K_{\mu\nu} = H_{\mu\nu} + \sum_{\bar{k}} \langle \mu\nu \| \bar{k} \rangle x_{\bar{k}} + \frac{\partial E_{xc}[\tilde{\rho}]}{\partial P_{\mu\nu}} \tag{2.18}$$

The exchange-correlation term is evaluated as:

$$\frac{\partial E_{xc}[\tilde{\rho}]}{\partial P_{\mu\nu}} = \int \frac{\delta E_{xc}[\tilde{\rho}(\mathbf{r})]}{\delta \tilde{\rho}(\mathbf{r})} \frac{\partial \tilde{\rho}(\mathbf{r})}{\partial P_{\mu\nu}} d\mathbf{r} = \sum_{\bar{k}} \frac{\partial x_{\bar{k}}}{\partial P_{\mu\nu}} \int v_{xc}[\tilde{\rho}(\mathbf{r})] \bar{k}(\mathbf{r}) d\mathbf{r} \tag{2.19}$$

with:

$$v_{xc}[\tilde{\rho}(\mathbf{r})] \equiv \frac{\delta E_{xc}[\tilde{\rho}]}{\delta \tilde{\rho}(\mathbf{r})} \tag{2.20}$$

The derivatives of the Coulomb fitting coefficients are obtained using Eq. (2.10) giving:

$$\frac{\partial x_{\bar{k}}}{\partial P_{\mu\nu}} = \sum_{\bar{l}} G^{-1}_{\bar{k}\bar{l}} \langle \bar{l} \| \mu\nu \rangle \tag{2.21}$$

Here $G^{-1}_{\bar{k}\bar{l}}$ refers to the $\bar{k}, \bar{l}$ element of G^{-1}. Introducing the exchange-correlation fitting coefficient vector, $\mathbf{z}$, with elements,

$$z_{\bar{k}} = \sum_{\bar{l}} G^{-1}_{\bar{k}\bar{l}} \left\langle \bar{l} \mid v_{xc}[\tilde{\rho}(\mathbf{r})] \right\rangle \tag{2.22}$$

we can rewrite Eq. (2.18) as

$$K_{\mu\nu} = H_{\mu\nu} + \sum_{\bar{k}} \langle \mu\nu \| \bar{k} \rangle \left(x_{\bar{k}} + z_{\bar{k}} \right) \tag{2.23}$$

It is important to point out that $z_{\bar{k}}$ is a spin-dependent quantity. Its different values for α and β spin densities determine the differences between the α and β Kohn-Sham matrices in open-shell calculations. Similar to Eq. (2.9), an inhomogeneous equation system can be formulated

$$\mathbf{G}\mathbf{z} = \mathbf{L} \tag{2.24}$$

with

$$\mathbf{L} = \begin{pmatrix} \langle \nu_{xc} \mid \bar{1} \rangle \\ \langle \nu_{xc} \mid \bar{2} \rangle \\ \vdots \\ \langle \nu_{xc} \mid \bar{m} \rangle \end{pmatrix} \tag{2.25}$$

In order to keep the calculation variational $\tilde{\rho}(\mathbf{r})$ has to be used directly without modifications from the solution of the Coulomb fitting for the evaluation of the exchange-correlation potential. However, this is not mandatory for the calculation of the Coulomb contribution in the SCF energy expression. As a result, there are two sets of fitting coefficients in deMon2k calculations. The first one refers to the solution to Eq. (2.9), and the other results from SCF acceleration techniques, such as fitting coefficient mixing or Direct Inversion of the Iterative Space (DIIS) [62–64], which are used to build the Coulomb part of the Kohn-Sham matrix.

Because the approximated density is a linear combination of auxiliary functions, the density calculation at each grid point becomes linear, i.e. the numerical integration scaling becomes $N_{aux} \times G$. With the above described ADFT approach the computational bottleneck for the numerical integration disappears. In combination with a sophisticated implementation of the three-center ERI calculations, the Coulomb contribution can be computed in an almost linear scaling effort by using the double-asymptotic expansion technique [65]. The computational bottleneck is now shifted to linear algebra operations,

mainly the diagonalization and multiplication of matrices. In particular, the diagonalization of the Coulomb matrix, associated with the TED, is the single most demanding linear algebra task in deMon2k. The second most demanding linear algebra task represents the solution of the Kohn-Sham equation system. It consists of the transformation of the general eigenvalue equation system into its special form and the diagonalization of the corresponding Kohn-Sham matrix. These operations are performed using optimized computational libraries [66–71]. The current implementation in deMon2k allows routine calculations of systems with up to 10,000 basis functions and has already been successfully applied to systems with more than 25,000 basis functions. If the molecular system under consideration exhibits non-trivial degrees of symmetry these limits can be further enlarged due to the symmetry-adapted blocking of the Kohn-Sham and Coulomb matrices. Therefore, from a computational point of view, the main advantage of symmetry adaptation in ADFT calculations is the transformation of the associated linear algebra tasks into block-diagonal form. Furthermore, symmetry adaptation is also a valuable tool for analyzing ADFT results. The next chapter will describe how to explore symmetry in the framework of ADFT.

3

SYMMETRY-ADAPTED AUXILIARY DENSITY FUNCTIONAL THEORY

3.1 Selection rules

In order to introduce symmetry into ADFT, we are initially concerned with the application of the following symmetry selection rules [72]:

$$\langle \psi^{\Gamma(\gamma)} | \phi^{\Gamma'(\gamma')} \rangle = \delta_{\Gamma\Gamma'} \delta_{\gamma\gamma'} \langle \psi^{\Gamma(\gamma)} | \phi^{\Gamma(\gamma)} \rangle \tag{3.1}$$

$$\langle \psi^{\Gamma(\gamma)} | \hat{O}^{A} | \phi^{\Gamma'(\gamma')} \rangle = \delta_{\Gamma\Gamma'} \delta_{\gamma\gamma'} \langle \psi^{\Gamma(\gamma)} | \hat{O}^{A} | \phi^{\Gamma(\gamma)} \rangle \tag{3.2}$$

Here, the operator $\hat{O}^{A}$ belongs to the totally symmetry representation A, the functions $\psi^{\Gamma(\gamma)}(\mathbf{r})$ and $\phi^{\Gamma'(\gamma')}(\mathbf{r})$ are symmetry-adapted functions belonging to the real irreducible representations Γ and Γ', respectively, and to the columns of these irreducible representations denoted by γ and γ'. The indices γ and γ' take values from 1 to the dimension of the irreducible representations d_{Γ} and $d_{\Gamma'}$, respectively. Proof of these equations are found in [73]. Usually the symmetry-adapted functions are constructed by projection operators, $\hat{P}_{\gamma\gamma}$,

$$\hat{P}^{\Gamma}_{\gamma\gamma} \phi(\mathbf{r}) = \phi^{\Gamma(\gamma)}(\mathbf{r}) \tag{3.3}$$

and transfer operators,

$$\hat{P}^{\Gamma}_{\gamma'\gamma} \phi^{\Gamma(\gamma)}(\mathbf{r}) = \phi^{\Gamma(\gamma')}(\mathbf{r}) \tag{3.4}$$

In the special case of complex irreducible representations, we employ corresponding real forms, which may have increased dimensions, in order to avoid complex algebra in the code. The enlarged real representations are called in the literature minimal representations [74]. For them the following modified selection rules apply:

$$\langle \psi^{\Gamma(\gamma)} | \phi^{\Gamma'(\gamma')} \rangle = \delta_{\Gamma\Gamma'} \langle \psi^{\Gamma(\gamma)} | \phi^{\Gamma(\gamma')} \rangle \tag{3.5}$$

$$\langle \psi^{\Gamma(\gamma)} | \hat{O}^{A} | \phi^{\Gamma'(\gamma')} \rangle = \delta_{\Gamma\Gamma'} \langle \psi^{\Gamma(\gamma)} | \hat{O}^{A} | \phi^{\Gamma(\gamma')} \rangle \tag{3.6}$$

Thus, functions belonging to minimal representations are only orthogonal by symmetry between different irreducible representations. For irreducible representations (not minimal), we also rely on the next identity [72]:

$$\langle \psi^{\Gamma(\gamma)} | \hat{O}^{A} | \phi^{\Gamma(\gamma)} \rangle = \langle \psi^{\Gamma(\gamma')} | \hat{O}^{A} | \phi^{\Gamma(\gamma')} \rangle \tag{3.7}$$

Eq. (3.7) allows the calculation of matrix elements of a multi-dimensional irreducible representation Γ from its degenerate symmetry-adapted functions of one column. A very important operator that is totally symmetric is the molecular Hamiltonian, Eq. (1.2). Totally symmetric operators commute with symmetry operations $\hat{R}$, i.e. the eigenfunctions of $\hat{O}^{A}$ are also eigenfunctions of $\hat{R}$. This fact allows us to connect the transformation properties of symmetry-adapted functions with the transformation properties of eigenfunctions of totally symmetric operators. Namely, as symmetry-adapted functions transform under symmetry operations accordingly to [75],

$$\hat{R}\phi^{\Gamma(\gamma')}(\mathbf{r}) = \sum_{\gamma} \chi^{\Gamma}_{\gamma\gamma'}(\hat{R}) \phi^{\Gamma(\gamma)}(\mathbf{r}) \tag{3.8}$$

where $\chi^{\Gamma}_{\gamma\gamma'}(\hat{R})$ is a matrix element of the irreducible representation Γ for the symmetry operation $\hat{R}$, then, the eigenfunctions of $\hat{O}^{A}$ transform in the same way. Therefore, each eigenfunction of $\hat{O}^{A}$ can be assigned to an irreducible representation $\Gamma(\gamma)$ [76]. A simple

C_5	$\hat{E}$	$\hat{C}_5$	$\hat{C}_5^2$	$\hat{C}_5^3$	$\hat{C}_5^4$
A	1	1	1	1	1
...					

$$\hat{R}\psi(\mathbf{r}) = 1\psi(\mathbf{r}) \quad \forall \quad \hat{R}$$
$$\therefore \ \psi(\mathbf{r}) \rightarrow \psi^A(\mathbf{r})$$

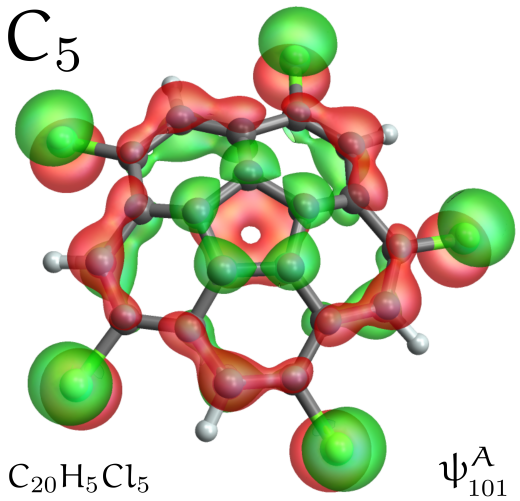

Figure 3.1: A molecular orbital of the system $C_{20}H_5Cl_5$ with symmetry C_5 that transforms as the totally symmetric irreducible representation A. This is seen by applying all symmetry operations $\hat{R}$ of the point group C_5 to the molecular orbital and noting that the resulting function has coefficients equal to 1 for all $\hat{R}$.

example of an eigenfunction of a totally symmetric operator which can be assigned to a single irreducible representation is given in Figure 3.1.

We will see that the selection rules simplify the calculations in ADFT. In this thesis, we treat only point group symmetry operations describing rotations performed on a given molecule. Now we apply these selection rules to the Kohn-Sham equations and Coulomb fitting equations.

3.2 Symmetry-adapted Kohn-Sham equations

For clarity of presentation, we restrict the following discussion to real one-dimensional irreducible representations. The extension to higher-dimensional irreducible representations is given later on. The symmetry-adapted Kohn-Sham equations are obtained by choosing symmetry-adapted basis functions for its matrix representation. The symmetry-adapted basis consists of a function set $\{\mathring{a}^\Gamma(\mathbf{r})\}$ in which each function is labeled with Γ

according to the irreducible representation to which it belongs. We call these functions Symmetry-Adapted Orbitals (SAOs). They are expressed as linear combinations of AOs:

$$\mathring{a}^{\Gamma}(\mathbf{r}) = \sum_{\mu} U^{\Gamma}_{\mu\mathring{a}}\mu(\mathbf{r}) \tag{3.9}$$

We call the basis $\{\mathring{a}^{\Gamma}(\mathbf{r})\}$ the SAO basis. This basis can be constructed by applying symmetry projectors and transfer operators to the AO basis. By construction the SAOs $\{\mathring{a}^{\Gamma}(\mathbf{r})\}$ span the same space as the AOs, and therefore we can express the Kohn-Sham matrix elements in the SAO representation as:

$$K^{\Gamma\Gamma'}_{\mathring{a}\mathring{b}} = \langle \mathring{a}^{\Gamma}|\hat{K}|\mathring{b}^{\Gamma'}\rangle = \sum_{\mu,\nu} U^{\Gamma\ T}_{\mathring{a}\mu} K_{\mu\nu} U^{\Gamma'}_{\nu\mathring{b}} \tag{3.10}$$

Thus, the symmetry-adapted Kohn-Sham matrix can be obtained by a transformation of the Kohn-Sham matrix in AO representation with the symmetrization matrix $\mathbf{U}$. We can express this in linear algebra notation as:

$$\mathbb{K} = \mathbf{U}^{\mathsf{T}}\mathbf{K}\mathbf{U} \tag{3.11}$$

For the symmetry-adapted matrices, here the Kohn-Sham matrix, we use in linear algebra notation the blackboard bold font. Similarly, we find for the overlap matrix elements in SAO representation:

$$S^{\Gamma\Gamma'}_{\mathring{a}\mathring{b}} = \langle \mathring{a}^{\Gamma}|\mathring{b}^{\Gamma'}\rangle = \sum_{\mu,\nu} U^{\Gamma\ T}_{\mathring{a}\mu} S_{\mu\nu} U^{\Gamma'}_{\nu\mathring{b}} \tag{3.12}$$

The corresponding linear algebra notation is given as:

$$\mathbb{S} = \mathbf{U}^{\mathsf{T}}\mathbf{S}\mathbf{U} \tag{3.13}$$

Assuming the Kohn-Sham operator is totally symmetric, i.e. $\hat{K} \to \hat{K}^{A}$, only the Kohn-Sham matrix elements with SAOs from the same irreducible representation will not vanish according to Eq. (3.2). Taking this integral selection rule into account we find:

$$K^{\Gamma\Gamma'}_{\mathring{a}\mathring{b}} = \langle \mathring{a}^{\Gamma} | \hat{K}^{A} | \mathring{b}^{\Gamma'} \rangle = \delta_{\Gamma\Gamma'} \langle \mathring{a}^{\Gamma} | \hat{K}^{A} | \mathring{b}^{\Gamma} \rangle = \delta_{\Gamma\Gamma'} K^{\Gamma}_{\mathring{a}\mathring{b}} \tag{3.14}$$

Therefore, the Kohn-Sham matrix in SAO representation is block diagonal since the matrix elements with $\Gamma \neq \Gamma'$ are zero. Furthermore, we can contract the irreducible representation labeling to one superscript for the diagonal blocks. The same holds for the overlap matrix elements in SAO representation:

$$S^{\Gamma\Gamma'}_{\mathring{a}\mathring{b}} = \langle \mathring{a}^{\Gamma} | \mathring{b}^{\Gamma'} \rangle = \delta_{\Gamma\Gamma'} \langle \mathring{a}^{\Gamma} | \mathring{b}^{\Gamma} \rangle = \delta_{\Gamma\Gamma'} S^{\Gamma}_{\mathring{a}\mathring{b}} \tag{3.15}$$

Therefore, the Kohn-Sham and overlap matrix in SAO representation have the general structure:

$$\mathbb{M} = \begin{pmatrix} \mathbf{M}^{\Gamma} & \mathbf{0} & \dots & \mathbf{0} \\ \mathbf{0} & \mathbf{M}^{\Gamma'} & \dots & \mathbf{0} \\ \vdots & \vdots & \ddots & \vdots \\ \mathbf{0} & \mathbf{0} & \dots & \mathbf{M}^{\Gamma''} \end{pmatrix} \tag{3.16}$$

In Eq. (3.16) Γ, Γ', ... Γ'' are different irreducible representations of the point group under consideration and each block $\mathbf{M}^{\Gamma}$ is a square matrix. These blocks have dimension $n^{\Gamma} \times n^{\Gamma}$, where n^{Γ} is the number of SAOs belonging to the irreducible representation Γ. In general, the blocks have different dimensions. It is convenient to write block diagonal matrices as a direct sum of their diagonal block matrices in the form:

$$\mathbb{M} = \mathbf{M}^{\Gamma} \oplus \mathbf{M}^{\Gamma'} \oplus \cdots \oplus \mathbf{M}^{\Gamma''} \tag{3.17}$$

To proceed, we now write the Kohn-Sham equations in SAO representation:

$$\mathbb{K}\mathbb{c} = \mathbb{S}\mathbb{c}\boldsymbol{\epsilon} \tag{3.18}$$

Because $\mathbb{K}$ and $\mathbb{S}$ are block diagonal, the MO coefficient matrix in SAO representation, $\mathbb{c}$, becomes block diagonal, too. Therefore, the Kohn-Sham equations in SAO representation can be partitioned into individual Roothaan-Hall type equation systems for each irreducible representation:

$$\mathbf{K}^{\Gamma}\mathbf{c}^{\Gamma} = \mathbf{S}^{\Gamma}\mathbf{c}^{\Gamma}\boldsymbol{\epsilon}^{\Gamma} \qquad \forall \quad \Gamma \tag{3.19}$$

From a computational point of view it is important to note that the equation systems for each irreducible representation can be solved separately from each other. In the deMon2k implementation developed in this thesis, the blocking of the Kohn-Sham equations proceeds along the following steps. First the overlap matrix is transformed into SAO representation according to Eq. (3.13). Next, a canonical orthogonalization [37] is performed separately for each block:

$$\mathbf{S}^{\Gamma}\mathbf{V}^{\Gamma} = \mathbf{V}^{\Gamma}\mathbf{D}^{\Gamma} \qquad \forall \quad \Gamma \tag{3.20}$$

$$\mathbf{Y}^{\Gamma} = \mathbf{V}^{\Gamma}\mathbf{D}^{\Gamma^{-\frac{1}{2}}} \qquad \forall \quad \Gamma \tag{3.21}$$

The resulting orthogonalization blocks $\{\mathbf{Y}^{\Gamma}\}$ are assembled,

$$\mathbf{Y} = \mathbf{Y}^{\Gamma} \oplus \mathbf{Y}^{\Gamma'} \oplus \ldots \tag{3.22}$$

and the final orthogonalization matrix is built as:

$$\mathbf{X} = \mathbf{U}\mathbf{Y} \tag{3.23}$$

With the matrix $\mathbf{X}$, which is not block diagonal, the Kohn-Sham equations can be directly transformed into an orthonormal SAO representation:

$$\mathbf{X}^{\mathsf{T}}\mathbf{K}\mathbf{X}\mathbf{X}^{-1}\mathbf{c} = \mathbf{X}^{\mathsf{T}}\mathbf{S}\mathbf{X}\mathbf{X}^{-1}\mathbf{c}\boldsymbol{\epsilon} \tag{3.24}$$

This yields the following block diagonal form,

$$\check{\mathbb{K}}\check{\mathbf{c}} = \check{\mathbf{c}}\boldsymbol{\epsilon} \tag{3.25}$$

which can be solved for each irreducible representation separately:

$$\check{\mathbf{K}}^{\Gamma}\check{\mathbf{c}}^{\Gamma} = \check{\mathbf{c}}^{\Gamma}\boldsymbol{\epsilon}^{\Gamma} \qquad \forall \quad \Gamma \tag{3.26}$$

The MO coefficients in the orthonormal SAO representation are assembled as:

$$\check{\mathbf{c}} = \check{\mathbf{c}}^{\Gamma} \oplus \check{\mathbf{c}}^{\Gamma'} \oplus \ldots \tag{3.27}$$

Afterwards, the MO coefficients in AO representation are obtained by the back transformation:

$$\mathbf{c} = \mathbf{X}\check{\mathbf{c}} \tag{3.28}$$

With these MO coefficients the density matrix and energy can be calculated and, if convergence is not reached, the next SCF cycle can be initialized.

In the case of multi-dimensional real irreducible representations an additional degree of blocking is possible since we have two symmetry labels, the irreducible representation Γ and the column of the irreducible representation γ. We then can apply an additional selection rule:

$$\langle \mathring{a}^{\Gamma(\gamma)}|\hat{K}^{A}|\mathring{b}^{\Gamma'(\gamma')}\rangle = \delta_{\Gamma\Gamma'}\delta_{\gamma\gamma'}\langle \mathring{a}^{\Gamma(\gamma)}|\hat{K}^{A}|\mathring{b}^{\Gamma(\gamma)}\rangle = \delta_{\Gamma\Gamma'}\delta_{\gamma\gamma'}K^{\Gamma(\gamma)}_{\mathring{a}\mathring{b}} \tag{3.29}$$

This gives rise to the following set of Kohn-Sham equations:

$$\breve{\mathbf{K}}^{\Gamma(\gamma)}\breve{\mathbf{c}}^{\Gamma(\gamma)} = \breve{\mathbf{c}}^{\Gamma(\gamma)}\boldsymbol{\epsilon}^{\Gamma(\gamma)} \qquad \forall \quad \Gamma, \gamma \tag{3.30}$$

In Eq. (3.30) γ takes the values 1, 2, ..., d_Γ with d_Γ being the dimension of the irreducible representation Γ. From the identity in Eq. (3.7) we observe that the matrix $\breve{\mathbf{K}}^{\Gamma(1)}$ is equal to $\breve{\mathbf{K}}^{\Gamma(\gamma)}$ for any γ if the Kohn-Sham operator is totally symmetric. However, in general the used Kohn-Sham operators are not totally symmetric because of the asymmetry of the electron density [77] and the approximate nature of the density functional when using non-symmetry-dependent functionals and potentials [78]. Therefore, the degeneracies are broken and not applying the identity of Eq. (3.7) allows us to detect this symmetry breaking. In this case the blocks $\breve{\mathbf{K}}^{\Gamma(\gamma)}$ and $\breve{\mathbf{K}}^{\Gamma(\gamma')}$ for $\gamma \neq \gamma'$ are different. As a result, the corresponding MO coefficients, $\breve{\mathbf{c}}^{\Gamma(\gamma)}$, and MO energies, $\boldsymbol{\epsilon}^{\Gamma(\gamma)}$, are different from $\breve{\mathbf{c}}^{\Gamma(\gamma')}$ and $\boldsymbol{\epsilon}^{\Gamma(\gamma')}$ for $\gamma \neq \gamma'$. In particular, the MO energies are sensitive indicators for symmetry breaking due to a not totally symmetric Kohn-Sham operator. For this reason, we enforce in our symmetry-adapted ADFT implementation in deMon2k orthogonality between different irreducible representations Γ and Γ' as well as between different degeneracies (columns) γ and γ' of multi-dimensional irreducible representations. However we allow $\breve{\mathbf{K}}^{\Gamma(\gamma)}$ to be different from $\breve{\mathbf{K}}^{\Gamma(\gamma')}$ for $\gamma \neq \gamma'$. The practical implication of this symmetry breaking is discussed in the validation chapter. A detailed discussion of the problem of asymmetry in density functional theory, its consequences and recent advances can be found in [77–87]. In the case of minimal representations there is no additional degree of blocking, i.e. we use Eq. (3.26) instead of (3.30), with:

$$\breve{\mathbf{K}}^{\Gamma} = \begin{pmatrix} \breve{\mathbf{K}}^{\Gamma(1)\Gamma(1)} & \breve{\mathbf{K}}^{\Gamma(1)\Gamma(2)} \\ \breve{\mathbf{K}}^{\Gamma(2)\Gamma(1)} & \breve{\mathbf{K}}^{\Gamma(2)\Gamma(2)} \end{pmatrix} \tag{3.31}$$

Here γ has taken the values of 1 and 2 because the minimal representations used in deMon2k are always two-dimensional. The point groups that contain them are T, T_h,

C_n, C_{nh} with $n > 2$ and S_{2m} with $m \geqslant 2$. We now turn to the symmetry adaptation of the Coulomb and exchange-correlation fitting equations.

3.3 Symmetry-adapted fitting equations

As already discussed, density fitting is characteristic to DF-DFT and ADFT. The resulting fitting equation systems can also be transformed into symmetry-adapted representation. In order to obtain the fitting equations in symmetry-adapted representation, we introduce symmetry-adapted auxiliary functions, $\mathring{k}^{\Gamma}(\mathbf{r})$, that span the same space as the primitive Hermite Gaussian ones. Therefore, an alternative expansion of the auxiliary density, Eq. (2.2), is given by:

$$\tilde{\rho}(\mathbf{r}) = \sum_{\Gamma} \sum_{\mathring{k} \in \Gamma} x_{\mathring{k}}^{\Gamma} \mathring{k}^{\Gamma}(\mathbf{r}) \tag{3.32}$$

Here, the sum over Γ runs over all irreducible representations of the underlying point group that are present in the symmetry-adapted auxiliary function set and the sum over $\mathring{k} \in \Gamma$ runs over all linear independent symmetry-adapted functions belonging to the same irreducible representation Γ. For clarity of presentation, we restrict the following discussion to real one-dimensional irreducible representations. However, our actual implementation covers higher-dimensional irreducible representations, too, as shown in the validation and application chapters. Inserting the auxiliary density expansion of Eq. (3.32) into the fitting error expression, Eq. (2.4), and minimizing ε_2, now with respect to the symmetry-adapted Coulomb fitting coefficients $x_{\mathring{k}}^{\Gamma}$, yields:

$$\sum_{\mu,\nu} P_{\mu\nu} \langle \mu\nu \| \mathring{k}^{\Gamma} \rangle = \sum_{\Gamma'} \sum_{\mathring{l} \in \Gamma'} x_{\mathring{l}}^{\Gamma'} \langle \mathring{l}^{\Gamma'} \| \mathring{k}^{\Gamma} \rangle \qquad \forall \quad \mathring{k}^{\Gamma} \wedge \Gamma \tag{3.33}$$

Because the Coulomb operator is totally symmetric only Coulomb matrix elements with symmetry-adapted auxiliary functions of the same irreducible representation will not vanish. Taking this integral selection rule into account modifies Eq. (3.33) to:

$$\sum_{\mu,\nu} P_{\mu\nu}\langle\mu\nu||\mathring{k}^{\Gamma}\rangle = \sum_{\Gamma'}\sum_{\mathring{l}\in\Gamma'} x_{\mathring{l}}^{\Gamma'}\langle\mathring{l}^{\Gamma'}||\mathring{k}^{\Gamma}\rangle\delta_{\Gamma'\Gamma} = \sum_{\mathring{l}\in\Gamma} x_{\mathring{l}}^{\Gamma}\langle\mathring{l}^{\Gamma}||\mathring{k}^{\Gamma}\rangle \qquad \forall \quad \mathring{k}^{\Gamma} \wedge \Gamma \tag{3.34}$$

Casting the symmetry-adapted density-fitting equations, Eq. (3.34), into matrix notation, yields an equation system for each irreducible representation of the form:

$$\mathbf{G}^{\Gamma}\mathbf{x}^{\Gamma} = \mathbf{J}^{\Gamma} \qquad \forall \quad \Gamma \tag{3.35}$$

Note that these equation systems are independent of each other.

To proceed, we now expand the symmetry-adapted auxiliary functions, $\mathring{k}^{\Gamma}(\mathbf{r})$, in terms of the normalized primitive atom-centered Hermite auxiliary functions that form our auxiliary function set:

$$\mathring{k}^{\Gamma}(\mathbf{r}) = \sum_{\bar{l}} \bar{l}(\mathbf{r})U_{\bar{l}\mathring{k}}^{\Gamma} \tag{3.36}$$

The corresponding auxiliary density expansion is then given by:

$$\tilde{\rho}(\mathbf{r}) = \sum_{\Gamma}\sum_{\mathring{k}\in\Gamma} x_{\mathring{k}}^{\Gamma}\mathring{k}^{\Gamma}(\mathbf{r}) = \sum_{\Gamma}\sum_{\mathring{k}\in\Gamma}\sum_{\bar{l}} x_{\mathring{k}}^{\Gamma}U_{\mathring{k}\bar{l}}^{\Gamma\ T}\bar{l}(\mathbf{r}) \tag{3.37}$$

Comparison of Eq. (3.37) with Eq. (2.2) yields for the Coulomb fitting coefficients the relation:

$$x_{\bar{l}} = \sum_{\Gamma}\sum_{\mathring{k}\in\Gamma} x_{\mathring{k}}^{\Gamma}U_{\mathring{k}\bar{l}}^{\Gamma\ T} \tag{3.38}$$

Therefore, the standard Coulomb fitting coefficients can be directly obtained from their symmetry-adapted equivalents calculated by Eq. (3.35) with the symmetrization matrix $\mathbf{U}$. On the other hand, the symmetry-adapted Coulomb vector, $\mathbf{J}^{\Gamma}$, and Coulomb matrix,

$\mathbf{G}^{\Gamma}$, elements can be obtained by inserting the expansion of the symmetry-adapted auxiliary functions, Eq. (3.36), as:

$$J^{\Gamma}_{\mathring{k}} = \sum_{\mu,\nu} P_{\mu\nu} \langle \mu\nu \| \mathring{k}^{\Gamma} \rangle = \sum_{\mu,\nu} \sum_{\bar{l}} P_{\mu\nu} \langle \mu\nu \| \bar{l} \rangle U^{\Gamma}_{\bar{l}\mathring{k}} \tag{3.39}$$

$$G^{\Gamma}_{\mathring{k}\mathring{l}} = \langle \mathring{k}^{\Gamma} \| \mathring{l}^{\Gamma} \rangle = \sum_{\bar{m},\bar{n}} U^{\Gamma\ T}_{\mathring{k}\bar{m}} \langle \bar{m} \| \bar{n} \rangle U^{\Gamma}_{\bar{n}\mathring{l}} \tag{3.40}$$

The corresponding matrix equations are:

$$\mathbf{J}^{\Gamma} = \mathbf{U}^{\Gamma\,\mathrm{T}} \mathbf{J}; \qquad \mathbf{G}^{\Gamma} = \mathbf{U}^{\Gamma\,\mathrm{T}} \mathbf{G} \mathbf{U}^{\Gamma} \tag{3.41}$$

Therefore, the symmetry-adapted Coulomb vector and matrix can be straightforwardly calculated from the corresponding standard Coulomb vector and matrix with the symmetrization matrix $\mathbf{U}$, too. Once these quantities are at hand, the symmetry-adapted fitting equation systems can be solved separately for each irreducible representation and the resulting symmetry-adapted fitting coefficients can be back-transformed into standard Coulomb fitting coefficients according to Eq. (3.38). This concludes the symmetry-adapted Coulomb fitting.

Besides the Coulomb fitting coefficients, exchange-correlation coefficients have to be calculated in ADFT, too. For symmetry-adapted exchange-correlation coefficients holds:

$$z^{\Gamma}_{\mathring{k}} = \sum_{\mathring{l} \in \Gamma} \langle \mathring{k}^{\Gamma} \| \mathring{l}^{\Gamma} \rangle^{-1} \langle \mathring{l}^{\Gamma} | \nu_{xc}[\tilde{\rho}] \rangle = \sum_{\mathring{l} \in \Gamma} G^{\Gamma\ -1}_{\mathring{k}\mathring{l}} \langle \mathring{l}^{\Gamma} | \nu_{xc}[\tilde{\rho}] \rangle \tag{3.42}$$

Eq. (3.42) can be reformulated as a linear equation system for each irreducible representation analog to the Coulomb fitting equation systems in Eq. (3.35):

$$\mathbf{G}^{\Gamma} \mathbf{z}^{\Gamma} = \mathbf{L}^{\Gamma} \qquad \forall \quad \Gamma \tag{3.43}$$

Also these equation systems are independent of each other. Similar to the Coulomb vector, the elements of the symmetry-adapted exchange-correlation vector, $L^{\Gamma}_{\mathring{k}}$, can be directly calculated from the corresponding standard exchange-correlation vector elements:

$$L^{\Gamma}_{\mathring{k}} = \sum_{\bar{l}} L_{\bar{l}} U^{\Gamma}_{\bar{l}\mathring{k}} = \sum_{\bar{l}} \langle \nu_{xc}[\tilde{\rho}] | \bar{l} \rangle U^{\Gamma}_{\bar{l}\mathring{k}} \tag{3.44}$$

The exchange-correlation integrals in Eq. (3.44) are calculated by numerical integration. Due to the spin polarization of the exchange-correlation potential, the exchange-correlation vector elements are also spin polarized. As a consequence also the exchange-correlation coefficients are spin polarized. Once the symmetry-adapted exchange-correlation vectors are at hand, the relevant equation systems of Eq. (3.43) are solved. Afterwards, the standard ADFT exchange-correlation coefficients can be obtained through the following back-transformation:

$$z_{\bar{k}} = \sum_{\Gamma} \sum_{\mathring{l} \in \Gamma} z^{\Gamma}_{\mathring{l}} U^{\Gamma\,T}_{\mathring{l}\bar{k}} \tag{3.45}$$

In order to extend our discussion to the case of real multi-dimensional irreducible representations, we rewrite Eq. (3.37) as:

$$\tilde{\rho}(\mathbf{r}) = \sum_{\Gamma} \sum_{\gamma} \sum_{\mathring{k} \in \Gamma(\gamma)} x^{\Gamma(\gamma)}_{\mathring{k}} \mathring{k}^{\Gamma(\gamma)}(\mathbf{r}) \tag{3.46}$$

As for the extension of the symmetry-adapted Kohn-Sham equations, Eq. (3.30), γ runs over the degeneracies of the irreducible representations. Again there are d_{Γ} degenerate functions which together form the irreducible representation Γ. As a consequence, the Coulomb fitting equation system can be written as:

$$\mathbf{G}^{\Gamma(\gamma)} \mathbf{x}^{\Gamma(\gamma)} = \mathbf{J}^{\Gamma(\gamma)} \qquad \forall \quad \Gamma, \gamma \tag{3.47}$$

Because the Coulomb operator is totally symmetric we can use Eq. (3.7) for the Coulomb matrix. Thus, it follows:

$$\mathbf{G}^{\Gamma(\gamma)} = \mathbf{G}^{\Gamma(\gamma')} \equiv \mathbf{G}^{\Gamma(1)} \tag{3.48}$$

Therefore, only one block corresponding to one of the degenerate functions has to be calculated, e.g. $\mathbf{G}^{\Gamma(1)}$. Note, however, that in general Eq. (3.7) cannot be applied to the Coulomb vector because the Kohn-Sham density propagates the symmetry breaking of the approximated exchange-correlation potential. Thus, we must assume for the different Coulomb vectors belonging to the same real multi-dimensional irreducible representation:

$$\mathbf{J}^{\Gamma(\gamma)} \neq \mathbf{J}^{\Gamma(\gamma)'} \tag{3.49}$$

Following these arguments, we can rewrite the symmetry-adapted Coulomb fitting equations, including real multi-dimensional irreducible representations as:

$$\mathbf{G}^{\Gamma(1)}\mathbf{x}^{\Gamma(\gamma)} = \mathbf{J}^{\Gamma(\gamma)} \qquad \forall \quad \Gamma, \gamma \tag{3.50}$$

After solving the symmetry-adapted fitting equation systems the symmetry-adapted Coulomb fitting coefficients can be back-transformed according to:

$$x_{\bar{l}} = \sum_{\Gamma} \sum_{\gamma} \sum_{\mathring{k} \in \Gamma(\gamma)} x_{\mathring{k}}^{\Gamma(\gamma)} U_{\mathring{k}\bar{l}}^{\Gamma(\gamma)^{T}} \tag{3.51}$$

Because the same argumentation holds also for the calculation of the exchange-correlation fitting coefficients, we find as symmetry-adapted exchange-correlation fitting equations:

$$\mathbf{G}^{\Gamma(1)}\mathbf{z}^{\Gamma(\gamma)} = \mathbf{L}^{\Gamma(\gamma)} \qquad \forall \quad \Gamma, \gamma \tag{3.52}$$

with

$$z_{\mathring{k}}^{\Gamma(\gamma)} = \sum_{\mathring{l}\in\Gamma(\gamma)} \langle \mathring{k}^{\Gamma(\gamma)} || \mathring{l}^{\Gamma(\gamma)} \rangle^{-1} \langle \mathring{l}^{\Gamma(\gamma)} | v_{xc}[\tilde{\rho}] \rangle = \sum_{\mathring{l}\in\Gamma(\gamma)} G_{\mathring{k}\mathring{l}}^{\Gamma(1)^{-1}} \langle \mathring{l}^{\Gamma(\gamma)} | v_{xc}[\tilde{\rho}] \rangle \quad (3.53)$$

Finally, for the case of the two-dimensional minimal irreducible representations, orthogonality between degenerate functions (i.e. functions belonging to Γ with different indices γ and γ') cannot be achieved using real projector and transfer operators. Therefore, only orthogonality between different irreducible representations Γ and Γ' can be exploited.

3.4 SYMMETRY-ADAPTED FITTING FOR TOTALLY SYMMETRIC DENSITIES

In the common situation of totally symmetric Kohn-Sham electron densities, which we will denote by $\rho(\mathbf{r}) \to \rho^A(\mathbf{r})$, the ADFT fitting equation systems will further simplify. Because the Coulomb operator is totally symmetric, the Coulomb fitting equation system reduces to its totally symmetric block:

$$\langle \rho^A || \mathring{k}^A \rangle = \sum_{\mathring{l}\in A} x_{\mathring{l}}^A \langle \mathring{l}^A || \mathring{k}^A \rangle \qquad \forall \quad \mathring{k}^A \quad (3.54)$$

Thus, only the totally symmetric equation system

$$\mathbf{G}^A \mathbf{x}^A = \mathbf{J}^A \quad (3.55)$$

has to be solved.

Because the auxiliary density is totally symmetric the calculation of the exchange-correlation fitting coefficients in ADFT simplifies, too. To show this, we calculate the exchange-correlation contribution to the ADFT Kohn-Sham matrix [58, 59] with the totally symmetric density as:

$$\frac{\partial E_{xc}[\tilde{\rho}^A]}{\partial P_{\mu\nu}} = \int \frac{\delta E_{xc}[\tilde{\rho}^A]}{\delta \tilde{\rho}^A(\mathbf{r})} \frac{\partial \tilde{\rho}^A(\mathbf{r})}{\partial P_{\mu\nu}} d\mathbf{r} \quad (3.56)$$

The here appearing partial derivative of the totally symmetric auxiliary density is given by:

$$\frac{\partial \tilde{\rho}^{A}(\mathbf{r})}{\partial P_{\mu\nu}} = \sum_{\mathring{k}\in A} \frac{\partial x^{A}_{\mathring{k}}}{\partial P_{\mu\nu}} \mathring{k}^{A}(\mathbf{r}) = \sum_{\mathring{k},\mathring{l}\in A} \langle \mu\nu \| \mathring{k}^{A} \rangle G^{\overline{A}^{-1}}_{\mathring{k}\mathring{l}} \mathring{l}^{A}(\mathbf{r}) \tag{3.57}$$

Inserting Eq. (3.57) into Eq. (3.56) and introducing the ADFT exchange-correlation potential as:

$$v_{xc}[\tilde{\rho}^{A}] \equiv \frac{\delta E_{xc}[\tilde{\rho}^{A}]}{\delta \tilde{\rho}^{A}(\mathbf{r})} \tag{3.58}$$

yields:

$$\frac{\partial E_{xc}[\tilde{\rho}^{A}]}{\partial P_{\mu\nu}} = \sum_{\mathring{k}\in A} \langle \mu\nu \| \mathring{k}^{A} \rangle z^{A}_{\mathring{k}}; \quad z^{A}_{\mathring{k}} = \sum_{\mathring{l}\in A} G^{\overline{A}^{-1}}_{\mathring{k}\mathring{l}} \langle \mathring{l}^{A} | v^{A}_{xc}[\tilde{\rho}^{A}] \rangle \tag{3.59}$$

Therefore, also for the exchange-correlation coefficients only the totally symmetric equation system,

$$\mathbf{G}^{A}\mathbf{z}^{A} = \mathbf{L}^{A} \tag{3.60}$$

has to be solved.

Figure 3.2 depicts the symmetry-adapted Coulomb matrices of benzene in D_{6h} symmetry (top) and dodecahedrane in I_h symmetry (bottom) employing the GEN-A2 and GEN-A2* auxiliary function sets for benzene and dodecahedrane, respectively. The first block, indicated by the red circle, corresponds to the totally symmetric irreducible representation. In the case of benzene, the dimension of this block is 28×28 whereas the dimension of the full Coulomb matrix is 288×288. In the case of dodecahedrane, its dimension is 43×43 whereas the dimension of the full Coulomb matrix is 2300×2300. This demonstrates the enormous reduction in the dimensionality of the fitting equation systems if totally symmetric auxiliary densities are used [88].

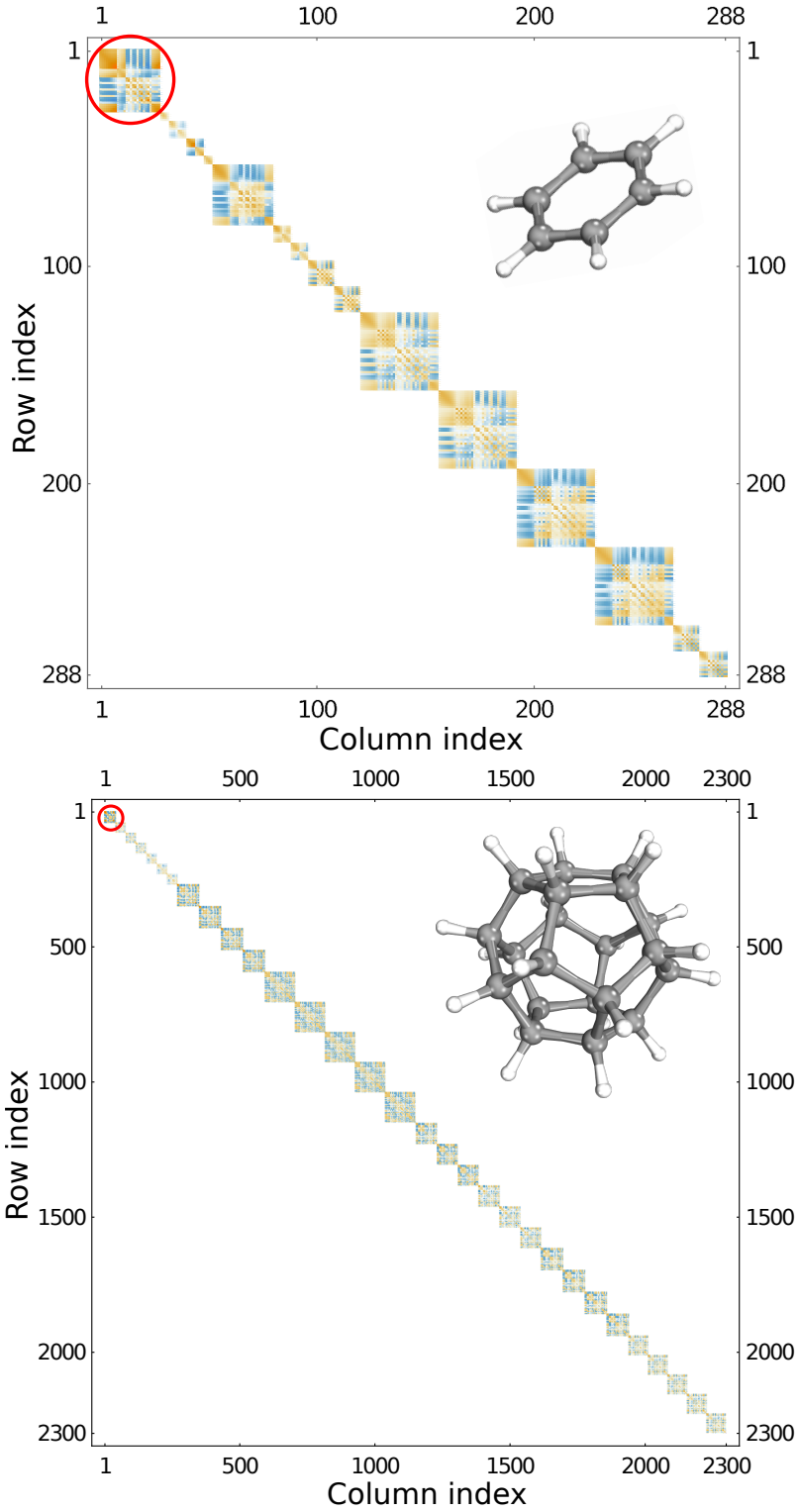

Figure 3.2: Symmetry-adapted Coulomb matrices of benzene in D_{6h} symmetry, top, and dodecahedrane in I_h symmetry, bottom. The first blocks, marked by red circles, belong to the totally symmetric irreducible representations. The color code indicates positive (towards red) and negative (towards blue) values.

3.5 Symmetry-adapted fitting implementation

We now describe the implementation of the symmetry-adapted calculation of Coulomb and exchange-correlation fitting coefficients as implemented in deMon2k. Instead of calculating the Coulomb matrix in auxiliary function representation $\mathbf{G}$, the blocks of the symmetry-adapted representation $\{\mathbf{G}^{\Gamma(1)}\}$ are calculated. For point groups with real multi-dimensional irreducible representations the degenerate blocks are copied from the first degenerate block, i.e. $\mathbf{G}^{\Gamma(\gamma)} \leftarrow \mathbf{G}^{\Gamma(1)}$. Note, however, that for the two-dimensional minimal representations the corresponding Coulomb matrix blocks are given by $\mathbf{G}^{\Gamma} = \mathbf{U}^{\Gamma\,\mathsf{T}}\mathbf{G}\mathbf{U}^{\Gamma}$ with the symmetrization matrix built as $\mathbf{U}^{\Gamma} = (\mathbf{U}^{\Gamma(1)}|\mathbf{U}^{\Gamma(2)})$. Also, note that the Coulomb matrix in the original auxiliary function representation $\mathbf{G}$ is normalized, i.e. the auxiliary functions are normalized with respect to the Coulomb norm. On the other hand, the Coulomb matrix in symmetry representation $\mathbb{G} = \bigoplus_{\Gamma(\gamma)} \mathbf{G}^{\Gamma(\gamma)}$ is not normalized since the symmetry-adapted auxiliary functions are not normalized. Therefore, the symmetry-adapted coefficients are expressing the auxiliary density in an unnormalized symmetry-adapted auxiliary function basis. Nevertheless, by the back-transformation, Eq. (3.51), the fitting coefficients in the original normalized auxiliary function basis are obtained in terms of the symmetrization matrix $\mathbf{U}$ and the symmetry-adapted fitting coefficients.

After building the symmetry-adapted Coulomb matrix blocks $\{\mathbf{G}^{\Gamma(1)}\}$, they are inverted and stored on tape. These blocks are used to solve equation system Eq. (3.50) for the symmetry-adapted Coulomb fitting coefficients in DF-DFT and ADFT calculations. In case of ADFT, they are also used to solve the equation system Eq. (3.52) for the symmetry-adapted exchange-correlation fitting coefficients. Scheme 3.1 depicts the pseudocode for the symmetry-adapted calculation and inversion of the Coulomb matrix.

Thus, the central quantity needed for the symmetry-adapted calculation of the Coulomb and exchange-correlation coefficients is the symmetrization matrix $\mathbf{U}$. At this point, it is important to note that the $\mathbf{U}$ symmetrization matrix for AOs and auxiliary functions

```
for Γ do
    for γ = 1, d_Γ do
        if γ = 1 then
            Build G^Γ(γ)
            Invert G^Γ(γ)
        else
            Copy G^Γ(γ)^-1 ← G^Γ(1)^-1
        end if
        Store G^Γ(γ)^-1
        if Only A_1 then
            Finish
        end if
    end for
end for
```

Scheme 3.1: Pseudocode for the inversion by blocks of the Coulomb matrix.

is identical if the same function type is used. Particularly important for the here presented implementation is that the same $\mathbf{U}$ symmetrization matrix can be used for Cartesian AOs, in form of contracted Gaussian type orbitals, and (primitive) Hermite Gaussian auxiliary functions. The details of the construction of the $\mathbf{U}$ symmetrization matrices are given in the next chapter.

4

CONSTRUCTION OF SYMMETRIZATION MATRICES

The central quantity needed for the symmetry-adapted calculation of the MO coefficients as well as the Coulomb and exchange-correlation coefficients is the symmetrization matrix $\mathbf{U}_{\text{bas}}$ for the basis functions and the symmetrization matrix $\mathbf{U}_{\text{aux}}$ for the auxiliary functions. It turns out that the symmetrization matrices for Hermite Gaussian auxiliary functions are identical to those for Cartesian Gaussian basis functions because Hermite polynomials transform under rotations in the same way as Cartesian monomials $x^p y^q z^r$ [89]. Because the symmetry adaptation of auxiliary functions has so far not been described in the literature, we use here the construction of the symmetrization matrix $\mathbf{U}_{\text{aux}}$ for auxiliary functions as a working example.

4.1 Construction of the U matrix for auxiliary functions

We start our description of the construction of the $\mathbf{U}$ symmetrization matrix for auxiliary (and Cartesian basis) functions with the definition of the primitive Hermite Gaussian auxiliary functions used in deMon2k. Such an (unnormalized) auxiliary function with exponent $\zeta_{\bar{k}}$ centered at atom K is given by:

$$\bar{k}(\mathbf{r};\zeta_{\bar{k}},\mathbf{K},\bar{\mathbf{k}}) = \left(\frac{\partial}{\partial K_x}\right)^{\bar{k}_x}\left(\frac{\partial}{\partial K_y}\right)^{\bar{k}_y}\left(\frac{\partial}{\partial K_z}\right)^{\bar{k}_z} e^{-\zeta_{\bar{k}}(\mathbf{r}-\mathbf{K})^2} \tag{4.1}$$

Here $\bar{\mathbf{k}} = (\bar{k}_x, \bar{k}_y, \bar{k}_z)$ is the angular momentum index of the auxiliary function with total angular momentum $\bar{k} = \bar{k}_x + \bar{k}_y + \bar{k}_z$. For the sake of simplicity in the following descriptions, we restrict ourselves to a particular set of auxiliary functions that is closed under symmetry operations. We call it an invariant [74]. From a technical point of view,

it is convenient to construct the **U** matrix in terms of a symmetrization matrix **V** for symmetry equivalent atoms and a symmetrization matrix **W** for (auxiliary) functions centered at the global origin.

To proceed, we first describe the construction of the symmetrization matrix **V**. As an example, we take the invariant consisting of the auxiliary functions at the three hydrogen atoms of ammonia in C_{3v} symmetry (see Scheme 4.1 and 4.2). The hydrogen atoms define our symmetry-equivalent atom set. We define the corresponding atomic permutation vectors $\mathbf{p}_A$, $\mathbf{p}_B$ and $\mathbf{p}_C$ as:

$$\mathbf{p}_A = \begin{pmatrix} 1 \\ 0 \\ 0 \end{pmatrix}, \qquad \mathbf{p}_B = \begin{pmatrix} 0 \\ 1 \\ 0 \end{pmatrix}, \qquad \mathbf{p}_C = \begin{pmatrix} 0 \\ 0 \\ 1 \end{pmatrix} \tag{4.2}$$

Scheme 4.1 and 4.2 show the construction of the atomic permutation matrices for the C_{3v} symmetry operations. Technically, these matrices can be built during the symmetry analysis of a molecule which yields its point group. The atomic permutation matrices express symmetry operations, $\hat{R}$, on the atomic permutation vectors given by Eq. (4.2).

$$\hat{R}\,\mathbf{p}_A \rightarrow \mathbf{P}(\hat{R})\mathbf{p}_A \tag{4.3}$$

With these assignment rules, we can now apply projection operators of real irreducible representations, Γ, here for the C_{3v} point group with $\Gamma = A_1, A_2, E$,

$$\begin{aligned}\hat{P}^{\Gamma}_{\gamma\gamma'} = \frac{d_\Gamma}{6}\Big(&\chi^{\Gamma}_{\gamma\gamma'}(\hat{E})\hat{E} + \chi^{\Gamma}_{\gamma\gamma'}(\hat{C}_3)\hat{C}_3 + \chi^{\Gamma}_{\gamma\gamma'}(\hat{C}_3^2)\hat{C}_3^2 + \\ &\chi^{\Gamma}_{\gamma\gamma'}(\hat{\sigma}_v)\hat{\sigma}_v + \chi^{\Gamma}_{\gamma\gamma'}(\hat{\sigma}'_v)\hat{\sigma}'_v + \chi^{\Gamma}_{\gamma\gamma'}(\hat{\sigma}''_v)\hat{\sigma}''_v\Big)\end{aligned} \tag{4.4}$$

as

$$\begin{aligned}\mathbf{P}^{\Gamma}_{\gamma\gamma'} = \frac{d_\Gamma}{6}\Big(&\chi^{\Gamma}_{\gamma\gamma'}(\hat{E})\mathbf{P}(\hat{E}) + \chi^{\Gamma}_{\gamma\gamma'}(\hat{C}_3)\mathbf{P}(\hat{C}_3) + \chi^{\Gamma}_{\gamma\gamma'}(\hat{C}_3^2)\mathbf{P}(\hat{C}_3^2) + \\ &\chi^{\Gamma}_{\gamma\gamma'}(\hat{\sigma}_v)\mathbf{P}(\hat{\sigma}_v) + \chi^{\Gamma}_{\gamma\gamma'}(\hat{\sigma}'_v)\mathbf{P}(\hat{\sigma}'_v) + \chi^{\Gamma}_{\gamma\gamma'}(\hat{\sigma}''_v)\mathbf{P}(\hat{\sigma}''_v)\Big)\end{aligned} \tag{4.5}$$

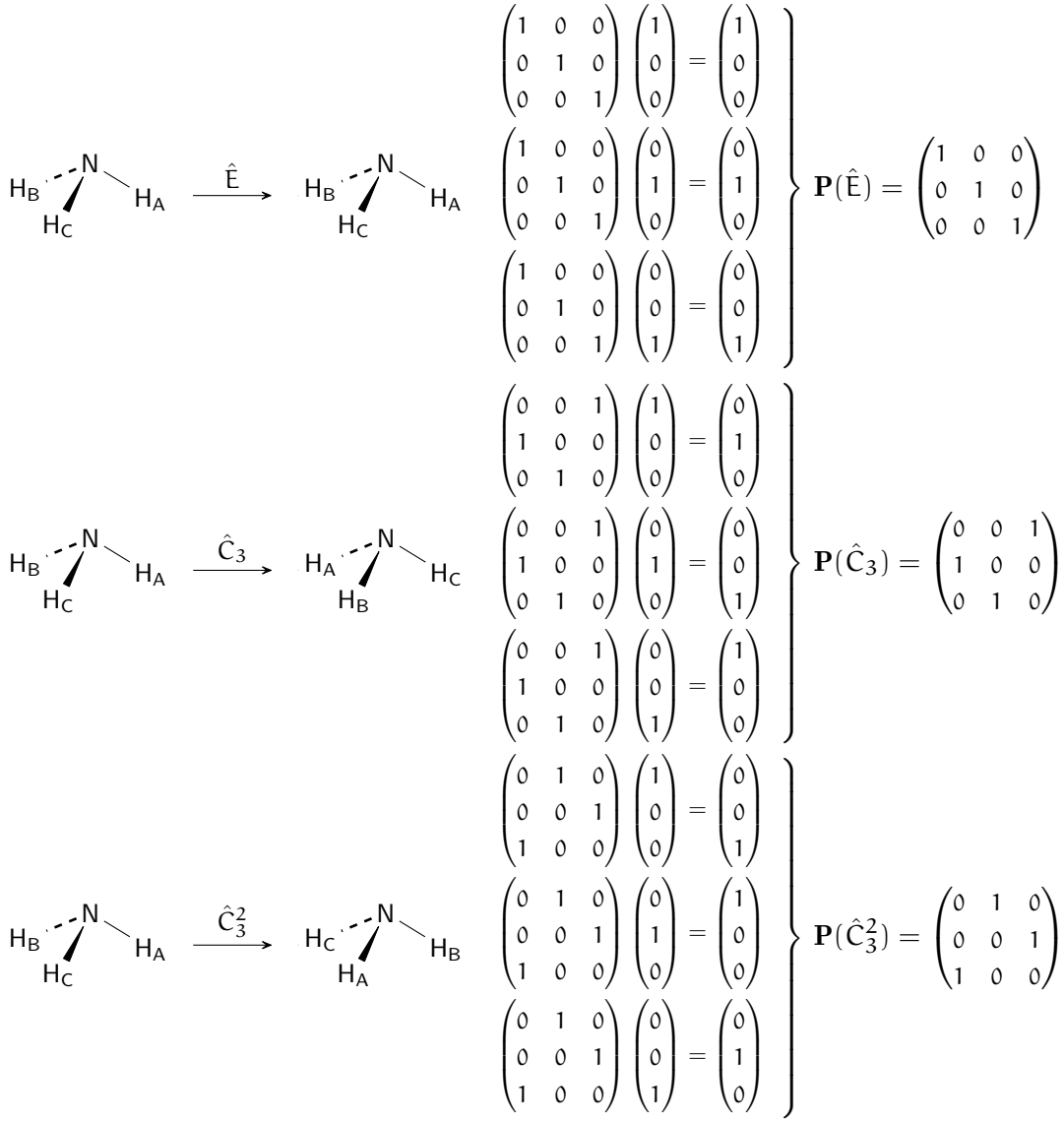

Scheme 4.1: Construction of atomic permutation matrices for the equivalent hydrogen atoms of ammonia in C_{3v} symmetry corresponding to the symmetry operations $\hat{E}$, $\hat{C}_3$ and $\hat{C}_3^2$. The rotations are right handed.

To further simplify these expressions we use the convention $\gamma' = 1$ for the operator $\mathbf{P}^{\Gamma}_{\gamma\gamma'}$ in our symmetry implementation in deMon2k. Therefore, we can drop the γ' index for the projection operators and irreducible representation matrix elements by defining:

$$\mathbf{P}^{\Gamma}_{\gamma} \equiv \mathbf{P}^{\Gamma}_{\gamma 1}; \quad \chi^{\Gamma}_{\gamma}(\hat{R}) \equiv \chi^{\Gamma}_{\gamma 1}(\hat{R}) \tag{4.6}$$

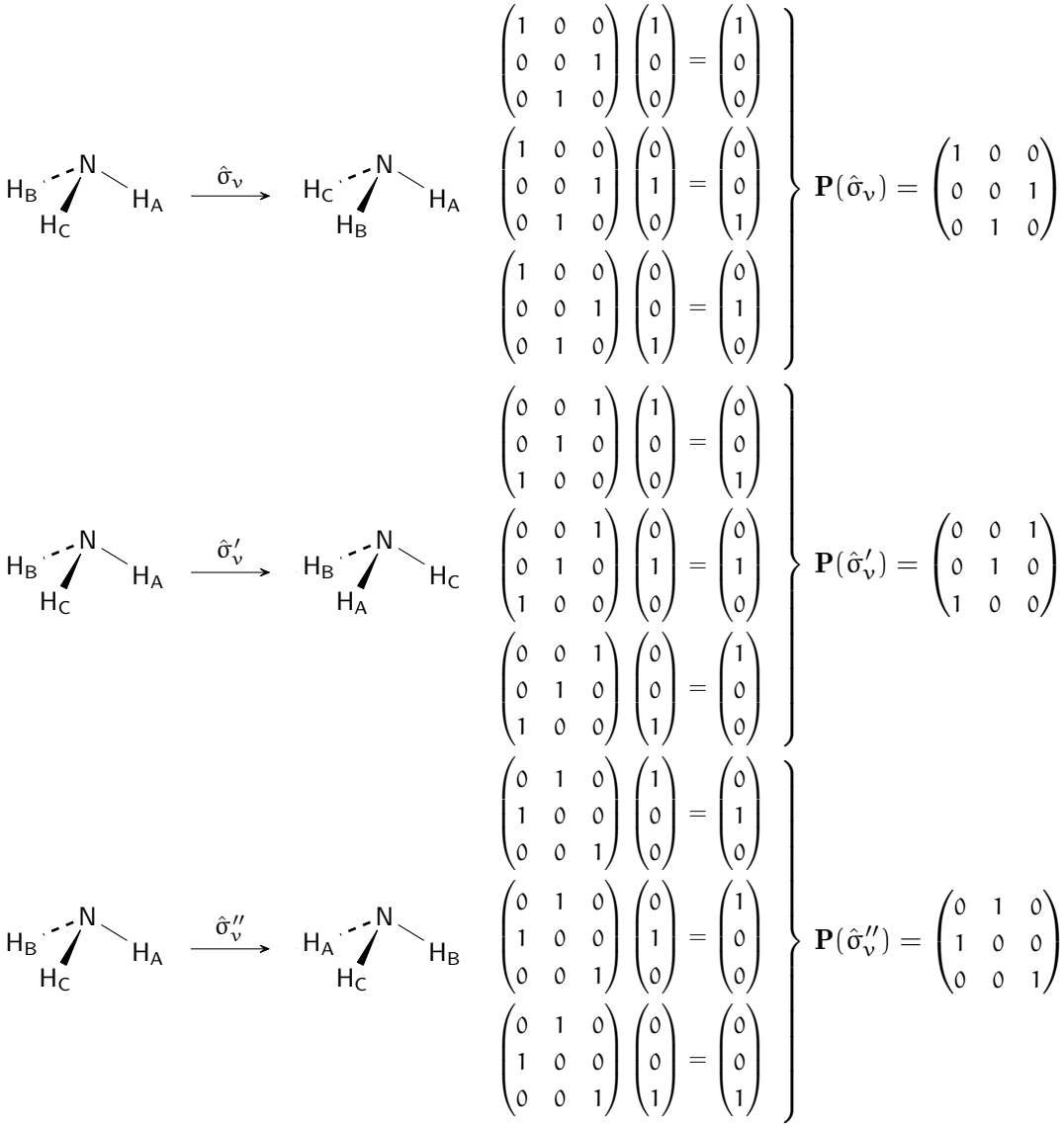

Scheme 4.2: Construction of atomic permutation matrices for the equivalent hydrogen atoms of ammonia in C_{3v} symmetry corresponding to the reflections.

The application of $\mathbf{P}^{\Gamma}_{\gamma}$, Eq. (4.5), on the atomic permutation vectors yields matrix vector products. Thus, the (unnormalized) symmetry-adapted permutation vectors are obtained as:

$$\begin{aligned}\mathbf{p}_K^{\Gamma(\gamma)} \equiv \mathbf{P}^{\Gamma}_{\gamma}\mathbf{p}_K = &\frac{d_\Gamma}{6}\chi^{\Gamma}_{\gamma}(\hat{E})\mathbf{P}(\hat{E})\mathbf{p}_K + \frac{d_\Gamma}{6}\chi^{\Gamma}_{\gamma}(\hat{C}_3)\mathbf{P}(\hat{C}_2)\mathbf{p}_K + \frac{d_\Gamma}{6}\chi^{\Gamma}_{\gamma}(\hat{C}_3^2)\mathbf{P}(\hat{C}_2)\mathbf{p}_K + \\ &\frac{d_\Gamma}{6}\chi^{\Gamma}_{\gamma}(\hat{\sigma}_\nu)\mathbf{P}(\hat{\sigma}_\nu)\mathbf{p}_K + \frac{d_\Gamma}{6}\chi^{\Gamma}_{\gamma}(\hat{\sigma}'_\nu)\mathbf{P}(\hat{\sigma}'_\nu)\mathbf{p}_K + \frac{d_\Gamma}{6}\chi^{\Gamma}_{\gamma}(\hat{\sigma}''_\nu)\mathbf{P}(\hat{\sigma}''_\nu)\mathbf{p}_K\end{aligned} \tag{4.7}$$

C_{3v}	$\hat{E}$	$\hat{C}_3$	$\hat{C}_3^2$	$\hat{\sigma}_v$	$\hat{\sigma}_v'$	$\hat{\sigma}_v''$
A_1	1	1	1	1	1	1
A_2	1	1	1	−1	−1	−1
E	$\begin{pmatrix} 1 & 0 \\ 0 & 1 \end{pmatrix}$	$\begin{pmatrix} -c & -s \\ s & -c \end{pmatrix}$	$\begin{pmatrix} -c & s \\ -s & -c \end{pmatrix}$	$\begin{pmatrix} 1 & 0 \\ 0 & -1 \end{pmatrix}$	$\begin{pmatrix} -c & -s \\ -s & c \end{pmatrix}$	$\begin{pmatrix} -c & s \\ s & c \end{pmatrix}$

$c = 1/2; \quad s = \sqrt{3}/2$

Table 4.1: C_{3v} point group table.

In Eq. (4.7) K denotes any atomic center on which the auxiliary functions of the invariant are centered. We perform these projections until we have found as many non-vanishing linear independent symmetry-adapted permutation vectors as initial atomic permutation vectors were used. Thus, in the case of our ammonia example for the equivalent hydrogen atoms, three linear independent symmetry-adapted permutation vectors are searched. The number of linear independent symmetry-adapted atomic permutation vectors can also be directly obtained from the character formula for the reduction of representations [76, 90, 91]. It is defined as follows for our ammonia example in C_{3v} point group:

$$\begin{aligned} a^{\Gamma} = \frac{1}{6}\Big(&\chi^{\Gamma}(\hat{E})\chi(\hat{E}) + \chi^{\Gamma}(\hat{C}_3)\chi(\hat{C}_3) + \chi^{\Gamma}(\hat{C}_3^2)\chi(\hat{C}_3^2) + \\ &\chi^{\Gamma}(\hat{\sigma}_v)\chi(\hat{\sigma}_v) + \chi^{\Gamma}(\hat{\sigma}_v')\chi(\hat{\sigma}_v') + \chi^{\Gamma}(\hat{\sigma}_v'')\chi(\hat{\sigma}_v'')\Big) \end{aligned} \tag{4.8}$$

In Eq. (4.8) $\chi^{\Gamma}(\hat{R})$ denote the characters of the irreducible representations. They can be obtained from the point group tables now available in deMon2k. Table 4.1 shows this table for the here discussed C_{3v} example. For one-dimensional irreducible representations, the character is simply the corresponding entry in the point group table. For multidimensional irreducible representations, it is given by the trace of the irreducible representation matrices. On the other hand, the characters of the reducible representations $\chi(\hat{E})$, $\chi(\hat{C}_3)$ and so on in Eq (4.8) are given by the traces of the corresponding permutation matrices, listed in Scheme 4.1 and 4.2. Thus, we find for $\chi(\hat{R}) = \mathrm{tr}(\mathbf{P}(\hat{R}))$:

$$\chi(\hat{E}) = 3,\ \chi(\hat{C}_3) = 0,\ \chi(\hat{C}_3^2) = 0,\ \chi(\hat{\sigma}_v) = 1,\ \chi(\hat{\sigma}_v') = 1,\ \chi(\hat{\sigma}_v'') = 1 \tag{4.9}$$

- $\Gamma = A_1; \gamma = 1; \chi^{A_1}(\hat{E}) = 1, \chi^{A_1}(\hat{C}_3) = 1, \chi^{A_1}(\hat{C}_3^2) = 1, \chi^{A_1}(\hat{\sigma}_v) = 1, \chi^{A_1}(\hat{\sigma}_v') = 1, \chi^{A_1}(\hat{\sigma}_v'') = 1; \mathbf{p}_A^{A_1} \equiv \mathbf{P}^{A_1}\mathbf{p}_A$

$$\mathbf{p}_A^{A_1} = \frac{1}{6}\,1\begin{pmatrix}1&0&0\\0&1&0\\0&0&1\end{pmatrix}\begin{pmatrix}1\\0\\0\end{pmatrix} + \frac{1}{6}\,1\begin{pmatrix}0&0&1\\1&0&0\\0&1&0\end{pmatrix}\begin{pmatrix}1\\0\\0\end{pmatrix} + \frac{1}{6}\,1\begin{pmatrix}0&1&0\\0&0&1\\1&0&0\end{pmatrix}\begin{pmatrix}1\\0\\0\end{pmatrix} +$$
$$\frac{1}{6}\,1\begin{pmatrix}1&0&0\\0&0&1\\0&1&0\end{pmatrix}\begin{pmatrix}1\\0\\0\end{pmatrix} + \frac{1}{6}\,1\begin{pmatrix}0&0&1\\0&1&0\\1&0&0\end{pmatrix}\begin{pmatrix}1\\0\\0\end{pmatrix} + \frac{1}{6}\,1\begin{pmatrix}0&1&0\\1&0&0\\0&0&1\end{pmatrix}\begin{pmatrix}1\\0\\0\end{pmatrix}$$
$$= \frac{1}{6}\left[\begin{pmatrix}1\\0\\0\end{pmatrix} + \begin{pmatrix}0\\1\\0\end{pmatrix} + \begin{pmatrix}0\\0\\1\end{pmatrix} + \begin{pmatrix}1\\0\\0\end{pmatrix} + \begin{pmatrix}0\\0\\1\end{pmatrix} + \begin{pmatrix}0\\1\\0\end{pmatrix}\right] = \begin{pmatrix}1/3\\1/3\\1/3\end{pmatrix}$$

store; enough for A_1; next projection in E

- $\Gamma = E; \gamma = 1; \chi_1^E(\hat{E}) = 1, \chi_1^E(\hat{C}_3) = -\frac{1}{2}, \chi_1^E(\hat{C}_3^2) = -\frac{1}{2}, \chi_1^E(\hat{\sigma}_v) = 1, \chi_1^E(\hat{\sigma}_v') = -\frac{1}{2}, \chi_1^E(\hat{\sigma}_v'') = -\frac{1}{2}; \mathbf{p}_A^{E(1)} \equiv \mathbf{P}_1^E\mathbf{p}_A$

$$\mathbf{p}_A^{E(1)} = \tfrac{2}{6}\,1\begin{pmatrix}1&0&0\\0&1&0\\0&0&1\end{pmatrix}\begin{pmatrix}1\\0\\0\end{pmatrix} + \tfrac{2}{6}\,\left(-\tfrac{1}{2}\right)\begin{pmatrix}0&0&1\\1&0&0\\0&1&0\end{pmatrix}\begin{pmatrix}1\\0\\0\end{pmatrix} + \tfrac{2}{6}\,\left(-\tfrac{1}{2}\right)\begin{pmatrix}0&1&0\\0&0&1\\1&0&0\end{pmatrix}\begin{pmatrix}1\\0\\0\end{pmatrix} +$$
$$\tfrac{2}{6}\,1\begin{pmatrix}1&0&0\\0&0&1\\0&1&0\end{pmatrix}\begin{pmatrix}1\\0\\0\end{pmatrix} + \tfrac{2}{6}\,\left(-\tfrac{1}{2}\right)\begin{pmatrix}0&0&1\\0&1&0\\1&0&0\end{pmatrix}\begin{pmatrix}1\\0\\0\end{pmatrix} + \tfrac{2}{6}\,\left(-\tfrac{1}{2}\right)\begin{pmatrix}0&1&0\\1&0&0\\0&0&1\end{pmatrix}\begin{pmatrix}1\\0\\0\end{pmatrix}$$
$$= \tfrac{2}{6}\left[\begin{pmatrix}1\\0\\0\end{pmatrix} - \tfrac{1}{2}\begin{pmatrix}0\\1\\0\end{pmatrix} - \tfrac{1}{2}\begin{pmatrix}0\\0\\1\end{pmatrix} + \begin{pmatrix}1\\0\\0\end{pmatrix} - \tfrac{1}{2}\begin{pmatrix}0\\0\\1\end{pmatrix} - \tfrac{1}{2}\begin{pmatrix}0\\1\\0\end{pmatrix}\right] = \begin{pmatrix}2/3\\-1/3\\-1/3\end{pmatrix}$$

store; find partner increasing γ

- $\Gamma = E; \gamma = 2; \chi_2^E(\hat{E}) = 0, \chi_2^E(\hat{C}_3) = \frac{\sqrt{3}}{2}, \chi_2^E(\hat{C}_3^2) = -\frac{\sqrt{3}}{2}, \chi_2^E(\hat{\sigma}_v) = 0, \chi_2^E(\hat{\sigma}_v') = -\frac{\sqrt{3}}{2}, \chi_2^E(\hat{\sigma}_v'') = \frac{\sqrt{3}}{2}; \mathbf{p}_A^{E(2)} \equiv \mathbf{P}_2^E\mathbf{p}_A$

$$\mathbf{p}_A^{E(2)} = \tfrac{2}{6}\,0\begin{pmatrix}1&0&0\\0&1&0\\0&0&1\end{pmatrix}\begin{pmatrix}1\\0\\0\end{pmatrix} + \tfrac{2}{6}\,\left(\tfrac{\sqrt{3}}{2}\right)\begin{pmatrix}0&0&1\\1&0&0\\0&1&0\end{pmatrix}\begin{pmatrix}1\\0\\0\end{pmatrix} + \tfrac{2}{6}\,\left(-\tfrac{\sqrt{3}}{2}\right)\begin{pmatrix}0&1&0\\0&0&1\\1&0&0\end{pmatrix}\begin{pmatrix}1\\0\\0\end{pmatrix} +$$
$$\tfrac{2}{6}\,0\begin{pmatrix}1&0&0\\0&0&1\\0&1&0\end{pmatrix}\begin{pmatrix}1\\0\\0\end{pmatrix} + \tfrac{2}{6}\,\left(-\tfrac{\sqrt{3}}{2}\right)\begin{pmatrix}0&0&1\\0&1&0\\1&0&0\end{pmatrix}\begin{pmatrix}1\\0\\0\end{pmatrix} + \tfrac{2}{6}\,\left(-\tfrac{\sqrt{3}}{2}\right)\begin{pmatrix}0&1&0\\1&0&0\\0&0&1\end{pmatrix}\begin{pmatrix}1\\0\\0\end{pmatrix}$$
$$= \tfrac{2}{6}\left[\tfrac{\sqrt{3}}{2}\begin{pmatrix}0\\1\\0\end{pmatrix} - \tfrac{\sqrt{3}}{2}\begin{pmatrix}0\\0\\1\end{pmatrix} - \tfrac{\sqrt{3}}{2}\begin{pmatrix}0\\0\\1\end{pmatrix} + \tfrac{\sqrt{3}}{2}\begin{pmatrix}0\\1\\0\end{pmatrix}\right] = \begin{pmatrix}0\\1/\sqrt{3}\\-1/\sqrt{3}\end{pmatrix}$$

store; all symmetry vectors found; finish

Scheme 4.3: Construction of symmetry-adapted permutation vectors for the equivalent hydrogen atoms of ammonia in C_{3v} symmetry.

Performing the resulting calculations according to Eq. (4.8) we obtain as only non-vanishing expansion coefficients for the irreducible representations $a^{A_1} = 1$, and $a^{E} = 1$. Considering that the irreducible representation E is two-dimensional, we must obtain in total three symmetry-adapted vectors, one belonging to A_1 and two belonging to E. Their construction according to the here outlined algorithm is depicted in Scheme 4.3. As this scheme shows, the three symmetry-adapted permutation vectors are $\mathbf{p}_A^{A_1}$ and the two $\mathbf{p}_A^{E}$ vectors.

In general, the (unnormalized) symmetry-adapted permutation vectors for a symmetry-equivalent atom set using real irreducible representations are obtained as:

$$\mathbf{p}_K^{\Gamma(\gamma)} = \frac{d_\Gamma}{h} \sum_{\hat{R}} \chi_\gamma^\Gamma(\hat{R}) \mathbf{P}(\hat{R}) \mathbf{p}_K \tag{4.10}$$

In Eq. (4.10) h denotes the order of the point group and $\mathbf{p}_K$ an atomic permutation vector from the symmetry-equivalent atom set of the invariant under consideration. The general form of the reduction formula is given by:

$$a^\Gamma = \frac{1}{h} \sum_R \chi^\Gamma(\hat{R}) \chi(\hat{R}) \tag{4.11}$$

The symmetry-adapted permutation vectors are stored in the $\mathbf{V}$ matrix as:

$$\mathbf{V} = \left(\mathbf{V}^{\Gamma(1)} \mid \mathbf{V}^{\Gamma(2)} \mid \ldots \mid \mathbf{V}^{\Gamma'(1)} \mid \mathbf{V}^{\Gamma'(2)} \mid \ldots \right) \tag{4.12}$$

$$\text{with} \quad \mathbf{V}^{\Gamma(\gamma)} = \left(\mathbf{p}_A^{\Gamma(\gamma)} \mid \mathbf{p}_B^{\Gamma(\gamma)} \mid \ldots \right) \tag{4.13}$$

In Eq. (4.12) Γ and Γ' are different irreducible representations of the point group under consideration.

After the symmetry-adapted atomic permutation vectors are calculated, we now turn to the construction of the symmetrization matrix $\mathbf{W}$ for the auxiliary functions. To this end, we assume (auxiliary) functions that are centered at the global origin. Take as

example the Hermite Gaussian d-type set of functions $\{\bar{d}_{xx}, \bar{d}_{xy}, \bar{d}_{xz}, \bar{d}_{yy}, \bar{d}_{yz}, \bar{d}_{zz}\}$. To proceed, we express the (auxiliary) function vectors $\{\mathbf{d_{xx}}, \mathbf{d_{xy}}, \mathbf{d_{xz}}, \mathbf{d_{yy}}, \mathbf{d_{yz}}, \mathbf{d_{zz}}\}$ as:

$$\mathbf{d_{xx}} = \begin{pmatrix}1\\0\\0\\0\\0\\0\end{pmatrix}, \mathbf{d_{xy}} = \begin{pmatrix}0\\1\\0\\0\\0\\0\end{pmatrix}, \mathbf{d_{xz}} = \begin{pmatrix}0\\0\\1\\0\\0\\0\end{pmatrix}, \mathbf{d_{yy}} = \begin{pmatrix}0\\0\\0\\1\\0\\0\end{pmatrix}, \mathbf{d_{yz}} = \begin{pmatrix}0\\0\\0\\0\\1\\0\end{pmatrix}, \mathbf{d_{zz}} = \begin{pmatrix}0\\0\\0\\0\\0\\1\end{pmatrix} \tag{4.14}$$

The auxiliary function transformations are depicted in Figure 4.1. For convenience of presentation, some symmetry operators are multiplied with a negative phase factor. The corresponding (auxiliary) function symmetrization matrices, $\mathbf{F}(\hat{R})$, are:

$$\begin{aligned}
\mathbf{F}(\hat{E}) &= \begin{pmatrix}1&0&0&0&0&0\\0&1&0&0&0&0\\0&0&1&0&0&0\\0&0&0&1&0&0\\0&0&0&0&1&0\\0&0&0&0&0&1\end{pmatrix}, \mathbf{F}(\hat{C}_3) = \begin{pmatrix}\frac{1}{4}&\frac{3}{4}&0&\frac{3}{4}&0&0\\-\frac{1}{2}&-\frac{1}{2}&0&\frac{1}{2}&0&0\\0&0&-\frac{1}{2}&0&-\frac{\sqrt{3}}{2}&0\\\frac{3}{4}&-\frac{3}{4}&0&\frac{1}{4}&0&0\\0&0&\frac{\sqrt{3}}{2}&0&-\frac{1}{2}&0\\0&0&0&0&0&1\end{pmatrix},\\
\mathbf{F}(\hat{C}_3^2) &= \begin{pmatrix}\frac{1}{4}&-\frac{3}{4}&0&\frac{3}{4}&0&0\\\frac{1}{2}&-\frac{1}{2}&0&-\frac{1}{2}&0&0\\0&0&-\frac{1}{2}&0&\frac{\sqrt{3}}{2}&0\\\frac{3}{4}&\frac{3}{4}&0&\frac{1}{4}&0&0\\0&0&-\frac{\sqrt{3}}{2}&0&-\frac{1}{2}&0\\0&0&0&0&0&1\end{pmatrix}, \mathbf{F}(\hat{\sigma}_v) = \begin{pmatrix}1&0&0&0&0&0\\0&-1&0&0&0&0\\0&0&1&0&0&0\\0&0&0&1&0&0\\0&0&0&0&-1&0\\0&0&0&0&0&1\end{pmatrix},\\
\mathbf{F}(\hat{\sigma}_v') &= \begin{pmatrix}\frac{1}{4}&\frac{3}{4}&0&\frac{3}{4}&0&0\\\frac{1}{2}&\frac{1}{2}&0&-\frac{1}{2}&0&0\\0&0&-\frac{1}{2}&0&-\frac{\sqrt{3}}{2}&0\\\frac{3}{4}&-\frac{3}{4}&0&\frac{1}{4}&0&0\\0&0&-\frac{\sqrt{3}}{2}&0&\frac{1}{2}&0\\0&0&0&0&0&1\end{pmatrix}, \mathbf{F}(\hat{\sigma}_v'') = \begin{pmatrix}\frac{1}{4}&-\frac{3}{4}&0&\frac{3}{4}&0&0\\-\frac{1}{2}&\frac{1}{2}&0&\frac{1}{2}&0&0\\0&0&-\frac{1}{2}&0&\frac{\sqrt{3}}{2}&0\\\frac{3}{4}&\frac{3}{4}&0&\frac{1}{4}&0&0\\0&0&\frac{\sqrt{3}}{2}&0&\frac{1}{2}&0\\0&0&0&0&0&1\end{pmatrix}
\end{aligned} \tag{4.15}$$

With these matrices the symmetry operations on the d-type Hermite Gaussian auxiliary functions are represented by matrix vector products according to:

$$\hat{R}\,\mathbf{d_\kappa} \rightarrow \mathbf{F}(\hat{R})\mathbf{d_\kappa} \tag{4.16}$$

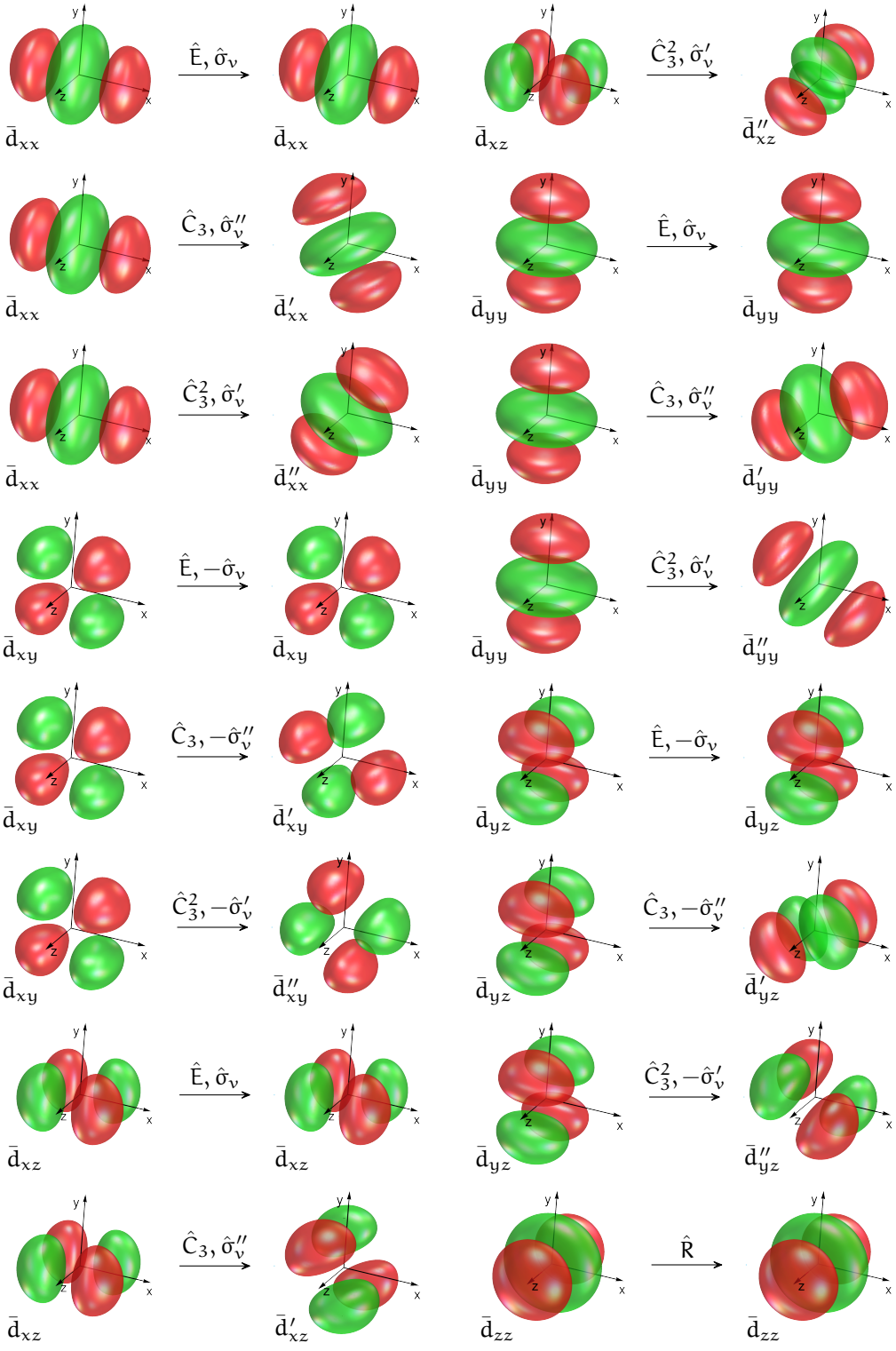

Figure 4.1: Transformation of d-type auxiliary functions under C_{3v} symmetry operations. The symbol $\hat{R}$ indicates any of the symmetry operations in the point group. The rotations $\hat{C}_3$ and $\hat{C}_3^2$ are right handed around the z axis. The mirror planes are $\sigma_v(xz) = \sigma_v(\perp \mathbf{y})$, $\sigma'_v(\perp \hat{C}_3\mathbf{y})$ and $\sigma''_v(\perp \hat{C}_3^2\mathbf{y})$.

Here $\mathbf{d}$ refers to the total angular momentum of the (auxiliary) function shell and $\boldsymbol{\kappa}$ is a specific angular momentum index, i.e. $\mathbf{xx} = (2,0,0)$, $\mathbf{xy} = (1,1,0)$ and so on. The elements of the symmetrization matrix $\mathbf{F}(\hat{R})$ for the function vectors of an (auxiliary) function shell are given by the formula:

$$F_{\kappa\lambda}(\hat{R}) = N_{\kappa\lambda} \sum_{a=0}^{\lambda_x} \sum_{b=0}^{a} \sum_{c=0}^{\lambda_y} \sum_{d=0}^{c} D(a,b,c,d)\ B_{abcd}\ S_{abcd}(\hat{R}) \tag{4.17}$$

In Eq. (4.17) κ and λ refer to (auxiliary) functions in the shell under consideration with corresponding angular momentum indices $\boldsymbol{\kappa} = (\kappa_x, \kappa_y, \kappa_z)$ and $\boldsymbol{\lambda} = (\lambda_x, \lambda_y, \lambda_z)$. The normalization constant in Eq. (4.17) is given as:

$$N_{\kappa\lambda} = \sqrt{\frac{(2\kappa_x - 1)!!(2\kappa_y - 1)!!(2\kappa_z - 1)!!}{(2\lambda_x - 1)!!(2\lambda_y - 1)!!(2\lambda_z - 1)!!}} \tag{4.18}$$

The $D(a,b,c,d)$ play the role of a Kronecker delta for sum terms according to:

$$D(a,b,c,d) = \begin{cases} 1 & 0 \leqslant \kappa_y + \kappa_z - a - c \leqslant \lambda_z \ \wedge\ 0 \leqslant \kappa_z - b - d \leqslant \kappa_y + \kappa_z - a - c \\ 0 & \text{else} \end{cases} \tag{4.19}$$

The other factors in Eq. (4.17) are products of binomial coefficients,

$$B_{abcd} = \binom{\lambda_x}{a}\binom{a}{b}\binom{\lambda_y}{c}\binom{c}{d}\binom{\lambda_z}{\kappa_y + \kappa_z - a - c}\binom{\kappa_y + \kappa_z - a - c}{\kappa_z - b - d} \tag{4.20}$$

and of the three-dimensional Cartesian representation matrices of the symmetry operation $\hat{R}$:

$$S_{abcd}(\hat{R}) = R_{11}^{\lambda_x - a} R_{12}^{\lambda_y - c} R_{13}^{a+c-\kappa_y-\kappa_z+\lambda_z} R_{21}^{a-b} R_{22}^{c-d} R_{23}^{-a+b-c+d+\kappa_y} R_{31}^{b} R_{32}^{d} R_{33}^{-b-d+\kappa_z} \tag{4.21}$$

Note that Eqs. (4.17) to (4.21) are valid for arbitrary angular momentum indices. For the C_{3v} example the three-dimensional Cartesian representation matrices are given by:

$$\begin{aligned}
\mathbf{F}(\hat{E}) &= \begin{pmatrix} 1 & 0 & 0 \\ 0 & 1 & 0 \\ 0 & 0 & 1 \end{pmatrix}, \mathbf{F}(\hat{C}_3) = \begin{pmatrix} -\frac{1}{2} & -\frac{\sqrt{3}}{2} & 0 \\ \frac{\sqrt{3}}{2} & -\frac{1}{2} & 0 \\ 0 & 0 & 1 \end{pmatrix}, \mathbf{F}(\hat{C}_3^2) = \begin{pmatrix} -\frac{1}{2} & \frac{\sqrt{3}}{2} & 0 \\ -\frac{\sqrt{3}}{2} & -\frac{1}{2} & 0 \\ 0 & 0 & 1 \end{pmatrix}, \\
\mathbf{F}(\hat{\sigma}_v) &= \begin{pmatrix} 1 & 0 & 0 \\ 0 & -1 & 0 \\ 0 & 0 & 1 \end{pmatrix}, \mathbf{F}(\hat{\sigma}_v') = \begin{pmatrix} -\frac{1}{2} & -\frac{\sqrt{3}}{2} & 0 \\ -\frac{\sqrt{3}}{2} & \frac{1}{2} & 0 \\ 0 & 0 & 1 \end{pmatrix}, \mathbf{F}(\hat{\sigma}_v'') = \begin{pmatrix} -\frac{1}{2} & \frac{\sqrt{3}}{2} & 0 \\ \frac{\sqrt{3}}{2} & \frac{1}{2} & 0 \\ 0 & 0 & 1 \end{pmatrix}
\end{aligned} \tag{4.22}$$

Technically, these matrices can be constructed in the initial symmetry analysis of a molecule which detects the point group of the molecule. However, the sorting of the symmetry operations in the point group detection algorithm in deMon2k is in general not the same as the sorting in the point group tables. Therefore, the three-dimensional Cartesian representations for the construction of symmetry-adapted basis and auxiliary functions are directly built from the point group tables in deMon2k. To this end, the irreducible representations in these tables that transform according to the Cartesian x, y and z basis are indicated, too. In the case of the C_{3v} example these are the two-dimensional irreducible representation E that transforms according to the (x, y) basis and the irreducible representation A_1 that transforms according to the z basis. Thus, the three-dimensional Cartesian representations can be constructed from Table 4.1 as:

$$\mathbf{R} = \boldsymbol{\chi}^{E}(\hat{R}) \oplus \boldsymbol{\chi}^{A_1}(\hat{R}) \qquad \forall \quad \hat{R} \tag{4.23}$$

With the three-dimensional Cartesian representation matrix elements at hand, the symmetrization matrix for the function vectors can be calculated. Developing the

formula of Eq. (4.17) in general for the d shell of (auxiliary) functions for any symmetry operation, the symmetrization matrix takes the generic form:

$$\mathbf{F}(\hat{R}) = \begin{pmatrix} R_{11}^2 & \sqrt{3}R_{11}R_{12} & \sqrt{3}R_{11}R_{13} & R_{12}^2 & \sqrt{3}R_{12}R_{13} & R_{13}^2 \\ \frac{2R_{11}R_{21}}{\sqrt{3}} & R_{12}R_{21}+R_{11}R_{22} & R_{13}R_{21}+R_{11}R_{23} & \frac{2R_{12}R_{22}}{\sqrt{3}} & R_{13}R_{22}+R_{12}R_{23} & \frac{2R_{13}R_{23}}{\sqrt{3}} \\ \frac{2R_{11}R_{31}}{\sqrt{3}} & R_{12}R_{31}+R_{11}R_{32} & R_{13}R_{31}+R_{11}R_{33} & \frac{2R_{12}R_{32}}{\sqrt{3}} & R_{13}R_{32}+R_{12}R_{33} & \frac{2R_{13}R_{33}}{\sqrt{3}} \\ R_{21}^2 & \sqrt{3}R_{21}R_{22} & \sqrt{3}R_{21}R_{23} & R_{22}^2 & \sqrt{3}R_{22}R_{23} & R_{23}^2 \\ \frac{2R_{21}R_{31}}{\sqrt{3}} & R_{22}R_{31}+R_{21}R_{32} & R_{23}R_{31}+R_{21}R_{33} & \frac{2R_{22}R_{32}}{\sqrt{3}} & R_{23}R_{32}+R_{22}R_{33} & \frac{2R_{23}R_{33}}{\sqrt{3}} \\ R_{31}^2 & \sqrt{3}R_{31}R_{32} & \sqrt{3}R_{31}R_{33} & R_{32}^2 & \sqrt{3}R_{32}R_{33} & R_{33}^2 \end{pmatrix} \tag{4.24}$$

Once the (auxiliary) function symmetrization matrices are available, we can formulate a projection operator in the same spirit as for the construction of the $\mathbf{V}$ symmetrization matrix. Thus, the symmetry-adapted d-type (auxiliary) function vectors, $\mathbf{d}_{\kappa}^{\Gamma(\gamma)} \equiv \mathbf{P}_{\gamma}^{\Gamma}\mathbf{d}_{\kappa}$, are calculated as:

$$\begin{aligned} \mathbf{d}_{\kappa}^{\Gamma(\gamma)} = &\frac{d_\Gamma}{6}\chi_\gamma^\Gamma(\hat{E})\mathbf{F}(\hat{E})\mathbf{d}_\kappa + \frac{d_\Gamma}{6}\chi_\gamma^\Gamma(\hat{C}_3)\mathbf{F}(\hat{C}_3)\mathbf{d}_\kappa + \frac{d_\Gamma}{6}\chi_\gamma^\Gamma(\hat{C}_3^2)\mathbf{F}(\hat{C}_3^2)\mathbf{d}_\kappa + \\ &\frac{d_\Gamma}{6}\chi_\gamma^\Gamma(\hat{\sigma}_\nu)\mathbf{F}(\hat{\sigma}_\nu)\mathbf{d}_\kappa + \frac{d_\Gamma}{6}\chi_\gamma^\Gamma(\hat{\sigma}'_\nu)\mathbf{F}(\hat{\sigma}'_\nu)\mathbf{d}_\kappa + \frac{d_\Gamma}{6}\chi_\gamma^\Gamma(\hat{\sigma}''_\nu)\mathbf{F}(\hat{\sigma}''_\nu)\mathbf{d}_\kappa \end{aligned} \tag{4.25}$$

Again, we perform these projections until we have found as many non-vanishing linear independent symmetry-adapted auxiliary function vectors as initial auxiliary function vectors were used. For this task we also take advantage of the reduction formula Eq. (4.11), taking $\chi(\hat{R})$ as the traces of the matrices given in Eq. (4.15). The only non-vanishing expansion coefficients are $a^{A_1} = 2$ and $a^{E} = 2$. Therefore, we search for two symmetry vectors belonging to A_1 and two pairs of symmetry vectors belonging to the two-dimensional E representation. In our example of d-type Hermite Gaussians auxiliary functions, which is worked out in Schemes 4.4 and 4.5, the $\mathbf{W}$ matrix is given by:

$$\mathbf{W} = (\mathbf{d}_{xx}^{A_1}|\mathbf{d}_{zz}^{A_1}|\mathbf{d}_{xx}^{E(1)}|\mathbf{d}_{xx}^{E(2)}|\mathbf{d}_{xz}^{E(1)}|\mathbf{d}_{xz}^{E(2)}) \tag{4.26}$$

- $\Gamma = A_1; \gamma = 1; \chi^{A_1}(\hat{E}) = 1, \chi^{A_1}(\hat{C}_3) = 1, \chi^{A_1}(\hat{C}_3^2) = 1, \chi^{A_1}(\hat{\sigma}_\nu) = 1, \chi^{A_1}(\hat{\sigma}'_\nu) = 1,$
  $\chi^{A_1}(\hat{\sigma}''_\nu) = 1; \mathbf{d}_{xx}^{A_1} \equiv \mathbf{P}_1^{A_1}\mathbf{d}_{xx}$

$$
\begin{aligned}
\mathbf{d}_{xx}^{A_1} &= \frac{1}{6}\,1\mathbf{F}(\hat{E})\mathbf{d}_{xx} + \frac{1}{6}\,1\mathbf{F}(\hat{C}_3)\mathbf{d}_{xx} + \frac{1}{6}\,1\mathbf{F}(\hat{C}_3^2)\mathbf{d}_{xx} + \frac{1}{6}\,1\mathbf{F}(\hat{\sigma}_\nu)\mathbf{d}_{xx} + \frac{1}{6}\,1\mathbf{F}(\hat{\sigma}'_\nu)\mathbf{d}_{xx} + \frac{1}{6}\,1\mathbf{F}(\hat{\sigma}''_\nu)\mathbf{d}_{xx} \\
&= \frac{1}{6}\,[1\mathbf{d}_{xx} + 1\mathbf{d}'_{xx} + 1\mathbf{d}''_{xx} + 1\mathbf{d}_{xx} + 1\mathbf{d}''_{xx} + 1\mathbf{d}'_{xx}] \\
&= \frac{1}{3}\,[\mathbf{d}_{xx} + \mathbf{d}'_{xx} + \mathbf{d}''_{xx}] \\
&= \frac{1}{3}\left[\mathbf{d}_{xx} + \left(\frac{1}{4}\mathbf{d}_{xx} - \frac{1}{2}\mathbf{d}_{xy} + \frac{3}{4}\mathbf{d}_{yy}\right) + \left(\frac{1}{4}\mathbf{d}_{xx} + \frac{1}{2}\mathbf{d}_{xy} + \frac{3}{4}\mathbf{d}_{yy}\right)\right] \\
&= \frac{1}{3}\left[\frac{3}{2}\mathbf{d}_{xx} + \frac{3}{2}\mathbf{d}_{yy}\right] = \frac{1}{2}\,[\mathbf{d}_{xx} + \mathbf{d}_{yy}] \quad \text{store; next projection} \\
\mathbf{d}_{xy}^{A_1} &\equiv \mathbf{P}_1^{A_1}\mathbf{d}_{xy} \\
\mathbf{d}_{xy}^{A_1} &= \frac{1}{6}\,1\mathbf{F}(\hat{E})\mathbf{d}_{xy} + \frac{1}{6}\,1\mathbf{F}(\hat{C}_3)\mathbf{d}_{xy} + \frac{1}{6}\,1\mathbf{F}(\hat{C}_3^2)\mathbf{d}_{xy} + \frac{1}{6}\,1\mathbf{F}(\hat{\sigma}_\nu)\mathbf{d}_{xy} + \frac{1}{6}\,1\mathbf{F}(\hat{\sigma}'_\nu)\mathbf{d}_{xy} + \frac{1}{6}\,1\mathbf{F}(\hat{\sigma}''_\nu)\mathbf{d}_{xy} \\
&= \frac{1}{6}\,[1\mathbf{d}_{xy} + 1\mathbf{d}'_{xy} + 1\mathbf{d}''_{xy} + 1(-\mathbf{d}_{xy}) + 1(-\mathbf{d}''_{xy}) + 1(-\mathbf{d}'_{xy})] \\
&= \mathbf{0} \quad \text{vanishes; next projection}
\end{aligned}
$$

...

$$
\begin{aligned}
\mathbf{d}_{yy}^{A_1} &\equiv \mathbf{P}_1^{A_1}\mathbf{d}_{yy} \\
\mathbf{d}_{yy}^{A_1} &= \frac{1}{6}\,1\mathbf{F}(\hat{E})\mathbf{d}_{yy} + \frac{1}{6}\,1\mathbf{F}(\hat{C}_3)\mathbf{d}_{yy} + \frac{1}{6}\,1\mathbf{F}(\hat{C}_3^2)\mathbf{d}_{yy} + \frac{1}{6}\,1\mathbf{F}(\hat{\sigma}_\nu)\mathbf{d}_{yy} + \frac{1}{6}\,1\mathbf{F}(\hat{\sigma}'_\nu)\mathbf{d}_{yy} + \frac{1}{6}\,1\mathbf{F}(\hat{\sigma}''_\nu)\mathbf{d}_{yy} \\
&= \frac{1}{6}\,[1\mathbf{d}_{yy} + 1\mathbf{d}'_{yy} + 1\mathbf{d}''_{yy} + 1\mathbf{d}_{yy} + 1\mathbf{d}''_{yy} + 1\mathbf{d}'_{yy}] \\
&= \frac{1}{3}\,[\mathbf{d}_{yy} + \mathbf{d}'_{yy} + \mathbf{d}''_{yy}] \\
&= \frac{1}{3}\left[\mathbf{d}_{yy} + \left(\frac{3}{4}\mathbf{d}_{xx} + \frac{1}{2}\mathbf{d}_{xy} + \frac{1}{4}\mathbf{d}_{yy}\right) + \left(\frac{3}{4}\mathbf{d}_{xx} - \frac{1}{2}\mathbf{d}_{xy} + \frac{1}{4}\mathbf{d}_{yy}\right)\right] \\
&= \frac{1}{3}\left[\frac{3}{2}\mathbf{d}_{xx} + \frac{3}{2}\mathbf{d}_{yy}\right] = \frac{1}{2}\,[\mathbf{d}_{xx} + \mathbf{d}_{yy}] \quad \text{linear dependent; next projection}
\end{aligned}
$$

...

$$
\begin{aligned}
\mathbf{d}_{zz}^{A_1} &\equiv \mathbf{P}_1^{A_1}\mathbf{d}_{zz} \\
\mathbf{d}_{zz}^{A_1} &= \frac{1}{6}\,1\mathbf{F}(\hat{E})\mathbf{d}_{zz} + \frac{1}{6}\,1\mathbf{F}(\hat{C}_3)\mathbf{d}_{zz} + \frac{1}{6}\,1\mathbf{F}(\hat{C}_3^2)\mathbf{d}_{zz} + \frac{1}{6}\,1\mathbf{F}(\hat{\sigma}_\nu)\mathbf{d}_{zz} + \frac{1}{6}\,1\mathbf{F}(\hat{\sigma}'_\nu)\mathbf{d}_{zz} + \frac{1}{6}\,1\mathbf{F}(\hat{\sigma}''_\nu)\mathbf{d}_{zz} \\
&= \frac{1}{6}\,[1\mathbf{d}_{zz} + 1\mathbf{d}_{zz} + 1\mathbf{d}_{zz} + 1\mathbf{d}_{zz} + 1\mathbf{d}_{zz} + 1\mathbf{d}_{zz}] \\
&= \mathbf{d}_{zz} \quad \text{store; enough for } A_1
\end{aligned}
$$

Scheme 4.4: Construction of symmetry-adapted (auxiliary) function vectors for the irreducible representation A_1. See Figure 4.1 for the actions of $\mathbf{F}(\hat{R})$ on the (auxiliary) function vectors $\mathbf{d}_\kappa$.

- $\Gamma = \mathrm{E};\gamma = 1;\chi_1^{\mathrm{E}}(\hat{\mathrm{E}}) = 1,\chi_1^{\mathrm{E}}(\hat{\mathrm{C}}_3) = -\frac{1}{2},\chi_1^{\mathrm{E}}(\hat{\mathrm{C}}_3^2) = -\frac{1}{2},\chi_1^{\mathrm{E}}(\hat{\sigma}_\nu) = 1,\chi_1^{\mathrm{E}}(\hat{\sigma}_\nu') = -\frac{1}{2},\chi_1^{\mathrm{E}}(\hat{\sigma}_\nu'') = -\frac{1}{2}$;
  $\mathbf{d}_{xx}^{\mathrm{E}(1)} \equiv \mathbf{P}_1^{\mathrm{E}}\mathbf{d}_{xx}$

$$\begin{aligned}
\mathbf{d}_{xx}^{\mathrm{E}(1)} &= \tfrac{2}{6}\left[1\mathbf{F}(\hat{\mathrm{E}})\mathbf{d}_{xx} + \left(-\tfrac{1}{2}\right)\mathbf{F}(\hat{\mathrm{C}}_3)\mathbf{d}_{xx} + \left(-\tfrac{1}{2}\right)\mathbf{F}(\hat{\mathrm{C}}_3^2)\mathbf{d}_{xx} + 1\mathbf{F}(\hat{\sigma}_\nu)\mathbf{d}_{xx} + \left(-\tfrac{1}{2}\right)\mathbf{F}(\hat{\sigma}_\nu')\mathbf{d}_{xx} + \left(-\tfrac{1}{2}\right)\mathbf{F}(\hat{\sigma}_\nu'')\mathbf{d}_{xx}\right] \\
&= \tfrac{2}{6}\left[1\mathbf{d}_{xx} + \left(-\tfrac{1}{2}\right)\mathbf{d}_{xx}' + \left(-\tfrac{1}{2}\right)\mathbf{d}_{xx}'' + 1\mathbf{d}_{xx} + \left(-\tfrac{1}{2}\right)\mathbf{d}_{xx}'' + \left(-\tfrac{1}{2}\right)\mathbf{d}_{xx}'\right] \\
&= \tfrac{2}{6}\left[2\mathbf{d}_{xx} - \mathbf{d}_{xx}' - \mathbf{d}_{xx}''\right] = \tfrac{2}{6}\left[2\mathbf{d}_{xx} - \left(\tfrac{1}{4}\mathbf{d}_{xx} - \tfrac{1}{2}\mathbf{d}_{xy} + \tfrac{3}{4}\mathbf{d}_{yy}\right) - \left(\tfrac{1}{4}\mathbf{d}_{xx} + \tfrac{1}{2}\mathbf{d}_{xy} + \tfrac{3}{4}\mathbf{d}_{yy}\right)\right] \\
&= \tfrac{2}{6}\left[\tfrac{3}{2}\mathbf{d}_{xx} - \tfrac{3}{2}\mathbf{d}_{yy}\right] = \tfrac{1}{2}\left[\mathbf{d}_{xx} - \mathbf{d}_{yy}\right] \quad \text{store; find partner increasing } \gamma
\end{aligned}$$

- $\Gamma = \mathrm{E};\gamma = 2;\chi_2^{\mathrm{E}}(\hat{\mathrm{E}}) = 0,\chi_2^{\mathrm{E}}(\hat{\mathrm{C}}_3) = \frac{\sqrt{3}}{2},\chi_2^{\mathrm{E}}(\hat{\mathrm{C}}_3^2) = -\frac{\sqrt{3}}{2},\chi_2^{\mathrm{E}}(\hat{\sigma}_\nu) = 0,\chi_2^{\mathrm{E}}(\hat{\sigma}_\nu') = -\frac{\sqrt{3}}{2},\chi_2^{\mathrm{E}}(\hat{\sigma}_\nu'') = \frac{\sqrt{3}}{2}$;
  $\mathbf{d}_{xx}^{\mathrm{E}(2)} \equiv \mathbf{P}_2^{\mathrm{E}}\mathbf{d}_{xx}$

$$\begin{aligned}
\mathbf{d}_{xx}^{\mathrm{E}(2)} &= \tfrac{2}{6}\left[0\mathbf{F}(\hat{\mathrm{E}})\mathbf{d}_{xx} + \left(\tfrac{\sqrt{3}}{2}\right)\mathbf{F}(\hat{\mathrm{C}}_3)\mathbf{d}_{xx} + \left(-\tfrac{\sqrt{3}}{2}\right)\mathbf{F}(\hat{\mathrm{C}}_3^2)\mathbf{d}_{xx} + 0\mathbf{F}(\hat{\sigma}_\nu)\mathbf{d}_{xx} + \left(-\tfrac{\sqrt{3}}{2}\right)\mathbf{F}(\hat{\sigma}_\nu')\mathbf{d}_{xx} + \left(\tfrac{\sqrt{3}}{2}\right)\mathbf{F}(\hat{\sigma}_\nu'')\mathbf{d}_{xx}\right] \\
&= \tfrac{2}{6}\left[\left(\tfrac{\sqrt{3}}{2}\right)\mathbf{d}_{xx}' + \left(-\tfrac{\sqrt{3}}{2}\right)\mathbf{d}_{xx}'' + \left(-\tfrac{\sqrt{3}}{2}\right)\mathbf{d}_{xx}'' + \left(\tfrac{\sqrt{3}}{2}\right)\mathbf{d}_{xx}'\right] \\
&= \tfrac{1}{\sqrt{3}}\left[\mathbf{d}_{xx}' - \mathbf{d}_{xx}''\right] = \tfrac{1}{\sqrt{3}}\left[\left(\tfrac{1}{4}\mathbf{d}_{xx} - \tfrac{1}{2}\mathbf{d}_{xy} + \tfrac{3}{4}\mathbf{d}_{yy}\right) - \left(\tfrac{1}{4}\mathbf{d}_{xx} + \tfrac{1}{2}\mathbf{d}_{xy} + \tfrac{3}{4}\mathbf{d}_{yy}\right)\right] \\
&= -\tfrac{1}{\sqrt{3}}\mathbf{d}_{xy} \quad \text{store; find next projection in } \Gamma = \mathrm{E},\gamma = 1
\end{aligned}$$

- $\Gamma = \mathrm{E};\gamma = 1;\chi_1^{\mathrm{E}}(\hat{\mathrm{E}}) = 1,\chi_1^{\mathrm{E}}(\hat{\mathrm{C}}_3) = -\frac{1}{2},\chi_1^{\mathrm{E}}(\hat{\mathrm{C}}_3^2) = -\frac{1}{2},\chi_1^{\mathrm{E}}(\hat{\sigma}_\nu) = 1,\chi_1^{\mathrm{E}}(\hat{\sigma}_\nu') = -\frac{1}{2},\chi_1^{\mathrm{E}}(\hat{\sigma}_\nu'') = -\frac{1}{2}$;
  $\mathbf{d}_{xy}^{\mathrm{E}(1)} \equiv \mathbf{P}_1^{\mathrm{E}}\mathbf{d}_{xy}$

$$\begin{aligned}
\mathbf{d}_{xy}^{\mathrm{E}(1)} &= \tfrac{2}{6}\left[1\mathbf{F}(\hat{\mathrm{E}})\mathbf{d}_{xy} + \left(-\tfrac{1}{2}\right)\mathbf{F}(\hat{\mathrm{C}}_3)\mathbf{d}_{xy} + \left(-\tfrac{1}{2}\right)\mathbf{F}(\hat{\mathrm{C}}_3^2)\mathbf{d}_{xy} + 1\mathbf{F}(\hat{\sigma}_\nu)\mathbf{d}_{xy} + \left(-\tfrac{1}{2}\right)\mathbf{F}(\hat{\sigma}_\nu')\mathbf{d}_{xy} + \left(-\tfrac{1}{2}\right)\mathbf{F}(\hat{\sigma}_\nu'')\mathbf{d}_{xy}\right] \\
&= \tfrac{2}{6}\left[1\mathbf{d}_{xy} + \left(-\tfrac{1}{2}\right)\mathbf{d}_{xy}' + \left(-\tfrac{1}{2}\right)\mathbf{d}_{xy}'' + 1\left(-\mathbf{d}_{xy}\right) + \left(-\tfrac{1}{2}\right)\left(-\mathbf{d}_{xy}''\right) + \left(-\tfrac{1}{2}\right)\left(-\mathbf{d}_{xy}'\right)\right] \\
&= \mathbf{0} \quad \text{vanishes; next projection}
\end{aligned}$$

$$\begin{aligned}
\mathbf{d}_{xz}^{\mathrm{E}(1)} &= \tfrac{2}{6}\left[1\mathbf{F}(\hat{\mathrm{E}})\mathbf{d}_{xz} + \left(-\tfrac{1}{2}\right)\mathbf{F}(\hat{\mathrm{C}}_3)\mathbf{d}_{xz} + \left(-\tfrac{1}{2}\right)\mathbf{F}(\hat{\mathrm{C}}_3^2)\mathbf{d}_{xz} + 1\mathbf{F}(\hat{\sigma}_\nu)\mathbf{d}_{xz} + \left(-\tfrac{1}{2}\right)\mathbf{F}(\hat{\sigma}_\nu')\mathbf{d}_{xz} + \left(-\tfrac{1}{2}\right)\mathbf{F}(\hat{\sigma}_\nu'')\mathbf{d}_{xz}\right] \\
&= \tfrac{2}{6}\left[1\mathbf{d}_{xz} + \left(-\tfrac{1}{2}\right)\mathbf{d}_{xz}' + \left(-\tfrac{1}{2}\right)\mathbf{d}_{xz}'' + 1\mathbf{d}_{xz} + \left(-\tfrac{1}{2}\right)\mathbf{d}_{xz}'' + \left(-\tfrac{1}{2}\right)\mathbf{d}_{xz}'\right] \\
&= \tfrac{2}{6}\left[2\mathbf{d}_{xz} - \mathbf{d}_{xz}' - \mathbf{d}_{xz}''\right] = \tfrac{2}{6}\left[2\mathbf{d}_{xz} - \left(-\tfrac{1}{2}\mathbf{d}_{xz} + \tfrac{\sqrt{3}}{2}\mathbf{d}_{yz}\right) - \left(-\tfrac{1}{2}\mathbf{d}_{xz} - \tfrac{\sqrt{3}}{2}\mathbf{d}_{yz}\right)\right] \\
&= \mathbf{d}_{xz} \quad \text{store; find partner increasing } \gamma
\end{aligned}$$

- $\Gamma = \mathrm{E};\gamma = 2;\chi_2^{\mathrm{E}}(\hat{\mathrm{E}}) = 0,\chi_2^{\mathrm{E}}(\hat{\mathrm{C}}_3) = \frac{\sqrt{3}}{2},\chi_2^{\mathrm{E}}(\hat{\mathrm{C}}_3^2) = -\frac{\sqrt{3}}{2},\chi_2^{\mathrm{E}}(\hat{\sigma}_\nu) = 0,\chi_2^{\mathrm{E}}(\hat{\sigma}_\nu') = -\frac{\sqrt{3}}{2},\chi_2^{\mathrm{E}}(\hat{\sigma}_\nu'') = \frac{\sqrt{3}}{2}$;
  $\mathbf{d}_{xz}^{\mathrm{E}(2)} \equiv \mathbf{P}_2^{\mathrm{E}}\mathbf{d}_{xz}$

$$\begin{aligned}
\mathbf{d}_{xz}^{\mathrm{E}(2)} &= \tfrac{2}{6}\left[0\mathbf{F}(\hat{\mathrm{E}})\mathbf{d}_{xz} + \left(\tfrac{\sqrt{3}}{2}\right)\mathbf{F}(\hat{\mathrm{C}}_3)\mathbf{d}_{xz} + \left(-\tfrac{\sqrt{3}}{2}\right)\mathbf{F}(\hat{\mathrm{C}}_3^2)\mathbf{d}_{xz} + 0\mathbf{F}(\hat{\sigma}_\nu)\mathbf{d}_{xz} + \left(-\tfrac{\sqrt{3}}{2}\right)\mathbf{F}(\hat{\sigma}_\nu')\mathbf{d}_{xz} + \left(\tfrac{\sqrt{3}}{2}\right)\mathbf{F}(\hat{\sigma}_\nu'')\mathbf{d}_{xz}\right] \\
&= \tfrac{2}{6}\left[\left(\tfrac{\sqrt{3}}{2}\right)\mathbf{d}_{xz}' + \left(-\tfrac{\sqrt{3}}{2}\right)\mathbf{d}_{xz}'' + \left(-\tfrac{\sqrt{3}}{2}\right)\mathbf{d}_{xz}'' + \left(\tfrac{\sqrt{3}}{2}\right)\mathbf{d}_{xz}'\right] \\
&= \tfrac{1}{\sqrt{3}}\left[\mathbf{d}_{xz}' - \mathbf{d}_{xz}''\right] = \tfrac{1}{\sqrt{3}}\left[\left(-\tfrac{1}{2}\mathbf{d}_{xz} + \tfrac{\sqrt{3}}{2}\mathbf{d}_{yz}\right) - \left(-\tfrac{1}{2}\mathbf{d}_{xz} - \tfrac{\sqrt{3}}{2}\mathbf{d}_{yz}\right)\right] \\
&= \mathbf{d}_{yz} \quad \text{store; six symmetry vectors found; finish}
\end{aligned}$$

Scheme 4.5: Construction of symmetry-adapted (auxiliary) function vectors for the irreducible representation E. See Figure 4.1 for the actions of $\mathbf{F}(\hat{\mathrm{R}})$ on the (auxiliary) function vectors $\mathbf{d}_\kappa$.

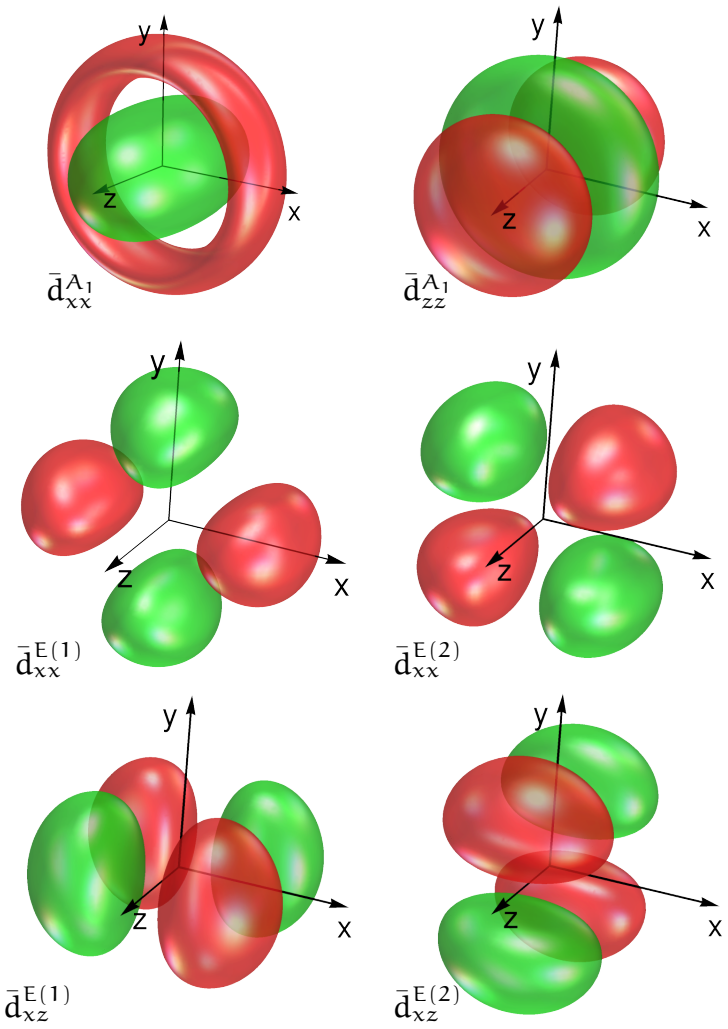

Figure 4.2: Origin-centered symmetry-adapted Hermite d-type functions.

The resulting symmetry-adapted functions are plotted in Figure 4.2. In general, the symmetry-adapted auxiliary function vectors for a particular angular momentum ℓ are obtained as:

$$\boldsymbol{\ell}_{\kappa}^{\Gamma(\gamma)} = \frac{d_{\Gamma}}{h} \sum_{R} \chi_{\gamma}^{\Gamma}(\hat{R}) \mathbf{F}(\hat{R}) \boldsymbol{\ell}_{\kappa} \tag{4.27}$$

These symmetry-adapted auxiliary function vectors are stored in the $\mathbf{W}$ matrix.

With the **V** and **W** matrices at hand, we now built a new basis by means of the direct product of these matrices (see appendix A)

$$\begin{aligned}\mathbf{B} =& \mathbf{V} \otimes \mathbf{W} \\ =& (\mathbf{p}_A^{A_1} | \mathbf{p}_A^{E(1)} | \mathbf{p}_A^{E(2)}) \otimes (\mathbf{d}_{xx}^{A_1} | \mathbf{d}_{zz}^{A_1} | \mathbf{d}_{xx}^{E(1)} | \mathbf{d}_{xz}^{E(1)} | \mathbf{d}_{xx}^{E(2)} | \mathbf{d}_{xz}^{E(2)})\end{aligned} \tag{4.28}$$

The resulting column vectors span the same space as the set of all vectors representing the original atom-centered auxiliary functions in the invariant under consideration. For point groups with only one-dimensional irreducible representations, the symmetrization matrix **U** is the matrix **B** with columns sorted by irreducible representations [88]. In general, the columns of the **U** symmetrization matrix are symmetry-adapted vectors built by applying the usual projector operator $\hat{P}_\gamma^\Gamma$ to the column vectors of **B**, i.e.

$$\mathbf{u}_{\mathring{l}}^{\Gamma(\gamma)} = \hat{P}_\gamma^\Gamma \left(\mathbf{p}_L^{\Gamma'(\gamma')} \otimes \boldsymbol{\ell}_\lambda^{\Gamma''(\gamma'')} \right) \tag{4.29}$$

In Eq. (4.29) $\mathring{l}$ is a cumulative index of the atom and function indices L and λ, the irreducible representations Γ' and Γ'', and the column indices γ' and γ'' of the atomic and function symmetry vectors. In our ammonia example, we are searching for $3 \cdot 6 = 18$ non-zero and linear independent symmetry-adapted vectors. To this end, we apply systematically the projection and transfer operators to the columns of **B** in the same way as we did for the symmetry-adapted permutation vectors and the symmetry-adapted function vectors. To do so, we have to build the matrix representations for the symmetry operations in the new basis given by the columns of **B**. The action of $\hat{R}$ on these vectors is given by the direct product of irreducible representations [92]:

$$\hat{R} \left(\mathbf{p}_L^{\Gamma'(\gamma')} \otimes \boldsymbol{\ell}_\lambda^{\Gamma''(\gamma'')} \right) = \sum_{\delta'}^{d_{\Gamma'}} \sum_{\delta''}^{d_{\Gamma''}} \chi_{\delta'\gamma'}^{\Gamma'}(\hat{R}) \, \chi_{\delta''\gamma''}^{\Gamma''}(\hat{R}) \, \mathbf{p}_L^{\Gamma'(\delta')} \otimes \boldsymbol{\ell}_\lambda^{\Gamma''(\delta'')} \tag{4.30}$$

Note that the expansion coefficients of the double sum in Eq. (4.30) are given by the product of irreducible representation matrix elements and, therefore, are independent of

L and λ. These coefficients depend only on the irreducible representations and their row and column indices. The space spanned by the columns of **B** can be split into invariant subspaces closed under the symmetry operations of the point group considered. These subspaces are built by the direct products of the degenerate symmetry vectors belonging to Γ' and Γ'', i.e. $\{\mathbf{p}_L^{\Gamma'(1)} \otimes \boldsymbol{\ell}_\lambda^{\Gamma''(1)}, \mathbf{p}_L^{\Gamma'(1)} \otimes \boldsymbol{\ell}_\lambda^{\Gamma''(2)}, ..., \mathbf{p}_L^{\Gamma'(d_{\Gamma'})} \otimes \boldsymbol{\ell}_\lambda^{\Gamma''(d_{\Gamma''})}\}$. For the ammonia example the invariant subspaces are given by the columns of the following rectangular matrices:

$$\mathbf{B}_1 = \left(\mathbf{p}_A^{A_1} \otimes \mathbf{d}_{xx}^{A_1}\right) \tag{4.31}$$

$$\mathbf{B}_2 = \left(\mathbf{p}_A^{A_1} \otimes \mathbf{d}_{zz}^{A_1}\right) \tag{4.32}$$

$$\mathbf{B}_3 = \left(\mathbf{p}_A^{A_1} \otimes \mathbf{d}_{xx}^{E(1)} | \mathbf{p}_A^{A_1} \otimes \mathbf{d}_{xx}^{E(2)}\right) \tag{4.33}$$

$$\mathbf{B}_4 = \left(\mathbf{p}_A^{A_1} \otimes \mathbf{d}_{xz}^{E(1)} | \mathbf{p}_A^{A_1} \otimes \mathbf{d}_{xz}^{E(2)}\right) \tag{4.34}$$

$$\mathbf{B}_5 = \left(\mathbf{p}_A^{E(1)} \otimes \mathbf{d}_{xx}^{A_1} | \mathbf{p}_A^{E(2)} \otimes \mathbf{d}_{xx}^{A_1}\right) \tag{4.35}$$

$$\mathbf{B}_6 = \left(\mathbf{p}_A^{E(1)} \otimes \mathbf{d}_{zz}^{A_1} | \mathbf{p}_A^{E(2)} \otimes \mathbf{d}_{zz}^{A_1}\right) \tag{4.36}$$

$$\mathbf{B}_7 = \left(\mathbf{p}_A^{E(1)} \otimes \mathbf{d}_{xx}^{E(1)} | \mathbf{p}_A^{E(1)} \otimes \mathbf{d}_{xx}^{E(2)} | \mathbf{p}_A^{E(2)} \otimes \mathbf{d}_{xx}^{E(1)} | \mathbf{p}_A^{E(2)} \otimes \mathbf{d}_{xx}^{E(2)}\right) \tag{4.37}$$

$$\mathbf{B}_8 = \left(\mathbf{p}_A^{E(1)} \otimes \mathbf{d}_{xz}^{E(1)} | \mathbf{p}_A^{E(1)} \otimes \mathbf{d}_{xz}^{E(2)} | \mathbf{p}_A^{E(2)} \otimes \mathbf{d}_{xz}^{E(1)} | \mathbf{p}_A^{E(2)} \otimes \mathbf{d}_{xz}^{E(2)}\right) \tag{4.38}$$

In general, we follow lexicographical ordering of the superscripts for building the subspace matrices, i.e.

$$\left(\mathbf{p}_L^{\Gamma'(1)} \otimes \boldsymbol{\ell}_\lambda^{\Gamma''(1)} | \mathbf{p}_L^{\Gamma'(1)} \otimes \boldsymbol{\ell}_\lambda^{\Gamma''(2)} | ... | \mathbf{p}_L^{\Gamma'(1)} \otimes \boldsymbol{\ell}_\lambda^{\Gamma''(d_{\Gamma''})} | \mathbf{p}_L^{\Gamma'(2)} \otimes \boldsymbol{\ell}_\lambda^{\Gamma''(1)} | ... | \mathbf{p}_L^{\Gamma'(d_{\Gamma'})} \otimes \boldsymbol{\ell}_\lambda^{\Gamma''(d_{\Gamma''})}\right) \tag{4.39}$$

To proceed, we now construct symmetry-adapted vectors for the subspaces given by the columns of matrices in Eqs. (4.31) to (4.38) using Eq. (4.30). Because the expansion coefficients are given by the products of irreducible representation matrices, we only need to calculate them for different direct products, here $A_1 \otimes A_1$, $A_1 \otimes E$ and $E \otimes E$. This projection procedure is known as the reduction of direct products of irreducible representations [73]. For real one-dimensional irreducible representations holds $\Gamma =$

$\Gamma' \otimes \Gamma''$. Therefore, we have implemented the reduction of direct products for this case, through the calculation of Clebsch-Gordan coefficients from the corresponding characters [93]:

$$C^{\Gamma}(\Gamma', \Gamma'') = \frac{1}{h} \sum_{\hat{R}} \chi^{\Gamma}(\hat{R}) \chi^{\Gamma'}(\hat{R}) \chi^{\Gamma''}(\hat{R}) \tag{4.40}$$

As a result, we find as expansion coefficients for $\mathbf{B}_1$ and $\mathbf{B}_2$:

$$C^{A_1}(A_1, A_1) = 1 \tag{4.41}$$

The corresponding column vectors of the symmetrization matrix $\mathbf{U}$ are given by:

$$\mathbf{u}_1^{A_1} = C^{A_1}(A_1, A_1) \cdot \mathbf{p}_A^{A_1} \otimes \mathbf{d}_{xx}^{A_1} = 1 \cdot \begin{pmatrix} \frac{1}{3} \\ \frac{1}{3} \\ \frac{1}{3} \end{pmatrix} \otimes \begin{pmatrix} \frac{1}{2} \\ 0 \\ 0 \\ \frac{1}{2} \\ 0 \\ 0 \end{pmatrix} \tag{4.42}$$

$$\mathbf{u}_2^{A_1} = C^{A_1}(A_1, A_1) \cdot \mathbf{p}_A^{A_1} \otimes \mathbf{d}_{zz}^{A_1} = 1 \cdot \begin{pmatrix} \frac{1}{3} \\ \frac{1}{3} \\ \frac{1}{3} \end{pmatrix} \otimes \begin{pmatrix} 0 \\ 0 \\ 0 \\ 0 \\ 0 \\ 1 \end{pmatrix} \tag{4.43}$$

For the two-dimensional $A_1 \otimes E$ subspaces given by the columns of $\mathbf{B}_3$, $\mathbf{B}_4$, $\mathbf{B}_5$, and $\mathbf{B}_6$ an explicit reduction is needed. From Eq. (4.11), using $\chi(\hat{R}) = \mathrm{tr}[\chi^{A_1}(\hat{R}) \cdot \boldsymbol{\chi}^{E}(\hat{R})]$, we obtain as only non-zero contribution $a^E = 1$. Therefore, we search for two symmetry-adapted vectors belonging to the E irreducible representation. We define the two-dimensional basis vectors $\mathbf{c}_1(E)$ and $\mathbf{c}_2(E)$ for the subspace spanned by the direct product vectors $\mathbf{p}_A^{A_1} \otimes \mathbf{d}_{xx}^{E(1)}$ and $\mathbf{p}_A^{A_1} \otimes \mathbf{d}_{xx}^{E(2)}$ in $\mathbf{B}_3$ as:

$$\mathbf{c}_1(E) = \begin{pmatrix} 1 \\ 0 \end{pmatrix}, \qquad \mathbf{c}_2(E) = \begin{pmatrix} 0 \\ 1 \end{pmatrix} \tag{4.44}$$

The matrix representations of the symmetry operations in this subspace are given by:

$$\mathbf{D}^{A_1 \otimes E}(\hat{R}) = \chi^{A_1}(\hat{R}) \cdot \boldsymbol{\chi}^{E}(\hat{R}) \qquad \forall \quad \hat{R} \tag{4.45}$$

As $\chi^{A_1}(\hat{R})$ is 1 for all symmetry operations we obtain:

$$\mathbf{D}^{A_1 \otimes E}(\hat{R}) = \boldsymbol{\chi}^{E}(\hat{R}) \qquad \forall \quad \hat{R} \tag{4.46}$$

With these representation matrices we can define the action of a symmetry operation in this subspace as:

$$\hat{R}\ \mathbf{c}_j(E) \rightarrow \mathbf{D}^{A_1 \otimes E}(\hat{R})\ \mathbf{c}_j(E) \qquad \forall \quad \hat{R} \wedge j \tag{4.47}$$

We now apply the projection operator $\hat{P}_1^E$ in order to obtain $\mathbf{c}_1^{E(1)}(A_1, E)$ as:

$$\begin{aligned} \mathbf{c}_1^{E(1)}(A_1, E) &= \hat{P}_1^E \mathbf{c}_1(E) \\ &= \frac{2}{6} \sum_{\hat{R}} \chi_1^E(\hat{R})\ \mathbf{D}^{A_1 \otimes E}(\hat{R})\ \mathbf{c}_1(E) \\ &= \frac{2}{6} \sum_{\hat{R}} \chi_1^E(\hat{R})\ \boldsymbol{\chi}^{E}(\hat{R})\ \mathbf{c}_1(E) \end{aligned} \tag{4.48}$$

The corresponding degenerate second component is given by:

$$\begin{aligned} \mathbf{c}_1^{E(2)}(A_1, E) &= \hat{P}_2^E \mathbf{c}_1(E) \\ &= \frac{2}{6} \sum_{\hat{R}} \chi_2^E(\hat{R})\ \mathbf{D}^{A_1 \otimes E}(\hat{R})\ \mathbf{c}_1(E) \\ &= \frac{2}{6} \sum_{\hat{R}} \chi_2^E(\hat{R})\ \boldsymbol{\chi}^{E}(\hat{R})\ \mathbf{c}_1(E) \end{aligned} \tag{4.49}$$

The explicit calculation of the symmetry-adapted vectors is shown in Scheme 4.6. As this scheme shows, the obtained symmetry-adapted vectors for the subspace given by the columns of $\mathbf{B}_3$ are:

$$\mathbf{c}_1^{E(1)}(A_1, E) = \begin{pmatrix} 1 \\ 0 \end{pmatrix} = \mathbf{c}_1(E), \quad \text{and} \quad \mathbf{c}_1^{E(2)}(A_1, E) = \begin{pmatrix} 0 \\ 1 \end{pmatrix} = \mathbf{c}_2(E) \tag{4.50}$$

The resulting column vectors of the E irreducible representation of the symmetrization matrix $\mathbf{U}$ are given by:

$$\begin{aligned} \mathbf{u}_3^{E(1)} &= \left(\mathbf{p}_A^{A_1} \otimes \mathbf{d}_{xx}^{E(1)} | \mathbf{p}_A^{A_1} \otimes \mathbf{d}_{xx}^{E(2)}\right) \mathbf{c}_1^{E(1)}(A_1, E) \\ &= \left(\mathbf{p}_A^{A_1} \otimes \mathbf{d}_{xx}^{E(1)} | \mathbf{p}_A^{A_1} \otimes \mathbf{d}_{xx}^{E(2)}\right) \begin{pmatrix} 1 \\ 0 \end{pmatrix} \\ &= \mathbf{p}_A^{A_1} \otimes \mathbf{d}_{xx}^{E(1)} = \begin{pmatrix} \frac{1}{3} \\ \frac{1}{3} \\ \frac{1}{3} \end{pmatrix} \otimes \begin{pmatrix} \frac{1}{2} \\ 0 \\ 0 \\ -\frac{1}{2} \\ 0 \\ 0 \end{pmatrix} \end{aligned} \tag{4.51}$$

and

$$\begin{aligned} \mathbf{u}_4^{E(2)} &= \left(\mathbf{p}_A^{A_1} \otimes \mathbf{d}_{xx}^{E(1)} | \mathbf{p}_A^{A_1} \otimes \mathbf{d}_{xx}^{E(2)}\right) \mathbf{c}_1^{E(2)}(A_1, E) \\ &= \left(\mathbf{p}_A^{A_1} \otimes \mathbf{d}_{xx}^{E(1)} | \mathbf{p}_A^{A_1} \otimes \mathbf{d}_{xx}^{E(2)}\right) \begin{pmatrix} 0 \\ 1 \end{pmatrix} \\ &= \mathbf{p}_A^{A_1} \otimes \mathbf{d}_{xx}^{E(2)} = \begin{pmatrix} \frac{1}{3} \\ \frac{1}{3} \\ \frac{1}{3} \end{pmatrix} \otimes \begin{pmatrix} 0 \\ -\frac{1}{\sqrt{3}} \\ 0 \\ 0 \\ 0 \\ 0 \end{pmatrix} \end{aligned} \tag{4.52}$$

For the subspaces given by the columns of $\mathbf{B}_4$, $\mathbf{B}_5$ and $\mathbf{B}_6$ the same projection holds. As a result, the column vectors of the symmetrization matrix arising from the subspace given by the columns of $\mathbf{B}_4$, as an example, are:

- $\Gamma = E; \gamma = 1; \chi_1^E(\hat{E}) = 1, \chi_1^E(\hat{C}_3) = -\frac{1}{2}, \chi_1^E(\hat{C}_3^2) = -\frac{1}{2}, \chi_1^E(\hat{\sigma}_v) = 1, \chi_1^E(\hat{\sigma}_v') = -\frac{1}{2}, \chi_1^E(\hat{\sigma}_v'') = -\frac{1}{2}; \mathbf{c}_1^{E(1)} \equiv \mathbf{P}_1^E \mathbf{c}_1$

$$\begin{aligned}
\mathbf{c}_1^{E(1)} &= \frac{2}{6}\Big[1\mathbf{D}^{A_1\otimes E}(\hat{E})\mathbf{c}_1 + (-\tfrac{1}{2})\mathbf{D}^{A_1\otimes E}(\hat{C}_3)\mathbf{c}_1 + (-\tfrac{1}{2})\mathbf{D}^{A_1\otimes E}(\hat{C}_3^2)\mathbf{c}_1 + 1\mathbf{D}^{A_1\otimes E}(\hat{\sigma}_v)\mathbf{c}_1 + \\
&\quad (-\tfrac{1}{2})\mathbf{D}^{A_1\otimes E}(\hat{\sigma}_v')\mathbf{c}_1 + (-\tfrac{1}{2})\mathbf{D}^{A_1\otimes E}(\hat{\sigma}_v'')\mathbf{c}_1\Big] \\
&= \frac{2}{6}\Big[1\chi^E(\hat{E})\mathbf{c}_1 + (-\tfrac{1}{2})\chi^E(\hat{C}_3)\mathbf{c}_1 + (-\tfrac{1}{2})\chi^E(\hat{C}_3^2)\mathbf{c}_1 + 1\chi^E(\hat{\sigma}_v)\mathbf{c}_1 + \\
&\quad (-\tfrac{1}{2})\chi^E(\hat{\sigma}_v')\mathbf{c}_1 + (-\tfrac{1}{2})\chi^E(\hat{\sigma}_v'')\mathbf{c}_1\Big] \\
&= \frac{2}{6}\left[1\begin{pmatrix}1&0\\0&1\end{pmatrix}\begin{pmatrix}1\\0\end{pmatrix} - \frac{1}{2}\begin{pmatrix}-\frac{1}{2}&-\frac{1}{2}\\ \frac{\sqrt{3}}{2}&-\frac{\sqrt{3}}{2}\end{pmatrix}\begin{pmatrix}1\\0\end{pmatrix} - \frac{1}{2}\begin{pmatrix}-\frac{1}{2}&\frac{1}{2}\\ -\frac{\sqrt{3}}{2}&-\frac{\sqrt{3}}{2}\end{pmatrix}\begin{pmatrix}1\\0\end{pmatrix} + \right. \\
&\quad \left. 1\begin{pmatrix}1&0\\0&-1\end{pmatrix}\begin{pmatrix}1\\0\end{pmatrix} - \frac{1}{2}\begin{pmatrix}-\frac{1}{2}&-\frac{1}{2}\\ -\frac{\sqrt{3}}{2}&\frac{\sqrt{3}}{2}\end{pmatrix}\begin{pmatrix}1\\0\end{pmatrix} - \frac{1}{2}\begin{pmatrix}-\frac{1}{2}&\frac{1}{2}\\ \frac{\sqrt{3}}{2}&\frac{\sqrt{3}}{2}\end{pmatrix}\begin{pmatrix}1\\0\end{pmatrix}\right] \\
&= \frac{2}{6}\left[1\begin{pmatrix}1\\0\end{pmatrix} - \frac{1}{2}\begin{pmatrix}-\frac{1}{2}\\ \frac{\sqrt{3}}{2}\end{pmatrix} - \frac{1}{2}\begin{pmatrix}-\frac{1}{2}\\ -\frac{\sqrt{3}}{2}\end{pmatrix} + 1\begin{pmatrix}1\\0\end{pmatrix} - \frac{1}{2}\begin{pmatrix}-\frac{1}{2}\\ -\frac{\sqrt{3}}{2}\end{pmatrix} - \frac{1}{2}\begin{pmatrix}-\frac{1}{2}\\ \frac{\sqrt{3}}{2}\end{pmatrix}\right] = \begin{pmatrix}1\\0\end{pmatrix}
\end{aligned}$$

store; find partner increasing γ

- $\Gamma = E; \gamma = 2; \chi_2^E(\hat{E}) = 0, \chi_2^E(\hat{C}_3) = \frac{\sqrt{3}}{2}, \chi_2^E(\hat{C}_3^2) = -\frac{\sqrt{3}}{2}, \chi_2^E(\hat{\sigma}_v) = 0, \chi_2^E(\hat{\sigma}_v') = -\frac{\sqrt{3}}{2}, \chi_2^E(\hat{\sigma}_v'') = \frac{\sqrt{3}}{2}; \mathbf{c}_1^{E(2)} \equiv \mathbf{P}_2^E \mathbf{c}_1$

$$\begin{aligned}
\mathbf{c}_1^{E(2)} &= \frac{2}{6}\Big[0\chi^E(\hat{E})\mathbf{c}_1 + (\tfrac{\sqrt{3}}{2})\chi^E(\hat{C}_3)\mathbf{c}_1 + (-\tfrac{\sqrt{3}}{2})\chi^E(\hat{C}_3^2)\mathbf{c}_1 + 0\chi^E(\hat{\sigma}_v)\mathbf{c}_1 + \\
&\quad (-\tfrac{\sqrt{3}}{2})\chi^E(\hat{\sigma}_v')\mathbf{c}_1 + (\tfrac{\sqrt{3}}{2})\chi^E(\hat{\sigma}_v'')\mathbf{c}_1\Big] \\
&= \frac{2}{6}\left[0\begin{pmatrix}1&0\\0&1\end{pmatrix}\begin{pmatrix}1\\0\end{pmatrix} + \frac{\sqrt{3}}{2}\begin{pmatrix}-\frac{1}{2}&-\frac{1}{2}\\ \frac{\sqrt{3}}{2}&-\frac{\sqrt{3}}{2}\end{pmatrix}\begin{pmatrix}1\\0\end{pmatrix} - \frac{\sqrt{3}}{2}\begin{pmatrix}-\frac{1}{2}&\frac{1}{2}\\ -\frac{\sqrt{3}}{2}&-\frac{\sqrt{3}}{2}\end{pmatrix}\begin{pmatrix}1\\0\end{pmatrix} + \right. \\
&\quad \left. 0\begin{pmatrix}1&0\\0&-1\end{pmatrix}\begin{pmatrix}1\\0\end{pmatrix} - \frac{\sqrt{3}}{2}\begin{pmatrix}-\frac{1}{2}&-\frac{1}{2}\\ -\frac{\sqrt{3}}{2}&\frac{\sqrt{3}}{2}\end{pmatrix}\begin{pmatrix}1\\0\end{pmatrix} + \frac{\sqrt{3}}{2}\begin{pmatrix}-\frac{1}{2}&\frac{1}{2}\\ \frac{\sqrt{3}}{2}&\frac{\sqrt{3}}{2}\end{pmatrix}\begin{pmatrix}1\\0\end{pmatrix}\right] \\
&= \frac{2}{6}\left[\frac{\sqrt{3}}{2}\begin{pmatrix}-\frac{1}{2}\\ \frac{\sqrt{3}}{2}\end{pmatrix} - \frac{\sqrt{3}}{2}\begin{pmatrix}-\frac{1}{2}\\ -\frac{\sqrt{3}}{2}\end{pmatrix} - \frac{\sqrt{3}}{2}\begin{pmatrix}-\frac{1}{2}\\ -\frac{\sqrt{3}}{2}\end{pmatrix} + \frac{\sqrt{3}}{2}\begin{pmatrix}-\frac{1}{2}\\ \frac{\sqrt{3}}{2}\end{pmatrix}\right] = \begin{pmatrix}0\\1\end{pmatrix}
\end{aligned}$$

two symmetry vectors found; finish

Scheme 4.6: Reduction of the direct product of the irreducible representations $A_1 \otimes E$ of the C_{3v} point group for the subspace given by the columns of $\mathbf{B}_3$. For clarity of presentation the basis vector $\mathbf{c}_1(E)$ is written as $\mathbf{c}_1$.

$$\mathbf{u}_5^{E(1)} = \left(\mathbf{p}_A^{A_1} \otimes \mathbf{d}_{xz}^{E(1)} | \mathbf{p}_A^{A_1} \otimes \mathbf{d}_{xz}^{E(2)}\right) \mathbf{c}_1^{E(1)}(A_1, E) = \mathbf{p}_A^{A_1} \otimes \mathbf{d}_{xz}^{E(1)} \tag{4.53}$$

$$\mathbf{u}_6^{E(2)} = \left(\mathbf{p}_A^{A_1} \otimes \mathbf{d}_{xz}^{E(1)} | \mathbf{p}_A^{A_1} \otimes \mathbf{d}_{xz}^{E(2)}\right) \mathbf{c}_1^{E(2)}(A_1, E) = \mathbf{p}_A^{A_1} \otimes \mathbf{d}_{xz}^{E(2)} \tag{4.54}$$

We can gather the symmetry-adapted vectors $\mathbf{c}_1^{E(1)}(A_1, E)$ and $\mathbf{c}_1^{E(2)}(A_1, E)$ in a matrix

$$\mathbf{C}^{E}(A_1, E) = (\mathbf{c}^{E(1)}(A_1, E)|\mathbf{c}^{E(2)}(A_1, E)) \tag{4.55}$$

This Clebsch-Gordan coefficient matrix for the direct product of $A_1 \otimes E$ is a straightforward extension of the scalar Clebsch-Gordan coefficient for one-dimensional irreducible representations given in Eq. (4.40) The projection procedure for the remaining four-dimensional subspaces is outlined in appendix B. In general, the overall symmetry-adapted vectors will be constructed as:

$$\mathbf{u}_i^{\Gamma(\gamma)} = (\,\mathbf{p}_L^{\Gamma'(1)} \otimes \boldsymbol{\ell}_\lambda^{\Gamma''(1)}|\,\mathbf{p}_L^{\Gamma'(1)} \otimes \boldsymbol{\ell}_\lambda^{\Gamma''(2)}|...|\,\mathbf{p}_L^{\Gamma'(d_{\Gamma'})} \otimes \boldsymbol{\ell}_\lambda^{\Gamma''(d_{\Gamma''})}\,)\; \mathbf{c}_j^{\Gamma(\gamma)}(\Gamma', \Gamma'') \tag{4.56}$$

The Clebsch-Gordan coefficient matrices for the C_{3v} example are given as:

$$C^{A_1}(A_1, A_1) = 1 \tag{4.57}$$

$$\mathbf{C}^{E}(A_1, E) = \begin{pmatrix} 1 & 0 \\ 0 & 1 \end{pmatrix} \tag{4.58}$$

$$\mathbf{C}^{E}(E, A_1) = \begin{pmatrix} 1 & 0 \\ 0 & 1 \end{pmatrix} \tag{4.59}$$

$$\left(\mathbf{C}^{A_1}(E, E)|\mathbf{C}^{A_2}(E, E)|\mathbf{C}^{E}(E, E)\right) = \left(\begin{array}{c|c|cc} \frac{1}{2} & 0 & \frac{1}{2} & 0 \\ 0 & \frac{1}{2} & 0 & -\frac{1}{2} \\ 0 & -\frac{1}{2} & 0 & -\frac{1}{2} \\ \frac{1}{2} & 0 & -\frac{1}{2} & 0 \end{array}\right) \tag{4.60}$$

Thus, if we resort the columns of $\mathbf{B}$ of our ammonia example according to its invariant subspaces,

$$\mathbf{B} = (\mathbf{B}_1|\mathbf{B}_2|\mathbf{B}_3|\mathbf{B}_4|\mathbf{B}_5|\mathbf{B}_6|\mathbf{B}_7|\mathbf{B}_8) \tag{4.61}$$

where the matrices $\mathbf{B}_i$ are built with the corresponding matrices for the subspaces in Eq. (4.31) to Eq. (4.38) then the $\mathbf{U}$ symmetrization matrix is given by:

$$\begin{aligned}\mathbf{U} = \mathbf{B}\Big(& C^{A_1}(A_1, A_1) \oplus C^{A_1}(A_1, A_1) \oplus \mathbf{C}^{E}(A_1, E) \oplus \mathbf{C}^{E}(A_1, E) \oplus \\ & \mathbf{C}^{E}(E, A_1) \oplus \mathbf{C}^{E}(E, A_1) \oplus \mathbf{C}(E, E) \oplus \mathbf{C}(E, E)\Big)\end{aligned} \tag{4.62}$$

Here $\mathbf{C}(E, E)$ is given by Eq. (4.60). Also it can be shown that Eq. (4.56) can be equivalently written as:

$$\mathbf{u}_{\mathring{i}}^{\Gamma(\gamma)} = \sum_{\delta'}^{d_{\Gamma'}} \sum_{\delta''}^{d_{\Gamma''}} C^{\Gamma(\gamma)}_{\delta'\delta'', \gamma'\gamma''}(\Gamma', \Gamma'')\, \mathbf{p}_L^{\Gamma'(\delta')} \otimes \boldsymbol{\ell}_{\lambda}^{\Gamma''(\delta'')} \tag{4.63}$$

The Clebsch-Gordan expansion coefficients in Eq. (4.63) can be calculated as [93]:

$$C^{\Gamma(\gamma)}_{\delta'\delta'', \gamma'\gamma''}(\Gamma', \Gamma'') = \frac{d_\Gamma}{h} \sum_{R}^{h} \chi^{\Gamma}_{\gamma}(\hat{R})\ \chi^{\Gamma'}_{\delta'\gamma'}(\hat{R})\ \chi^{\Gamma''}_{\delta''\gamma''}(\hat{R}) \tag{4.64}$$

The double-index notation can be contracted into a single-index notation by the formula $i = d_{\Gamma''}(\delta' - 1) + \delta''$ and $j = d_{\Gamma''}(\gamma' - 1) + \gamma''$. Whereas the i index denotes the row index of the Clebsch-Gordan coefficient matrix, the selection of γ' and γ'' is not unique [94]. In our implementation, we perform this selection by applying all the $\hat{P}^{\Gamma}_{\gamma}$ operators defined in the direct product space of the irreducible representations,

$$\hat{P}^{\Gamma}_{\gamma} \rightarrow \mathbf{P}^{\Gamma}_{\gamma} = \frac{d_\Gamma}{h} \sum_{\hat{R}} \chi^{\Gamma}_{\gamma}\, \mathbf{D}^{\Gamma'\otimes\Gamma''}(\hat{R}) \tag{4.65}$$

to the corresponding basis vectors of this space

$$\{\mathbf{c}_j(\Gamma', \Gamma'')\} = \{\mathbf{c}_1(\Gamma', \Gamma''), \mathbf{c}_2(\Gamma', \Gamma''), ..., \mathbf{c}_{d_{\Gamma'} d_{\Gamma''}}(\Gamma', \Gamma'')\} \tag{4.66}$$

These projections are performed until we have obtained as many non-zero, linear independent symmetry-adapted vectors as original basis vectors. This procedure is depicted in Scheme 4.7. In this Scheme we first loop over all irreducible representations Γ in the point group, then we loop over the basis vectors of the subspace given by Eq.

for Γ **do**
  for $j = 1, d_{\Gamma'} \cdot d_{\Gamma''}$ **do**
    if $\mathbf{P}_1^{\Gamma}\mathbf{c}_j(\Gamma', \Gamma'')$ is valid **then**
      $\mathbf{C} \leftarrow \hat{P}_1^{\Gamma}\mathbf{c}_j(\Gamma', \Gamma'')$
      for $\gamma = 2, d_{\Gamma}$ **do**
        $\mathbf{C} \leftarrow \hat{P}_{\gamma}^{\Gamma}\mathbf{c}_j(\Gamma', \Gamma'')$
      end for
      if $\mathrm{Rank}(\mathbf{C}) = d_{\Gamma'} \cdot d_{\Gamma''}$ **then**
        Finish
      end if
    end if
  end for
end for

Scheme 4.7: Pseudocode for building the Clebsch-Gordan coefficient matrix for the direct product of irreducible representations Γ' and Γ''. Here a symmetry-adapted column vector is "valid" when it is non-zero and linear independent to the previous found vectors stored in matrix $\mathbf{C}$. The left arrow means to add the column vector to the matrix $\mathbf{C}$ (initially empty).

(4.66) as a standard basis [95]. The projector matrix representations given by Eq. (4.65) are applied to the column vectors $\{\mathbf{c}_j(\Gamma', \Gamma'')\}$ until we have obtained $d_{\Gamma'} \cdot d_{\Gamma''}$ non-zero, linear independent symmetry-adapted vectors. With this procedure the columns of the Clebsch-Gordan coefficient matrix are uniquely defined.

To elaborate more on the cumulative column index $\mathring{l}$ of the $\mathbf{U}$ symmetrization matrix we list it in Table 4.2 for the here discussed example. The corresponding symmetry-adapted auxiliary functions are shown in Figure 4.3, 4.4 and 4.5. One of the interesting symmetries of the symmetry-adapted auxiliary functions in the ammonia example is the A_2 irreducible representation which arises from the direct product reduction of $E \otimes E$. The two symmetry-adapted A_2 auxiliary functions, $\mathring{k}_5^{A_2}$ and $\mathring{k}_6^{A_2}$ are depicted at the bottom of Figure 4.3. This irreducible representation is symmetric under the rotations $\hat{C}_3$ and $\hat{C}_3^2$ but antisymmetric under the reflections $\hat{\sigma}_v$, $\hat{\sigma}_v'$ and $\hat{\sigma}_v''$ of the C_{3v} point group. The symmetry-adapted auxiliary functions belonging to irreducible representation E are degenerate in couples. These couples are shown together in each row of the Figures 4.4 and 4.5.

$\mathring{l}$	Γ	γ	L	λ	Γ'	Γ''	γ'	γ''	$\mathbf{u}_{\mathring{l}}^{\Gamma(\gamma)}$
1	A_1	1	H_A	**xx**	A_1	A_1	1	1	$\mathbf{p}_A^{A_1} \otimes \mathbf{d}_{\mathbf{xx}}^{A_1}$
2	A_1	1	H_A	**zz**	A_1	A_1	1	1	$\mathbf{p}_A^{A_1} \otimes \mathbf{d}_{\mathbf{zz}}^{A_1}$
3	A_1	1	H_A	**xx**	E	E	1	1	$\frac{1}{2}\mathbf{p}_A^{E(1)} \otimes \mathbf{d}_{\mathbf{xx}}^{E(1)} + \frac{1}{2}\mathbf{p}_A^{E(2)} \otimes \mathbf{d}_{\mathbf{xx}}^{E(2)}$
4	A_1	1	H_A	**xz**	E	E	1	1	$\frac{1}{2}\mathbf{p}_A^{E(1)} \otimes \mathbf{d}_{\mathbf{xz}}^{E(1)} + \frac{1}{2}\mathbf{p}_A^{E(2)} \otimes \mathbf{d}_{\mathbf{xz}}^{E(2)}$
5	A_2	1	H_A	**xx**	E	E	1	2	$\frac{1}{2}\mathbf{p}_A^{E(1)} \otimes \mathbf{d}_{\mathbf{xx}}^{E(2)} - \frac{1}{2}\mathbf{p}_A^{E(2)} \otimes \mathbf{d}_{\mathbf{xx}}^{E(1)}$
6	A_2	1	H_A	**xz**	E	E	1	2	$\frac{1}{2}\mathbf{p}_A^{E(1)} \otimes \mathbf{d}_{\mathbf{xz}}^{E(2)} - \frac{1}{2}\mathbf{p}_A^{E(2)} \otimes \mathbf{d}_{\mathbf{xz}}^{E(1)}$
7	E	1	H_A	**xx**	A_1	E	1	1	$\mathbf{p}_A^{A_1} \otimes \mathbf{d}_{\mathbf{xx}}^{E(1)}$
8	E	1	H_A	**xz**	A_1	E	1	1	$\mathbf{p}_A^{A_1} \otimes \mathbf{d}_{\mathbf{xz}}^{E(1)}$
9	E	1	H_A	**xx**	E	A_1	1	1	$\mathbf{p}_A^{E(1)} \otimes \mathbf{d}_{\mathbf{xx}}^{A_1}$
10	E	1	H_A	**zz**	E	A_1	1	1	$\mathbf{p}_A^{E(1)} \otimes \mathbf{d}_{\mathbf{zz}}^{A_1}$
11	E	1	H_A	**xx**	E	E	1	1	$\frac{1}{2}\mathbf{p}_A^{E(1)} \otimes \mathbf{d}_{\mathbf{xx}}^{E(1)} - \frac{1}{2}\mathbf{p}_A^{E(2)} \otimes \mathbf{d}_{\mathbf{xx}}^{E(2)}$
12	E	1	H_A	**xz**	E	E	1	1	$\frac{1}{2}\mathbf{p}_A^{E(1)} \otimes \mathbf{d}_{\mathbf{xz}}^{E(1)} - \frac{1}{2}\mathbf{p}_A^{E(2)} \otimes \mathbf{d}_{\mathbf{xz}}^{E(2)}$
13	E	2	H_A	**xx**	A_1	E	1	1	$\mathbf{p}_A^{A_1} \otimes \mathbf{d}_{\mathbf{xx}}^{E(2)}$
14	E	2	H_A	**xz**	A_1	E	1	1	$\mathbf{p}_A^{A_1} \otimes \mathbf{d}_{\mathbf{xz}}^{E(2)}$
15	E	2	H_A	**xx**	E	A_1	1	1	$\mathbf{p}_A^{E(2)} \otimes \mathbf{d}_{\mathbf{xx}}^{A_1}$
16	E	2	H_A	**zz**	E	A_1	1	1	$\mathbf{p}_A^{E(2)} \otimes \mathbf{d}_{\mathbf{zz}}^{A_1}$
17	E	2	H_A	**xx**	E	E	1	1	$-\frac{1}{2}\mathbf{p}_A^{E(1)} \otimes \mathbf{d}_{\mathbf{xx}}^{E(2)} - \frac{1}{2}\mathbf{p}_A^{E(2)} \otimes \mathbf{d}_{\mathbf{xx}}^{E(1)}$
18	E	2	H_A	**xz**	E	E	1	1	$-\frac{1}{2}\mathbf{p}_A^{E(1)} \otimes \mathbf{d}_{\mathbf{xz}}^{E(2)} - \frac{1}{2}\mathbf{p}_A^{E(2)} \otimes \mathbf{d}_{\mathbf{xz}}^{E(1)}$

Table 4.2: List of the column indices of the overall **U** symmetrization matrix composed from symmetry-adapted atomic permutation vectors and symmetry-adapted function vectors for the ammonia example in C_{3v} symmetry. The vectors have been sorted by irreducible representations and enumerated.

In order to achieve block diagonalization of the **G** matrix for the invariant under consideration, the columns of **U** have to be sorted according to their irreducible representations. Furthermore, the here outlined construction of the symmetrization matrix part for an invariant has to be performed for all invariants of a molecule. The resulting symmetrization matrix blocks can then be combined into the complete **U** symmetrization matrix. However, in our actual deMon2k implementation the complete symmetrization matrix $\mathbf{U}_{\text{bas}}$ is only built for the blocking of the Kohn-Sham matrix. The corresponding symmetrization matrix for the auxiliary functions, $\mathbf{U}_{\text{aux}}$, is not explicitly constructed. Instead, we perform the transformation of the Coulomb matrix and vector into symmetry-adapted representations element by element, looping over the $\mathring{k}$ and $\mathring{l}$ cumulative indices of all the invariants for each pair Γ, γ. This approach is particularly memory efficient

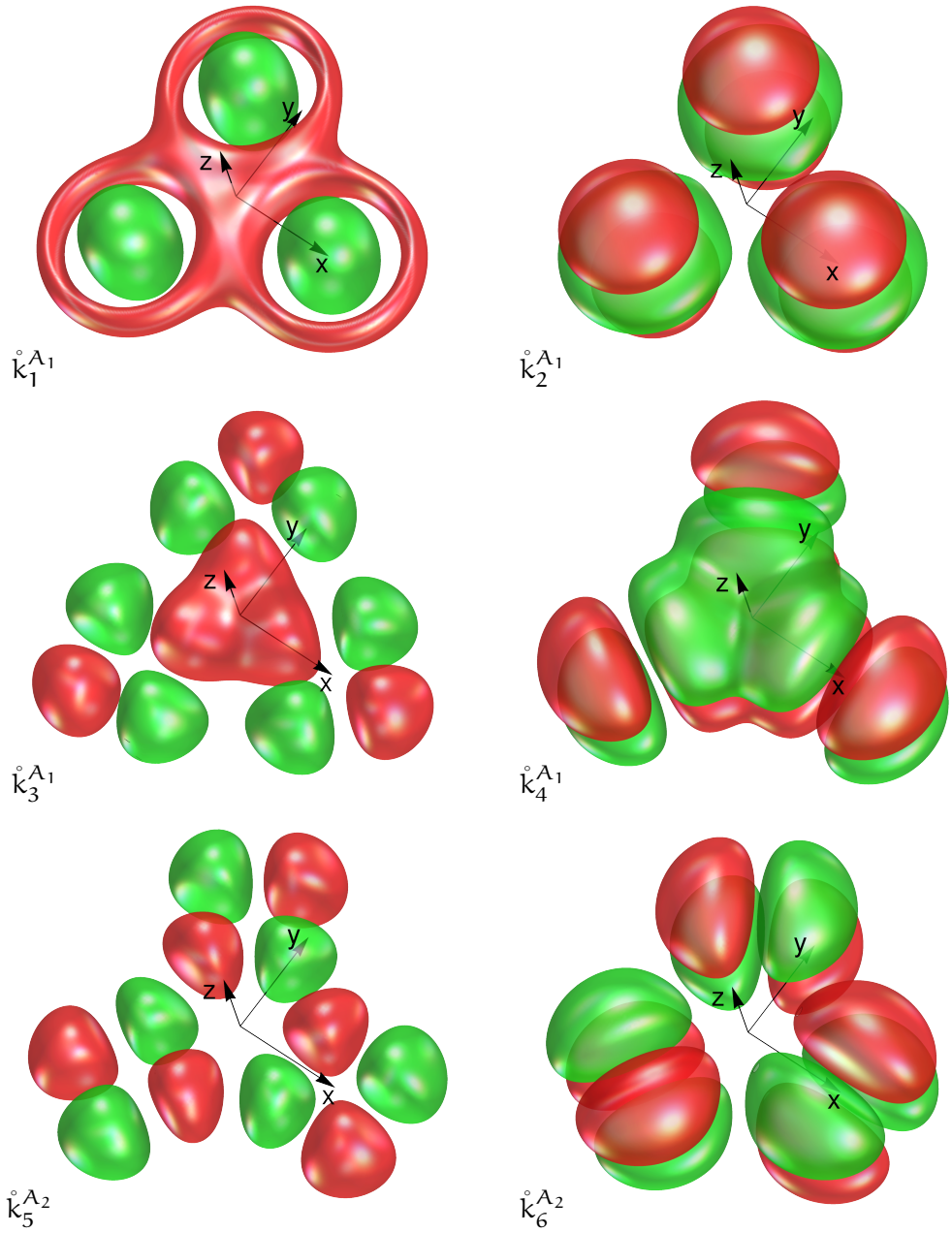

Figure 4.3: Symmetry-adapted auxiliary functions for the C_{3v} ammonia example with symmetry A_1 and A_2.

because only the **V** and **W** matrices need to be computed and stored. Take as example the dodecahedrane molecule $C_{20}H_{20}$ in I_h symmetry shown at the bottom of Figure 3.2. The two symmetry-equivalent atom sets of hydrogen and carbon atoms give rise to **V** matrices with dimensions of 20×20. If the GEN-A2 auxiliary function set is used, three

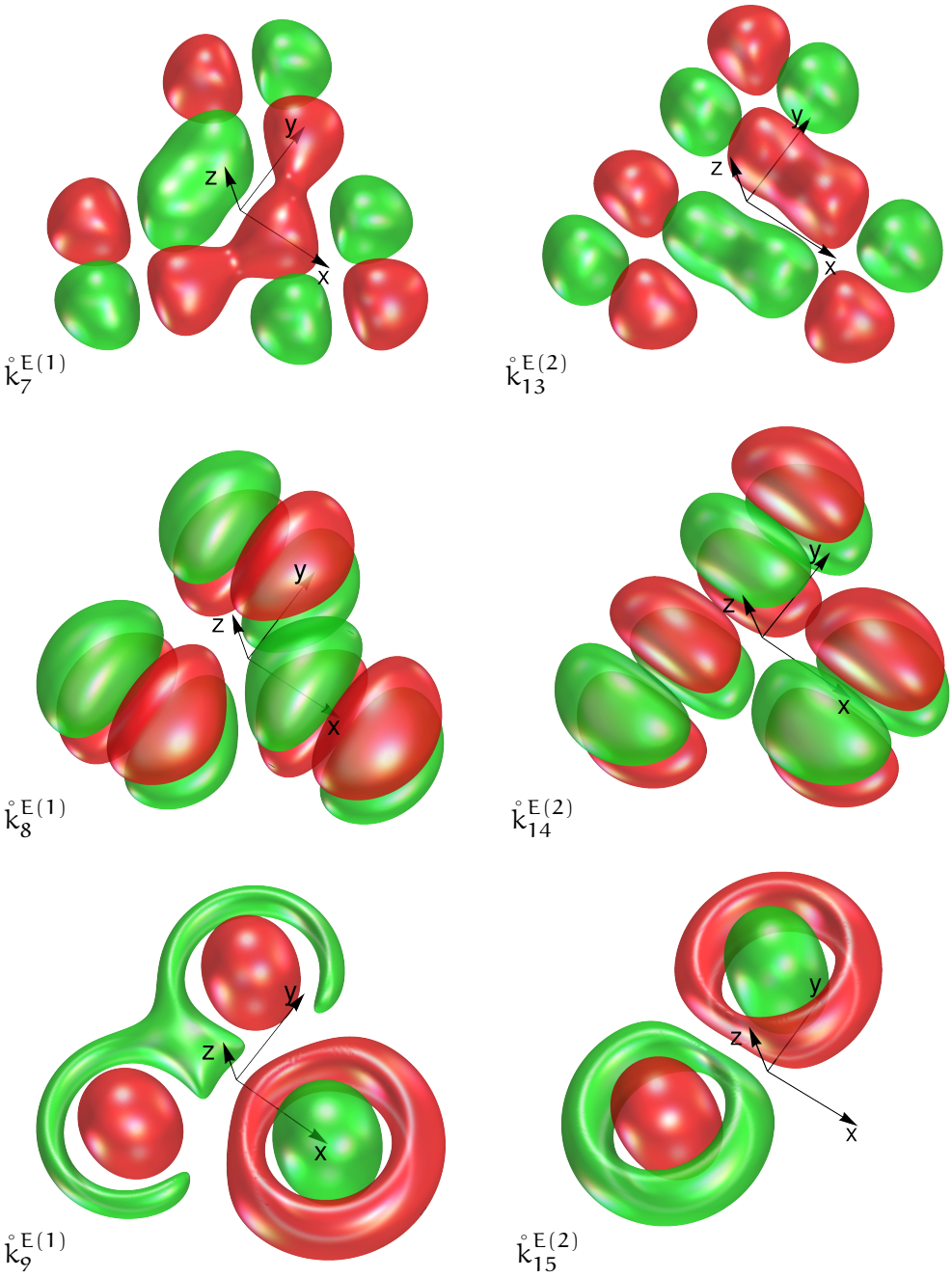

Figure 4.4: Symmetry-adapted auxiliary functions for the C_{3v} ammonia example with symmetry E (part 1).

W matrices for the s-, p- and d-type (auxiliary) functions are needed. Their matrix dimensions are 1×1, 3×3 and 6×6, respectively. In comparison, the complete **U** matrix has dimension 2300×2300. Obviously, this is an enormous reduction in memory demand.

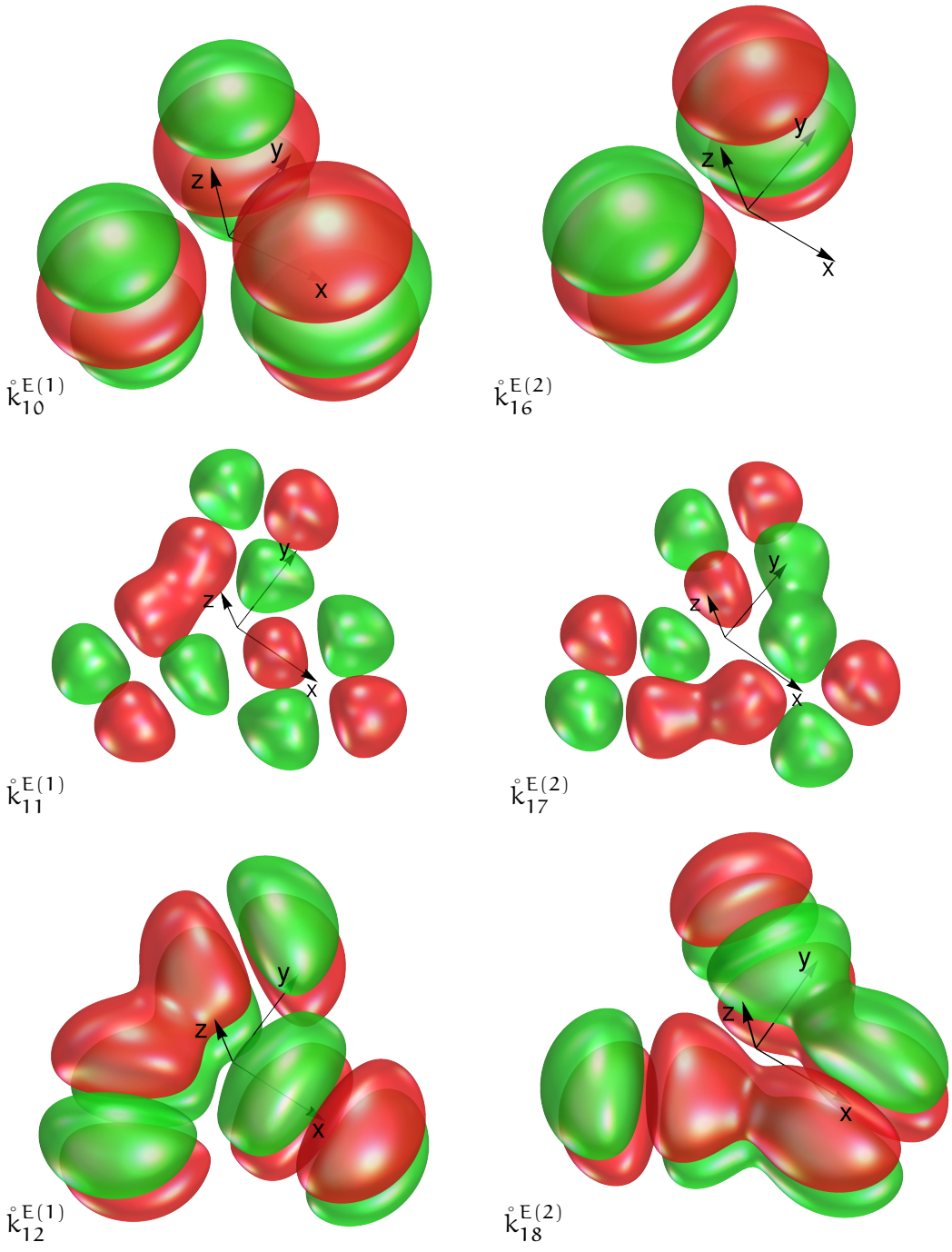

Figure 4.5: Symmetry-adapted auxiliary functions for the C_{3v} ammonia example with symmetry E (part 2).

4.2 Construction of the **U** matrix for spherical basis functions

In order to use the procedure outlined above for the construction of symmetrization matrices for spherical orbitals, the symmetrization matrix for Cartesian functions must be transformed to their spherical analog. To do so, we introduce the following basis transformation:

$$\mathbf{F}_{\text{sph}}(\hat{R}) = \mathbf{M}^{-}\,\mathbf{F}_{\text{Cart}}(\hat{R})\mathbf{M} \qquad \forall \quad \hat{R} \tag{4.67}$$

The matrix $\mathbf{M}$ is in general rectangular. This is so because the Cartesian matrix representations have dimension $(\frac{(\ell+1)(\ell+2)}{2}) \times (\frac{(\ell+1)(\ell+2)}{2})$ whereas the spherical matrix representations have dimension $(2\ell+1)\times(2\ell+1)$. Therefore, the matrix $\mathbf{M}^{-}$ is a Moore-Penrose pseudoinverse such that the matrix product $\mathbf{M}^{-}\mathbf{M}$ yields the identity matrix of dimension $(2\ell+1)\times(2\ell+1)$. The elements of $\mathbf{M}$ are given by [96]:

$$M_{a,\ell m} = \begin{cases} \frac{1}{\sqrt{2}}(c(\ell,m,\mathbf{a}) + c(\ell,-m,\mathbf{a})) & m < 0 \\ c(\ell,0,\mathbf{a}) & m = 0 \\ \frac{1}{\sqrt{-2}}(c(\ell,m,\mathbf{a}) - c(\ell,-m,\mathbf{a})) & m > 0 \end{cases} \tag{4.68}$$

with

$$\begin{aligned} c(\ell,m,\mathbf{a}) =& \frac{1}{2^{\ell}\ell!}\sqrt{\frac{(2a_x)!\,(2a_y)!\,(2a_z)!\ell!(\ell-|m|)!}{(2\ell)!a_x!a_y!a_z!(\ell+|m|)!}}\sum_{i=0}^{(\ell-|m|)/2}\binom{\ell}{i}\binom{i}{j}\frac{(-1)^i(2\ell-2i)!}{(\ell-|m|-2i)!} \\ &\cdot\sum_{k=0}^{j}\binom{j}{k}\binom{|m|}{a_x-2k} \\ &\cdot\begin{cases}(-1)^{(|m|-a_x+2k)/2} & m \geqslant 0 \\ (-1)^{-(|m|-a_x+2k)/2} & m < 0\end{cases};\ j = (a_x+a_y-|m|)/2 \end{aligned} \tag{4.69}$$

Here, $\mathbf{a} = (a_x, a_y, a_z)$ is the angular momentum index of the Cartesian function and the pair (ℓ, m) the pointer to real spherical (harmonics) Gaussian functions. If j is not an

integer, $M_{a,\ell m}$ is zero. Furthermore, any term that includes the factorial of a negative number is neglected. The elements of the back transformation matrix $\mathbf{M}^{-}$ are:

$$M^{-}_{\ell m,a} = \sum_{b_x+b_y+b_z=\ell} S_{ab} \cdot M_{b,\ell m} \tag{4.70}$$

with $\ell = a_x + a_y + a_z = b_x + b_y + b_z$ and

$$\begin{aligned} S_{ab} = &\left[\frac{(a_x+b_x)!\,(a_y+b_y)!\,(a_z+b_z)!}{((a_x+b_x)/2)!\,((a_y+b_y)/2)!\,((a_z+b_z)/2)!}\right] \\ &\cdot\left[\frac{(2a_x)!\,(2a_y)!\,(2a_z)!\,(2b_x)!\,(2b_y)!\,(2b_z)!}{a_x!a_y!a_z!b_x!b_y!b_z!}\right]^{-1/2} \end{aligned} \tag{4.71}$$

Here $(a_x+b_x)/2$, $(a_y+b_y)/2$ and $(a_z+b_z)/2$ must be integers, otherwise $S_{ab} = 0$. In deMon2k these transformation matrices are built and stored for angular momentum up to $\ell = 8$. For higher angular momentum the matrix elements can be calculated on the fly. In particular for d-type atomic orbitals the transformation matrices $\mathbf{M}$ and $\mathbf{M}^{-}$ are:

$$\mathbf{M} = \begin{pmatrix} 0 & 0 & -\frac{1}{2} & 0 & \frac{\sqrt{3}}{2} \\ 1 & 0 & 0 & 0 & 0 \\ 0 & 0 & 0 & 1 & 0 \\ 0 & 0 & -\frac{1}{2} & 0 & -\frac{\sqrt{3}}{2} \\ 0 & 1 & 0 & 0 & 0 \\ 0 & 0 & 1 & 0 & 0 \end{pmatrix}, \quad \mathbf{M}^{-} = \begin{pmatrix} 0 & 1 & 0 & 0 & 0 & 0 \\ 0 & 0 & 0 & 0 & 1 & 0 \\ -\frac{1}{3} & 0 & 0 & -\frac{1}{3} & 0 & \frac{2}{3} \\ 0 & 0 & 1 & 0 & 0 & 0 \\ \frac{1}{\sqrt{3}} & 0 & 0 & -\frac{1}{\sqrt{3}} & 0 & 0 \end{pmatrix} \tag{4.72}$$

After obtaining the spherical representations matrices of the symmetry operations, we use them in the usual reduction procedure to built a symmetrization matrix $\mathbf{W}$ for the spherical basis. For the ammonia example the (5×5) matrix representations $\mathbf{F}_{\text{sph}}(\hat{R})$ are:

$$\mathbf{F}(\hat{E}) = \begin{pmatrix} 1 & 0 & 0 & 0 & 0 \\ 0 & 1 & 0 & 0 & 0 \\ 0 & 0 & 1 & 0 & 0 \\ 0 & 0 & 0 & 1 & 0 \\ 0 & 0 & 0 & 0 & 1 \end{pmatrix}, \quad \mathbf{F}(\hat{C}_3) = \begin{pmatrix} -\frac{1}{2} & 0 & 0 & 0 & -\frac{\sqrt{3}}{2} \\ 0 & -\frac{1}{2} & 0 & \frac{\sqrt{3}}{2} & 0 \\ 0 & 0 & 1 & 0 & 0 \\ 0 & -\frac{\sqrt{3}}{2} & 0 & -\frac{1}{2} & 0 \\ \frac{\sqrt{3}}{2} & 0 & 0 & 0 & -\frac{1}{2} \end{pmatrix}, \tag{4.73}$$

$$\mathbf{F}(\hat{C}_3^2) = \begin{pmatrix} -\frac{1}{2} & 0 & 0 & 0 & \frac{\sqrt{3}}{2} \\ 0 & -\frac{1}{2} & 0 & -\frac{\sqrt{3}}{2} & 0 \\ 0 & 0 & 1 & 0 & 0 \\ 0 & \frac{\sqrt{3}}{2} & 0 & -\frac{1}{2} & 0 \\ -\frac{\sqrt{3}}{2} & 0 & 0 & 0 & -\frac{1}{2} \end{pmatrix}, \quad \mathbf{F}(\hat{\sigma}_v) = \begin{pmatrix} -1 & 0 & 0 & 0 & 0 \\ 0 & -1 & 0 & 0 & 0 \\ 0 & 0 & 1 & 0 & 0 \\ 0 & 0 & 0 & 1 & 0 \\ 0 & 0 & 0 & 0 & 1 \end{pmatrix}, \tag{4.74}$$

$$\mathbf{F}(\hat{\sigma}_v') = \begin{pmatrix} \frac{1}{2} & 0 & 0 & 0 & \frac{\sqrt{3}}{2} \\ 0 & \frac{1}{2} & 0 & -\frac{\sqrt{3}}{2} & 0 \\ 0 & 0 & 1 & 0 & 0 \\ 0 & -\frac{\sqrt{3}}{2} & 0 & -\frac{1}{2} & 0 \\ \frac{\sqrt{3}}{2} & 0 & 0 & 0 & -\frac{1}{2} \end{pmatrix}, \mathbf{F}(\hat{\sigma}_v'') = \begin{pmatrix} \frac{1}{2} & 0 & 0 & 0 & -\frac{\sqrt{3}}{2} \\ 0 & \frac{1}{2} & 0 & \frac{\sqrt{3}}{2} & 0 \\ 0 & 0 & 1 & 0 & 0 \\ 0 & \frac{\sqrt{3}}{2} & 0 & -\frac{1}{2} & 0 \\ -\frac{\sqrt{3}}{2} & 0 & 0 & 0 & -\frac{1}{2} \end{pmatrix} \tag{4.75}$$

In general, for any symmetry operation of any point group the spherical d-type function matrix representations are given in terms of the three-dimensional Cartesian representations by:

$$\mathbf{F}(\hat{R}) = \begin{pmatrix} R_{12}R_{21} + R_{11}R_{22} & R_{13}R_{22} + R_{12}R_{23} & \sqrt{3}R_{13}R_{23} & R_{13}R_{21} + R_{11}R_{23} & R_{11}R_{21} - R_{12}R_{22} \\ R_{22}R_{31} + R_{21}R_{32} & R_{23}R_{32} + R_{22}R_{33} & \sqrt{3}R_{23}R_{33} & R_{23}R_{31} + R_{21}R_{33} & R_{21}R_{31} - R_{22}R_{32} \\ \sqrt{3}R_{31}R_{32} & \sqrt{3}R_{32}R_{33} & \frac{3R_{33}^2}{2} - \frac{1}{2} & \sqrt{3}R_{31}R_{33} & \frac{1}{2}\sqrt{3}\left(R_{31}^2 - R_{32}^2\right) \\ R_{12}R_{31} + R_{11}R_{32} & R_{13}R_{32} + R_{12}R_{33} & \sqrt{3}R_{13}R_{33} & R_{13}R_{31} + R_{11}R_{33} & R_{11}R_{31} - R_{12}R_{32} \\ R_{11}R_{12} - R_{21}R_{22} & R_{12}R_{13} - R_{22}R_{23} & \frac{1}{2}\sqrt{3}\left(R_{13}^2 - R_{23}^2\right) & R_{11}R_{13} - R_{21}R_{23} & \frac{1}{2}\left(R_{11}^2 - R_{12}^2 - R_{21}^2 + R_{22}^2\right) \end{pmatrix} \tag{4.76}$$

Comparison of the symmetry-adapted d-type Cartesian atomic orbitals and the symmetry-adapted d-type spherical atomic orbitals are shown in Figure 4.6. As this figure shows the only difference is in the A_1 irreducible representation. The SAOs of the irreducible representation E are the same in Cartesian or spherical basis functions. As this discussion showed, for the construction of the symmetrization matrices **U** for the basis or auxiliary functions, we need the point group tables in order to define the projector and transfer operators. Their implementation into deMon2k is described in the next chapter.

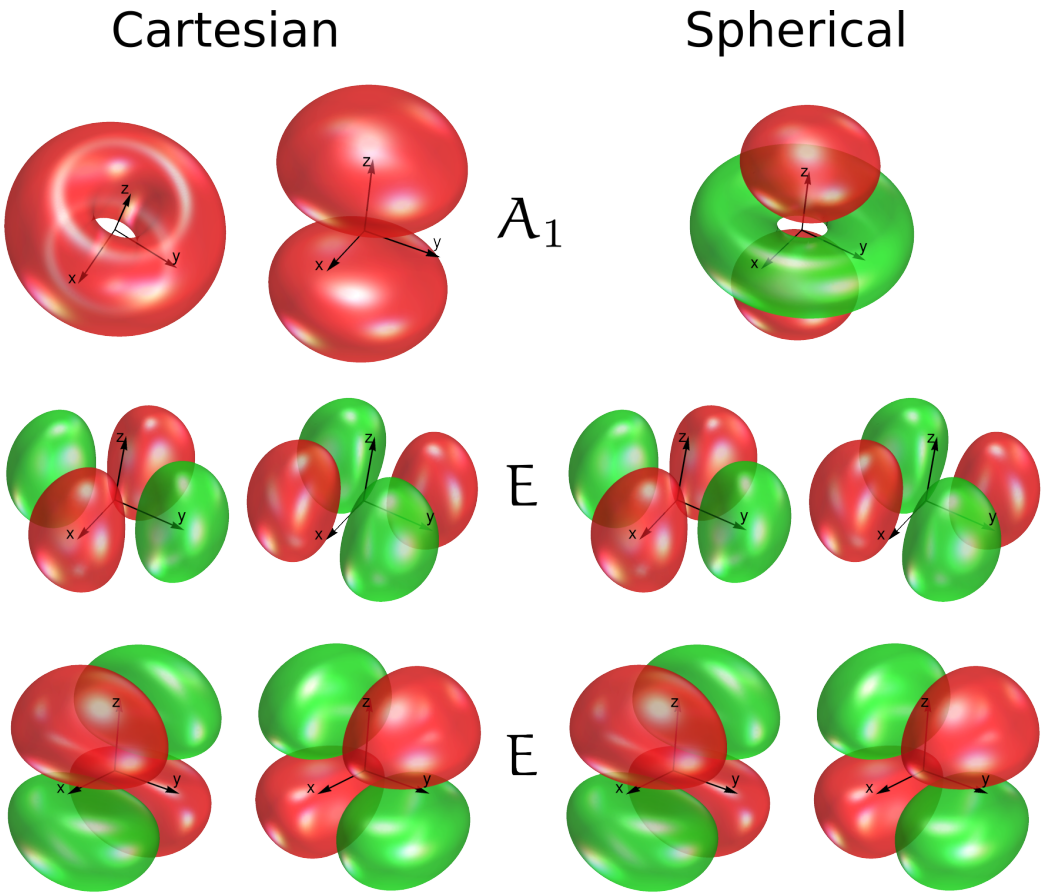

Figure 4.6: Comparison of real symmetry-adapted atomic d-orbitals from Cartesian and spherical basis functions.

5

POINT GROUP REPRESENTATIONS

5.1 Point group tables in deMon2k

The tables for the following point groups were included in deMon2k as part of the development of this thesis: C_i, C_s, C_n, C_{nv}, C_{nh}, D_n, D_{nd}, D_{nh}, S_4, S_6, T, T_d, T_h, O, O_h, I, I_h, $C_{\infty v}$ and $D_{\infty h}$, with $n = 2, ..., 6$. Most of these tables were taken from the StoBe code [97], which in turn took them from the literature [98]. Prior to implementation, they were transformed into real form in order to avoid complex arithmetic. The point group tables for I, I_h, $C_{\infty v}$ and $D_{\infty h}$ are generated in this thesis because they were not available in StoBe. For these tables, the same literature, albeit in a newer edition [72], was taken as reference. For the implementation in deMon2k, special care was taken to align the molecule into the (standard) orientation used in these tables.

5.2 Construction of $C_{\infty v}$ point group table cut outs

We now describe the construction of real irreducible representations for the point groups $C_{\infty v}$ in such a manner that they become finite and, therefore, can be computed. Our aim is to build projector and transfer operators for the symmetry adaptation of the AO basis and auxiliary functions. To this end, we need enough irreducible representations to span completely the space of the basis functions. Take as an example the $C_{\infty v}$ point group for which the Cartesian tensor bases of the initial irreducible representation are given in Table 5.1. As this table shows s-type basis functions with total angular momentum 0 only project on to the $\Sigma^+(A_1)$ irreducible representation. Furthermore, p-type functions with

	Rank of Cartesian tensor			
$C_{\infty v}$	0	1	2	3
$A_1\,(\Sigma^+)$	1	z	x^2+y^2, z^2	$(x^2+y^2)\,z, z^3$
$A_2\,(\Sigma^-)$				
$E_1(\Pi)$		(x, y)	(zx, yz)	$\{x\,(x^2+y^2), y\,(x^2+y^2)\}, (xz^2, yz^2)$
$E_2(\Delta)$			(xy, x^2-y^2)	$\{xyz, z\,(x^2-y^2)\}$
$E_3(\Phi)$				$\{x\,(x^2-3y^2), y\,(3x^2-y^2)\}$

Table 5.1: Symmetry-adapted Cartesian tensors of point group $C_{\infty v}$ [72].

total angular momentum 1 project on to the one-dimensional irreducible representation $\Sigma^+(A_1)$ and the two-dimensional irreducible representation $\Pi(E_1)$. The corresponding symmetry-adapted functions, in standard orientation, are $p_z^{\Sigma^+}$ and $(p_x, p_y)^{\Pi}$. For the d-type Cartesian function shell, we obtain as symmetry-adapted functions:

$$(d_{xx}+d_{yy})^{\Sigma^+}, d_{zz}^{\Sigma^+}, (d_{xz}, d_{yz})^{\Pi}, (d_{xy}, d_{xx}-d_{yy})^{\Delta} \tag{5.1}$$

The shell of the Cartesian f-type functions will also project on to the $\Phi(E_3)$ irreducible representation. This indicates that the number of irreducible representations needed to completely span the function space of the basis or auxiliary functions depends on the maximum total angular momentum of the underlying function set. Note that this number of necessary irreducible representations is the same for Cartesian and spherical Gaussian type orbitals as well as for Hermite Gaussian type auxiliary functions. Therefore, if the largest total angular momentum in the basis or auxiliary function set is $\ell = 1$ only the irreducible representations Σ^+ and Π are needed. Similarly, if the largest total angular momentum in the function set under consideration is $\ell = 2$ only the irreducible representations Σ^+, Π and Δ are needed. This can be straightforwardly generalized. Therefore, taking Σ^- also into account the number of irreducible representations, N_Γ, needed for the symmetry-adapted expansion of a basis or auxiliary function set with total angular momentum ℓ is given by:

$$N_\Gamma = 2 + \ell \tag{5.2}$$

The next step is to generate the matrix representations for the symmetry operations (rotations). The values of the determinants of these matrices are either $+1$ or -1. If the determinant value is $+1$ we call the symmetry operation a proper rotation, if it is -1 we call it an improper rotation. For $C_{\infty v}$ proper rotations refer to $\hat{C}$ rotations whereas improper rotations refer to $\hat{\sigma}$ reflections. The irreducible representations Σ^+ and Σ^- are one-dimensional. For Σ^+ all representations are $+1$ for proper rotations and -1 for improper rotations, i.e. reflections. All following irreducible representations in $C_{\infty v}$ are two-dimensional. They can be most conveniently expressed by the following complex form [72]:

$$\chi^{E_m}(\hat{C}(\phi)) = \begin{pmatrix} e^{-im\phi} & 0 \\ 0 & e^{im\phi} \end{pmatrix} \tag{5.3}$$

$$\chi^{E_m}(\hat{\sigma}(\phi)) = (-1)^m \begin{pmatrix} 0 & e^{-im\phi} \\ e^{im\phi} & 0 \end{pmatrix} \tag{5.4}$$

To ease the discussion, we switch to Mulliken notation that is more systematic but less common in Chemistry, where the spectroscopic notation with greek letters is preferred. To transform the complex two-dimensional irreducible representations of Eqs. (5.3) and (5.4) into real form we employ the following symmetrization matrix [76]:

$$\mathbf{U} = \frac{1}{\sqrt{2}} \begin{pmatrix} 1 & -i \\ 1 & i \end{pmatrix} \tag{5.5}$$

Thus, we obtain the following real two-dimensional representations:

$$\chi^{E_m}(\hat{C}(\phi)) = \begin{pmatrix} \cos(m\phi) & -\sin(m\phi) \\ \sin(m\phi) & \cos(m\phi) \end{pmatrix} \tag{5.6}$$

$$\chi^{E_m}(\hat{\sigma}(\phi)) = (-1)^m \begin{pmatrix} \cos(m\phi) & \sin(m\phi) \\ \sin(m\phi) & -\cos(m\phi) \end{pmatrix} \tag{5.7}$$

These representations are defined for any angle ϕ since the point group is infinite. As our purpose is to find a finite cut out of this infinite point group, we need to define a finite set of angles $\{\phi_n\}$ for each symmetry operation. These angles will depend on the number, h, of symmetry operations considered, and the symmetry operation index, n, that enumerates the proper rotations and reflections taking the values $n = 1, 2, ..., h/2$. For elucidating this dependency, we take the example of p-type functions. We demand that the p_x and p_y functions remain the same or transform into each other under application of any symmetry operation. For this we need symmetry operations that transform the functions as follows

$$\begin{aligned} &\hat{R}p_x = \pm p_x \\ \text{or} \quad &\hat{R}p_x = \pm p_y \end{aligned} \tag{5.8}$$

These equations are accompanied by analogous rotations for the p_y function. The proper rotations that accomplish Eq. (5.8) are the ones that divide the unit circle in quadrants, i.e. $2\pi(n-1)/4$ with $n = 1, 2, 3, 4$. These 4 proper rotations are accompanied in our $C_{\infty v}$ cut outs by four improper rotations, i.e. reflections. Therefore, the number of symmetry operations and, thus, the group order is $h = 8$. Knowledge of the rotation angles allow us to write the proper rotations in standard notation:

$$\hat{C}\left(\frac{2\pi(n-1)}{h/2}\right) = \hat{C}_{h/2}^{n-1} \tag{5.9}$$

Thus, the 8 symmetry operations we have are $\hat{E} = \hat{C}_4^0$, $\hat{C}_4$, $\hat{C}_4^2$, $\hat{C}_4^3$, $\hat{\sigma}_v$, $\hat{\sigma}_v^2$, $\hat{\sigma}_v^3$, and $\hat{\sigma}_v^4$. For convenience we have enumerated the reflection operations $\hat{\sigma}_v^n$ instead of using primes. This defines all symmetry operations in our finite dimension $C_{\infty v}$ point group cut out needed for function sets that contain up to p-type functions. Thus, we have

defined a set of angles to insert in Eq. (5.6) and Eq. (5.7). These angles are given in general by:

$$\phi_n = \frac{2\pi(n-1)}{h/2} \qquad \text{with} \qquad n = 1, 2, ..., h/2 \tag{5.10}$$

Therefore we can rewrite Eq. (5.6) and (5.7) as:

$$\chi^{E_m}(\hat{C}^{n-1}_{h/2}) = \begin{pmatrix} \cos(m\phi_n) & -\sin(m\phi_n) \\ \sin(m\phi_n) & \cos(m\phi_n) \end{pmatrix} \tag{5.11}$$

$$\chi^{E_m}(\hat{\sigma}^n_v) = (-1)^m \begin{pmatrix} \cos(m\phi_n) & \sin(m\phi_n) \\ \sin(m\phi_n) & -\cos(m\phi_n) \end{pmatrix} \tag{5.12}$$

The finite part of the infinite $C_{\infty v}$ point group given by the symmetry operations $\{\hat{E}, \hat{C}_4, \hat{C}_4^2, \hat{C}_4^3, \hat{\sigma}_v, \hat{\sigma}_v^2, \hat{\sigma}_v^3, \hat{\sigma}_v^4\}$ we just defined, is sufficient to describe the symmetry of s- and p-type functions, i.e. to built corresponding projection operators that generate symmetry-adapted s- and p-type functions for the irreducible representations under consideration. The generated point group table is depicted in Table 5.2.

$C_{\infty v}$	$\hat{E}$	$\hat{C}_4$	$\hat{C}_4^2$	$\hat{C}_4^3$	$\hat{\sigma}_v$	$\hat{\sigma}_v^2$	$\hat{\sigma}_v^3$	$\hat{\sigma}_v^4$
$A_1(\Sigma^+)$	1	1	1	1	1	1	1	1
$A_2(\Sigma^-)$	1	1	1	1	−1	−1	−1	−1
$E_1(\Pi)$	$\left(\begin{smallmatrix} 1 & 0 \\ 0 & 1 \end{smallmatrix}\right)$	$\left(\begin{smallmatrix} 0 & -1 \\ 1 & 0 \end{smallmatrix}\right)$	$\left(\begin{smallmatrix} -1 & 0 \\ 0 & -1 \end{smallmatrix}\right)$	$\left(\begin{smallmatrix} 0 & 1 \\ -1 & 0 \end{smallmatrix}\right)$	$\left(\begin{smallmatrix} -1 & 0 \\ 0 & 1 \end{smallmatrix}\right)$	$\left(\begin{smallmatrix} 0 & -1 \\ -1 & 0 \end{smallmatrix}\right)$	$\left(\begin{smallmatrix} 1 & 0 \\ 0 & -1 \end{smallmatrix}\right)$	$\left(\begin{smallmatrix} 0 & 1 \\ 1 & 0 \end{smallmatrix}\right)$

Table 5.2: Generated $C_{\infty v}$ point group table cut out for angular momentum up to $\ell = 1$.

The number of operations and therefore the angles ϕ_n will depend on the total angular momentum of the basis functions. To elucidate this dependency we take the example of the d-type functions depicted in Figure 5.1. We request that the functions $d_1 = 1/2(d_{xx} - d_{yy})$ and $d_2 = d_{xy}$ remain the same or transform into each other under

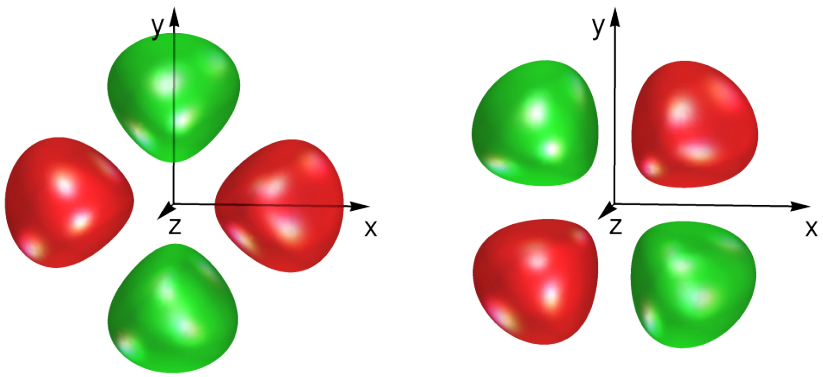

Figure 5.1: Hermite Gaussian functions $1/2(d_{xx} - d_{yy})$ at left and d_{xy} at right. These functions transform into each other according to the Δ irreducible representation of the $C_{\infty v}$ point group.

application of any symmetry operation. For this we need rotations that transform the functions as follows,

$$\begin{aligned} \hat{R}d_1 &= \pm d_1 \\ \text{or} \quad \hat{R}d_1 &= \pm d_2 \end{aligned} \tag{5.13}$$

and similar for the d_2 functions. The proper rotations that accomplish Eq. (5.13) are the ones that divide the unit circle in octants, i.e. $2\pi(n-1)/8$ with $n = 1, 2, ..., 8$. In the same way there are eight reflections that accomplish Eq. (5.13) and, therefore, we find as group order $h = 16$. The corresponding rotation angles are again given by Eq. (5.10). In order to be able to compare the differences between the different cut outs of $C_{\infty v}$ here presented, the generated point group table cut out for angular momentum up to d-type functions is shown in Tables 5.3 and 5.4.

In conclusion, we find that the group order for finite dimension cut outs of $C_{\infty v}$ is given in general by:

$$h = 8\ell \tag{5.14}$$

Here ℓ denotes the largest total angular momentum of the function set under consideration. By construction, the here derived finite-dimensional cut outs of the infinite point group

$C_{\infty v}$	$\hat{E}$	$\hat{C}_8$	$\hat{C}_8^2$	$\hat{C}_8^3$	$\hat{C}_8^4$	$\hat{C}_8^5$	$\hat{C}_8^6$	$\hat{C}_8^7$
A_1	1	1	1	1	1	1	1	1
A_2	1	1	1	1	1	1	1	1
$E_1(\Pi)$	$\begin{pmatrix} 1 & 0 \\ 0 & 1 \end{pmatrix}$	$\begin{pmatrix} q & -q \\ q & q \end{pmatrix}$	$\begin{pmatrix} 0 & -1 \\ 1 & 0 \end{pmatrix}$	$\begin{pmatrix} -q & -q \\ q & -q \end{pmatrix}$	$\begin{pmatrix} -1 & 0 \\ 0 & -1 \end{pmatrix}$	$\begin{pmatrix} -q & q \\ -q & -q \end{pmatrix}$	$\begin{pmatrix} 0 & 1 \\ -1 & 0 \end{pmatrix}$	$\begin{pmatrix} q & q \\ -q & q \end{pmatrix}$
$E_2(\Delta)$	$\begin{pmatrix} 1 & 0 \\ 0 & 1 \end{pmatrix}$	$\begin{pmatrix} 0 & -1 \\ 1 & 0 \end{pmatrix}$	$\begin{pmatrix} -1 & 0 \\ 0 & -1 \end{pmatrix}$	$\begin{pmatrix} 0 & 1 \\ -1 & 0 \end{pmatrix}$	$\begin{pmatrix} 1 & 0 \\ 0 & 1 \end{pmatrix}$	$\begin{pmatrix} 0 & -1 \\ 1 & 0 \end{pmatrix}$	$\begin{pmatrix} -1 & 0 \\ 0 & -1 \end{pmatrix}$	$\begin{pmatrix} 0 & 1 \\ -1 & 0 \end{pmatrix}$

$q = \frac{1}{\sqrt{2}}$

Table 5.3: Generated $C_{\infty v}$ point group table cut out for angular momentum up to $\ell = 2$ (part 1).

$C_{\infty v}$	$\hat{\sigma}_v$	$\hat{\sigma}_v^2$	$\hat{\sigma}_v^3$	$\hat{\sigma}_v^4$	$\hat{\sigma}_v^5$	$\hat{\sigma}_v^6$	$\hat{\sigma}_v^7$	$\hat{\sigma}_v^8$
A_1	1	1	1	1	1	1	1	1
A_2	−1	−1	−1	−1	−1	−1	−1	−1
$E_1(\Pi)$	$\begin{pmatrix} -1 & 0 \\ 0 & 1 \end{pmatrix}$	$\begin{pmatrix} -q & -q \\ -q & q \end{pmatrix}$	$\begin{pmatrix} 0 & -1 \\ -1 & 0 \end{pmatrix}$	$\begin{pmatrix} q & -q \\ -q & -q \end{pmatrix}$	$\begin{pmatrix} 1 & 0 \\ 0 & -1 \end{pmatrix}$	$\begin{pmatrix} q & q \\ q & -q \end{pmatrix}$	$\begin{pmatrix} 0 & 1 \\ 1 & 0 \end{pmatrix}$	$\begin{pmatrix} -q & q \\ q & q \end{pmatrix}$
$E_2(\Delta)$	$\begin{pmatrix} 1 & 0 \\ 0 & -1 \end{pmatrix}$	$\begin{pmatrix} 0 & 1 \\ 1 & 0 \end{pmatrix}$	$\begin{pmatrix} -1 & 0 \\ 0 & 1 \end{pmatrix}$	$\begin{pmatrix} 0 & -1 \\ -1 & 0 \end{pmatrix}$	$\begin{pmatrix} 1 & 0 \\ 0 & -1 \end{pmatrix}$	$\begin{pmatrix} 0 & 1 \\ 1 & 0 \end{pmatrix}$	$\begin{pmatrix} -1 & 0 \\ 0 & 1 \end{pmatrix}$	$\begin{pmatrix} 0 & -1 \\ -1 & 0 \end{pmatrix}$

$q = \frac{1}{\sqrt{2}}$

Table 5.4: Generated $C_{\infty v}$ point group table cut out for angular momentum up to $\ell = 2$ (part 2).

$C_{\infty v}$ are not complete. As a result, the well-known relation between dimensionality of irreducible representations and group order,

$$\sum_{\Gamma} d_{\Gamma}^2 = h \tag{5.15}$$

is modified for the finite dimensional cut outs to:

$$\sum_{\Gamma} 2d_{\Gamma}^2 - 4 = h \tag{5.16}$$

Also, in our finite-dimensional cut outs, the number of classes [75] does not coincide with the number of irreducible representations. For example, the symmetry operations of Table 5.2 are the same of the C_{4v} point group, nevertheless, in our cut out table we do not have the B_1 and B_2 irreducible representations found in the C_{4v} point group table [72]. This represents no problem since the B irreducible representations are absent in the complete $C_{\infty v}$ point group, and, therefore, we do not need them. Also, we can compare

the C_{8v} point group table with the $C_{\infty v}$ cut out table we built for d-type functions (shown in Tables 5.3 and 5.3). The C_{8v} and our cut out tables have the same symmetry operations. We observed that in our cut out, not only the B irreducible representations are absent but also a double degenerated irreducible representation, E_3, which can characterize Cartesian tensors of rank 3, i.e., f-type functions. This suggest that we are taking more symmetry operations than the minimum needed for the symmetry adaptation of functions. Nevertheless, this causes no problem in practice. Finally, we have to consider an additional circumstance. The electron density is given by the squares of MOs which at the end are given by the squares of SAOs. Therefore, we will have irreducible representation products of the form $\Gamma \otimes \Gamma$. For the two-dimensional irreducible representations of $C_{\infty v}$ we see from the point group tables that $E_m \otimes E_m = \Sigma^+ \oplus \Sigma^- \oplus E_{2m}$. In order to span the space for such direct products we need to double its dimension. Therefore, we set in our implementation:

$$N_\Gamma = 2 + 2\ell \tag{5.17}$$

$$h = 16\,\ell \tag{5.18}$$

Again ℓ denotes in Eq. (5.17) and (5.18) the maximum total angular momentum of the underlying function set.

5.3 Generation of I point group table in real form

Another point group table that was not available in the StoBe code was the one for the icosahedral group I. In the literature, it is built from the generator matrices shown in Table 5.5 given by Altmann and Herzig [72]. The matrix multiplication of the generators yields all symmetry operation matrix representations for the irreducible representations of the point group I. The expressions of the symmetry operations in terms of the generators are

I	$\hat{C}^{+}_{51}$	$\hat{C}^{+}_{31}$	$\hat{C}_{2a}$
A	1	1	1
T_1	$\frac{1}{2}\begin{bmatrix} g_- & \bar{\imath} & i\bar{g}_+ \\ \bar{\imath} & g_+ & \bar{g}_- \\ i\bar{g}_+ & \bar{g}_- & 1 \end{bmatrix}$	$\begin{bmatrix} 0 & 0 & \bar{\imath} \\ \bar{\imath} & 0 & 0 \\ 0 & \bar{1} & 0 \end{bmatrix}$	$\begin{bmatrix} \bar{1} & 0 & 0 \\ 0 & \bar{1} & 0 \\ 0 & 0 & 1 \end{bmatrix}$
T_2	$\frac{1}{2}\begin{bmatrix} \bar{g}_+ & \bar{\imath} & ig_- \\ \bar{\imath} & \bar{g}_- & g_+ \\ ig_- & g_+ & 1 \end{bmatrix}$	$\begin{bmatrix} 0 & 0 & \bar{\imath} \\ \bar{\imath} & 0 & 0 \\ 0 & \bar{1} & 0 \end{bmatrix}$	$\begin{bmatrix} \bar{1} & 0 & 0 \\ 0 & \bar{1} & 0 \\ 0 & 0 & 1 \end{bmatrix}$
F	$\frac{1}{4}\begin{bmatrix} \bar{1} & \bar{t} & i\bar{t} & i\bar{t} \\ \bar{t} & \bar{1} & 3i & \bar{\imath} \\ i\bar{t} & 3i & 1 & 1 \\ i\bar{t} & \bar{\imath} & 1 & \bar{3} \end{bmatrix}$	$\begin{bmatrix} 1 & 0 & 0 & 0 \\ 0 & 0 & 0 & \bar{\imath} \\ 0 & \bar{\imath} & 0 & 0 \\ 0 & 0 & \bar{1} & 0 \end{bmatrix}$	$\begin{bmatrix} 1 & 0 & 0 & 0 \\ 0 & \bar{1} & 0 & 0 \\ 0 & 0 & \bar{1} & 0 \\ 0 & 0 & 0 & 1 \end{bmatrix}$
H	$\frac{1}{2}\begin{bmatrix} 0 & \lambda^2\omega^* & \bar{\lambda} & i\lambda\bar{\omega}^* & i\lambda\bar{\omega} \\ (\lambda^*)^2\,\omega & 0 & \bar{\lambda}^* & i\lambda^*\bar{\omega} & i\lambda^*\bar{\omega}^* \\ \bar{\lambda}^* & \bar{\lambda} & 1 & 0 & i \\ i\lambda^*\bar{\omega} & i\lambda\bar{\omega}^* & 0 & \bar{1} & \bar{1} \\ i\lambda^*\bar{\omega}^* & i\lambda\bar{\omega} & i & \bar{1} & 0 \end{bmatrix}$	$\begin{bmatrix} \omega & 0 & 0 & 0 & 0 \\ 0 & \omega^* & 0 & 0 & 0 \\ 0 & 0 & 0 & 0 & \bar{\imath} \\ 0 & 0 & \bar{\imath} & 0 & 0 \\ 0 & 0 & 0 & \bar{1} & 0 \end{bmatrix}$	$\begin{bmatrix} 1 & 0 & 0 & 0 & 0 \\ 0 & 1 & 0 & 0 & 0 \\ 0 & 0 & \bar{1} & 0 & 0 \\ 0 & 0 & 0 & \bar{1} & 0 \\ 0 & 0 & 0 & 0 & 1 \end{bmatrix}$

$$\lambda = \exp\left(i \arctan\left(\sqrt{5/3}\right)\right),\ g_\pm = \left(\sqrt{5} \pm 1\right)/2,\ t = \sqrt{5},\ \omega = \exp(2\pi i/3),\ \bar{\imath} = -i$$

Table 5.5: Generators for the icosahedral point group as given in [72]. Letters and numbers with a bar denote their negative values.

shown in Table 5.6. As these generators are in complex form, the challenge was to find a similarity transformation that transforms the irreducible representations into real form:

$$\mathbf{U}^{\Gamma\,\dagger}\boldsymbol{\chi}^{\Gamma}_{\text{Complex}}(\hat{R})\,\mathbf{U}^{\Gamma} = \boldsymbol{\chi}^{\Gamma}_{\text{Real}}(\hat{R}) \qquad \forall \quad \hat{R},\ \Gamma \tag{5.19}$$

The adjoint superscript † denotes a transposed, complex conjugated matrix. The $\mathbf{U}^{\Gamma}$ transfomation matrices I derived are shown in Fig. 5.2. Using these unitary matrices the generators become real. The orthonormal matrices of the real generators are explicitly shown in Table 5.7. The matrix $\mathbf{U}^{T_1}$ was not needed since the real generators for the irreducible representation T_1 are also given in the tables [72] (see also Table 5.7). Furthermore, the T_1 irreducible representation corresponds to the transformation of the Cartesian basis $\mathbf{x}$, $\mathbf{y}$, $\mathbf{z}$. It is used to align the molecule into standard orientation and

I		I	
E	$\hat{C}_{2a}\hat{C}_{2a}$	$\hat{C}^{+}_{36}$	$\hat{C}^{+}_{31}\hat{C}_{2a}\hat{C}^{+}_{51}\hat{C}^{+}_{31}\hat{C}_{2a}$
$\hat{C}^{+}_{51}$	$\hat{C}^{+}_{51}$	$\hat{C}^{+}_{37}$	$\hat{C}_{2a}\hat{C}^{+}_{31}\hat{C}_{2a}\hat{C}^{+}_{51}$
$\hat{C}^{+}_{52}$	$\hat{C}^{+}_{51}\hat{C}^{+}_{51}\hat{C}_{2a}\hat{C}^{+}_{31}$	$\hat{C}^{+}_{38}$	$\hat{C}_{2a}\hat{C}^{+}_{51}\hat{C}_{2a}\hat{C}^{+}_{31}$
$\hat{C}^{+}_{53}$	$\hat{C}^{+}_{51}\hat{C}_{2a}\hat{C}^{+}_{31}\hat{C}^{+}_{51}$	$\hat{C}^{+}_{39}$	$\hat{C}^{+}_{31}\hat{C}^{+}_{51}\hat{C}_{2a}\hat{C}^{+}_{31}$
$\hat{C}^{+}_{54}$	$\hat{C}^{+}_{31}\hat{C}^{+}_{51}\hat{C}_{2a}$	$\hat{C}^{+}_{3,10}$	$\hat{C}^{+}_{31}\hat{C}_{2a}\hat{C}^{+}_{51}\hat{C}_{2a}$
$\hat{C}^{+}_{55}$	$\hat{C}^{+}_{51}\hat{C}_{2a}\hat{C}^{+}_{51}\hat{C}_{2a}$	$\hat{C}^{-}_{31}$	$\hat{C}^{+}_{31}\hat{C}^{+}_{31}$
$\hat{C}^{+}_{56}$	$\hat{C}_{2a}\hat{C}^{+}_{51}\hat{C}_{2a}\hat{C}^{+}_{51}$	$\hat{C}^{-}_{32}$	$\hat{C}_{2a}\hat{C}^{+}_{31}\hat{C}^{+}_{31}$
$\hat{C}^{-}_{51}$	$\hat{C}^{+}_{31}\hat{C}^{+}_{51}\hat{C}^{+}_{31}$	$\hat{C}^{-}_{33}$	$\hat{C}^{+}_{31}\hat{C}_{2a}\hat{C}^{+}_{31}$
$\hat{C}^{-}_{52}$	$\hat{C}_{2a}\hat{C}^{+}_{51}\hat{C}_{2a}$	$\hat{C}^{-}_{34}$	$\hat{C}^{+}_{31}\hat{C}^{+}_{31}\hat{C}_{2a}$
$\hat{C}^{-}_{53}$	$\hat{C}^{+}_{51}\hat{C}^{+}_{31}\hat{C}^{+}_{31}$	$\hat{C}^{-}_{35}$	$\hat{C}^{+}_{51}\hat{C}_{2a}\hat{C}^{+}_{31}\hat{C}_{2a}$
$\hat{C}^{-}_{54}$	$\hat{C}_{2a}\hat{C}^{+}_{31}\hat{C}^{+}_{51}$	$\hat{C}^{-}_{36}$	$\hat{C}^{+}_{31}\hat{C}^{+}_{51}\hat{C}_{2a}\hat{C}^{+}_{51}$
$\hat{C}^{-}_{55}$	$\hat{C}^{+}_{31}\hat{C}^{+}_{31}\hat{C}^{+}_{51}$	$\hat{C}^{-}_{37}$	$\hat{C}_{2a}\hat{C}^{+}_{51}\hat{C}^{+}_{51}$
$\hat{C}^{-}_{56}$	$\hat{C}^{+}_{51}\hat{C}_{2a}\hat{C}^{+}_{31}$	$\hat{C}^{-}_{38}$	$\hat{C}^{+}_{31}\hat{C}^{+}_{51}\hat{C}^{+}_{51}$
$\hat{C}^{2+}_{51}$	$\hat{C}^{+}_{51}\hat{C}^{+}_{51}$	$\hat{C}^{-}_{39}$	$\hat{C}^{+}_{51}\hat{C}^{+}_{51}\hat{C}^{+}_{31}$
$\hat{C}^{2+}_{52}$	$\hat{C}^{+}_{31}\hat{C}_{2a}\hat{C}^{+}_{51}$	$\hat{C}^{-}_{3,10}$	$\hat{C}^{+}_{51}\hat{C}^{+}_{51}\hat{C}_{2a}$
$\hat{C}^{2+}_{53}$	$\hat{C}^{+}_{31}\hat{C}_{2a}\hat{C}^{+}_{31}\hat{C}^{+}_{51}$	$\hat{C}_{2a}$	$\hat{C}_{2a}$
$\hat{C}^{2+}_{54}$	$\hat{C}^{+}_{51}\hat{C}^{+}_{31}\hat{C}_{2a}$	$\hat{C}_{2b}$	$\hat{C}^{+}_{31}\hat{C}_{2a}\hat{C}^{+}_{31}\hat{C}^{+}_{31}$
$\hat{C}^{2+}_{55}$	$\hat{C}_{2a}\hat{C}^{+}_{31}\hat{C}^{+}_{51}\hat{C}^{+}_{31}$	$\hat{C}_{2c}$	$\hat{C}^{+}_{31}\hat{C}^{+}_{31}\hat{C}_{2a}\hat{C}^{+}_{31}$
$\hat{C}^{2+}_{56}$	$\hat{C}^{+}_{31}\hat{C}^{+}_{51}\hat{C}^{+}_{31}\hat{C}_{2a}$	$\hat{C}_{2d}$	$\hat{C}^{+}_{31}\hat{C}^{+}_{51}$
$\hat{C}^{2-}_{51}$	$\hat{C}^{+}_{51}\hat{C}^{+}_{51}\hat{C}^{+}_{51}$	$\hat{C}_{2e}$	$\hat{C}^{+}_{31}\hat{C}_{2a}\hat{C}^{+}_{51}\hat{C}^{+}_{31}$
$\hat{C}^{2-}_{52}$	$\hat{C}_{2a}\hat{C}^{+}_{51}\hat{C}^{+}_{51}\hat{C}_{2a}$	$\hat{C}_{2f}$	$\hat{C}^{+}_{51}\hat{C}^{+}_{31}\hat{C}_{2a}\hat{C}^{+}_{51}$
$\hat{C}^{2-}_{53}$	$\hat{C}^{+}_{31}\hat{C}^{+}_{31}\hat{C}_{2a}\hat{C}^{+}_{51}\hat{C}_{2a}$	$\hat{C}_{2g}$	$\hat{C}^{+}_{51}\hat{C}^{+}_{31}$
$\hat{C}^{2-}_{54}$	$\hat{C}_{2a}\hat{C}^{+}_{51}\hat{C}^{+}_{31}$	$\hat{C}_{2h}$	$\hat{C}^{+}_{51}\hat{C}^{+}_{51}\hat{C}^{+}_{31}\hat{C}_{2a}$
$\hat{C}^{2-}_{55}$	$\hat{C}^{+}_{51}\hat{C}_{2a}$	$\hat{C}_{2i}$	$\hat{C}_{2a}\hat{C}^{+}_{51}\hat{C}^{+}_{31}\hat{C}^{+}_{31}$
$\hat{C}^{2-}_{56}$	$\hat{C}_{2a}\hat{C}^{+}_{51}$	$\hat{C}_{2j}$	$\hat{C}_{2a}\hat{C}^{+}_{51}\hat{C}^{+}_{31}\hat{C}_{2a}$
$\hat{C}^{+}_{31}$	$\hat{C}^{+}_{31}$	$\hat{C}_{2k}$	$\hat{C}^{+}_{51}\hat{C}^{+}_{31}\hat{C}^{+}_{31}\hat{C}_{2a}$
$\hat{C}^{+}_{32}$	$\hat{C}^{+}_{31}\hat{C}_{2a}$	$\hat{C}_{2l}$	$\hat{C}_{2a}\hat{C}^{+}_{51}\hat{C}^{+}_{51}\hat{C}^{+}_{31}$
$\hat{C}^{+}_{33}$	$\hat{C}_{2a}\hat{C}^{+}_{31}\hat{C}_{2a}$	$\hat{C}_{2m}$	$\hat{C}_{2a}\hat{C}^{+}_{31}\hat{C}^{+}_{51}\hat{C}_{2a}$
$\hat{C}^{+}_{34}$	$\hat{C}_{2a}\hat{C}^{+}_{31}$	$\hat{C}_{2n}$	$\hat{C}^{+}_{31}\hat{C}^{+}_{31}\hat{C}_{2a}\hat{C}^{+}_{51}$
$\hat{C}^{+}_{35}$	$\hat{C}^{+}_{51}\hat{C}_{2a}\hat{C}^{+}_{51}$	$\hat{C}_{2o}$	$\hat{C}^{+}_{31}\hat{C}^{+}_{51}\hat{C}_{2a}\hat{C}^{+}_{51}\hat{C}_{2a}$

Table 5.6: Symmetry operations of the I point group in terms of its generators as given in [72].

it provides the matrix representations used for building the symmetrization matrices for atom permutations, $\mathbf{V}$, and origin-centered functions, $\mathbf{W}$, given in the previous chapter. Thus, with the real generators at hand, we can build any symmetry operation matrix representation for any of the irreducible representations. As an example, take the symmetry operation $\hat{C}^{+}_{52}$ which is given in terms of the generators (see Table 5.6) as:

$$\hat{C}^{+}_{52} = \hat{C}^{+}_{51}\hat{C}^{+}_{51}\hat{C}_{2a}\hat{C}^{+}_{31} \tag{5.20}$$

$$\mathbf{U}^{T_2} = \frac{1}{\sqrt{2}} \begin{pmatrix} i & 0 & -i \\ 0 & \sqrt{2} & 0 \\ -1 & 0 & -1 \end{pmatrix}$$

$$\mathbf{U}^{F} = \frac{1}{\sqrt{2}} \begin{pmatrix} -i & 0 & i & 0 \\ 0 & i & 0 & -i \\ 1 & 0 & 1 & 0 \\ 0 & -1 & 0 & -1 \end{pmatrix}$$

$$\mathbf{U}^{H} = \frac{1}{2\sqrt{2}} \begin{pmatrix} \sqrt{2}-i & \sqrt{2}+i & 0 & -i\sqrt{2} & 0 \\ \sqrt{2}+i & \sqrt{2}-i & 0 & i\sqrt{2} & 0 \\ 0 & 0 & -2 & 0 & 2 \\ -i\sqrt{2} & i\sqrt{2} & 0 & 2i & 0 \\ 0 & 0 & 2i & 0 & 2i \end{pmatrix}$$

Figure 5.2: Transfomation matrices for the construction of real generators for the icosahedral point group. See text for details.

The corresponding real matrix representation for the F irreducible representation is obtained with the real generators from Table 5.7 by:

$$\begin{aligned} \chi^{F}(\hat{C}_{52}^{+}) &= \chi^{F}(\hat{C}_{51}^{+})\chi^{F}(\hat{C}_{51}^{+})\chi^{F}(\hat{C}_{2a})\chi^{F}(\hat{C}_{31}^{+}) \\ &= \begin{pmatrix} 0 & \frac{1}{2} & \frac{1}{4}\left(1+\sqrt{5}\right) & \frac{1}{4}\left(\sqrt{5}-1\right) \\ \frac{1}{4}\left(-1-\sqrt{5}\right) & -\frac{1}{2} & \frac{1}{4}\left(\sqrt{5}-1\right) & 0 \\ \frac{1}{4}\left(1-\sqrt{5}\right) & \frac{1}{2} & 0 & \frac{1}{4}\left(-1-\sqrt{5}\right) \\ \frac{1}{2} & -\frac{1}{2} & \frac{1}{2} & -\frac{1}{2} \end{pmatrix} \end{aligned} \tag{5.21}$$

The validity of the generated I point group table was confirmed by calculating the multiplication table of the point group [99] and consecutive checking of its properties (rearrangement theorem, criteria of irreducibility, orthonormality, group order and number of irreducible representations relation). The building of the multiplication table of the group and its validation were programmed in the software Maple [100]. The generated real point group table was directly exported to Fortran code in order to include it into deMon2k.

I	$\hat{C}_{51}^{+}$	$\hat{C}_{31}^{+}$	$\hat{C}_{2a}$
A	1	1	1
T_1	$\frac{1}{4}\begin{pmatrix} 2 & -1-\sqrt{5} & \sqrt{5}-1 \\ 1+\sqrt{5} & \sqrt{5}-1 & -2 \\ \sqrt{5}-1 & 2 & 1+\sqrt{5} \end{pmatrix}$	$\begin{pmatrix} 0 & 0 & 1 \\ 1 & 0 & 0 \\ 0 & 1 & 0 \end{pmatrix}$	$\begin{pmatrix} 1 & 0 & 0 \\ 0 & -1 & 0 \\ 0 & 0 & -1 \end{pmatrix}$
T_2	$\frac{-1}{2\left(1+\sqrt{5}\right)}\begin{pmatrix} 1 & \sqrt{2}\left(2+\sqrt{5}\right) & -\sqrt{5} \\ \sqrt{2} & 2 & \sqrt{2}\left(2+\sqrt{5}\right) \\ -4-\sqrt{5} & \sqrt{2} & 1 \end{pmatrix}$	$\frac{1}{2\sqrt{2}}\begin{pmatrix} \sqrt{2} & 2 & \sqrt{2} \\ 2 & 0 & -2 \\ -\sqrt{2} & 2 & -\sqrt{2} \end{pmatrix}$	$\begin{pmatrix} 0 & 0 & 1 \\ 0 & -1 & 0 \\ 1 & 0 & 0 \end{pmatrix}$
F	$\frac{-1}{4}\begin{pmatrix} 0 & 2 & -1-\sqrt{5} & \sqrt{5}-1 \\ -1-\sqrt{5} & 2 & \sqrt{5}-1 & 0 \\ \sqrt{5}-1 & 2 & 0 & -1-\sqrt{5} \\ 2 & 2 & 2 & 2 \end{pmatrix}$	$\frac{1}{2}\begin{pmatrix} 1 & 1 & -1 & -1 \\ 1 & 1 & 1 & 1 \\ -1 & 1 & 1 & -1 \\ 1 & -1 & 1 & -1 \end{pmatrix}$	$\begin{pmatrix} 0 & 0 & -1 & 0 \\ 0 & 0 & 0 & 1 \\ -1 & 0 & 0 & 0 \\ 0 & 1 & 0 & 0 \end{pmatrix}$
H	$\chi^{H}(\hat{C}_{51}^{+})$	$\frac{1}{4}\begin{pmatrix} -\frac{3}{2} & -\frac{1}{2}-\sqrt{6} & -\sqrt{2} & \frac{\sqrt{6}-1}{\sqrt{2}} & \sqrt{2} \\ \sqrt{6}-\frac{1}{2} & -\frac{3}{2} & \sqrt{2} & \sqrt{\frac{7}{2}+\sqrt{6}} & -\sqrt{2} \\ \sqrt{2} & -\sqrt{2} & -2 & -2 & -2 \\ -\sqrt{\frac{7}{2}+\sqrt{6}} & \frac{1}{\sqrt{2}}-\sqrt{3} & 2 & -1 & -2 \\ \sqrt{2} & -\sqrt{2} & 2 & -2 & 2 \end{pmatrix}$	$\frac{1}{2\sqrt{2}}\begin{pmatrix} \sqrt{2} & \sqrt{2} & 0 & 2 & 0 \\ \sqrt{2} & \sqrt{2} & 0 & -2 & 0 \\ 0 & 0 & 0 & 0 & 2\sqrt{2} \\ 2 & -2 & 0 & 0 & 0 \\ 0 & 0 & 2\sqrt{2} & 0 & 0 \end{pmatrix}$

$$\chi^{H}(\hat{C}_{51}^{+}) = \frac{1}{64}\begin{pmatrix} -7+3\sqrt{5}+2\sqrt{6}\left(\sqrt{5}-1\right) & 11+9\sqrt{5}+4\sqrt{6}\left(\sqrt{5}-1\right) & -4\sqrt{\left(3-\sqrt{5}\right)\left(7+2\sqrt{6}\right)} & a & b \\ 11+9\sqrt{5}+4\sqrt{6}-4\sqrt{30} & -7+3\sqrt{5}+2\sqrt{6}-2\sqrt{30} & -4\sqrt{\left(3-\sqrt{5}\right)\left(7-2\sqrt{6}\right)} & c & d \\ 2\sqrt{2}\left(7-3\sqrt{5}+3\sqrt{6}+\sqrt{30}\right) & 4\sqrt{89-3\sqrt{5}+2\sqrt{6}\left(\sqrt{5}-3\right)} & 16 & -4\left(1+3\sqrt{5}\right) & 16 \\ -2\sqrt{153+29\sqrt{5}+30\sqrt{6}-2\sqrt{30}} & 2\sqrt{153+29\sqrt{5}+2\sqrt{6}\left(\sqrt{5}-15\right)} & -4\left(7+\sqrt{5}\right) & -6\left(3+\sqrt{5}\right) & 4\left(3\sqrt{5}-7\right) \\ 4\sqrt{45+\sqrt{5}-2\sqrt{6}+6\sqrt{30}} & -4\sqrt{45+\sqrt{5}+2\sqrt{6}-6\sqrt{30}} & -48 & 4\left(\sqrt{5}-1\right) & 16 \end{pmatrix}$$

$$a = 2\sqrt{345-35\sqrt{5}-42\sqrt{6}+54\sqrt{30}};\ b = -2\sqrt{345-35\sqrt{5}+42\sqrt{6}-54\sqrt{30}};\ c = -4\sqrt{65+21\sqrt{5}-2\sqrt{6}\left(9+5\sqrt{5}\right)};\ d = -2\sqrt{2}\left(1+3\sqrt{5}+3\sqrt{6}+\sqrt{30}\right)$$

Table 5.7: Real generators for the icosahedral point group.

5.4 Direct products of groups

We now turn to the construction of point group tables through direct products of groups. In our implementation the following direct products of groups are implemented:

$$D_{\infty h} = C_{\infty v} \otimes C_i \tag{5.22}$$

$$I_{\infty h} = I \otimes C_i \tag{5.23}$$

To proceed, we first review some general definitions and concepts for direct products of groups [101]. To this end, we define the group S of order h_S with elements (symmetry operations) $\hat{s}_1, \hat{s}_2, \ldots \hat{s}_{h_S}$ as:

$$S = \{\hat{s}_1, \hat{s}_2, \ldots \hat{s}_{h_S}\}$$

In the same way we define the group T as:

$$T = \left\{\hat{t}_1, \hat{t}_2, \ldots \hat{t}_{h_T}\right\}$$

If the intersection of these groups is only the identity operation,

$$S \cap T = \hat{E} \tag{5.24}$$

then the elements of S will commute with the elements of T

$$\hat{s}_i \hat{t}_j = \hat{t}_j \hat{s}_i \qquad \forall \quad i = 1, ..., h_S \ \wedge \ j = 1, ..., h_T \tag{5.25}$$

Under this condition we can define the group G as the direct product of the groups S and T:

$$G = S \otimes T \tag{5.26}$$

The so-defined group G contains as elements all possible pairs of the elements from S and T. Thus, the elements of G are given by:

$$\begin{aligned} G &= \{\hat{g}_1 \quad , \hat{g}_2 \quad , \ldots , \hat{g}_{h_S} \quad , \hat{g}_{h_S+1}, \hat{g}_{h_S+2}, \ldots , \hat{g}_{h_S h_T}\} \\ &= \{\hat{s}_1\hat{t}_1, \hat{s}_2\hat{t}_1, \ldots , \hat{s}_{h_S}\hat{t}_1, \hat{s}_1\hat{t}_2 \quad , \hat{s}_2\hat{t}_2 \quad , \ldots , \hat{s}_{h_S}\hat{t}_{h_T}\} \end{aligned} \tag{5.27}$$

From this definition of G follows that its group order is just the product of the group orders of S and T:

$$h_G = h_S \cdot h_T \tag{5.28}$$

The construction of G as a direct product of the groups S and T also permits to calculate its irreducible representations, Γ_i, as direct products of the irreducible representation matrices of S and T. To do so, we denote the irreducible representations of S and T as

$$\{\Sigma_1, \Sigma_2, \ldots , \Sigma_{k_S}\} \tag{5.29}$$

and

$$\{\Theta_1, \Theta_2, \ldots , \Theta_{k_T}\} \tag{5.30}$$

respectively. Here k_S and k_T denote the number of irreducible representations in the groups S and T. An irreducible representation of the direct product group G is then given by:

$$\Gamma_i = \Sigma_j \otimes \Theta_k \qquad \forall \quad j = 1, 2, .., k_S \ \wedge \ k = 1, 2, .., k_T \tag{5.31}$$

Thus, the irreducible representations of G are given by:

$$\begin{aligned} \{\Gamma\} &= \{\Gamma_1 \quad , \Gamma_2 \quad , \ldots , \Gamma_{k_S} \quad , \Gamma_{k_S+1} \quad , \Gamma_{k_S+2} \quad , \ldots , \Gamma_{k_S k_T}\} \\ \{\Gamma\} &= \{\Sigma_1 \otimes \Theta_1, \Sigma_2 \otimes \Theta_1, \ldots , \Sigma_{k_S} \otimes \Theta_1, \Sigma_1 \otimes \Theta_2, \Sigma_2 \otimes \Theta_2, \ldots , \Sigma_{k_S} \otimes \Theta_{k_T}\} \end{aligned} \tag{5.32}$$

From this definition follows immediately that the number of irreducible representations in G, k_G, is just the product of the numbers of irreducible representations in S and T:

$$k_G = k_S \cdot k_T \tag{5.33}$$

For the explicit calculation of the direct product in Eq. (5.31) we recall that the irreducible representations of S and T are in general expressed by irreducible representation matrices with elements $\chi^{\Sigma}_{\sigma\sigma'}(\hat{s})$ and $\chi^{\Theta}_{\theta\theta'}(\hat{t})$. Thus, the direct product in Eq. (5.31) is calculated as a direct product of matrices (see appendix A) by:

$$\boldsymbol{\chi}^{\Gamma}(\hat{g}) = \boldsymbol{\chi}^{\Sigma}(\hat{s}) \otimes \boldsymbol{\chi}^{\Theta}(\hat{t}) \tag{5.34}$$

The dimension of $\boldsymbol{\chi}^{\Gamma}(\hat{g})$ is given by:

$$d_{\Gamma} = d_{\Sigma} \cdot d_{\Theta} \tag{5.35}$$

As this discussion shows, the point group table of G can be straightforwardly built from the point group tables of S and T. In our implementation we sort the G point group table according to Eqs. (5.27) and (5.32).

The here outlined constructions of direct products of groups and corresponding irreducible representations were implemented in a general form through the subroutine protab.f in deMon2k. In this thesis, they are used for the on-the-fly construction of the $D_{\infty h}$ and I_h point groups. Extension to other direct products is straightforward.

5.4.1 *Construction of* $D_{\infty h} = C_{\infty v} \otimes C_i$ *point group table cut outs*

In order to illustrate the direct product generation of $D_{\infty h} = C_{\infty v} \otimes C_i$, we use the $C_{\infty v}$ cut out from Table 5.2 and the C_i point group table given in Table 5.8.

C_i	$\hat{E}$	$\hat{i}$
A_g	1	1
A_u	1	-1

Table 5.8: C_i point group table.

The resulting $D_{\infty h}$ finite point group table cut out has the generic structure shown in Table 5.9. In this table, Γ denotes any of the irreducible representations of $C_{\infty v}$ and $\hat{R}$ any of the symmetry operations of $C_{\infty v}$. The Tables 5.10 and 5.11 show the explicit form of the multiplications based on Table 5.9. The resulting $D_{\infty h}$ point group cut out for angular momentum up to $\ell = 1$ is given in Table 5.12.

$D_{\infty h}$	$\hat{R}\,\hat{E}$	$\hat{R}\,\hat{i}$
$\Gamma \otimes A_g$	$\chi^\Gamma(\hat{R}) \otimes 1$	$\chi^\Gamma(\hat{R}) \otimes 1$
$\Gamma \otimes A_u$	$\chi^\Gamma(\hat{R}) \otimes 1$	$\chi^\Gamma(\hat{R}) \otimes (-1)$

Table 5.9: Generic $D_{\infty h}$ point group table form in terms of direct products of the irreducible representations of the point groups $C_{\infty v}$ and C_i. See text for further details.

$C_{\infty v} \otimes C_i$	$\hat{E}\,\hat{E}$	$\hat{C}_4\,\hat{E}$	$\hat{C}_4^2\,\hat{E}$	$\hat{C}_4^3\,\hat{E}$	$\hat{\sigma}_v\,\hat{E}$	$\hat{\sigma}_v^2\,\hat{E}$	$\hat{\sigma}_v^3\,\hat{E}$	$\hat{\sigma}_v^4\,\hat{E}$
$\Sigma^+ \otimes A_g$	$1 \otimes 1$	$1 \otimes 1$	$1 \otimes 1$	$1 \otimes 1$	$1 \otimes 1$	$1 \otimes 1$	$1 \otimes 1$	$1 \otimes 1$
$\Sigma^- \otimes A_g$	$1 \otimes 1$	$1 \otimes 1$	$1 \otimes 1$	$1 \otimes 1$	$(-1) \otimes 1$	$(-1) \otimes 1$	$(-1) \otimes 1$	$(-1) \otimes 1$
$\Pi \otimes A_g$	$\left(\begin{smallmatrix} 1 & 0 \\ 0 & 1 \end{smallmatrix}\right) \otimes 1$	$\left(\begin{smallmatrix} 0 & -1 \\ 1 & 0 \end{smallmatrix}\right) \otimes 1$	$\left(\begin{smallmatrix} -1 & 0 \\ 0 & -1 \end{smallmatrix}\right) \otimes 1$	$\left(\begin{smallmatrix} 0 & 1 \\ -1 & 0 \end{smallmatrix}\right) \otimes 1$	$\left(\begin{smallmatrix} -1 & 0 \\ 0 & 1 \end{smallmatrix}\right) \otimes 1$	$\left(\begin{smallmatrix} 0 & -1 \\ -1 & 0 \end{smallmatrix}\right) \otimes 1$	$\left(\begin{smallmatrix} 1 & 0 \\ 0 & -1 \end{smallmatrix}\right) \otimes 1$	$\left(\begin{smallmatrix} 0 & 1 \\ 1 & 0 \end{smallmatrix}\right) \otimes 1$
$\Sigma^+ \otimes A_u$	$1 \otimes 1$	$1 \otimes 1$	$1 \otimes 1$	$1 \otimes 1$	$1 \otimes 1$	$1 \otimes 1$	$1 \otimes 1$	$1 \otimes 1$
$\Sigma^- \otimes A_u$	$1 \otimes 1$	$1 \otimes 1$	$1 \otimes 1$	$1 \otimes 1$	$(-1) \otimes 1$	$(-1) \otimes 1$	$(-1) \otimes 1$	$(-1) \otimes 1$
$\Pi \otimes A_u$	$\left(\begin{smallmatrix} 1 & 0 \\ 0 & 1 \end{smallmatrix}\right) \otimes 1$	$\left(\begin{smallmatrix} 0 & -1 \\ 1 & 0 \end{smallmatrix}\right) \otimes 1$	$\left(\begin{smallmatrix} -1 & 0 \\ 0 & -1 \end{smallmatrix}\right) \otimes 1$	$\left(\begin{smallmatrix} 0 & 1 \\ -1 & 0 \end{smallmatrix}\right) \otimes 1$	$\left(\begin{smallmatrix} -1 & 0 \\ 0 & 1 \end{smallmatrix}\right) \otimes 1$	$\left(\begin{smallmatrix} 0 & -1 \\ -1 & 0 \end{smallmatrix}\right) \otimes 1$	$\left(\begin{smallmatrix} 1 & 0 \\ 0 & -1 \end{smallmatrix}\right) \otimes 1$	$\left(\begin{smallmatrix} 0 & 1 \\ 1 & 0 \end{smallmatrix}\right) \otimes 1$

Table 5.10: $D_{\infty h} = C_{\infty v} \otimes C_i$ multiplications for angular momentum up to $\ell = 1$ (part 1).

$C_{\infty v} \otimes C_i$	$\hat{E}\,\hat{i}$	$\hat{C}_4\,\hat{i}$	$\hat{C}_4^2\,\hat{i}$	$\hat{C}_4^3\,\hat{i}$	$\hat{\sigma}_v\,\hat{i}$	$\hat{\sigma}_v^2\,\hat{i}$	$\hat{\sigma}_v^3\,\hat{i}$	$\hat{\sigma}_v^4\,\hat{i}$
$\Sigma^+ \otimes A_g$	$1 \otimes 1$	$1 \otimes 1$	$1 \otimes 1$	$1 \otimes 1$	$1 \otimes 1$	$1 \otimes 1$	$1 \otimes 1$	$1 \otimes 1$
$\Sigma^- \otimes A_g$	$1 \otimes 1$	$1 \otimes 1$	$1 \otimes 1$	$1 \otimes 1$	$(-1) \otimes 1$	$(-1) \otimes 1$	$(-1) \otimes 1$	$(-1) \otimes 1$
$\Pi \otimes A_g$	$\left(\begin{smallmatrix} 1 & 0 \\ 0 & 1 \end{smallmatrix}\right) \otimes 1$	$\left(\begin{smallmatrix} 0 & -1 \\ 1 & 0 \end{smallmatrix}\right) \otimes 1$	$\left(\begin{smallmatrix} -1 & 0 \\ 0 & -1 \end{smallmatrix}\right) \otimes 1$	$\left(\begin{smallmatrix} 0 & 1 \\ -1 & 0 \end{smallmatrix}\right) \otimes 1$	$\left(\begin{smallmatrix} -1 & 0 \\ 0 & 1 \end{smallmatrix}\right) \otimes 1$	$\left(\begin{smallmatrix} 0 & -1 \\ -1 & 0 \end{smallmatrix}\right) \otimes 1$	$\left(\begin{smallmatrix} 1 & 0 \\ 0 & -1 \end{smallmatrix}\right) \otimes 1$	$\left(\begin{smallmatrix} 0 & 1 \\ 1 & 0 \end{smallmatrix}\right) \otimes 1$
$\Sigma^+ \otimes A_u$	$1 \otimes (-1)$	$1 \otimes (-1)$	$1 \otimes (-1)$	$1 \otimes (-1)$	$1 \otimes (-1)$	$1 \otimes (-1)$	$1 \otimes (-1)$	$1 \otimes (-1)$
$\Sigma^- \otimes A_u$	$1 \otimes (-1)$	$1 \otimes (-1)$	$1 \otimes (-1)$	$1 \otimes (-1)$	$(-1) \otimes (-1)$	$(-1) \otimes (-1)$	$(-1) \otimes (-1)$	$(-1) \otimes (-1)$
$\Pi \otimes A_u$	$\left(\begin{smallmatrix} 1 & 0 \\ 0 & 1 \end{smallmatrix}\right) \otimes (-1)$	$\left(\begin{smallmatrix} 0 & -1 \\ 1 & 0 \end{smallmatrix}\right) \otimes (-1)$	$\left(\begin{smallmatrix} -1 & 0 \\ 0 & -1 \end{smallmatrix}\right) \otimes (-1)$	$\left(\begin{smallmatrix} 0 & 1 \\ -1 & 0 \end{smallmatrix}\right) \otimes (-1)$	$\left(\begin{smallmatrix} -1 & 0 \\ 0 & 1 \end{smallmatrix}\right) \otimes (-1)$	$\left(\begin{smallmatrix} 0 & -1 \\ -1 & 0 \end{smallmatrix}\right) \otimes (-1)$	$\left(\begin{smallmatrix} 1 & 0 \\ 0 & -1 \end{smallmatrix}\right) \otimes (-1)$	$\left(\begin{smallmatrix} 0 & 1 \\ 1 & 0 \end{smallmatrix}\right) \otimes (-1)$

Table 5.11: $D_{\infty h} = C_{\infty v} \otimes C_i$ multiplications for angular momentum up to $\ell = 1$ (part 2).

$D_{\infty h}$	$\hat{E}$	$\hat{C}_4$	$\hat{C}_4^2$	$\hat{C}_4^3$	$\hat{\sigma}_v$	$\hat{\sigma}_v'$	$\hat{\sigma}_v''$	$\hat{\sigma}_v'''$	$\hat{i}$	$\hat{S}_4^3$	$\hat{\sigma}_h$	$\hat{S}_4$	$\hat{C}_2$	$\hat{C}_2'$	$\hat{C}_2''$	$\hat{C}_2'''$
Σ_g^+	1	1	1	1	1	1	1	1	1	1	1	1	1	1	1	1
Σ_g^-	1	1	1	1	−1	−1	−1	−1	1	1	1	1	−1	−1	−1	−1
Π_g	$\left(\begin{smallmatrix} 1 & 0 \\ 0 & 1 \end{smallmatrix}\right)$	$\left(\begin{smallmatrix} 0 & -1 \\ 1 & 0 \end{smallmatrix}\right)$	$\left(\begin{smallmatrix} -1 & 0 \\ 0 & -1 \end{smallmatrix}\right)$	$\left(\begin{smallmatrix} 0 & 1 \\ -1 & 0 \end{smallmatrix}\right)$	$\left(\begin{smallmatrix} -1 & 0 \\ 0 & 1 \end{smallmatrix}\right)$	$\left(\begin{smallmatrix} 0 & -1 \\ -1 & 0 \end{smallmatrix}\right)$	$\left(\begin{smallmatrix} 1 & 0 \\ 0 & -1 \end{smallmatrix}\right)$	$\left(\begin{smallmatrix} 0 & 1 \\ 1 & 0 \end{smallmatrix}\right)$	$\left(\begin{smallmatrix} 1 & 0 \\ 0 & 1 \end{smallmatrix}\right)$	$\left(\begin{smallmatrix} 0 & -1 \\ 1 & 0 \end{smallmatrix}\right)$	$\left(\begin{smallmatrix} -1 & 0 \\ 0 & -1 \end{smallmatrix}\right)$	$\left(\begin{smallmatrix} 0 & 1 \\ -1 & 0 \end{smallmatrix}\right)$	$\left(\begin{smallmatrix} -1 & 0 \\ 0 & 1 \end{smallmatrix}\right)$	$\left(\begin{smallmatrix} 0 & -1 \\ -1 & 0 \end{smallmatrix}\right)$	$\left(\begin{smallmatrix} 1 & 0 \\ 0 & -1 \end{smallmatrix}\right)$	$\left(\begin{smallmatrix} 0 & 1 \\ 1 & 0 \end{smallmatrix}\right)$
Σ_u^+	1	1	1	1	1	1	1	1	−1	−1	−1	−1	−1	−1	−1	−1
Σ_u^-	1	1	1	1	−1	−1	−1	−1	−1	−1	−1	−1	1	1	1	1
Π_u	$\left(\begin{smallmatrix} 1 & 0 \\ 0 & 1 \end{smallmatrix}\right)$	$\left(\begin{smallmatrix} 0 & -1 \\ 1 & 0 \end{smallmatrix}\right)$	$\left(\begin{smallmatrix} -1 & 0 \\ 0 & -1 \end{smallmatrix}\right)$	$\left(\begin{smallmatrix} 0 & 1 \\ -1 & 0 \end{smallmatrix}\right)$	$\left(\begin{smallmatrix} -1 & 0 \\ 0 & 1 \end{smallmatrix}\right)$	$\left(\begin{smallmatrix} 0 & -1 \\ -1 & 0 \end{smallmatrix}\right)$	$\left(\begin{smallmatrix} 1 & 0 \\ 0 & -1 \end{smallmatrix}\right)$	$\left(\begin{smallmatrix} 0 & 1 \\ 1 & 0 \end{smallmatrix}\right)$	$\left(\begin{smallmatrix} -1 & 0 \\ 0 & -1 \end{smallmatrix}\right)$	$\left(\begin{smallmatrix} 0 & 1 \\ -1 & 0 \end{smallmatrix}\right)$	$\left(\begin{smallmatrix} 1 & 0 \\ 0 & 1 \end{smallmatrix}\right)$	$\left(\begin{smallmatrix} 0 & -1 \\ 1 & 0 \end{smallmatrix}\right)$	$\left(\begin{smallmatrix} 1 & 0 \\ 0 & -1 \end{smallmatrix}\right)$	$\left(\begin{smallmatrix} 0 & 1 \\ 1 & 0 \end{smallmatrix}\right)$	$\left(\begin{smallmatrix} -1 & 0 \\ 0 & 1 \end{smallmatrix}\right)$	$\left(\begin{smallmatrix} 0 & -1 \\ -1 & 0 \end{smallmatrix}\right)$

Table 5.12: Generated $D_{\infty h} = C_{\infty v} \otimes C_i$ point group table cut out for angular momentum up to $\ell = 1$.

5.4.2 *Construction of* $I_h = I \otimes C_i$

The other point group in our deMon2k implementation that is generated on-the-fly as a direct product is $I_h = I \otimes C_i$. Table 5.13 lists the generic structure of the generated I_h point group table. In this table Γ denotes any of the irreducible representations of I and $\hat{R}$ denotes any of the symmetry operations of I.

I_h	$\hat{R}\hat{E}$	$\hat{R}\hat{i}$
$\Gamma \otimes A_g$	$\chi^{\Gamma}(\hat{R}) \otimes 1$	$\chi^{\Gamma}(\hat{R}) \otimes 1$
$\Gamma \otimes A_u$	$\chi^{\Gamma}(\hat{R}) \otimes 1$	$\chi^{\Gamma}(\hat{R}) \otimes (-1)$

Table 5.13: Generic structure of I_h point group table.

Take as example the matrix representation of the symmetry operation $\hat{C}^{+}_{52}\hat{i}$ in the irreducible representation $F_u = F \otimes A_u$. It is given by:

$$\begin{aligned} \chi^{F_u}(\hat{C}^{+}_{52}\hat{i}) &= \chi^{F}(\hat{C}^{+}_{52}) \otimes \chi^{A_u}(\hat{i}) \\ \chi^{F_u}(\hat{C}^{+}_{52}\hat{i}) &= \chi^{F}(\hat{C}^{+}_{52}) \otimes (-1) \end{aligned} \tag{5.36}$$

This is just the negative of Eq. (5.21). As can be seen from Table 5.13 the only matrix representations that are different from the ones in the I point group table are the $\Gamma_u = \Gamma \otimes A_u$ irreducible representations. An extract of the point group table of I_h is shown in Table 5.14. In this table the following notations are used:

$$\hat{S}^{-}_{10,2} = \hat{C}^{+}_{52}\hat{i}, \quad \hat{S}^{-}_{6,2} = \hat{C}^{+}_{32}\hat{i}, \quad \hat{\sigma}_{va} = \hat{C}_{2a}\hat{i} \tag{5.37}$$

The complete list of the 120 symmetry operations of the I_h point group is given in Figure 5.3. In this list, the second half of the symmetry operations are the result of $\hat{R}\hat{i}$, where $\hat{R}$ denotes any of the symmetry operations of the first half of the list.

I_h	...	$\hat{C}^+_{52}$	$\hat{C}^+_{32}$	$\hat{C}_{2a}$	$\hat{S}^{3-}_{10,2}$	$\hat{S}^-_{6,2}$	$\hat{\sigma}_a$	...
A_g		$\chi^A(\hat{C}^+_{52})$	$\chi^A(\hat{C}^+_{32})$	$\chi^A(\hat{C}_{2a})$	$\chi^A(\hat{C}^+_{52})$	$\chi^A(\hat{C}^+_{32})$	$\chi^A(\hat{C}_{2a})$	
T_{1g}		$\chi^{T_1}(\hat{C}^+_{52})$	$\chi^{T_1}(\hat{C}^+_{32})$	$\chi^{T_1}(\hat{C}_{2a})$	$\chi^{T_1}(\hat{C}^+_{52})$	$\chi^{T_1}(\hat{C}^+_{32})$	$\chi^{T_1}(\hat{C}_{2a})$	
T_{2g}		$\chi^{T_2}(\hat{C}^+_{52})$	$\chi^{T_2}(\hat{C}^+_{32})$	$\chi^{T_2}(\hat{C}_{2a})$	$\chi^{T_2}(\hat{C}^+_{52})$	$\chi^{T_2}(\hat{C}^+_{32})$	$\chi^{T_2}(\hat{C}_{2a})$	
F_g		$\chi^F(\hat{C}^+_{52})$	$\chi^F(\hat{C}^+_{32})$	$\chi^F(\hat{C}_{2a})$	$\chi^F(\hat{C}^+_{52})$	$\chi^F(\hat{C}^+_{32})$	$\chi^F(\hat{C}_{2a})$	
H_g		$\chi^H(\hat{C}^+_{52})$	$\chi^H(\hat{C}^+_{32})$	$\chi^H(\hat{C}_{2a})$	$\chi^H(\hat{C}^+_{52})$	$\chi^H(\hat{C}^+_{32})$	$\chi^H(\hat{C}_{2a})$	
A_u		$\chi^A(\hat{C}^+_{52})$	$\chi^A(\hat{C}^+_{32})$	$\chi^A(\hat{C}_{2a})$	$-\chi^A(\hat{C}^+_{52})$	$-\chi^A(\hat{C}^+_{32})$	$-\chi^A(\hat{C}_{2a})$	
T_{1u}		$\chi^{T_1}(\hat{C}^+_{52})$	$\chi^{T_1}(\hat{C}^+_{32})$	$\chi^{T_1}(\hat{C}_{2a})$	$-\chi^{T_1}(\hat{C}^+_{52})$	$-\chi^{T_1}(\hat{C}^+_{32})$	$-\chi^{T_1}(\hat{C}_{2a})$	
T_{2u}		$\chi^{T_2}(\hat{C}^+_{52})$	$\chi^{T_2}(\hat{C}^+_{32})$	$\chi^{T_2}(\hat{C}_{2a})$	$-\chi^{T_2}(\hat{C}^+_{52})$	$-\chi^{T_2}(\hat{C}^+_{32})$	$-\chi^{T_2}(\hat{C}_{2a})$	
F_u		$\chi^F(\hat{C}^+_{52})$	$\chi^F(\hat{C}^+_{32})$	$\chi^F(\hat{C}_{2a})$	$-\chi^F(\hat{C}^+_{52})$	$-\chi^F(\hat{C}^+_{32})$	$-\chi^F(\hat{C}_{2a})$	
H_u		$\chi^H(\hat{C}^+_{52})$	$\chi^H(\hat{C}^+_{32})$	$\chi^H(\hat{C}_{2a})$	$-\chi^H(\hat{C}^+_{52})$	$-\chi^H(\hat{C}^+_{32})$	$-\chi^H(\hat{C}_{2a})$	

Table 5.14: Extract of the I_h point group table in terms of the generators of the I point group.

$$
\begin{aligned}
&\hat{E}, \left(\hat{C}^+_{51}, \hat{C}^+_{52}, \hat{C}^+_{53}, \hat{C}^+_{54}, \hat{C}^+_{55}, \hat{C}^+_{56}, \hat{C}^-_{51}, \hat{C}^-_{52}, \hat{C}^-_{53}, \hat{C}^-_{54}, \hat{C}^-_{55}, \hat{C}^-_{56}\right),\\
&\left(\hat{C}^{2+}_{51}, \hat{C}^{2+}_{52}, \hat{C}^{2+}_{53}, \hat{C}^{2+}_{54}, \hat{C}^{2+}_{55}, \hat{C}^{2+}_{56}, \hat{C}^{2-}_{51}, \hat{C}^{2-}_{52}, \hat{C}^{2-}_{53}, \hat{C}^{2-}_{54}, \hat{C}^{2-}_{55}, \hat{C}^{2-}_{56}\right),\\
&\Big(\hat{C}^+_{31}, \hat{C}^+_{32}, \hat{C}^+_{33}, \hat{C}^+_{34}, \hat{C}^+_{35}, \hat{C}^+_{36}, \hat{C}^+_{37}, \hat{C}^+_{38}, \hat{C}^+_{39}, \hat{C}^+_{3,10},\\
&\quad \hat{C}^-_{31}, \hat{C}^-_{32}, \hat{C}^-_{33}, \hat{C}^-_{34}, \hat{C}^-_{35}, \hat{C}^-_{36}, \hat{C}^-_{37}, \hat{C}^-_{38}, \hat{C}^-_{39}, \hat{C}^-_{3,10}\Big),\\
&\left(\hat{C}_{2a}, \hat{C}_{2b}, \hat{C}_{2c}, \hat{C}_{2d}, \hat{C}_{2e}, \hat{C}_{2f}, \hat{C}_{2g}, \hat{C}_{2h}, \hat{C}_{2i}, \hat{C}_{2j}, \hat{C}_{2k}, \hat{C}_{2l}, \hat{C}_{2m}, \hat{C}_{2n}, \hat{C}_{2o}\right),\\
&\hat{i}, \left(\hat{S}^{3-}_{10,1}, \hat{S}^{3-}_{10,2}, \hat{S}^{3-}_{10,3}, \hat{S}^{3-}_{10,4}, \hat{S}^{3-}_{10,5}, \hat{S}^{3-}_{10,6}, \hat{S}^{3+}_{10,1}, \hat{S}^{3+}_{10,2}, \hat{S}^{3+}_{10,3}, \hat{S}^{3+}_{10,4}, \hat{S}^{3+}_{10,5}, \hat{S}^{3+}_{10,6}\right),\\
&\left(\hat{S}^-_{10,1}, \hat{S}^-_{10,2}, \hat{S}^-_{10,3}, \hat{S}^-_{10,4}, \hat{S}^-_{10,5}, \hat{S}^-_{10,6}, \hat{S}^+_{10,1}, \hat{S}^+_{10,2}, \hat{S}^+_{10,3}, \hat{S}^+_{10,4}, \hat{S}^+_{10,5}, \hat{S}^+_{10,6}\right),\\
&\Big(\hat{S}^-_{61}, \hat{S}^-_{62}, \hat{S}^-_{63}, \hat{S}^-_{64}, \hat{S}^-_{65}, \hat{S}^-_{66}, \hat{S}^-_{67}, \hat{S}^-_{68}, \hat{S}^-_{69}, \hat{S}^-_{6,10},\\
&\quad \hat{S}^+_{61}, \hat{S}^+_{62}, \hat{S}^+_{63}, \hat{S}^+_{64}, \hat{S}^+_{65}, \hat{S}^+_{66}, \hat{S}^+_{67}, \hat{S}^+_{68}, \hat{S}^+_{69}, \hat{S}^+_{6,10}\Big),\\
&\left(\hat{\sigma}_a, \hat{\sigma}_b, \hat{\sigma}_c, \hat{\sigma}_d, \hat{\sigma}_e, \hat{\sigma}_f, \hat{\sigma}_g, \hat{\sigma}_h, \hat{\sigma}_i, \hat{\sigma}_j, \hat{\sigma}_k, \hat{\sigma}_l, \hat{\sigma}_m, \hat{\sigma}_n, \hat{\sigma}_o\right).
\end{aligned}
$$

Figure 5.3: List of symmetry operations in the I_h point group as given in [72].

6

VALIDATION

The validation of our symmetry-adapted SCF and density-fitting implementation consisted of four steps. First, we prepared molecular test inputs for all point groups accessible to the implementation presented in this thesis. In the next step, we validated that the **U** symmetrization matrices for the AO basis and the auxiliary functions transform the overlap and Coulomb matrix into block-diagonal form. This validation was performed for all implemented point groups varying the angular momentum of the underlying function sets. The next step was to compare total energies from symmetry-adapted ADFT Kohn-Sham and Hartree-Fock calculations with their unconstrained counterparts. For these calculations, the default settings of deMon2k were used. In the last step, the same is done for the symmetry-adapted density fitting for a subset of molecules increasing the angular momentum of the auxiliary functions and varying corresponding fitting thresholds.

6.1 Molecular test set

Molecules, 3D models, tables and geometric examples for the here discussed point groups can be found in [102] and [103]. Most of the validation test set molecules were taken from there. The selected molecules are listed in Table 6.1. All molecular geometries except Au_{72} were optimized with the PBE exchange-correlation functional [24] in combination with the DZVP [104] basis and GEN-A2 [105] auxiliary function sets. The optimized geometry of Au_{72} was taken from [106]. After the molecular structure optimizations, the molecular geometries were symmetrized either with SYMMOL [107] or VMD [108]. Next, structure similarity analyses between the symmetrized and optimized structures

	Point group	Formula	Name
1	C_2	H_2O_2	Hydrogen peroxide [102]
2	C_{2v}	H_2O	Water [102]
3	C_{2h}	N_2F_2	trans-Diflurodiazene [102]
4	C_3	$P(C_6H_5)_3$	Triphenylphosphine [109]
5	C_{3v}	NH_3	Ammonia [102]
6	C_{3h}	$B(OH)_3$	Boric acid [110]
7	C_4	$CuC_8H_{16}N_4(CH_3)_4{}^{2+}$	Tetramethyl-1,4,7,10-tetraazacyclododecane copper(II) dication [111]
8	C_{4v}	BrF_5	Bromine pentafluoride [112, 113]
9	C_{4h}	$CuN_{12}{}^{2-}$	Tetraazidocopper(II) dianion [114]
10	C_5	$C_{20}H_5Cl_5$	Pentachlorocorannulene [115]
11	C_{5v}	$NiNOC_5(CH_3)_5$	Pentamethylcyclopentadienyl nickel nitrosyl [116]
12	C_{5h}	$C_5(CH_3)_5{}^-$	Pentamethylcyclopentadienyl anion [117]
13	C_6	$(C_6O_2H_7(OH)_3)_6$	α-Cyclodextrin [118]
14	C_{6v}	$B_7{}^+$	Boronheptamer cation cluster [119]
15	C_{6h}	$C_6(N(CH_3)_2)_6$	Hexakis(dimethylamino)benzene [120]
16	D_2	$C_{10}H_{16}$	Twistane [102]
17	D_{2d}	C_3H_4	Allene [102]
18	D_{2h}	N_2O_4	Dinitrogen tetroxide [102]
19	D_3	$Fe(C_2O_4)_3{}^{3-}$	Tris(oxalato)iron(III) trianion [121]
20	D_{3d}	C_2H_6	Ethane [102]
21	D_{3h}	C_3H_6	Cyclopropane [102]
22	D_4	$C_8H_{16}S_4$	1,4,7,10-Tetrathiacyclododecane [122]
23	D_{4d}	S_8	Octasulfur [102]
24	D_{4h}	$BrF_4{}^-$	Tetrafluorobromate anion [123]
25	D_5	$YbI_2(OC_4H_8)_5{}^+$	trans-Diiodopentakis(tetrahydrofuran)ytterbium(III) cation [124]
26	D_{5d}	$Fe(C_5H_5)_2$	Ferrocene [102]
27	D_{5h}	C_{10}	Cyclo[10]carbon cluster [125]
28	D_6	$C_6N_6O_{12}$	Hexanitrobenzene [126]
29	D_{6d}	Au_{26}	D_{6d} [26]Gold cluster [127]
30	D_{6h}	C_6H_6	Benzene [102]
31	$C_{\infty v}$	HCN	Hydrogen cyanide [102]
32	$D_{\infty h}$	H_2	Hydrogen
34	C_s	C_2H_2BrCl	cis-1-Bromo-2-chloroethene [102]
33	C_i	$C_2H_2Br_2Cl_2$	1,2-Dibromo-1,2-dichloroethane [102]
35	S_4	$C_8H_4(CH_3)_4$	1,3,5,7-Tetramethylcycloocta-cis,cis,cis-1,3,5,7-tetraene [128]
36	S_6	$(C_2H_4O)_6$	1,4,7,10,13,16-hexaoxacyclooctadecane [129]
37	T	$C_{60}F_{36}$	[36]Fluorinated [60]fullerene [130, 131]
38	T_d	CH_4	Methane [102]
39	T_h	$Th(NO_3)_6{}^{2-}$	Hexanitratothorate(IV) dianion [132]
40	O	$(NC_3H_6)_8$	Dodeka(ethylene)octamine [133]
41	O_h	SF_6	Sulfur hexafluoride [102]
42	I	Au_{72}	[72]Gold fullerene [106]
43	I_h	$C_{20}H_{20}$	Dodecahedrane [134]

Table 6.1: List of test molecules.

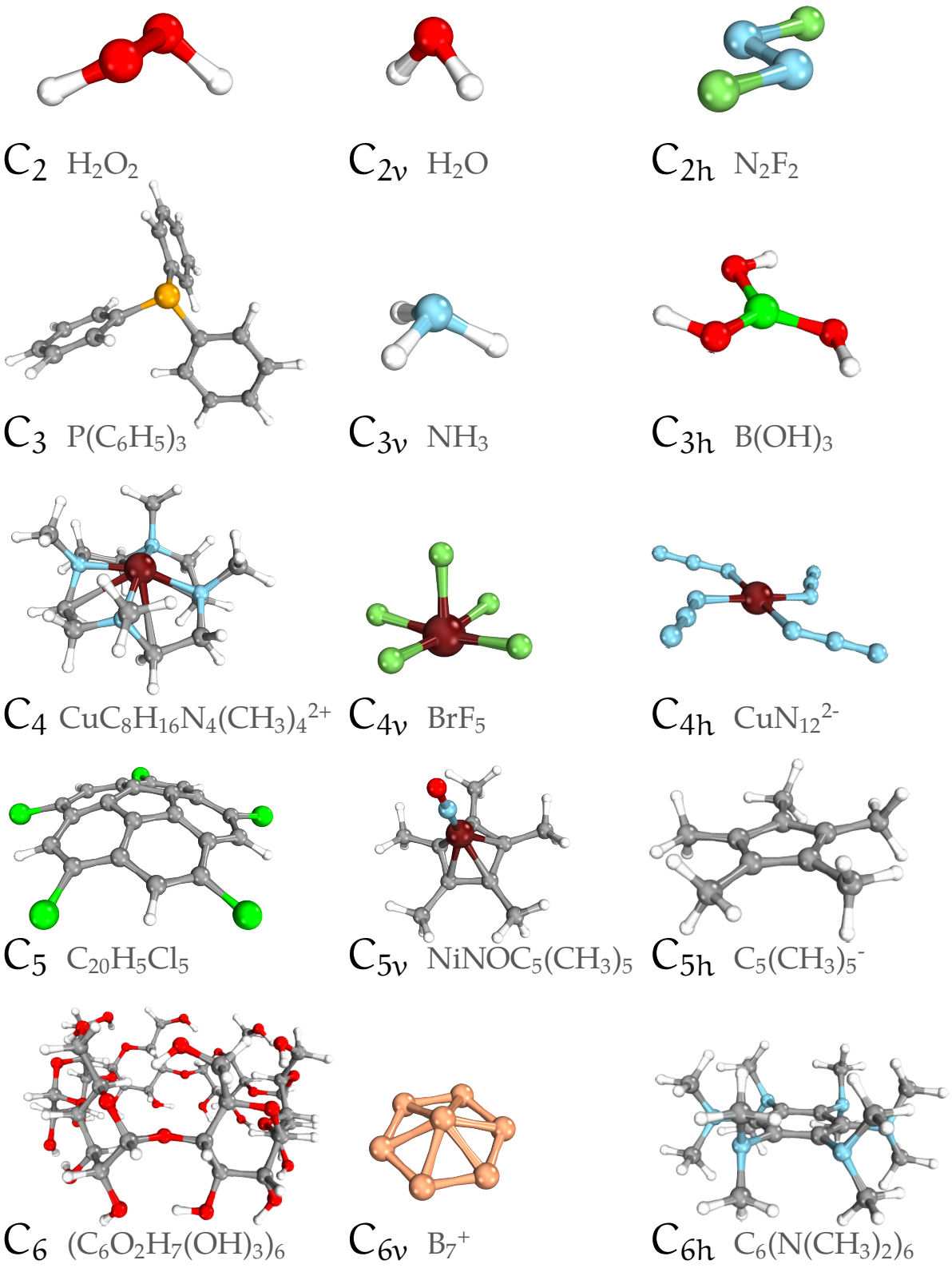

Figure 6.1: Test molecules with symmetry C_n, C_{nv} and C_{nh} with $n = 2,\ldots,6$.

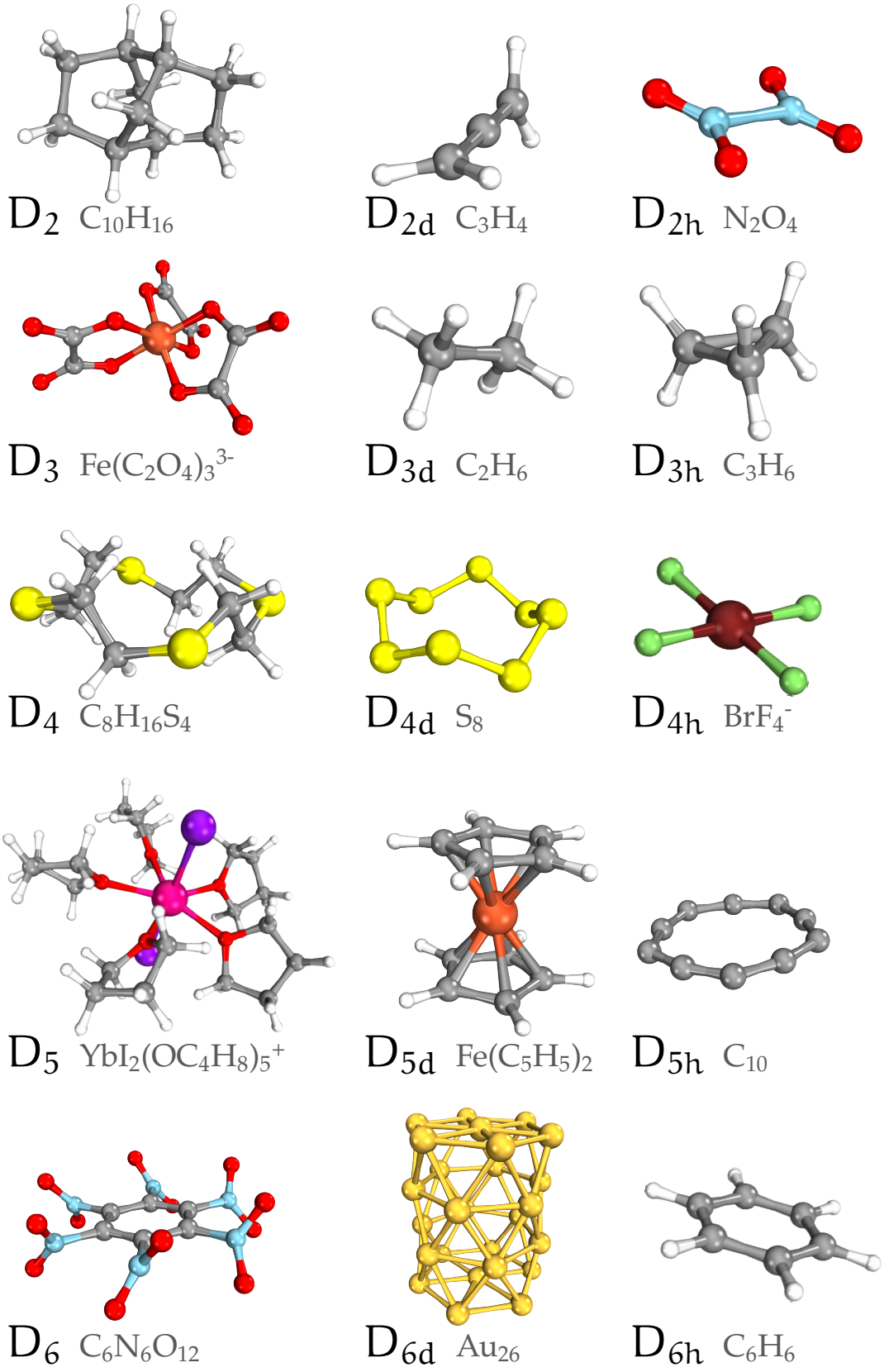

Figure 6.2: Test molecules with symmetry D_n, D_{nd} and D_{nh} with $n = 2,\ldots,6$.

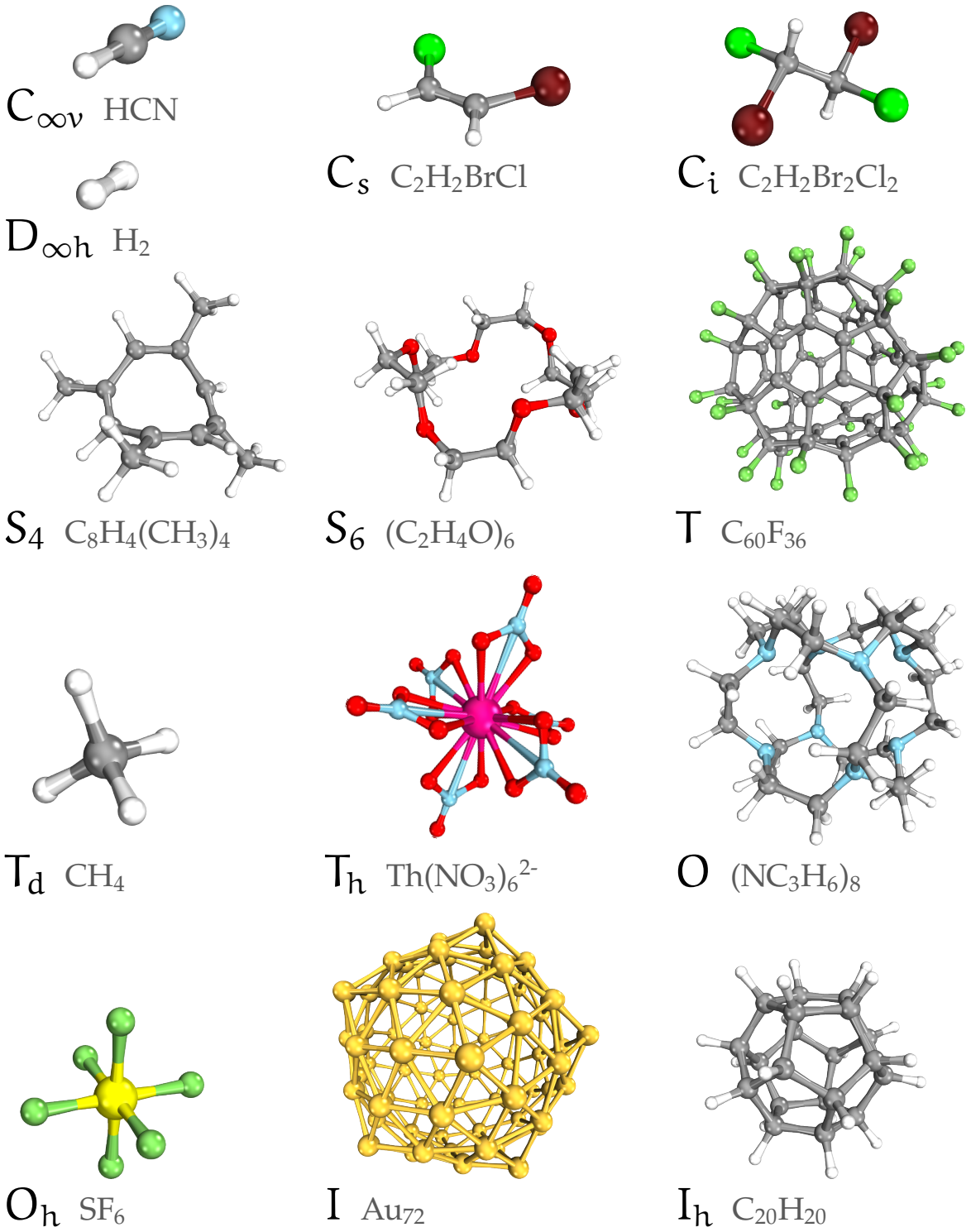

Figure 6.3: Test molecules with symmetry $C_{\infty v}$, $D_{\infty h}$, C_i, C_s, S_4, S_6, T, T_d, T_h, O, O_h, I and I_h.

were performed. The resulting similarity index [135] was in all cases larger than 0.99, which indicates an almost perfect match between the two structures. The so-obtained molecular structures are shown in Figures 6.1, 6.2 and 6.3.

6.2 Blocking of overlap and Coulomb matrices

As the unit and Coulomb operators are totally symmetric, their symmetry-adapted matrix representation must be in block-diagonal form. To probe these block-diagonal structures of the overlap and Coulomb matrix, we use basis and auxiliary functions with angular momentum up to 6, i.e. i-type functions. This limit was chosen because it covers all basis and auxiliary function sets used in this thesis. We emphasize that it does not represent a physical limit for the here presented implementation in deMon2k. For the validation of the block-diagonal form of the overlap matrix, we also employed Cartesian and spherical basis functions. For these tests, we prepared a custom basis set that has only one shell for each angular momentum with diffuse functions in such a way that the overlap matrix remains dense in the original AO basis. For the auxiliary functions, we used the GEN-A2** auxiliary function set [136] together with the custom basis set just described. This generates auxiliary functions from s- to i-type and a dense Coulomb matrix in the original auxiliary function representation. We calculated the matrices $\mathbf{S}_{\text{Cart}}$, $\mathbf{S}_{\text{Sph}}$ and $\mathbf{G}$ in the original representation as well as the corresponding symmetrization matrices $\mathbf{U}_{\text{Cart}}$, $\mathbf{U}_{\text{Sph}}$ and $\mathbf{U}_{\text{aux}}$. These matrices were exported in the matrix market format [137]. Afterwards, the relevant matrix multiplications were performed with the software Mathematica [138]. After obtaining the symmetry-adapted representations of the overlap and Coulomb matrices, we observed that all matrix elements outside the diagonal blocks of the irreducible representations are in absolute below 10^{-6} for all tests. Figure 6.4 shows the largest absolute matrix elements out of the diagonal blocks for all test molecules listed in Table 6.1. According to this figure, all outer block matrix elements are in absolute below 10^{-6}, which is the default integral threshold in deMon2k. Therefore, we conclude

from these results that the newly implemented construction of the symmetrization matrices is correct.

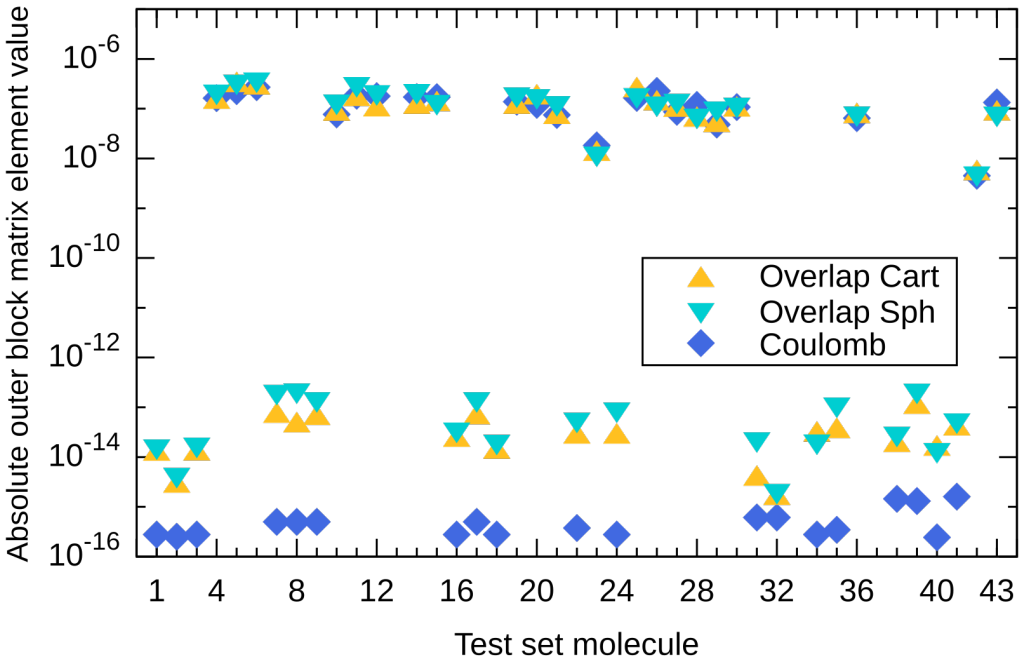

Figure 6.4: Largest absolute values of outer block matrix elements for the symmetry-adapted Cartesian and spherical overlap (triangles) and Coulomb (diamonds) matrices. See text for further details.

6.3 Symmetry-adapted DF-DFT and ADFT SCF calculations

After the construction of the symmetrization matrices has been successfully validated, we now turn to symmetry-adapted SCF calculations. To this end, we performed Hartree-Fock, DF-DFT and ADFT single-point energy calculations employing symmetry-adapted Hartree-Fock or Kohn-Sham matrices. For the validation, we calculated the differences of converged SCF energies from symmetry-adapted and unconstrained SCF runs for all molecules from Table 6.1 as:

$$\Delta E \equiv E_{SCF}^{Sym} - E_{SCF} \tag{6.1}$$

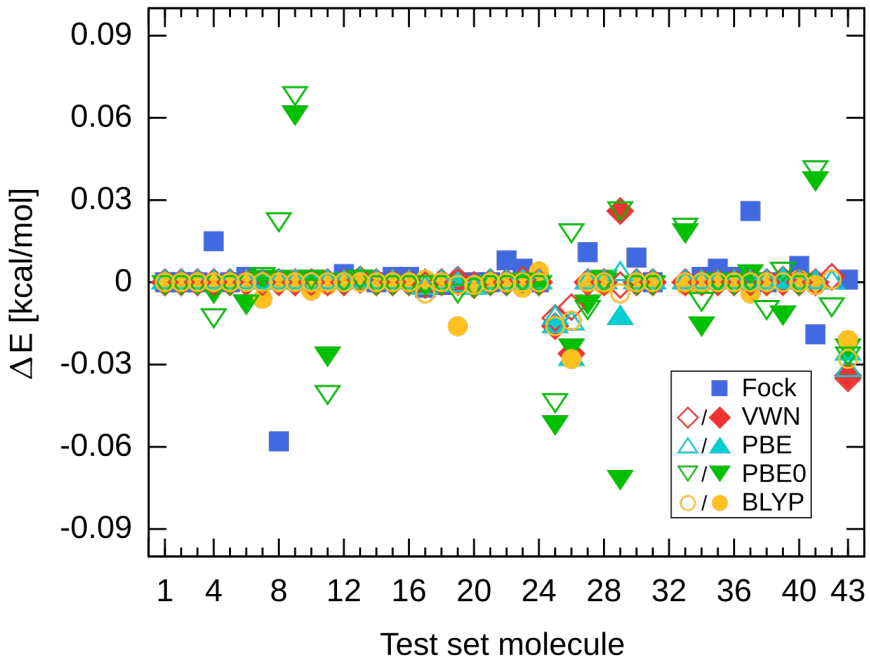

Figure 6.5: Single-point energy differences between symmetry-adapted DF-DFT (empty symbols) and ADFT (filled symbols) SCF calculations and their unconstrained counterparts. The DZVP/GEN-A2 basis and auxiliary function sets were used. See text for further details.

These calculations were performed with the DZVP basis and GEN-A2 auxiliary function set [104, 105]. Figure 6.5 depicts the energy differences for Hartree-Fock (Fock), using the variational fitting of Fock exchange [139], the local LDA with the Dirac exchange [16] and VWN [17] correlation functional, the GGA [18, 19] in form of the BLYP [20–23] and PBE [24] functionals, and the global PBE0 [26, 27] hybrid functional. As Figure 6.5 shows $|\Delta E|$ is always below 0.1 kcal/mol. Furthermore, note that $|\Delta E|$ for the Hartree-Fock calculations, which employ totally symmetric operators by construction, for the set of molecules tested, the value is smaller than 0.06 kcal/mol. This value marks the here used default SCF energy convergence threshold of 10^{-5} a.u. in deMon2k. Because the corresponding deviations for the studied density functionals are usually smaller or only insignificantly larger than this threshold, we conclude that symmetry breaking in the SCF due to the approximate nature of the exchange-correlation functionals or their unconstrained numerical integration can be neglected in symmetry-adapted DF-DFT and ADFT SCF calculations.

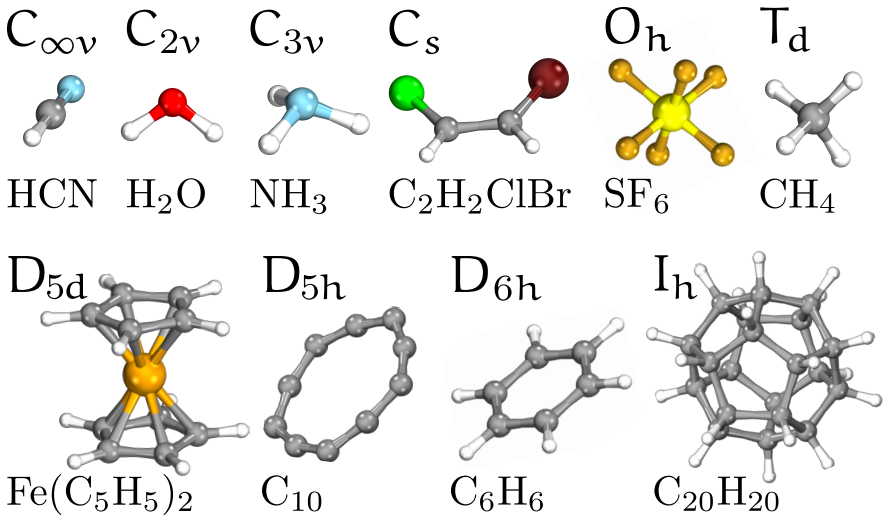

Figure 6.6: Test set of molecules for calculations with the cc-pVTZ basis set.

Aux. set	PG	System	Fock	VWN	BLYP	PBE	PBE0	LCPBE	HSE06
GEN-A2	$C_{\infty v}$	HCN	0.000	0.000	0.000	0.000	0.000	0.000	0.000
	C_{2v}	H_2O	0.000	0.000	0.000	0.000	0.000	0.000	0.000
	C_{3v}	NH_3	0.000	0.000	0.000	0.000	0.000	0.000	0.000
	C_s	C_2H_2ClBr	0.109	0.000	0.000	0.000	-0.017	0.000	-0.016
	D_{5d}	$Fe(C_5H_5)_2$	0.014	-0.001	-0.001	-0.001	-0.002	-0.001	0.000
	D_{5h}	C_{10}	0.011	0.000	0.000	0.000	-0.006	0.000	-0.006
	D_{6h}	C_6H_6	0.012	0.000	0.000	0.000	0.002	0.000	0.002
	O_h	SF_6	0.010	0.000	0.000	0.000	0.115	0.000	0.047
	T_d	CH_4	0.000	0.000	0.000	0.000	0.000	0.000	0.000
	I_h	$C_{20}H_{20}$	0.000	0.000	0.000	0.000	0.000	0.000	0.000
GEN-A2*	$C_{\infty v}$	HCN	0.000	0.000	0.000	0.000	0.000	0.000	0.000
	C_{2v}	H_2O	0.000	0.000	0.000	0.000	0.000	0.000	0.000
	C_{3v}	NH_3	0.000	0.000	0.000	0.000	0.000	0.000	0.000
	C_s	C_2H_2ClBr	-0.038	0.000	0.000	0.000	0.006	0.000	0.004
	D_{5d}	$Fe(C_5H_5)_2$	-0.005	-0.001	-0.001	-0.001	0.000	0.000	-0.001
	D_{5h}	C_{10}	-0.008	0.000	0.000	0.000	-0.003	0.000	-0.003
	D_{6h}	C_6H_6	0.002	0.000	0.000	0.000	0.001	0.000	0.001
	O_h	SF_6	0.000	0.000	0.000	0.000	0.046	0.000	-0.048
	T_d	CH_4	0.000	0.000	0.000	0.000	0.000	0.000	0.000
	I_h	$C_{20}H_{20}$	0.000	0.000	0.000	0.000	0.000	0.000	0.001

Table 6.2: Single point energy differences [kcal/mol] between symmetry-adapted ADFT and unconstrained SCF calculations with the cc-pVTZ basis set. See text for further details.

In order to investigate the influence of the basis and auxiliary function sets on these results, we performed the same validation for ADFT albeit with a smaller test set depicted in Figure 6.6, with the cc-pVTZ basis [140, 141] in combination with the GEN-A2 and GEN-A2* auxiliary function sets. The corresponding energy differences according to Eq. (6.1) are listed in Table 6.2. To this table we also added the recently implemented variational fitted range-separated LCPBE [24, 142] and HSE06 [143] hybrid functionals. As Table 6.2 shows the change of basis and auxiliary function set has no significant effect on the here discussed energy differences. Therefore, we conclude that symmetry-adapted DF-DFT and ADFT SCF calculations yield converged energies that are indistinguishable, within the SCF convergence threshold, from their unconstrained counterparts.

In order to investigate the effect of symmetry breaking in more detail, we calculated nitric oxide, NO, in $C_{\infty\nu}$ symmetry employing PBE/DZVP/GEN-A2* level of theory. Due to the odd number of electrons in this system the NO doublet ground state possesses one unpaired electron in a doubly degenerate π MO (see Figure 6.7). Therefore, a symmetry-adapted description of NO with only one Slater determinant is impossible. This is also seen by the corresponding density contribution from the single occupied π MO , given by $\pi \times \pi = \Sigma^+ + \Sigma^- + \Delta$, which yields an overall non-totally-symmetric density. In Table 6.3 the MO energies from a symmetry-adapted Kohn-Sham calculation (Sym.) are compared with those from a symmetry-unconstrained reference SCF (Ref.).

The symmetry breaking is clearly observable from the symmetry assignment of the MOs in the symmetry-adapted Kohn-Sham calculation. It is significantly stronger in the β than in the α spin manifold. This is surprising because the symmetry is broken by the occupation of the α spin manifold. The converged (unrestricted Kohn-Sham) SCF energy difference between these two calculations is only 0.3 kcal/mol. This shows that the here presented symmetry-adapted SCF implementation permits the calculation and identification of symmetry-broken SCF solutions. For comparison, we also list in Table 6.3 the results from a Kohn-Sham calculation with fractional occupation (Smear) of the highest occupied π MO. In the corresponding eigenvalue spectrum, no symmetry

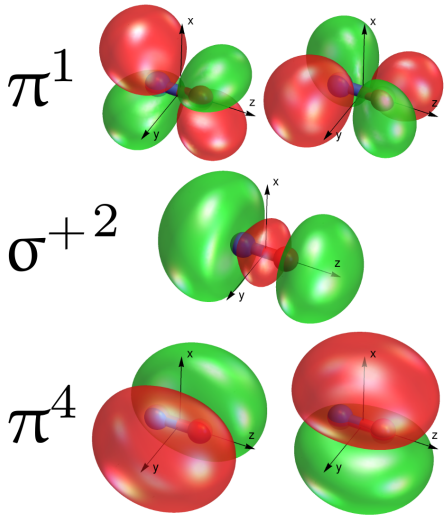

Figure 6.7: Last occupied molecular orbitals of NO corresponding to the symmetry-adapted calculation in Table 6.3. Only α MOs are shown.

	Sym.					Ref.				Smear			
	Spin α			Spin β		Spin α		Spin β		Spin α		Spin β	
n	ϵ [a.u.]	Γ	n	ϵ [a.u.]	Γ	n	ϵ [a.u.]	n	ϵ [a.u.]	n	ϵ [a.u.]	n	ϵ [a.u.]
0	0.384	$\pi(1)$	0	0.422	$\pi(1)$	0	0.383	0	0.422	0	0.384	0	0.410
0	0.387	$\pi(2)$	0	0.397	$\pi(2)$	0	0.387	0	0.397	0	0.384	0	0.410
0	0.197	σ^+	0	0.210	σ^+	0	0.197	0	0.210	0	0.197	0	0.210
0	-0.161	$\pi(2)$	0	-0.101	$\pi(1)$	0	-0.160	0	-0.101	0.5	-0.167	0	-0.123
1	-0.168	$\pi(1)$	0	-0.145	$\pi(2)$	1	-0.169	0	-0.145	0.5	-0.167	0	-0.123
1	-0.425	σ^+	1	-0.404	σ^+	1	-0.425	1	-0.404	1	-0.426	1	-0.404
1	-0.462	$\pi(1)$	1	-0.415	$\pi(1)$	1	-0.462	1	-0.415	1	-0.464	1	-0.434
1	-0.463	$\pi(2)$	1	-0.453	$\pi(2)$	1	-0.463	1	-0.453	1	-0.464	1	-0.434

Table 6.3: Molecular orbital energies (ϵ), occupations (n) and symmetry assignments (Γ) for NO. The data refer to symmetry-adapted (Sym.), unconstrained reference (Ref.) and fractional occupied (Smear) SCF calculations employing PBE/DZVP/GEN-A2* level of theory.

breaking is observed. However, the converged SCF energy of this calculation is over 1 kcal/mol above the reference energy. Thus, we find the following ordering for the converged SCF energies of the calculations in Table 6.3:

$$E_{SCF} \leqslant E_{SCF}^{Sym} < E_{SCF}^{Smear} \tag{6.2}$$

As the energy E_{SCF}^{Smear} is the highest, this underlines the variational problematic of fractional occupied Kohn-Sham calculations.

6.4 Symmetry-adapted density fitting

The just outlined symmetry-adapted SCF calculations can be further extended by a symmetry-adapted density fitting. This has been so far not discussed in the literature. In order to validate the newly developed symmetry-adapted density fitting, we performed single-point ADFT energy calculations of the molecules depicted in Figure 6.6 employing the indicated point-group symmetries for the solution of the fitting equation systems. All calculations were carried out with a SCF density fitting convergence of 10^{-5} atomic units [62]. The threshold for the TED of the Coulomb matrix was set to 10^{-7}. For the numerical integration of the exchange-correlation energy and potential the pruned fixed (75,302)p grid [144] was used. For all other keywords, the default settings of deMon2k were employed. For the single-point SCF ADFT calculations the all-electron cc-pVTZ basis [140] was used. Table 6.4 lists the energy differences between SCF calculations with symmetry-adapted density fitting, using only auxiliary functions of the totally symmetric irreducible representations, and symmetry-unconstrained SCF calculations. The listed energy differences are calculated as:

$$\Delta E \equiv E_{Fit}^{Sym} - E_{SCF} \tag{6.3}$$

The energy differences in Table 6.4 are given for Hartree-Fock (Fock), using the variational fitting of Fock exchange [139], the LDA with the Dirac exchange [16] and VWN [17] correlation functional, the GGA [18, 19] in form of the BLYP [20–23] and PBE [24] functionals, the global PBE0 [26, 27] hybrid functional and the range-separated LCPBE [24, 142] and HSE06 [143] hybrid functionals. All calculations were performed with the GEN-A2, GEN-A2* as well as GEN-A4* auxiliary function sets. As Table 6.4 shows $|\Delta E|$ is always well below 1 kcal/mol. The energy differences for the GEN-A2 auxiliary function set, which includes only s, p and d Hermite Gaussian auxiliary functions, are in absolute usually smaller than for the GEN-A2* or GEN-A4* auxiliary function sets, which include s, p, d, f and g auxiliary functions.

Aux. set	PG	System	Fock	VWN	BLYP	PBE	PBE0	LCPBE	HSE06
GEN-A2	$C_{\infty v}$	HCN	0.000	0.000	0.000	0.000	0.000	0.000	0.000
	C_{2v}	H_2O	0.000	0.000	0.000	0.000	0.000	0.000	0.000
	C_{3v}	NH_3	0.000	0.000	0.000	0.000	0.000	0.000	0.000
	C_s	C_2H_2ClBr	0.002	0.000	0.000	0.000	0.000	-0.001	0.000
	D_{5d}	$Fe(C_5H_5)_2$	0.045	0.062	0.059	0.070	0.063	0.062	0.069
	D_{5h}	C_{10}	-0.047	0.081	0.143	0.045	0.028	-0.028	0.040
	D_{6h}	C_6H_6	0.007	0.005	0.006	0.006	0.006	0.006	0.006
	O_h	SF_6	0.011	0.000	0.000	0.000	0.073	0.000	-0.035
	T_d	CH_4	0.000	0.000	0.000	0.000	0.000	0.000	0.000
	I_h	$C_{20}H_{20}$	0.005	0.001	0.001	0.001	0.002	0.003	0.002
GEN-A2*	$C_{\infty v}$	HCN	0.000	0.000	0.000	0.000	0.000	0.000	0.000
	C_{2v}	H_2O	0.000	0.000	0.000	0.000	0.000	0.000	0.000
	C_{3v}	NH_3	0.000	-0.017	-0.013	-0.014	-0.011	-0.001	-0.013
	C_s	C_2H_2ClBr	0.001	-0.001	-0.001	0.000	-0.001	-0.001	-0.001
	D_{5d}	$Fe(C_5H_5)_2$	0.025	0.058	0.004	0.011	0.025	0.048	0.025
	D_{5h}	C_{10}	-0.039	-0.049	-0.079	-0.075	-0.068	-0.058	-0.073
	D_{6h}	C_6H_6	0.006	0.008	0.015	0.021	0.016	0.001	0.022
	O_h	SF_6	-0.006	0.000	0.000	0.000	0.052	-0.001	-0.050
	T_d	CH_4	0.000	0.002	0.002	0.000	0.000	0.001	0.000
	I_h	$C_{20}H_{20}$	-0.038	-0.667	-0.532	-0.382	-0.423	-0.088	-0.503
GEN-A4*	$C_{\infty v}$	HCN	0.000	0.000	-0.001	-0.001	-0.001	-0.001	-0.001
	C_{2v}	H_2O	0.000	-0.001	-0.001	-0.001	-0.001	0.000	-0.001
	C_{3v}	NH_3	-0.001	-0.003	0.007	0.006	0.004	0.002	0.007
	C_s	C_2H_2ClBr	-0.002	-0.002	-0.001	-0.002	-0.003	-0.001	-0.003
	D_{5d}	$Fe(C_5H_5)_2$	0.029	-0.154	-0.185	-0.065	0.041	-0.058	-0.018
	D_{5h}	C_{10}	-0.026	-0.026	-0.202	0.022	0.049	0.008	0.051
	D_{6h}	C_6H_6	0.004	-0.008	-0.102	0.035	0.047	-0.004	0.053
	O_h	SF_6	-0.055	0.005	-0.089	-0.087	-0.051	-0.075	-0.086
	T_d	CH_4	0.000	-0.001	-0.002	-0.003	-0.003	-0.002	-0.003
	I_h	$C_{20}H_{20}$	-0.011	-0.019	-0.370	0.053	0.092	-0.115	0.126

Table 6.4: Energy differences [kcal/mol] of converged SCF energies employing symmetry-adapted density fitting using only the totally symmetric block of the Coulomb matrix and unconstrained density fitting. The cc-pVTZ basis set was used in all calculations. See text for further details.

At this point, it is important to note that the eigenvalues of the symmetry-adapted Coulomb matrix are different from those of the symmetry-unconstrained Coulomb

matrix. The Coulomb matrix eigenvalue spectra of ferrocene and dodecahedrane for unconstrained and symmetry-adapted density fitting are shown in Figures 6.8 and 6.9.

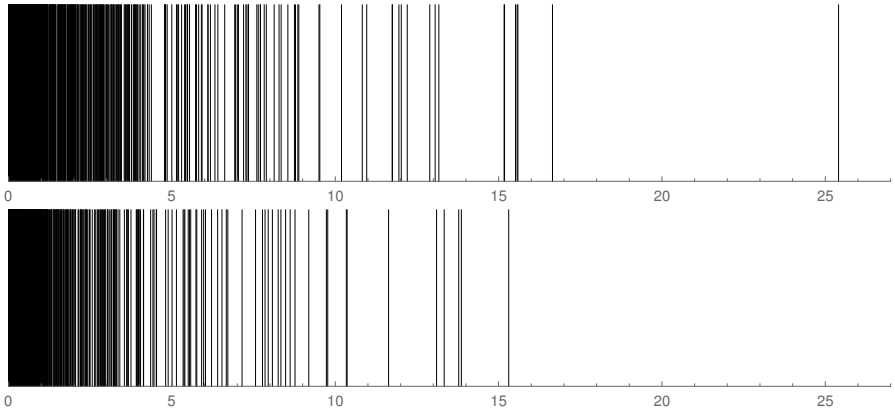

Figure 6.8: D_{5d} ferrocene cc-pVTZ/GEN-A2* eigenvalue spectrum of the Coulomb matrix in the original auxiliary function representation (top) and in symmetry-adapted auxiliary function representation including normalization (bottom).

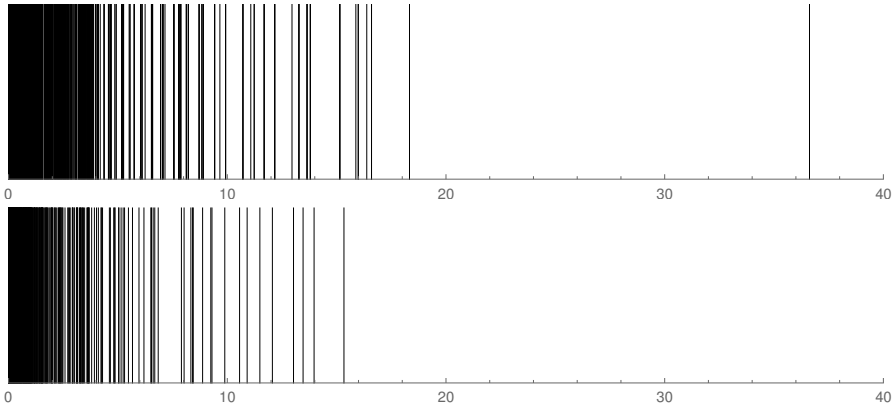

Figure 6.9: I_h dodecahedrane cc-pVTZ/GEN-A2* eigenvalue spectrum of the Coulomb matrix in the original auxiliary function representation (top) and in symmetry-adapted auxiliary function representation including normalization (bottom).

The different eigenvalue spectra of the Coulomb matrix become particularly important for the symmetry-adapted density fitting with TED. The TED, which truncates eigenvalues of the auxiliary function set according to a given threshold, acts differently in the symmetry-adapted and unconstrained density fitting. As a consequence, the converged SCF energies differ slightly. As can be seen from Table 6.4 this energy difference is for the fully analytic Hartree-Fock method always in the range of the used SCF convergence,

PG	System	Tol 10^{-x}	Fock	VWN	BLYP	PBE	PBE0	LCPBE	HSE06
D_{5d}	$Fe(C_5H_5)_2$	6	-0.076	-0.817	1.080	0.008	-0.454	-0.795	-0.400
		7	0.025	0.058	0.004	0.011	0.025	0.048	0.025
		8	0.024	0.023	-0.145	-0.034	-0.004	0.003	-0.004
D_{6h}	C_6H_6	6	-0.058	-0.498	0.956	0.042	-0.342	-0.812	-0.275
		7	0.006	0.008	0.015	0.021	0.016	0.001	0.022
		8	0.013	0.023	0.056	0.073	0.058	-0.007	0.078
O_h	SF_6	6	-0.063	-0.384	-0.880	-0.918	-0.689	-0.411	-0.767
		7	-0.006	0.000	0.000	0.000	0.052	-0.001	-0.050
		8	0.007	0.000	0.000	0.000	0.044	-0.001	-0.051
I_h	$C_{20}H_{20}$	6	-0.281	-3.495	1.132	-2.202	-2.787	-1.814	-3.153
		7	-0.038	-0.667	-0.532	-0.382	-0.423	-0.088	-0.503
		8	-0.003	0.025	-0.389	-0.356	-0.218	-0.090	-0.252

Table 6.5: Energy differences [kcal/mol] of converged SCF energies between unconstrained and symmetry-adapted density fitting using only the totally symmetric block of the Coulomb matrix. The cc-pVTZ/GEN-A2* basis and auxiliary function sets were used in all calculations. The Tol 10^{-x} column denotes the TED tolerance. See text for further details.

whereas larger deviations of around 0.5 kcal/mol are observed for LDA, GGA and hybrid functionals. At first glance, it is tempting to attribute these larger deviations to the unsymmetrical numerical integration grid. However, closer inspection reveals that numerical integration errors are at least one order of magnitude smaller than the energy differences found in Table 6.4 for $C_{20}H_{20}$ with the GEN-A2* auxiliary function set and LDA, GGA or hybrid functionals. In fact, these energy differences can be substantially reduced if the Coulomb matrix TED in the symmetry-adapted density fitting only acts on negative eigenvalues. Therefore, the larger energy differences in Table 6.4 are caused by the TED of the Coulomb matrix. To explore this behavior in more detail we conducted cc-pVTZ/GEN-A2* calculations using different TED tolerances. The results are shown in Table 6.5. As can be seen from this table, a substantial reduction of the energy difference is obtained when the TED tolerance is tightened from 10^{-6} to 10^{-7}. This is the reason why we set the TED tolerance to 10^{-7} for all symmetry-adapted density fitting calculations.

In order to investigate the effect of reducing the Coulomb matrix to its totally symmetric block, Eq. (3.55), we performed the calculations of Table 6.4 once again but now using

all symmetry-adapted blocks of the Coulomb matrix. These results are listed in Table 6.6. As the comparison with Table 6.4 shows, the reduction of the Coulomb matrix to its totally symmetric block introduces no additional deviations with respect to the symmetry-unconstrained reference. In fact, we even find the contrary, namely smaller deviations for the symmetry-adapted density fitting using only the totally symmetric block of the Coulomb matrix. This unexpected result can be rationalized by the different eigenvalue spectra (see Figures 6.8 and 6.9) of the unconstrained and symmetry-adapted Coulomb matrix. If only the totally symmetric block of the Coulomb matrix is used, this difference becomes smaller because the effect of TED in the symmetry-adapted density fitting is minimized. On the other hand, if the eigenvalue spectrum of the Coulomb matrix would be homogeneously dense, the effect of different TEDs would become negligible. This is the reason why on average the energy deviations in Table 6.4 and 6.6 decrease when going from GEN-A2* to GEN-A4*.

So far we have investigated symmetry-adapted density fitting using symmetry-unconstrained SCF calculations. Now we combine symmetry-adapted density fitting with symmetry-adapted SCF calculations. To this end, we performed once again the calculations of Table 6.4, however now with symmetry-adapted SCF . These results are listed in Table 6.7. Comparison with Table 6.4 shows that symmetry adaptation of the SCF has on average little to no effect on the observed energy deviations. The same holds for the symmetry-adapted density fitting using all symmetry-adapted blocks of the Coulomb matrix as the comparison of Table 6.7 and 6.8 shows. We observe that the energy differences decrease for the I_h system when using the GEN-A4* instead of the GEN-A2* auxiliary function set. However, such an improvement is not found for all systems. In general, the best agreement between unconstrained and symmetry-adapted density fitting calculations is found for GEN-A2 and GEN-A4*. From these calculations we conclude that it is best to use in symmetry-adapted density fitting only the totally symmetric part of the auxiliary density. In combination with symmetry-adapted Kohn-Sham SCF calculations, this approach yields converged energies that are in good agreement

with symmetry-unconstrained results. In fact, for the GEN-A2 auxiliary function set the observed deviations are negligible.

Aux. set	PG	System	Fock	VWN	BLYP	PBE	PBE0	LCPBE	HSE06
GEN-A2	$C_{\infty v}$	HCN	0.000	0.000	0.000	0.000	0.000	0.000	0.000
	C_{2v}	H_2O	0.000	0.000	0.000	0.000	0.000	0.000	0.000
	C_{3v}	NH_3	0.000	0.000	0.000	0.000	0.000	0.000	0.000
	C_s	C_2H_2ClBr	0.000	0.000	0.000	0.000	0.000	-0.001	0.000
	D_{5d}	$Fe(C_5H_5)_2$	0.053	0.061	0.058	0.068	0.067	0.058	0.069
	D_{5h}	C_{10}	-0.028	-0.021	-0.020	-0.022	-0.023	-0.030	-0.023
	D_{6h}	C_6H_6	0.007	0.005	0.005	0.006	0.006	0.006	0.006
	O_h	SF_6	-0.097	0.000	0.000	0.000	-0.035	-0.001	-0.038
	T_d	CH_4	0.000	0.000	0.001	0.000	0.000	0.000	0.000
	I_h	$C_{20}H_{20}$	0.003	-0.002	-0.005	-0.006	-0.003	-0.003	-0.004
GEN-A2*	$C_{\infty v}$	HCN	0.000	0.000	0.000	0.000	0.000	0.000	0.000
	C_{2v}	H_2O	0.000	0.000	0.000	0.000	0.000	0.000	0.000
	C_{3v}	NH_3	0.002	-0.002	0.038	0.036	0.025	0.021	0.035
	C_s	C_2H_2ClBr	0.018	0.044	-0.576	-0.338	-0.196	-0.349	-0.221
	D_{5d}	$Fe(C_5H_5)_2$	0.025	-0.002	-0.009	-0.008	0.004	0.035	0.005
	D_{5h}	C_{10}	-0.046	-0.048	-0.085	-0.051	-0.045	-0.037	-0.048
	D_{6h}	C_6H_6	0.007	-0.014	-0.001	-0.008	-0.005	-0.003	-0.006
	O_h	SF_6	-0.003	0.223	0.176	0.236	0.216	0.009	0.182
	T_d	CH_4	0.000	0.002	0.002	0.000	0.000	0.001	0.000
	I_h	$C_{20}H_{20}$	-0.032	-0.735	-0.627	-0.459	-0.476	-0.116	-0.563
GEN-A4*	$C_{\infty v}$	HCN	0.000	0.000	-0.001	-0.001	-0.001	-0.001	-0.001
	C_{2v}	H_2O	0.000	-0.001	-0.001	-0.001	-0.001	0.000	-0.001
	C_{3v}	NH_3	-0.001	-0.007	0.008	0.003	0.001	0.001	0.003
	C_s	C_2H_2ClBr	-0.003	-0.002	-0.002	-0.002	-0.003	-0.001	-0.003
	D_{5d}	$Fe(C_5H_5)_2$	0.035	-0.535	-0.713	-0.464	-0.637	-0.288	-0.376
	D_{5h}	C_{10}	-0.023	-0.056	-0.250	-0.014	0.020	-0.016	0.021
	D_{6h}	C_6H_6	0.007	-0.065	-0.183	-0.023	0.001	-0.030	0.003
	O_h	SF_6	-0.003	0.004	-0.089	-0.087	-0.066	-0.075	-0.036
	T_d	CH_4	0.000	-0.001	-0.002	-0.003	-0.003	-0.002	-0.003
	I_h	$C_{20}H_{20}$	-0.004	-0.127	-0.493	-0.068	-0.004	-0.162	0.019

Table 6.6: Energy differences [kcal/mol] of converged SCF energies employing symmetry-adapted and unconstrained density fitting. The cc-pVTZ basis set was used in all calculations. See text for further details.

Aux. set	PG	System	Fock	VWN	BLYP	PBE	PBE0	LCPBE	HSE06
GEN-A2	$C_{\infty v}$	HCN	0.000	0.000	0.000	0.000	0.000	0.000	0.000
	C_{2v}	H_2O	0.000	0.000	0.000	0.000	0.000	0.000	0.000
	C_{3v}	NH_3	0.000	0.000	0.000	0.000	0.000	0.000	0.000
	C_s	C_2H_2ClBr	0.109	0.000	0.000	0.000	-0.017	-0.001	-0.016
	D_{5d}	$Fe(C_5H_5)_2$	0.013	0.061	0.059	0.069	0.070	0.058	0.069
	D_{5h}	C_{10}	-0.029	-0.020	-0.021	-0.021	-0.027	-0.029	-0.027
	D_{6h}	C_6H_6	0.018	0.005	0.006	0.006	0.009	0.006	0.009
	O_h	SF_6	0.000	0.000	0.000	0.000	-0.007	-0.001	-0.095
	T_d	CH_4	0.000	0.000	0.001	0.000	0.000	0.000	0.000
	I_h	$C_{20}H_{20}$	0.001	0.001	0.001	0.001	0.001	0.000	0.001
GEN-A2*	$C_{\infty v}$	HCN	0.000	0.000	0.000	0.000	0.000	0.000	0.000
	C_{2v}	H_2O	0.000	0.000	0.000	0.000	0.000	0.000	0.000
	C_{3v}	NH_3	0.002	-0.001	0.037	0.037	0.026	0.021	0.035
	C_s	C_2H_2ClBr	-0.020	0.044	-0.576	-0.338	-0.189	-0.349	-0.218
	D_{5d}	$Fe(C_5H_5)_2$	0.031	0.035	0.039	0.029	0.034	0.048	0.040
	D_{5h}	C_{10}	-0.046	-0.043	-0.075	-0.046	-0.044	-0.035	-0.045
	D_{6h}	C_6H_6	0.008	0.021	0.039	0.029	0.025	0.006	0.030
	O_h	SF_6	0.003	0.223	0.176	0.236	0.258	0.009	0.214
	T_d	CH_4	0.000	0.002	0.002	0.000	0.000	0.001	0.000
	I_h	$C_{20}H_{20}$	-0.040	-0.667	-0.532	-0.382	-0.423	-0.091	-0.502
GEN-A4*	$C_{\infty v}$	HCN	0.000	0.000	-0.001	-0.001	-0.001	-0.001	-0.001
	C_{2v}	H_2O	0.000	-0.001	-0.001	-0.001	-0.001	0.000	-0.001
	C_{3v}	NH_3	-0.001	-0.003	0.007	0.006	0.004	0.002	0.007
	C_s	C_2H_2ClBr	-0.049	-0.002	-0.003	-0.003	-0.003	-0.003	-0.001
	D_{5d}	$Fe(C_5H_5)_2$	0.028	-0.156	-0.186	-0.065	-0.300	-0.058	-0.018
	D_{5h}	C_{10}	-0.026	-0.026	-0.201	0.022	0.048	0.008	0.050
	D_{6h}	C_6H_6	0.004	-0.008	-0.102	0.035	0.047	-0.004	0.053
	O_h	SF_6	-0.005	0.005	-0.089	-0.087	-0.050	-0.075	-0.051
	T_d	CH_4	0.000	-0.001	-0.002	-0.003	-0.003	-0.002	-0.003
	I_h	$C_{20}H_{20}$	-0.012	-0.019	-0.370	0.053	0.092	-0.115	0.126

Table 6.7: Energy differences [kcal/mol] of converged symmetry-adapted SCF energies employing symmetry-adapted density fitting using only the totally symmetric block of the Coulomb matrix and unconstrained SCF calculation. The cc-pVTZ basis set was used in all calculations. See text for further details.

Aux. set	PG	System	Fock	VWN	BLYP	PBE	PBE0	LCPBE	HSE06
GEN-A2	$C_{\infty v}$	HCN	0.000	0.000	0.000	0.000	0.000	0.000	0.000
	C_{2v}	H_2O	0.000	0.000	0.000	0.000	0.000	0.000	0.000
	C_{3v}	NH_3	0.000	0.000	0.000	0.000	0.000	0.000	0.000
	C_s	C_2H_2ClBr	0.108	0.000	0.000	0.000	-0.017	-0.001	-0.016
	D_{5d}	$Fe(C_5H_5)_2$	0.058	0.060	0.058	0.067	0.069	0.058	0.071
	D_{5h}	C_{10}	-0.029	-0.021	-0.020	-0.022	-0.028	-0.030	-0.029
	D_{6h}	C_6H_6	0.018	0.005	0.005	0.006	0.008	0.006	0.008
	O_h	SF_6	-0.030	0.000	0.000	0.000	0.118	-0.001	-0.046
	T_d	CH_4	0.000	0.000	0.001	0.000	0.000	0.000	0.000
	I_h	$C_{20}H_{20}$	0.003	-0.002	-0.004	-0.005	-0.003	-0.003	-0.004
GEN-A2*	$C_{\infty v}$	HCN	0.000	0.000	0.000	0.000	0.000	0.000	0.000
	C_{2v}	H_2O	0.000	0.000	0.000	0.000	0.000	0.000	0.000
	C_{3v}	NH_3	0.002	-0.002	0.038	0.036	0.025	0.021	0.035
	C_s	C_2H_2ClBr	-0.020	0.043	-0.576	-0.338	-0.189	-0.349	-0.218
	D_{5d}	$Fe(C_5H_5)_2$	0.025	-0.003	-0.009	-0.008	0.003	0.035	0.005
	D_{5h}	C_{10}	-0.046	-0.048	-0.085	-0.051	-0.048	-0.037	-0.050
	D_{6h}	C_6H_6	0.010	-0.013	-0.003	-0.007	-0.004	-0.003	-0.004
	O_h	SF_6	0.002	0.223	0.176	0.236	0.218	0.009	0.193
	T_d	CH_4	0.000	0.002	0.002	0.000	0.000	0.001	0.000
	I_h	$C_{20}H_{20}$	-0.031	-0.734	-0.626	-0.458	-0.475	-0.115	-0.562
GEN-A4*	$C_{\infty v}$	HCN	0.000	0.000	-0.001	-0.001	-0.001	-0.001	-0.001
	C_{2v}	H_2O	0.000	-0.001	-0.001	-0.001	-0.001	0.000	-0.001
	C_{3v}	NH_3	-0.001	-0.007	0.008	0.003	0.001	0.001	0.003
	C_s	C_2H_2ClBr	-0.046	-0.002	-0.002	-0.002	-0.004	-0.002	0.000
	D_{5d}	$Fe(C_5H_5)_2$	0.038	-0.535	-0.713	-0.464	-0.636	-0.288	-0.375
	D_{5h}	C_{10}	-0.023	-0.056	-0.250	-0.014	0.018	-0.016	0.019
	D_{6h}	C_6H_6	0.007	-0.065	-0.183	-0.023	0.001	-0.030	0.003
	O_h	SF_6	0.003	0.005	-0.089	-0.087	-0.075	-0.075	-0.076
	T_d	CH_4	0.000	-0.001	-0.002	-0.003	-0.003	-0.002	-0.003
	I_h	$C_{20}H_{20}$	-0.004	-0.126	-0.493	-0.067	-0.004	-0.161	0.019

Table 6.8: Energy differences [kcal/mol] of converged symmetry-adapted SCF energies employing symmetry-adapted density fitting and unconstrained SCF calculation. The cc-pVTZ basis set was used in all calculations. See text for further details.

7

APPLICATIONS

7.1 Fullerenes

After the symmetry-adapted fitting of Coulomb and exchange-correlation coefficients has been validated, we now analyze the computational performance for the symmetry-adapted density fitting using only totally symmetric auxiliary functions. To this end, we carried out single-point ADFT energy calculations of icosahedral fullerenes ranging from C_{20} to C_{2160}. The geometries were provided from Dr. Pedroza-Montero [145] except for the geometry of C_{2160}, which was taken from the literature [146]. The here presented calculations were performed with the PBE/DZVP/GEN-A2* methodology. Figures 7.1 and 7.2 compare Central Processing Unit (CPU) timings between the recently developed MINRES fitting approach [54] and the here proposed symmetry-adapted TED fitting (SYMTED) using only the totally symmetric block of the Coulomb matrix in symmetry representation. The calculations were performed using 24 Intel(R) Xeon(R) CPU cores with 20 GB of Random Access Memory (RAM) per core. As Figures 7.1 and 7.2 show symmetry-adapted density fitting is for these systems always computationally more efficient than MINRES without symmetry constraints. The CPU times of the different density fitting approaches along with their RAM demands per core are listed in Table 7.1. For comparison, we also include in this table the reference data for the unconstrained TED density fitting. For the fullerene, C_{960}, symmetry-adapted TED density fitting is more than 250 times faster than its unconstrained reference and still more than 7 times faster than unconstrained MINRES. For the largest fullerene, C_{2160}, symmetry-adapted

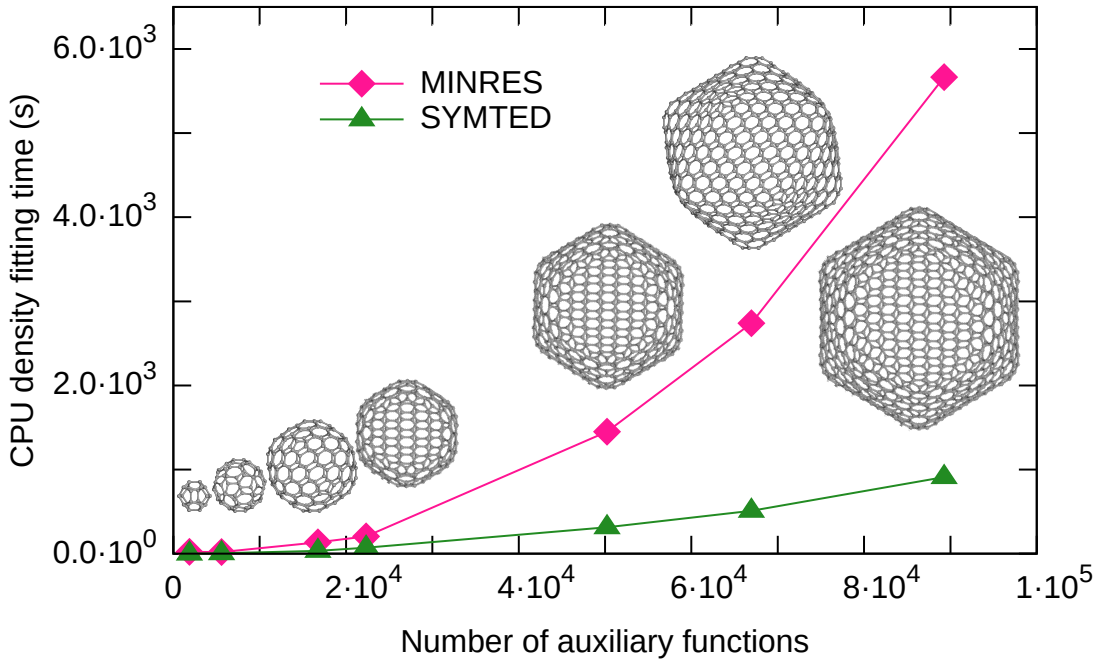

Figure 7.1: CPU time for MINRES and symmetry-adapted TED (SYMTED) density fitting in icosahedral fullerenes up to C_{960} [88] using PBE/DZVP/GEN-A2* methodology. To guide the eye, the data points are connected by lines.

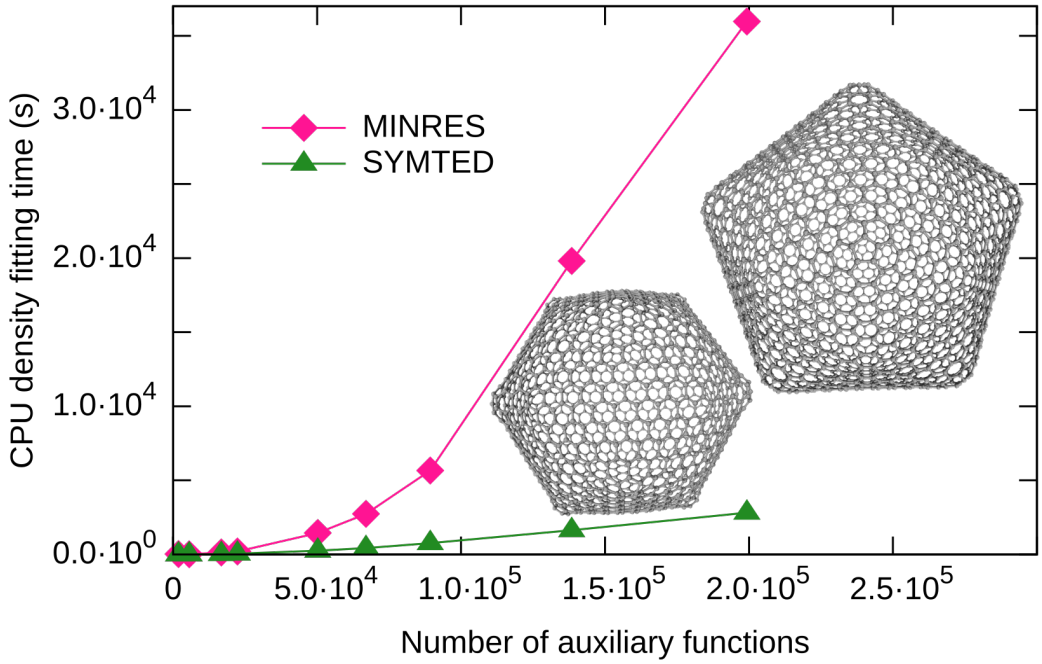

Figure 7.2: CPU time for MINRES and symmetry-adapted TED (SYMTED) density fitting in the icosahedral fullerenes C_{1500} and C_{2160} using PBE/DZVP/GEN-A2* methodology. To guide the eye, the data points are connected by lines.

	Fitting CPU time [s]			Fitting RAM demand [MB]		
System	TED	MINRES	SYMTED	TED	MINRES	SYMTED
C_{20}	1.7	20.4	0.3	1.19	4.63	0.55
C_{60}	61.6	17.7	2.2	10.02	7.83	0.68
C_{180}	1573.1	134.9	22.9	89.30	17.72	1.25
C_{240}	3694.4	206.2	53.5	158.63	22.83	1.61
C_{540}	43150.6	1450.2	254.4	802.23	50.03	4.29
C_{720}	103841.7	2740.6	432.0	1425.94	67.67	6.57
C_{960}	255725.4	5665.9	759.0	2534.70	92.72	10.38
C_{1500}	1017714.2*	19802.9	1635.3	6187.39	155.52	22.25
C_{2160}	3119399.4*	35972.1	2819.9	12829.41	244.36	43.00

Table 7.1: Fitting CPU times [s] and RAM demands [MB/core] for single-point energy calculations of icosahedral fullerenes employing the TED, MINRES and SYMTED density fitting approaches. Values with * are estimated.

TED density fitting is estimated to be more than 1101 times faster than its unconstrained reference and still more than 20 times faster than unconstrained MINRES density fitting. The estimations (values with * in Table 7.1) were performed by fitting the calculated data points to a polynomial of degree 3, $a + bx + cx^2 + dx^3$, where the a, b, c and d coefficients are determined to -3.74×10^2, 1.12×10^{-1}, -5.85×10^{-6} and 4.11×10^{-10}. The estimated calculations, although still feasible, would take months to finish.

Furthermore, as Table 7.1 shows, symmetry-adapted density fitting shows sub-quadratic scaling for the CPU time with respect to the fullerene system sizes and dramatically reduced RAM demand. Thus, the here used large RAM node is mainly necessary for the TED reference calculations and the RAM demand of the SCF .

7.2 Uranium dimer

The here presented U_2 studies were performed in collaboration with Dr. Pérez-Figueroa [136]. She performed symmetry-adapted calculations with the Kohn-Sham matrix in symmetry representation in an unrestricted Kohn-Sham methodology using effective core potentials. These calculations provided molecular orbitals that are symmetry-adapted.

On the other hand, symmetry-unconstrained calculations yield MOs that are symmetry distorted. The resulting MO diagrams of the optimized system [136] are shown in Figure 7.3. This diagram was calculated using the PBE exchange-correlation functional with a 32 valence electron quasi-relativistic pseudo potential [147] from the Stuttgart-Dresden group in combination with a corresponding energy-optimized valence basis set [148]. For the density fitting the GEN-A2** auxiliary function set [136] was used. As can be seen

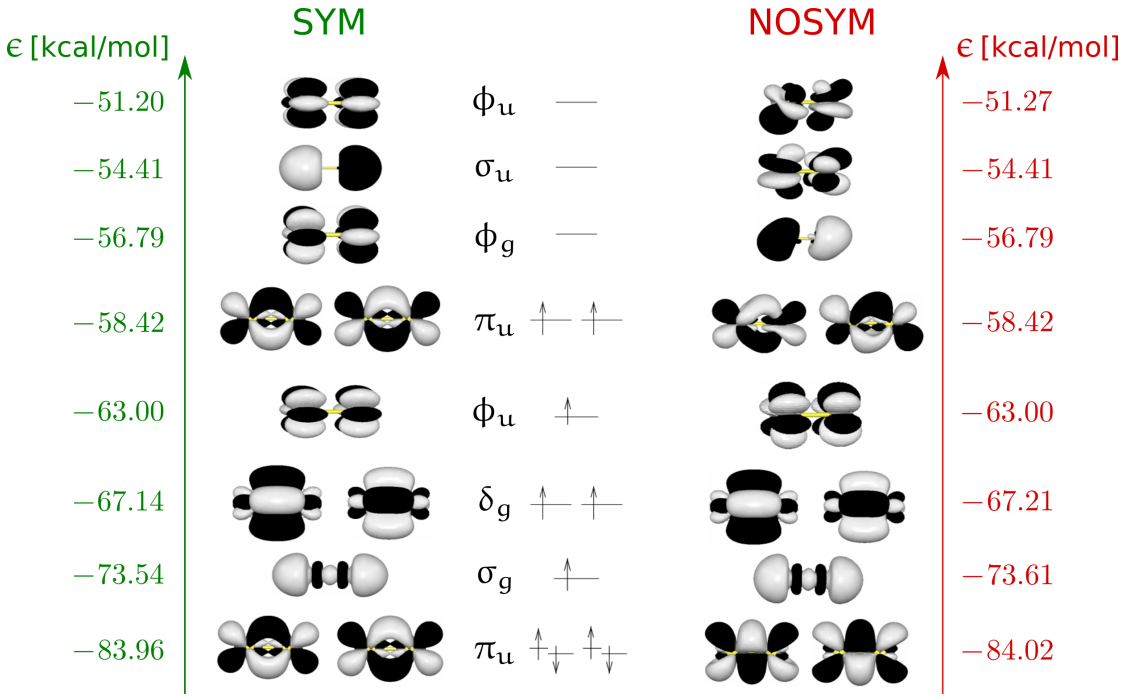

Figure 7.3: Uranium dimer ground state molecular orbital diagram from symmetry-adapted (left) and symmetry-unconstrained (right) calculation. Only the α MOs and energies are shown.

from Figure 7.3 the MO symmetry distortion in the symmetry-unconstrained calculation is most pronounced at the Fermi level and above. On the other hand, the symmetry-adapted calculation shows a symmetry breaking due to the single occupation of the doubly degenerate ϕ_u MO. Therefore, the electron density from the symmetry-adapted calculation of this system has contributions other than the totally symmetric one due to:

$$\phi_u \otimes \phi_u = \Sigma_g^+ + \Sigma_g^- + I_g \tag{7.1}$$

As a result, the Kohn-Sham operator and, thus, the Kohn-Sham matrix are symmetry broken. This manifests itself in the different energies and occupations of symmetry-degenerate orbitals as in the example of NO (see Table 6.3). For the uranium dimer, this symmetry breaking is most pronounced by the different occupations of the symmetry-degenerate ϕ_u MOs in Figure 7.3.

	SYM		NOSYM	
Mult.	r_e [Å]	ΔE [kcal/mol]	r_e [Å]	ΔE [kcal/mol]
5	2.31	4.63	2.24	4.34
7	2.27	0.00	2.27	**0.00**
9	2.45	6.53	2.46	6.53
11	2.61	5.61	2.60	5.61
D_e [kcal/mol]	97.86 (65.14)		97.86 (72.16)	

Table 7.2: Optimized bond lengths and relative energies of symmetry-adapted (SYM) and symmetry-unconstrained (NOSYM) PBE/QECP32/GEN-A4** calculations of U_2 with different spin multiplicities. The dissociation energy refers to the septet ground state. Values in parentheses are from single-point PBE0 calculations on top of PBE optimized structures.

The only experimental data available for neutral U_2 is its dissociation energy of 52 ± 5 kcal/mol [149]. This value was obtained at temperatures in the range of 2500−2700 K under the assumption of a bond length of 3.0 Å. Table 7.2 lists optimized equilibrium distances of U_2 using multiplicities 5, 7, 9 and 11 from symmetry-adapted and symmetry-unconstrained SCF calculations. These calculations were performed using the previously mentioned level of theory together with the GEN-A4** auxiliary function set. As can be seen from this table the calculations agree for multiplicities 7, 9 and 11, whereas for multiplicity 5 there is a deviation of 0.07 Å in the bond length, with a larger optimized distance from the symmetry-adapted SCF. Also in Table 7.2 are shown the dissociation energies calculated with PBE and PBE0 exchange-correlation functionals using symmetry-adapted and symmetry-unconstrained SCF calculations at the optimized bond length of 2.27 Å with multiplicity 7. The dissociation energies calculated with the PBE functional agree well with each other. For the PBE0 calculations the dissociation energies differ by

8.46 kcal/mol. As expected from the variational principle the symmetry-adapted PBE0 dissociation energy is smaller. As a result, it is closer to the experimental reference.

7.3 TD-ADFT

In the Time Dependent Auxiliary Density Functional Theory (TD-ADFT) methodology, employing the random phase approximation, the excited states are calculated as eigenvectors of the eigenvalue equation [50, 150, 151]:

$$\mathbf{\Omega F} = \omega^2 \mathbf{F} \tag{7.2}$$

The elements of the matrix $\mathbf{\Omega}$ are given by:

$$\Omega_{ia,jb} = \delta_{ab}\delta_{ij}\left(\epsilon_a - \epsilon_i\right)^2 + 2\sqrt{\epsilon_a - \epsilon_i}K_{ia,jb}\sqrt{\epsilon_b - \epsilon_j} \tag{7.3}$$

with:

$$\begin{aligned} K_{ia,jb} = &\sum_{\bar{m},\bar{n}} \langle ia\|\bar{m}\rangle G^{-1}_{\bar{m}\bar{n}} \langle \bar{n}\|jb\rangle + \\ &\sum_{\bar{m},\bar{n}}\sum_{\bar{k},\bar{l}} \langle ia\|\bar{k}\rangle G^{-1}_{\bar{k}\bar{l}} \left\langle \bar{l}\left|f_{xc}[\tilde{\rho}]\right|\bar{m}\right\rangle G^{-1}_{\bar{m}\bar{n}} \langle \bar{n}\|jb\rangle \end{aligned} \tag{7.4}$$

In Eq. (7.4) $f_{xc}[\tilde{\rho}]$ is the ADFT exchange-correlation kernel $\frac{\delta^2 E_{xc}[\tilde{\rho}]}{\delta\tilde{\rho}(\mathbf{r})\delta\tilde{\rho}(\mathbf{r}')}$. From the solution of Eq. (7.2), the excitation energies, ω, and the oscillator strengths can be obtained. The elements of the eigenvectors $\mathbf{F}$ are double-index labeled by occupied MOs, ψ_i^Γ, and unoccupied MOs, $\psi_a^{\Gamma'}$, denoting the product $\psi_i^\Gamma\psi_a^{\Gamma'}$. Here we have added to the MOs irreducible representation labels since each MO is assigned to an irreducible representation when the TD-ADFT calculation is performed on top of a symmetry-adapted Kohn-Sham SCF. As a result, each element of the eigenvectors $\mathbf{F}$ can be assigned to an irreducible representation, which reflects the corresponding excitation. Thus, for labeling the excitation contributions to the excitation energies, the direct product of

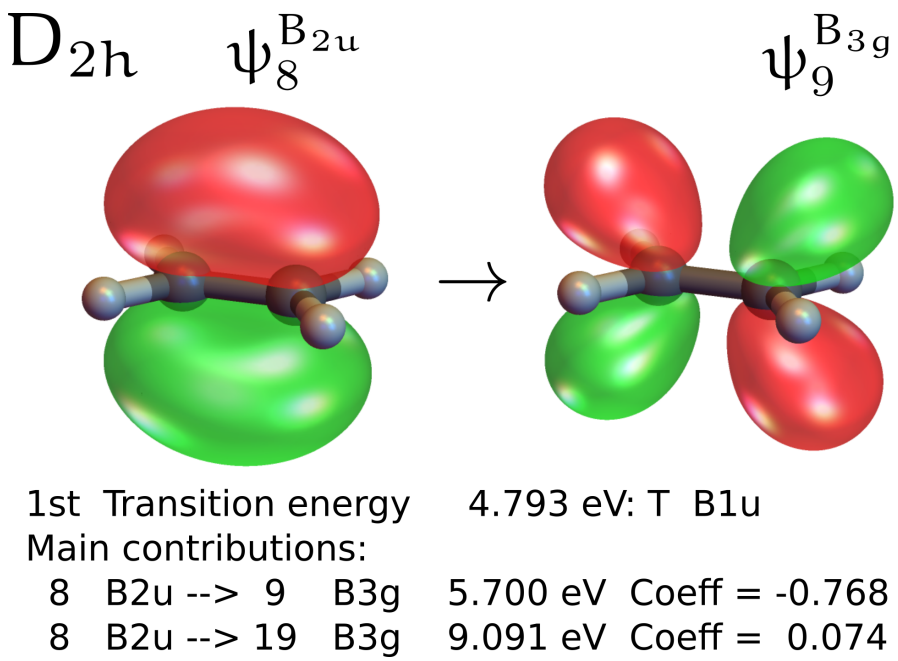

Figure 7.4: First excited state of ethylene. The lines of text are a sample of the new TD-ADFT output in deMon2k.

irreducible representations must be calculated. To this end, we use Clebsch-Gordan coefficients. The addition of irreducible representation labels to the transition energies and the use of Clebsch-Gordan coefficients to determine the resulting symmetry of the excitation energies in the deMon2k TD-ADFT module were realized in collaboration with Lic. L. I. Hernandez-Segura. The situation is particularly simple if one or both irreducible representations in the direct product $\Gamma \times \Gamma'$ are one-dimensional. In this case, the results are single irreducible representations. As a pictorial example for this case, we show in Figure 7.4 the main contribution of the $\mathbf{F}$ eigenvector for the first excited state of ethylene in D_{2h} symmetry. The resulting B_{1u} excited state assignment is simply the direct product of the irreducible representations of the involved MOs, here $B_{2u} \times B_{3g}$ (note that in this particular example the direct product can be calculated from the irreducible representation characters). As Figure 7.4 shows this symmetry information is now added to the new TD-ADFT output in deMon2k. A list of symmetry assignment of the 12 lowest-lying excited states of ethylene at the PBE/aug-cc-pVTZ/GEN-A2* level

E.s.	Mult.	Sym.	$\Delta E[eV]$	λ [nm]	O.s.
1	T	B_{1u}	4.79	258.67	0.00
2	T	B_{2u}	6.46	191.81	0.00
3	S	B_{2u}	6.57	188.80	0.05
4	T	B_{3g}	6.92	179.03	0.00
5	S	B_{3g}	6.98	177.50	0.00
6	T	B_{1g}	6.99	177.31	0.00
7	S	B_{1g}	7.04	176.08	0.00
8	T	B_{1g}	7.19	172.54	0.00
9	S	B_{1u}	7.61	162.99	0.27
10	S	B_{1g}	7.71	160.78	0.00
11	T	A_u	7.74	160.27	0.00
12	S	A_u	7.74	160.08	0.00

Table 7.3: First 12 excited states of ethylene. With symmetry labeling at the PBE/aug-cc-pVTZ/GEN-A2* level of theory. E.s., Mult., Sym. and O.s. denote the excited state, its multiplicity (Singlet or Triplet), its symmetry and the corresponding transition oscillator strength, respectively.

of theory is given in Table 7.3. Because the main contributions to the excitation energy (the larges coefficients in absolute value) have the same irreducible representation direct product the excited state symmetry labeling is straightforward.

For the benzene molecule the situation is different. In this case, direct products of two-dimensional irreducible representations must be calculated. The result is a direct sum of several irreducible representations. If the column indices of the two-dimensional irreducible representation components of the degenerate MOs are known, we can calculate linear combinations of direct products of these column components. Take as example the first excitation in benzene (see Figure 7.5) given by $E_{1g} \times E_{2u}$ as:

$$-0.52(E_{1g}(1) \otimes E_{2u}(2)) + 0.52(E_{1g}(2) \otimes E_{2u}(1)) \tag{7.5}$$

For the expansion of the here appearing direct products of two-dimensional column components the corresponding (normalized) Clebsch-Gordan coefficients matrix is needed. For the $E_{1g} \times E_{2u}$ example, this matrix is depicted in Table 7.4. Its elements are

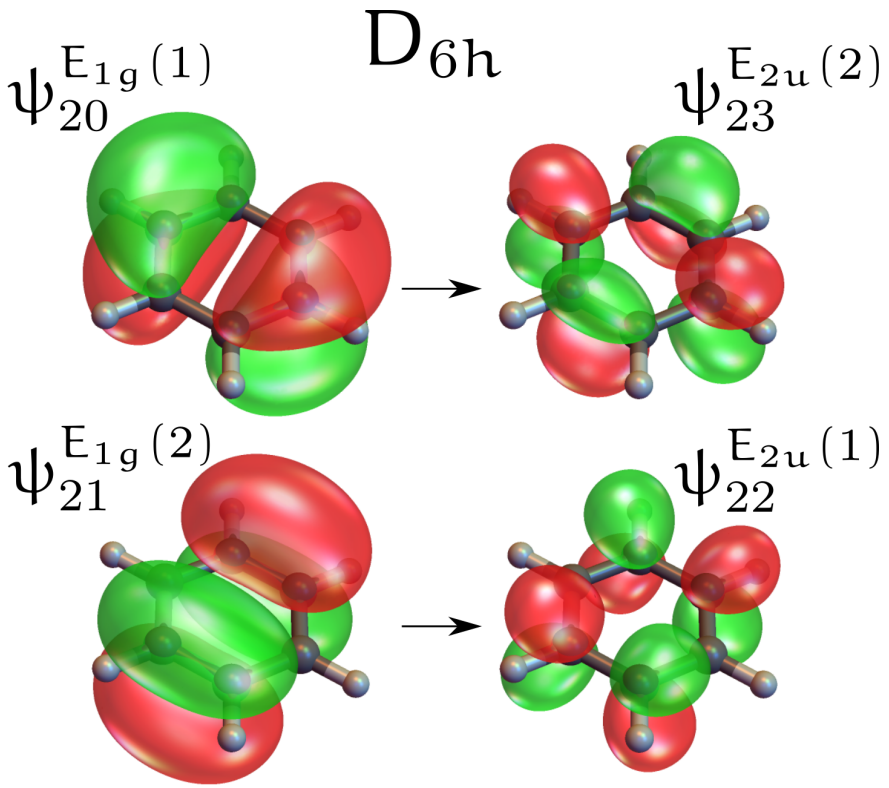

Figure 7.5: First excited state of benzene. The lines of text are a sample of the new TD-ADFT output in deMon2k.

$E_{1g} \otimes E_{2u}$	B_{1u}	B_{2u}	$E_{1u}(1)$	$E_{1u}(2)$
$E_{1g}(1)E_{2u}(1)$	$\frac{1}{\sqrt{2}}$	0	$\frac{1}{\sqrt{2}}$	0
$E_{1g}(1)E_{2u}(2)$	0	$\frac{1}{\sqrt{2}}$	0	$-\frac{1}{\sqrt{2}}$
$E_{1g}(2)E_{2u}(1)$	0	$-\frac{1}{\sqrt{2}}$	0	$-\frac{1}{\sqrt{2}}$
$E_{1g}(2)E_{2u}(2)$	$\frac{1}{\sqrt{2}}$	0	$-\frac{1}{\sqrt{2}}$	0

Table 7.4: The normalized Clebsch-Gordan coefficient matrix for the direct product of irreducible representations $E_{1g} \otimes E_{2u}$ in the point group D_{6h} as calculated in deMon2k.

		deMon2k					Gaussian			
E.s.	Mult.	Sym.	ΔE [eV]	λ [nm]	O.s.	E.s.	Mult.	Sym.	ΔE [eV]	λ [nm]	O.s.
1	T	B_{2u}	4.74	261.58	0.00	1	T	?	4.46	278.08	0.00
2	T	E_{1u}	4.96	249.85	0.00	2	T	?	4.83	256.80	0.00
3	T	E_{1u}	4.96	249.85	0.00	3	T	?	4.83	256.80	0.00
4	T	B_{1u}	5.14	241.06	0.00	4	T	?	5.10	243.09	0.00
5	S	B_{1u}	5.42	228.93	0.00	5	S	?	5.36	231.33	0.00
6	S	B_{2u}	6.39	194.11	0.00	6	S	?	6.24	198.67	0.00
7	T	A_{2u}	6.99	177.41	0.00	7	T	?	6.94	178.61	0.00
8	T	E_{2u}	7.00	176.97	0.00	8	T	?	6.96	178.08	0.00
9	T	E_{2u}	7.00	176.97	0.00	9	T	?	6.96	178.08	0.00
10	T	A_{1u}	7.02	176.56	0.00	10	T	?	6.98	177.51	0.00
11	S	A_{1u}	7.15	173.34	0.00	11	S	?	7.11	174.39	0.00
12	S	E_{2u}	7.26	170.84	0.00	12	S	?	7.21	171.94	0.00
13	S	E_{2u}	7.26	170.84	0.00	13	S	?	7.21	171.94	0.00
14	S	A_{2u}	7.29	169.95	0.00	14	S	?	7.24	171.19	0.00

Table 7.5: Excited states of Benzene molecule calculated in deMon2k and Gaussian. E.s., Mult., Sym. and O.s. denote the excited state, its multiplicity (Singlet or Triplet), its symmetry and the corresponding transition oscillator strength, respectively.

calculated according to Eq. (4.64). With the Clebsch-Gordan coefficients at hand we can expand Eq. (7.5) as:

$$-0.52\left(\frac{1}{\sqrt{2}}B_{2u}-\frac{1}{\sqrt{2}}E_{1u}(2)\right)+0.52\left(-\frac{1}{\sqrt{2}}B_{2u}-\frac{1}{\sqrt{2}}E_{1u}(2)\right)=-\frac{1.04}{\sqrt{2}}B_{2u} \quad (7.6)$$

This allows the determination of an overall single irreducible representation label for the excited state in question. Table 7.5 compares the calculated excited states in deMon2k with those from Gaussian [48] employing the VWN/6-31G** level of theory. For the TD-ADFT calculations in deMon2k, the GEN-A2* auxiliary function set was used. Note that in Gaussian the excited state symmetries arising from products of multi-dimensional irreducible representations are not assigned, whereas this assignment is now possible in deMon2k.

8

CONCLUSIONS AND PERSPECTIVES

8.1 Conclusions

This thesis describes the derivation and implementation of symmetry-adapted Hartree-Fock, DF-DFT and ADFT calculations in deMon2k. The work is based on the symmetry adaptation of the Hartree-Fock or Kohn-Sham matrix and the symmetry adaptation of the Coulomb fitting equations. The now implemented point groups in deMon2k are: C_i, C_s, C_n, C_{nv}, C_{nh}, D_n, D_{nd}, D_{nh}, S_4, S_6, T, T_d, T_h, O, O_h, I, I_h, $C_{\infty v}$ and $D_{\infty h}$, with $n = 2, ..., 6$. The icosahedral point group tables, as well as the linear infinity point group table cutouts, were generated in this work. All other real point group tables were taken from StoBe [97]. Noticeable characteristics of this implementation and corresponding resulting studies are the following:

- The working equations for the symmetry-adapted calculation of Coulomb and exchange-correlation fitting coefficients in ADFT (and DF-DFT) are derived in this thesis and published in [88].
- The here presented formulas for the symmetry adaptation of the Kohn-Sham matrix and fitting equations are general. In particular, no restriction for the angular momentum of the Cartesian and spherical atomic orbital basis as well as for the Hermite Gaussian auxiliary functions exists.
- It was found that for totally symmetric densities only the fitting equation systems of the totally symmetric irreducible representation have to be solved. This results in a huge dimension reduction of the linear equation systems that have to be solved

for the calculation of the Coulomb and exchange-correlation fitting coefficients in ADFT (and DF-DFT).

- To illustrate the advantages of symmetry-adapted density fitting, icosahedral giant fullerenes up to C_{2160} were calculated employing different density fitting approaches. These calculations show that symmetry-adapted density fitting is superior to all other tested approaches in terms of CPU time as well as in RAM demand. This underlines the potential of the here presented fitting approach.

- The assignment of molecular orbitals and auxiliary functions according to their irreducible representations is now available in deMon2k.

- The direct products of groups, irreducible representations and matrices were implemented in a general form in deMon2k. Thus, additional point groups or extensions, e.g. double groups for relativistic two-component wave functions, can be straightforwardly implemented.

- The symmetry-adapted fitting was implemented in a memory-efficient form allowing the study of large systems. Key to success is the on-the-fly calculation of the symmetrization matrix elements in terms of of the symmetrization matrix for atom permutation vectors and the symmetrization matrix for origin-centered (auxiliary) functions. With this methodology the construction of the complete $\mathbf{U}$ transformation matrix can be avoided allowing a memory-efficient implementation.

- The study of the symmetry-adapted density fitting showed energy deviations from the corresponding symmetry-unconstrained calculations of up to around 0.5 kcal/mol. Our analysis reveals that these deviations originate from the truncated eigenvalue decomposition of the Coulomb matrix due to its different eigenvalue spectrum in symmetry-adapted and unconstrained form. Therefore, we recommend to use symmetry-adapted density fitting only in studies where all calculations are symmetry-adapted.

- The here presented implementation of symmetry-adapted SCF calculations permits the identification of symmetry breaking by analyzing the MO energies of degenerate orbitals. As this kind of symmetry breaking is allowed in our implementation it is expected that the total energy differences between symmetry-adapted and unconstrained calculations are small in general.

- As the direct products of irreducible representations are calculated as well as the corresponding Clebsch-Gordan coefficients, the irreducible representation labeling of the Kohn-Sham states and excited states in TD-ADFT become possible in deMon2k.

8.2 Perspectives

From this work the following perspectives arise:

- To implement symmetry-adapted molecular structure optimization. This will reduce the degrees of freedom in molecular geometry optimization by fixing the point group of the molecule.

- To develop a reduced memory SCF implementation for the Kohn-Sham matrix. This involves the calculation of the symmetry-adapted Kohn-Sham matrix irreducible representation blocks directly without the construction of the complete Kohn-Sham matrix in the original AO representation. This implies a further reduction of RAM, which will allow the calculation of even larger systems.

- To increase the efficiency of the symmetry-adapted density fitting by building the symmetry-adapted matrix representations in a more efficient way or/and to use the double coset decomposition methodology [152]. It has to be pointed out that currently for the symmetry-adapted fitting 99% of the CPU time is used for the building of the symmetry-adapted Coulomb matrix.

- To augment the number of point groups implemented. There are several strategies to achieve this: 1) To code more point group tables. 2) To perform direct products of already implemented point groups. 3) Generate character tables for any point group [153] (not the complete matrix representations) and use the subduction methodology [154] for the building of symmetry-adapted basis and auxiliary functions. 4) To generate directly the complete matrix representation tables for any point group [155].

- Include space groups in the symmetry-adapted SCF and density fitting in order to use it within the cyclic cluster model [156] methodology. This uses periodic boundary conditions to model systems such as crystals, surfaces and polymers. As translational symmetry is always used in this method, the use of symmetry-adapted SCF and fitting is unavoidable and therefore exploitable.

- Use symmetry-adapted approximate Kohn-Sham operators for non-symmetric molecules by perturbation theory [157].

APPENDIX

A

DIRECT PRODUCT OF MATRICES

The direct product of matrices, also named Kronecker or outer product of the $m \times n$ matrix $\mathbf{A}$ and the $p \times q$ matrix $\mathbf{B}$ yields the $(m \cdot p) \times (n \cdot q)$ matrix $\mathbf{C}$ given by:

$$\mathbf{C} = \mathbf{A} \otimes \mathbf{B} = \begin{bmatrix} A_{11}\mathbf{B} & \cdots & A_{1n}\mathbf{B} \\ \vdots & \ddots & \vdots \\ A_{m1}\mathbf{B} & \cdots & A_{mn}\mathbf{B} \end{bmatrix} \tag{A.1}$$

The elements of $\mathbf{C}$ are calculated as:

$$C_{p(i-1)+k,q(j-1)+l} = A_{ij}B_{kl} \tag{A.2}$$

Example:

$$\begin{pmatrix} 0 & 1 \\ 1 & 0 \end{pmatrix} \otimes \begin{pmatrix} 0 & -1 & 0 \\ 1 & 0 & 0 \\ 0 & 0 & 1 \end{pmatrix} = \begin{pmatrix} 0 & 0 & 0 & 0 & -1 & 0 \\ 0 & 0 & 0 & 1 & 0 & 0 \\ 0 & 0 & 0 & 0 & 0 & 1 \\ 0 & -1 & 0 & 0 & 0 & 0 \\ 1 & 0 & 0 & 0 & 0 & 0 \\ 0 & 0 & 1 & 0 & 0 & 0 \end{pmatrix} \tag{A.3}$$

B

REDUCTION OF $E \otimes E$ IN C_{3v}

This appendix outlines the reduction of the four-dimensional subspace that results from the direct product $E \otimes E$ in C_{3v} for the ammonia example of Chapter 4. The corresponding invariant example subspaces are given by the columns of $\mathbf{B}_7$ and $\mathbf{B}_8$, see Eqs. (4.37) and (4.38):

$$\mathbf{B}_7 = \left(\mathbf{p}_A^{E(1)} \otimes \mathbf{d}_{xx}^{E(1)} | \mathbf{p}_A^{E(1)} \otimes \mathbf{d}_{xx}^{E(2)} | \mathbf{p}_A^{E(2)} \otimes \mathbf{d}_{xx}^{E(1)} | \mathbf{p}_A^{E(2)} \otimes \mathbf{d}_{xx}^{E(2)}\right) \tag{B.1}$$

$$\mathbf{B}_8 = \left(\mathbf{p}_A^{E(1)} \otimes \mathbf{d}_{xz}^{E(1)} | \mathbf{p}_A^{E(1)} \otimes \mathbf{d}_{xz}^{E(2)} | \mathbf{p}_A^{E(2)} \otimes \mathbf{d}_{xz}^{E(1)} | \mathbf{p}_A^{E(2)} \otimes \mathbf{d}_{xz}^{E(2)}\right) \tag{B.2}$$

From the character reduction formula, Eq. (4.11), follows:

$$E \otimes E = A_1 \oplus A_2 \oplus E \tag{B.3}$$

Thus, the four-dimensional subspace must consist of 4 vectors, one belonging to the irreducible representation A_1, another to the irreducible representation A_2 and two degenerate vectors belonging to the two-dimensional irreducible representation E. A basis for this four-dimensional subspace is given by:

$$\mathbf{c}_1 = \begin{pmatrix} 1 \\ 0 \\ 0 \\ 0 \end{pmatrix}, \quad \mathbf{c}_2 = \begin{pmatrix} 0 \\ 1 \\ 0 \\ 0 \end{pmatrix}, \quad \mathbf{c}_3 = \begin{pmatrix} 0 \\ 0 \\ 1 \\ 0 \end{pmatrix}, \quad \mathbf{c}_4 = \begin{pmatrix} 0 \\ 0 \\ 0 \\ 1 \end{pmatrix} \tag{B.4}$$

A representation of the symmetry operations in this basis can be obtained by the direct products of the corresponding irreducible representation matrices [73]:

$$\mathbf{D}^{E\otimes E}(\hat{R}) = \boldsymbol{\chi}^{E}(\hat{R}) \otimes \boldsymbol{\chi}^{E}(\hat{R}) \qquad \forall \quad \hat{R} \tag{B.5}$$

The resulting representation matrices for C_{3v} are:

$$\mathbf{D}^{E\otimes E}(\hat{E}) = \begin{pmatrix} 1 & 0 \\ 0 & 1 \end{pmatrix} \otimes \begin{pmatrix} 1 & 0 \\ 0 & 1 \end{pmatrix} = \begin{pmatrix} 1 & 0 & 0 & 0 \\ 0 & 1 & 0 & 0 \\ 0 & 0 & 1 & 0 \\ 0 & 0 & 0 & 1 \end{pmatrix} \tag{B.6}$$

$$\mathbf{D}^{E\otimes E}(\hat{C}_3) = \begin{pmatrix} -\frac{1}{2} & -\frac{\sqrt{3}}{2} \\ \frac{\sqrt{3}}{2} & -\frac{1}{2} \end{pmatrix} \otimes \begin{pmatrix} -\frac{1}{2} & -\frac{\sqrt{3}}{2} \\ \frac{\sqrt{3}}{2} & -\frac{1}{2} \end{pmatrix} = \begin{pmatrix} \frac{1}{4} & \frac{\sqrt{3}}{4} & \frac{\sqrt{3}}{4} & \frac{3}{4} \\ -\frac{\sqrt{3}}{4} & \frac{1}{4} & -\frac{3}{4} & \frac{\sqrt{3}}{4} \\ -\frac{\sqrt{3}}{4} & -\frac{3}{4} & \frac{1}{4} & \frac{\sqrt{3}}{4} \\ \frac{3}{4} & -\frac{\sqrt{3}}{4} & -\frac{\sqrt{3}}{4} & \frac{1}{4} \end{pmatrix} \tag{B.7}$$

$$\mathbf{D}^{E\otimes E}(\hat{C}_3^2) = \begin{pmatrix} -\frac{1}{2} & \frac{\sqrt{3}}{2} \\ -\frac{\sqrt{3}}{2} & -\frac{1}{2} \end{pmatrix} \otimes \begin{pmatrix} -\frac{1}{2} & \frac{\sqrt{3}}{2} \\ -\frac{\sqrt{3}}{2} & -\frac{1}{2} \end{pmatrix} = \begin{pmatrix} \frac{1}{4} & -\frac{\sqrt{3}}{4} & -\frac{\sqrt{3}}{4} & \frac{3}{4} \\ \frac{\sqrt{3}}{4} & \frac{1}{4} & -\frac{3}{4} & -\frac{\sqrt{3}}{4} \\ \frac{\sqrt{3}}{4} & -\frac{3}{4} & \frac{1}{4} & -\frac{\sqrt{3}}{4} \\ \frac{3}{4} & \frac{\sqrt{3}}{4} & \frac{\sqrt{3}}{4} & \frac{1}{4} \end{pmatrix} \tag{B.8}$$

$$\mathbf{D}^{E\otimes E}(\hat{\sigma}_v) = \begin{pmatrix} 1 & 0 \\ 0 & -1 \end{pmatrix} \otimes \begin{pmatrix} 1 & 0 \\ 0 & -1 \end{pmatrix} = \begin{pmatrix} 1 & 0 & 0 & 0 \\ 0 & -1 & 0 & 0 \\ 0 & 0 & -1 & 0 \\ 0 & 0 & 0 & 1 \end{pmatrix} \tag{B.9}$$

$$\mathbf{D}^{E\otimes E}(\hat{\sigma}_v') = \begin{pmatrix} -\frac{1}{2} & -\frac{\sqrt{3}}{2} \\ -\frac{\sqrt{3}}{2} & \frac{1}{2} \end{pmatrix} \otimes \begin{pmatrix} -\frac{1}{2} & -\frac{\sqrt{3}}{2} \\ -\frac{\sqrt{3}}{2} & \frac{1}{2} \end{pmatrix} = \begin{pmatrix} \frac{1}{4} & \frac{\sqrt{3}}{4} & \frac{\sqrt{3}}{4} & \frac{3}{4} \\ \frac{\sqrt{3}}{4} & -\frac{1}{4} & \frac{3}{4} & -\frac{\sqrt{3}}{4} \\ \frac{\sqrt{3}}{4} & \frac{3}{4} & -\frac{1}{4} & -\frac{\sqrt{3}}{4} \\ \frac{3}{4} & -\frac{\sqrt{3}}{4} & -\frac{\sqrt{3}}{4} & \frac{1}{4} \end{pmatrix} \tag{B.10}$$

$$\mathbf{D}^{E\otimes E}(\hat{\sigma}_v'') = \begin{pmatrix} -\frac{1}{2} & \frac{\sqrt{3}}{2} \\ \frac{\sqrt{3}}{2} & \frac{1}{2} \end{pmatrix} \otimes \begin{pmatrix} -\frac{1}{2} & \frac{\sqrt{3}}{2} \\ \frac{\sqrt{3}}{2} & \frac{1}{2} \end{pmatrix} = \begin{pmatrix} \frac{1}{4} & -\frac{\sqrt{3}}{4} & -\frac{\sqrt{3}}{4} & \frac{3}{4} \\ -\frac{\sqrt{3}}{4} & -\frac{1}{4} & \frac{3}{4} & \frac{\sqrt{3}}{4} \\ -\frac{\sqrt{3}}{4} & \frac{3}{4} & -\frac{1}{4} & \frac{\sqrt{3}}{4} \\ \frac{3}{4} & \frac{\sqrt{3}}{4} & \frac{\sqrt{3}}{4} & \frac{1}{4} \end{pmatrix} \tag{B.11}$$

With these matrices, we can express the symmetry operations of the C_{3v} point group on the basis vectors of Eq. (B.4) as matrix vector products. As an example, take the $\hat{C}_3$ rotation applied to the first basis vector of Eq. (B.4):

$$\hat{C}_3 \mathbf{c}_1 \rightarrow \mathbf{D}^{E\otimes E}(\hat{C}_3)\mathbf{c}_1 \tag{B.12}$$

With Eq. (B.7) we find:

$$\mathbf{D}^{E\otimes E}(\hat{C}_3)\ \mathbf{c}_1 = \frac{1}{4}\ \mathbf{c}_1 - \frac{\sqrt{3}}{4}\ \mathbf{c}_2 - \frac{\sqrt{3}}{4}\ \mathbf{c}_3 + \frac{3}{4}\ \mathbf{c}_4 \tag{B.13}$$

In the same way we can now express corresponding projection operators for the basis vectors in Eq. (B.4) of the form:

$$\mathbf{P}^{\Gamma}_{\gamma} = \frac{d_\Gamma}{h} \sum_{\hat{R}} \chi^{\Gamma}_{\gamma}(\hat{R})\, \mathbf{D}^{E\otimes E}(\hat{R}) \tag{B.14}$$

The projection of the basis vectors from Eq. (B.4) on to the irreducible representations A_1, A_2 and E is depicted in Scheme B.1 and B.2. The resulting four symmetry-adapted basis vectors, $\{\mathbf{c}^{\Gamma(\gamma)}\}$, are collected in the so-called Clebsch-Gordan coefficient matrix as:

$$\mathbf{C} = (\mathbf{c}_1^{A_1}|\mathbf{c}_2^{A_2}|\mathbf{c}_1^{E(1)}|\mathbf{c}_1^{E(2)}) \tag{B.15}$$

This is the Clebsch-Gordan coefficient matrix for the reduction of the direct product of irreducible representation $E \otimes E$. Thus, the subspace given by the columns of matrix $\mathbf{B}_7$ of dimension 18×4 takes the form:

$$\mathbf{B}_7 = (\mathbf{p}_A^{E(1)} \otimes \mathbf{d}_{xx}^{E(1)}|\mathbf{p}_A^{E(1)} \otimes \mathbf{d}_{xx}^{E(2)}|\mathbf{p}_A^{E(2)} \otimes \mathbf{d}_{xx}^{E(1)}|\mathbf{p}_A^{E(2)} \otimes \mathbf{d}_{xx}^{E(2)}) \tag{B.16}$$

The four resulting symmetry-adapted vectors corresponding to the subspace given by the columns of $\mathbf{B}_7$, according to the here presented procedure, are given by:

$$\mathbf{B}_7\mathbf{C} = (\mathbf{u}_3^{A_1}|\mathbf{u}_5^{A_2}|\mathbf{u}_{11}^{E(1)}|\mathbf{u}_{17}^{E(2)}) \tag{B.17}$$

- $\Gamma = A_1; \gamma = 1; \chi^{A_1}(\hat{E}) = 1, \chi^{A_1}(\hat{C}_3) = 1, \chi^{A_1}(\hat{C}_3^2) = 1, \chi^{A_1}(\hat{\sigma}_v) = 1, \chi^{A_1}(\hat{\sigma}_v') = 1, \chi^{A_1}(\hat{\sigma}_v'') = 1;$ $\mathbf{c}_1^{A_1} \equiv \mathbf{P}_1^{A_1}\mathbf{c}_1$

$$\mathbf{c}_1^{A_1} = \frac{1}{6}\Big[1\mathbf{D}^{E\otimes E}(\hat{E})\mathbf{c}_1 + 1\mathbf{D}^{E\otimes E}(\hat{C}_3)\mathbf{c}_1 + 1\mathbf{D}^{E\otimes E}(\hat{C}_3^2)\mathbf{c}_1 + 1\mathbf{D}^{E\otimes E}(\hat{\sigma}_v)\mathbf{c}_1 + 1\mathbf{D}^{E\otimes E}(\hat{\sigma}_v')\mathbf{c}_1 + 1\mathbf{D}^{E\otimes E}(\hat{\sigma}_v'')\mathbf{c}_1\Big]$$

$$= \frac{1}{6}\left[1\begin{pmatrix}1\\0\\0\\0\end{pmatrix} + 1\begin{pmatrix}\frac{1}{4}\\-\frac{\sqrt{3}}{4}\\-\frac{\sqrt{3}}{4}\\\frac{3}{4}\end{pmatrix} + 1\begin{pmatrix}\frac{1}{4}\\\frac{\sqrt{3}}{4}\\\frac{\sqrt{3}}{4}\\\frac{3}{4}\end{pmatrix} + 1\begin{pmatrix}1\\0\\0\\0\end{pmatrix} + 1\begin{pmatrix}\frac{1}{4}\\\frac{\sqrt{3}}{4}\\\frac{\sqrt{3}}{4}\\\frac{3}{4}\end{pmatrix} + 1\begin{pmatrix}\frac{1}{4}\\-\frac{\sqrt{3}}{4}\\-\frac{\sqrt{3}}{4}\\\frac{3}{4}\end{pmatrix}\right] = \begin{pmatrix}\frac{1}{2}\\0\\0\\\frac{1}{2}\end{pmatrix}$$

store; enough for A_1; next projection in A_2

- $\Gamma = A_2; \gamma = 1; \chi^{A_2}(\hat{E}) = 1, \chi^{A_2}(\hat{C}_3) = 1, \chi^{A_2}(\hat{C}_3^2) = 1, \chi^{A_2}(\hat{\sigma}_v) = -1, \chi^{A_2}(\hat{\sigma}_v') = -1,$ $\chi^{A_2}(\hat{\sigma}_v'') = -1; \mathbf{c}_1^{A_2} \equiv \mathbf{P}_1^{A_2}\mathbf{c}_1$

$$\mathbf{c}_1^{A_2} = \frac{1}{6}\Big[1\mathbf{D}^{E\otimes E}(\hat{E})\mathbf{c}_1 + 1\mathbf{D}^{E\otimes E}(\hat{C}_3)\mathbf{c}_1 + 1\mathbf{D}^{E\otimes E}(\hat{C}_3^2)\mathbf{c}_1 + (-1)\mathbf{D}^{E\otimes E}(\hat{\sigma}_v)\mathbf{c}_1 + (-1)\mathbf{D}^{E\otimes E}(\hat{\sigma}_v')\mathbf{c}_1 + (-1)\mathbf{D}^{E\otimes E}(\hat{\sigma}_v'')\mathbf{c}_1\Big]$$

$$= \frac{1}{6}\left[1\begin{pmatrix}1\\0\\0\\0\end{pmatrix} + 1\begin{pmatrix}\frac{1}{4}\\-\frac{\sqrt{3}}{4}\\-\frac{\sqrt{3}}{4}\\\frac{3}{4}\end{pmatrix} + 1\begin{pmatrix}\frac{1}{4}\\\frac{\sqrt{3}}{4}\\\frac{\sqrt{3}}{4}\\\frac{3}{4}\end{pmatrix} - 1\begin{pmatrix}1\\0\\0\\0\end{pmatrix} - 1\begin{pmatrix}\frac{1}{4}\\\frac{\sqrt{3}}{4}\\\frac{\sqrt{3}}{4}\\\frac{3}{4}\end{pmatrix} - 1\begin{pmatrix}\frac{1}{4}\\-\frac{\sqrt{3}}{4}\\-\frac{\sqrt{3}}{4}\\\frac{3}{4}\end{pmatrix}\right] = \begin{pmatrix}0\\0\\0\\0\end{pmatrix}$$

vanishes; next projection

$$\mathbf{c}_2^{A_2} \equiv \mathbf{P}_1^{A_2}\mathbf{c}_2$$

$$= \frac{1}{6}\Big[1\mathbf{D}^{E\otimes E}(\hat{E})\mathbf{c}_2 + 1\mathbf{D}^{E\otimes E}(\hat{C}_3)\mathbf{c}_2 + 1\mathbf{D}^{E\otimes E}(\hat{C}_3^2)\mathbf{c}_2 + (-1)\mathbf{D}^{E\otimes E}(\hat{\sigma}_v)\mathbf{c}_2 + (-1)\mathbf{D}^{E\otimes E}(\hat{\sigma}_v')\mathbf{c}_2 + (-1)\mathbf{D}^{E\otimes E}(\hat{\sigma}_v'')\mathbf{c}_2\Big]$$

$$= \frac{1}{6}\left[1\begin{pmatrix}0\\1\\0\\0\end{pmatrix} + 1\begin{pmatrix}\frac{\sqrt{3}}{4}\\\frac{1}{4}\\-\frac{3}{4}\\-\frac{\sqrt{3}}{4}\end{pmatrix} + 1\begin{pmatrix}-\frac{\sqrt{3}}{4}\\\frac{1}{4}\\-\frac{3}{4}\\\frac{\sqrt{3}}{4}\end{pmatrix} - 1\begin{pmatrix}0\\-1\\0\\0\end{pmatrix} - 1\begin{pmatrix}\frac{\sqrt{3}}{4}\\-\frac{1}{4}\\\frac{3}{4}\\-\frac{\sqrt{3}}{4}\end{pmatrix} - 1\begin{pmatrix}-\frac{\sqrt{3}}{4}\\-\frac{1}{4}\\\frac{3}{4}\\\frac{\sqrt{3}}{4}\end{pmatrix}\right] = \begin{pmatrix}0\\\frac{1}{2}\\-\frac{1}{2}\\0\end{pmatrix}$$

store; enough for A_2; next projection in E

Scheme B.1: Reduction of the direct product of irreducible representations, $E \otimes E$, of the C_{3v} point group for the irreducible representations A_1 and A_2.

In Eq. (B.17) we have enumerated the overall symmetry-adapted vectors $\mathbf{u}_{\mathring{l}}^{\Gamma(\gamma)}$ to coincide with Table 4.2. For the basis given by the columns of $\mathbf{B}_8$, we do not have to repeat the reduction procedure. The subspace given by the columns of the matrix $\mathbf{B}_8$ of dimensions 18×4 has the form:

$$\mathbf{B}_8 = (\mathbf{p}_A^{E(1)} \otimes \mathbf{d}_{xz}^{E(1)} | \mathbf{p}_A^{E(1)} \otimes \mathbf{d}_{xz}^{E(2)} | \mathbf{p}_A^{E(2)} \otimes \mathbf{d}_{xz}^{E(1)} | \mathbf{p}_A^{E(2)} \otimes \mathbf{d}_{xz}^{E(2)}) \tag{B.18}$$

- $\Gamma = E; \gamma = 1; \chi_1^E(\hat{E}) = 1, \chi_1^E(\hat{C}_3) = -\frac{1}{2}, \chi_1^E(\hat{C}_3^2) = -\frac{1}{2}, \chi_1^E(\hat{\sigma}_v) = 1, \chi_1^E(\hat{\sigma}_v') = -\frac{1}{2}, \chi_1^E(\hat{\sigma}_v'') = -\frac{1}{2}$; $\mathbf{c}_1^{E(1)} \equiv \mathbf{P}_1^E \mathbf{c}_1$

$$\mathbf{c}_1^{E(1)} = \frac{2}{6}\Big[1\mathbf{D}^{E\otimes E}(\hat{E})\mathbf{c}_1 + (-\tfrac{1}{2})\mathbf{D}^{E\otimes E}(\hat{C}_3)\mathbf{c}_1 + (-\tfrac{1}{2})\mathbf{D}^{E\otimes E}(\hat{C}_3^2)\mathbf{c}_1 + 1\mathbf{D}^{E\otimes E}(\hat{\sigma}_v)\mathbf{c}_1 + (-\tfrac{1}{2})\mathbf{D}^{E\otimes E}(\hat{\sigma}_v')\mathbf{c}_1 + (-\tfrac{1}{2})\mathbf{D}^{E\otimes E}(\hat{\sigma}_v'')\mathbf{c}_1\Big]$$
$$= \frac{2}{6}\left[1\begin{pmatrix}1\\0\\0\\0\end{pmatrix} - \frac{1}{2}\begin{pmatrix}\frac{1}{4}\\-\frac{\sqrt{3}}{4}\\-\frac{\sqrt{3}}{4}\\\frac{3}{4}\end{pmatrix} - \frac{1}{2}\begin{pmatrix}\frac{1}{4}\\\frac{\sqrt{3}}{4}\\\frac{\sqrt{3}}{4}\\\frac{3}{4}\end{pmatrix} + 1\begin{pmatrix}1\\0\\0\\0\end{pmatrix} - \frac{1}{2}\begin{pmatrix}\frac{1}{4}\\\frac{\sqrt{3}}{4}\\\frac{\sqrt{3}}{4}\\\frac{3}{4}\end{pmatrix} - \frac{1}{2}\begin{pmatrix}\frac{1}{4}\\-\frac{\sqrt{3}}{4}\\-\frac{\sqrt{3}}{4}\\\frac{3}{4}\end{pmatrix}\right] = \begin{pmatrix}\frac{1}{2}\\0\\0\\-\frac{1}{2}\end{pmatrix}$$

store; find partner increasing γ

- $\Gamma = E; \gamma = 2; \chi_2^E(\hat{E}) = 0, \chi_2^E(\hat{C}_3) = \frac{\sqrt{3}}{2}, \chi_2^E(\hat{C}_3^2) = -\frac{\sqrt{3}}{2}, \chi_2^E(\hat{\sigma}_v) = 0, \chi_2^E(\hat{\sigma}_v') = -\frac{\sqrt{3}}{2}, \chi_2^E(\hat{\sigma}_v'') = \frac{\sqrt{3}}{2}$; $\mathbf{c}_1^{E(2)} \equiv \mathbf{P}_2^E \mathbf{c}_1$

$$\mathbf{c}_1^{E(2)} = \frac{2}{6}\Big[0\mathbf{D}^{E\otimes E}(\hat{E})\mathbf{c}_1 + (\tfrac{\sqrt{3}}{2})\mathbf{D}^{E\otimes E}(\hat{C}_3)\mathbf{c}_1 + (-\tfrac{\sqrt{3}}{2})\mathbf{D}^{E\otimes E}(\hat{C}_3^2)\mathbf{c}_1 + 0\mathbf{D}^{E\otimes E}(\hat{\sigma}_v)\mathbf{c}_1 + (-\tfrac{\sqrt{3}}{2})\mathbf{D}^{E\otimes E}(\hat{\sigma}_v')\mathbf{c}_1 + (\tfrac{\sqrt{3}}{2})\mathbf{D}^{E\otimes E}(\hat{\sigma}_v'')\mathbf{c}_1\Big]$$
$$= \frac{2}{6}\left[\frac{\sqrt{3}}{2}\begin{pmatrix}\frac{1}{4}\\-\frac{\sqrt{3}}{4}\\-\frac{\sqrt{3}}{4}\\\frac{3}{4}\end{pmatrix} - \frac{\sqrt{3}}{2}\begin{pmatrix}\frac{1}{4}\\\frac{\sqrt{3}}{4}\\\frac{\sqrt{3}}{4}\\\frac{3}{4}\end{pmatrix} - \frac{\sqrt{3}}{2}\begin{pmatrix}\frac{1}{4}\\\frac{\sqrt{3}}{4}\\\frac{\sqrt{3}}{4}\\\frac{3}{4}\end{pmatrix} + \frac{\sqrt{3}}{2}\begin{pmatrix}\frac{1}{4}\\-\frac{\sqrt{3}}{4}\\-\frac{\sqrt{3}}{4}\\\frac{3}{4}\end{pmatrix}\right] = \begin{pmatrix}0\\-\frac{1}{2}\\-\frac{1}{2}\\0\end{pmatrix}$$

four symmetry vectors found; finish

Scheme B.2: Reduction of the direct product of irreducible representations, $E \otimes E$, of the C_{3v} point group for the irreducible representation E.

The corresponding four resulting symmetry-adapted vectors are:

$$\mathbf{B}_8\mathbf{C} = (\mathbf{u}_4^{A_1}|\mathbf{u}_6^{A_2}|\mathbf{u}_{12}^{E(1)}|\mathbf{u}_{18}^{E(2)}) \tag{B.19}$$

Again the enumeration of the symmetry-adapted column vectors $\mathbf{u}_i^{\Gamma(\gamma)}$ coincide with Table 4.2.

BIBLIOGRAPHY

[1]R. P. Crease and C. C. Mann, *The second creation. Makers of the revolution in twentieth-century physics* (Rutgers university press, Brunswick, 1996), 187.

[2]M. Born and R. Oppenheimer, "Zur Quantentheorie der Molekeln", Ann. Phys. **389**, 457 (1927).

[3]M. Born and K. Huang, *Dynamical theory of crystal lattices* (Oxford university press, Oxford, 1954), 408.

[4]N. C. Handy and A. M. Lee, "The adiabatic approximation", Chem. Phys. Lett. **252**, 425 (1996).

[5]R. G. Parr and W. Yang, *Density-functional theory of atoms and molecules* (Oxford university press, Oxford, 1989).

[6]P. Hohenberg and W. Kohn, "Inhomogeneous electron gas", Phys. Rev. **136**, B864 (1964).

[7]L. H. Thomas, "The calculation of atomic fields", Math. Proc. Cambridge Philos. Soc. **23**, 542 (1927).

[8]E. Fermi, "Un metodo statistico per la determinazione di alcune prioprietà dell'atomo", Rend. Accad. Naz. Lincei **6**, 602 (1927).

[9]E. Teller, "On the stability of molecules in the Thomas-Fermi theory", Rev. Mod. Phys. **34**, 627 (1962).

[10]W. Kohn and L. J. Sham, "Self-consistent equations including exchange and correlation effects", Phys. Rev. **140**, A1133 (1965).

[11]Q. Zhao and R. G. Parr, "Quantities T_s[n] and T_c[n] in density-functional theory", Phys. Rev. A **46**, 2337 (1992).

[12]Q. Zhao and R. G. Parr, "Constrained-search method to determine electronic wave functions from electronic densities", J. Chem. Phys. **98**, 543 (1993).

[13]Q. Zhao, R. C. Morrison, and R. G. Parr, "From electron densities to Kohn-Sham kinetic energies, orbital energies, exchange-correlation potentials, and exchange-correlation energies", Phys. Rev. A **50**, 2138 (1994).

[14]J. P. Perdew and S. Kurth, "Density functionals for non-relativistic Coulomb systems in the new century", in *A primer in density functional theory*, edited by C. Fiolhais, F. Nogueira, and M. A. L. Marques (Springer, Berlin, 2003).

[15]W. Koch and M. C. Holthausen, *A chemist's guide to density functional theory* (John Wiley and sons, Ltd., Weinheim, 2001) Chap. 5, 47.

[16]P. A. M. Dirac, "Note on exchange phenomena in the Thomas atom", Math. Proc. Cambridge Philos. Soc. **26**, 376 (1930).

[17]S. H. Vosko, L. Wilk, and M. Nusair, "Accurate spin-dependent electron liquid correlation energies for local spin density calculations: A critical analysis", Can. J. Phys. **58**, 1200 (1980).

[18]D. C. Langreth and M. J. Mehl, "Beyond the local-density approximation in calculations of ground-state electronic properties", Phys. Rev. B **28**, 1809 (1983).

[19]J. P. Perdew and W. Yue, "Accurate and simple density functional for the electronic exchange energy: Generalized gradient approximation", Phys. Rev. B **33**, 8800 (1986).

[20]A. D. Becke, "Density-functional exchange-energy approximation with correct asymptotic behavior", Phys. Rev. A **38**, 3098 (1988).

[21]R. Colle and D. Salvetti, "Approximate calculation of the correlation energy for the closed shells", Theor. Chim. Acta **37**, 329 (1975).

[22]R. Colle and D. Salvetti, "A general method for approximating the electronic correlation energy in molecules and solids", J. Chem. Phys. **79**, 1404 (1983).

[23]C. Lee, W. Yang, and R. G. Parr, "Development of the Colle-Salvetti correlation-energy formula into a functional of the electron density", Phys. Rev. B **37**, 785 (1988).

[24]J. P. Perdew, K. Burke, and M. Ernzerhof, "Generalized gradient approximation made simple", Phys. Rev. Lett. **77**, 3865 (1996).

[25]A. D. Becke, "Density-functional thermochemistry. III. The role of exact exchange", J. Chem. Phys. **98**, 5648 (1993).

[26]C. Adamo and V. Barone, "Toward reliable density functional methods without adjustable parameters: The PBE0 model", J. Chem. Phys. **110**, 6158 (1999).

[27]M. Ernzerhof and G. E. Scuseria, "Assessment of the Perdew-Burke-Ernzerhof exchange-correlation functional", J. Chem. Phys. **110**, 5029 (1999).

[28]E. J. Baerends, D. E. Ellis, and P. Ros, "Self-consistent molecular Hartree-Fock-Slater calculations I. The computational procedure", Chem. Phys. **2**, 41 (1973).

[29]G. te Velde and E. J. Baerends, "Numerical integration for polyatomic systems", J. Comput. Phys. **99**, 84 (1992).

[30]B. Delley, "An all-electron numerical method for solving the local density functional for polyatomic molecules", J. Chem. Phys. **92**, 508 (1990).

[31]A. M. Köster, G. Geudtner, A. Alvarez-Ibarra, P. Calaminici, M. E. Casida, J. Carmona-Espindola, V. D. Dominguez, R. Flores-Moreno, G. U. Gamboa, A. Goursot, T. Heine, A. Ipatov, A. de la Lande, F. Janetzko, J. M. del Campo, D. Mejia-Rodriguez, J. U. Reveles, J. Vasquez-Perez, A. Vela, B. Zuniga-Gutierrez, and D. R. Salahub, *deMon2k Version 6, The deMon developers*, Cinvestav, Mexico city, 2018.

[32]C. C. J. Roothaan, "New developments in molecular orbital theory", Rev. Mod. Phys. **23**, 69 (1951).

[33]G. G. Hall, "The molecular orbital theory of chemical valency. VIII. A method of calculating ionization potentials", Proc. R. Soc. Lond. A **205**, 541 (1951).

[34]C. C. J. Roothaan, "Self-consistent field theory for open shells of electronic systems", Rev. Mod. Phys. **32**, 179 (1960).

[35]J. A. Pople and R. K. Nesbet, "Self-consistent orbitals for radicals", J. Chem. Phys. **22**, 571 (1954).

[36]J. S. Binkley, J. A. Pople, and P. A. Dobosh, "The calculation of spin-restricted single-determinant wavefunctions", Mol. Phys. **28**, 1423 (1974).

[37]A. Szabo and N. S. Ostlund, *Modern quantum chemistry: Introduction to advanced electronic structure theory* (Dover publications, Mineola, 1996).

[38]P.-O. Löwdin, "On the non-orthogonality problem connected with the use of atomic wave functions in the theory of molecules and crystals", J. Chem. Phys. **18**, 365 (1950).

[39]P.-O. Löwdin, "On the non-orthogonality problem", Adv. Quantum Chem. **5**, 185 (1970).

[40]B. I. Dunlap, J. W. D. Connolly, and J. R. Sabin, "On some approximations in applications of Xα theory", J. Chem. Phys. **71**, 3396 (1979).

[41]B. I. Dunlap, J. W. D. Connolly, and J. R. Sabin, "On first-row diatomic molecules and local density models", J. Chem. Phys. **71**, 4993 (1979).

[42]J. W. Mintmire and B. I. Dunlap, "Fitting the Coulomb potential variationally in linear combination of atomic orbitals density functional calculations", Phys. Rev. A **25**, 88 (1982).

[43]A. M. Köster, "Hermite Gaussian auxiliary functions for the variational fitting of the Coulomb potential in density functional methods", J. Chem. Phys. **118**, 9943 (2003).

[44]M. E. Casida, C. Daul, A. Goursot, A. M. Köster, L. G. M. Pettersson, E. Proynov, A. St-Amant, D. R. Salahub, H. Duarte, N. Godbout, J. Guan, C. Jamorski, M. Leboeuf, V. Malkin, O. Malkina, F. Sim, and A. Vela, *deMon-KS version 3.4, deMon software, Montreal*, 1996.

[45]J. Andzelm and E. Wimmer, "Density functional Gaussian-type-orbital approach to molecular geometries, vibrations, and reaction energies", J. Chem. Phys. **96**, 1280 (1992).

[46]O. Vahtras, J. Almlöf, and M. W. Feyereisen, "Integral approximations for LCAO-SCF calculations", Chem. Phys. Lett. **213**, 514 (1993).

[47]R. Ahlrichs, "Efficient evaluation of three-center two-electron integrals over Gaussian functions", Phys. Chem. Chem. Phys. **6**, 5119 (2004).

[48]M. J. Frisch et al., *Gaussian 03, Revision C.02*, Gaussian, Inc., Wallingford, CT, 2004.

[49]B. I. Dunlap, N. Rösch, and S. B. Trickey, "Variational fitting methods for electronic structure calculations", Mol. Phys. **108**, 3167 (2010).

[50]A. Ipatov, A. Fouqueau, C. P. del Valle, F. Cordova, M. E. Casida, A. M. Köster, A. Vela, and C. J. Jamorski, "Excitation energies from an auxiliary-function formulation of time-dependent density-functional response theory with charge conservation constraint", J. Mol. Struct. THEOCHEM **762**, 179 (2006).

[51]J. Andzelm, E. Radzio, and D. R. Salahub, "Compact basis sets for LCAO-LSD calculations. Part I: Method and bases for Sc to Zn", J. Comput. Chem. **6**, 520 (1985).

[52]J. Andzelm, N. Russo, and D. R. Salahub, "Ground and excited states of group IVA diatomics from local-spin-density calculations: Model potentials for Si, Ge, and Sd", J. Chem. Phys. **87**, 6562 (1987).

[53]A. M. Köster, "Efficient recursive computation of molecular integrals for density functional methods", J. Chem. Phys. **104**, 4114 (1996).

[54]J. N. Pedroza-Montero, J. L. Morales, G. Geudtner, A. Álvarez-Ibarra, P. Calaminici, and A. M. Köster, "Variational density fitting with a Krylov subspace method", J. Chem. Theory Comput. **16**, 2965 (2020).

[55]*The deMon2k users' guide (2nd ed.)* `http://www.demon-software.com/public_html/support/htmlug/index.html`.

[56]B. I. Dunlap, "Robust and variational fitting: Removing the four-center integrals from center stage in quantum chemistry", J. Mol. Struct. THEOCHEM **529**, 37 (2000).

[57]P. M. W. Gill, "Density functional theory (DFT), Hartree–Fock (HF), and the self-consistent field", in *Encyclopedia of computational chemistry* (Wiley, New York, 2002), 678.

[58]D. N. Laikov, "Fast evaluation of density functional exchange-correlation terms using the expansion of the electron density in auxiliary basis sets", Chem. Phys. Lett. **281**, 151 (1997).

[59]A. M. Köster, J. U. Reveles, and J. M. del Campo, "Calculation of exchange-correlation potentials with auxiliary function densities", J. Chem. Phys. **121**, 3417 (2004).

[60]U. Birkenheuer, A. B. Gordienko, V. A. Nasluzov, M. K. Fuchs-Rohr, and N. Rösch, "Model density approach to the Kohn–Sham problem: Efficient extension of the density fitting technique", Int. J. Quantum Chem. **102**, 743 (2005).

[61]B. G. Johnson and D. A. Holder, "A generalized formulation of density functional theory with auxiliary basis sets", in *The j-matrix method: Developments and applications*, edited by A. D. Alhaidari, H. A. Yamani, E. J. Heller, and M. S. Abdelmonem (Springer, Dordrecht, 2008), 311.

[62]A. M. Köster, J. M. del Campo, F. Janetzko, and B. Zuniga-Gutierrez, "A MinMax self-consistent-field approach for auxiliary density functional theory", J. Chem. Phys. **130**, 114106 (2009).

[63]P. Pulay, "Convergence acceleration of iterative sequences. The case of SCF iteration", Chem. Phys. Let. **73**, 393 (1980).

[64]P. Pulay, "Improved SCF convergence acceleration", J. Comput. Chem. **3**, 556 (1982).

[65]A. Alvarez-Ibarra and A. M. Köster, "Double asymptotic expansion of three-center electronic repulsion integrals", J. Chem. Phys. **139**, 024102 (2013).

[66]C. L. Lawson, R. J. Hanson, D. R. Kincaid, and F. T. Krogh, "Basic linear algebra subprograms for Fortran usage", ACM Trans. Math. Softw. **5**, 308 (1979).

[67]J. J. Dongarra, J. Du Croz, S. Hammarling, and R. J. Hanson, "An extended set of FORTRAN basic linear algebra subprograms", ACM Trans. Math. Softw. **14**, 1 (1988).

[68]J. J. Dongarra, J. Du Croz, S. Hammarling, and R. J. Hanson, "Algorithm 656: An extended set of basic linear algebra subprograms: Model implementation and test programs", ACM Trans. Math. Softw. **14**, 18 (1988).

[69]J. J. Dongarra, J. Du Croz, S. Hammarling, and I. S. Duff, "A set of level 3 basic linear algebra subprograms", ACM Trans. Math. Softw. **16**, 1 (1990).

[70]J. J. Dongarra, J. Du Croz, S. Hammarling, and I. S. Duff, "Algorithm 679: A set of level 3 basic linear algebra subprograms: Model implementation and test programs", ACM Trans. Math. Softw. **16**, 18 (1990).

[71]E. Anderson, Z. Bai, C. Bischof, L. S. Blackford, J. Demmel, J. J. Dongarra, J. Du Croz, S. Hammarling, A. Greenbaum, A. McKenney, and D. Sorensen, *Lapack users' guide (3rd ed.)* https://www.netlib.org/lapack/lug/, (1999)

[72]S. L. Altmann and P. Herzig, *Point-group theory tables*, 2nd ed., https://phaidra.univie.ac.at/view/o:104731 (University of Vienna, Vienna, 2011).

[73]R. McWeeny, *Symmetry: An introduction to group theory and its applications* (Dover publications, Oxford, 2012).

[74]L. Kantorovich and A. Livshits, "A novel approach for constructing symmetry-adapted basis sets for quantum-chemical calculations. I. Real symmetry-adapted orbitals", Phys. Stat. Sol. B **174**, 79 (1992).

[75]M. Hamermesh, *Group theory and its application to physical problems* (Addison-Wesley, Massachusetts, 1989).

[76]D. M. Bishop, *Group theory and chemistry* (Dover publications, Oxford, 1993).

[77]H. A. Fertig and W. Kohn, "Symmetry of the atomic electron density in Hartree, Hartree-Fock, and density-functional theories", Phys. Rev. A **62**, 052511 (2000).

[78]A. Görling, "Symmetry in density-functional theory", Phys. Rev. A **47**, 2783 (1993).

[79]B. I. Dunlap, "Symmetry and degeneracy in Xα and density functional theory", in *Advances in chemical physics* (John Wiley and sons, Ltd., Chichester, 1987) Chap. 5, 287.

[80]B. Weiner and S. B. Trickey, "Fukutome symmetry classification of the Kohn–Sham auxiliary one-matrix and its associated state or ensemble", Int. J. Quantum Chem. **69**, 451 (1998).

[81] A. K. Theophilou and P. Papaconstantinou, "Some properties of the KS potential, concerning degenerate and nearly degenerate states", J. Mol. Struct. THEOCHEM **501**, 85 (2000).

[82] J. Katriel, F. Zahariev, and K. Burke, "Symmetry and degeneracy in density functional theory", Int. J. Quantum Chem. **85**, 432 (2001).

[83] A. K. Theophilou, "Does the Kohn and Sham potential have the symmetry of the external potential?", AIP Conf. Proc. **1642**, 187 (2015).

[84] A. K. Theophilou, "A novel density functional theory for atoms, molecules, and solids", J. Chem. Phys. **149**, 074104 (2018).

[85] Á. Nagy, "Density functional theory from spherically symmetric densities", J. Chem. Phys. **149**, 204112 (2018).

[86] V. N. Glushkov and S. I. Fesenko, "Parameterized effective potential for excited states and its application to the calculation of transition dipole moments", Opt. Spectrosc. **128**, 437 (2020).

[87] Á. Nagy, "Subspace theory with spherically symmetric densities", J. Chem. Phys. **154**, 074103 (2021).

[88] A. A. M. Carranza and A. M. Köster, "Symmetry-adapted density fitting in auxiliary density functional theory", Theor. Chem. Acc. **140**, 32 (2021).

[89] B. Yang, J. Flusser, and T. Suk, "3D rotation invariants of Gaussian–Hermite moments", Pattern Recognit. Lett. **54**, 18 (2015).

[90] P. W. Atkins and R. S. Friedman, *Molecular quantum mechanics, 5th Ed.* (Oxford university press, Oxford, 2011).

[91] G. Fieck, "Symmetry adaption reduced to tabulated quantities", Theor. Chim. Acta **44**, 279 (1977).

[92] S. Dresselhaus, G. Dresselhaus, and A. Jorio, *Group theory: Application to the physics of condensed matter* (Springer, Heidelberg, 2008).

[93]P. M. van Den Broek and J. F. Cornwell, "Clebsch-Gordan coefficients of symmetry groups", Phys. Stat. Sol. B **90**, 211 (1978).

[94]R. Dirl, "Clebsch-Gordan coefficients: General theory", J. Math. Phys. **20**, 659 (1979).

[95]S. Axler, "Finite-dimensional vector spaces.", in *Linear algebra done right* (Springer, Cham, 2015).

[96]H. B. Schlegel and M. J. Frisch, "Transformation between Cartesian and pure spherical harmonic Gaussians", Int. J. Quantum Chem. **54**, 83 (1995).

[97]K. Hermann, L. G. M. Pettersson, M. E. Casida, C. Daul, A. Goursot, A. Koester, E. Proynov, A. St-Amant, and D. R. Salahub, *StoBe-deMon version 3.3v*, 2014.

[98]S. L. Altmann and P. Herzig, *Point-group theory tables* (Clarendon press, Oxford, 1994).

[99]T. Inui, Y. Tanabe, and Y. Onodera, "Vector spaces", in *Group theory and its applications in physics* (Springer, Heidelberg, 1990), 30.

[100]*Maple, version 2016.1. Maplesoft, a division of Waterloo Maple Inc.* Waterloo, Ontario.

[101]M. Tinkham, *Group theory and quantum mechanics* (Dover publications, Mineola, 2003).

[102]*Symmetry resources at Otterbein University. The symmetry gallery: A collection of over 120 unique molecules and polyhedra with interactive display of all symmetry elements and animation of all operations.* https://symotter.org/gallery, Westerville, 2021.

[103]G. Katzer, *Character tables for point groups used in chemistry. Character tables are an important tool derived from group theory and are used in many parts of molecular chemistry, particularly in spectroscopy. Examples (both geometrical object and molecules) are given for every point group if possible.* http://gernot-katzers-spice-pages.com/character_tables/.

[104]N. Godbout, D. R. Salahub, J. Andzelm, and E. Wimmer, "Optimization of Gaussian-type basis sets for local spin density functional calculations. Part I. Boron through neon, optimization technique and validation", Can. J. Chem. **70**, 560 (1992).

[105]P. Calaminici, F. Janetzko, A. M. Köster, R. Mejia-Olvera, and B. Zuniga-Gutierrez, "DFT optimized basis sets for gradient corrected functionals: 3d transition metal systems", J. Chem. Phys. **126**, 044108 (2007).

[106] A. J. Karttunen, M. Linnolahti, T. A. Pakkanen, and P. Pyykkö, "Icosahedral Au_{72}: A predicted chiral and spherically aromatic golden fullerene", Chem. Commun., 465 (2008).

[107] T. Pilati and A. Forni, "SYMMOL: A program to find the maximum symmetry group in an atom cluster, given a prefixed tolerance", J. Appl. Crystallogr. **31**, 503 (1998).

[108] W. Humphrey, A. Dalke, and K. Schulten, "VMD – visual molecular dynamics", J. Mol. Graph **14**, 33 (1996).

[109] B. Ziemer, A. Rabis, and H.-U. Steinberger, "Triclinic polymorphs of triphenylphosphine and triphenylphosphine sulfide", Acta Crystallogr. C **56**, e58 (2000).

[110] D. M. Schubert, D. T. Natan, D. C. Wilson, and K. I. Hardcastle, "Facile synthesis and structures of cyclic triimidazole and its boric acid adduct", Cryst. Growth Des. **11**, 843 (2011).

[111] J. H. Coates, D. A. Hadi, and S. F. Lincoln, "The preparation, characterization and solution chemistry of some nickel(II) and copper(II) complexes of 1,4,7,10-tetramethyl-1,4,7,10-tetraazacyclododecane", Aust. J. Chem. **35**, 903 (1982).

[112] R. N. Clayton and T. K. Mayeda, "The use of bromine pentafluoride in the extraction of oxygen from oxides and silicates for isotopic analysis", Geochim. Cosmochim. Acta **27**, 43 (1963).

[113] S. Adam, A. Ellern, and K. Seppelt, "Structural principles of the coordination number eight: WF, ReF, and XeF", Chem. Eur. J. **2**, 398 (1996).

[114] M. A. S. Goher, A. E. H. Abdou, M. A. M. Abu-Youssef, and F. A. Mautner, "Bis-(tetraethylammonium)[tetraazidocuprate(II)] and catena-di-μ-1,1-azido-[di-μ-1,1-azido-bis-(2,4-dimethylpyridine)dicopper(II)]", Transit. Met. Chem. **26**, 39 (2001).

[115] E. M. Muzammil, D. Halilovic, and M. C. Stuparu, "Synthesis of corannulene-based nanographenes", Commun. Chem. **2**, 58 (2019).

[116]D. V. Fomitchev, T. R. Furlani, and P. Coppens, "Combined x-ray diffraction and density functional study of [Ni(NO)(η5-Cp*)] in the ground and light-induced metastable states", Inorg. Chem. **37**, 1519 (1998).

[117]F. M. Geisler and G. Helmchen, "A straightforward synthesis of (3S)-4-methoxybutane-1,3-diol and its use as chiral auxiliary for the preparation of (pS)-1-(diphenylphosphino)-2-formyl-1',2',3',4',5'-pentamethylferrocene", Synthesis **13**, 2201 (2006).

[118]G. Le Bas and S. A. Mason, "Neutron diffraction structure of α-cyclodextrin cyclopentanone hydrate at 20 K: Host–guest interactive disorder", Acta Crystallogr. B **50**, 717 (1994).

[119]Q.-S. Li, L.-F. Gong, and Z.-M. Gao, "Structures and stabilities of B7, B7+ and B7- clusters", Chem. Phys. Lett. **390**, 220 (2004).

[120]J. M. Chance, B. Kahr, A. B. Buda, J. P. Toscano, and K. Mislow, "Stereochemistry of hexakis(dimethylamino)benzene and its dication", J. Org. Chem. **53**, 3226 (1988).

[121]R. Wartchow, "Crystal structure of potassium tris(oxalato)ferrate(III) trihydrate doped with sodium, $K_{2.9}Na_{0.1}Fe(C_2O_4)_3$ $3H_2O$", Z. Kristallogr. NCS **212**, 83 (1997).

[122]R. E. Wolf, J. R. Hartman, J. M. E. Storey, B. M. Foxman, and S. R. Cooper, "Crown thioether chemistry: Structural and conformational studies of tetrathia-12-crown-4, pentathia-15-crown-5, and hexathia-18-crown-6. Implications for ligand design", J. Am. Chem. Soc. **109**, 4328 (1987).

[123]W. W. Wilson and K. O. Christe, "Tetramethylammonium salts of tetrafluorochlorate(1-), tetrafluorobromate(1-) and hexafluorobromate(1-)", Inorg. Chem. **28**, 4172 (1989).

[124]M. Niemeyer, "trans-Diiodopentakis(tetrahydrofuran)ytterbium(III) tetraiodo-trans-bis(tetrahydrofuran)ytterbium(III)", Acta Crystallogr. E **57**, m363 (2001).

[125]H. L. Anderson, C. W. Patrick, L. M. Scriven, and S. L. Woltering, "A short history of cyclocarbons", Bull. Chem. Soc. Jpn. **94**, 798 (2021).

[126]R. L. Atkins, R. A. Hollins, and W. S. Wilson, "Synthesis of polynitro compounds. Hexasubstituted benzenes", J. Org. Chem. **51**, 3261 (1986).

[127]K. Joshi and S. Krishnamurty, "Au_{26}: A case of fluxionality/co-existence", Phys. Chem. Chem. Phys. **20**, 8616 (2018).

[128]G. Avitabile, P. Ganis, and V. Petraccone, "Crystal and molecular structure of 1,3,5,7-tetramethylcycloocta-cis,cis,cis-1,3,5,7-tetraene", J. Phys. Chem. **73**, 2378 (1969).

[129]N. A. Al-Jallal, A. A. Al-Kahtani, and A. A. El-Azhary, "Conformational study of the structure of free 18-crown-6", J. Phys. Chem. A **109**, 3694 (2005).

[130]P. B. Hitchcock and R. Taylor, "Single crystal x-ray structure of tetrahedral $C_{60}F_{36}$: The most aromatic and distorted fullerene", Chem. Commun., 2078 (2002).

[131]A. A. Gakh and A. A. Tuinman, "The structure of $C_{60}F_{36}$", Tetrahedron Lett. **42**, 7133 (2001).

[132]M. Wang, B. Wang, P. Zheng, W. Wang, and J. Lin, "Structure of the extraction complex bis[(dicyclohexano-18-crown-6)oxonium] hexanitratothorate(IV) isomer A", Acta Crystallogr. C **44**, 1913 (1988).

[133]M. Bühl, "Dodeka(ethylene)octamine", Chem. Eur. J. **17**, 3575 (2011).

[134]M. Bertau, F. Wahl, A. Weiler, K. Scheumann, J. Wörth, M. Keller, and H. Prinzbach, "From pagodanes to dodecahedranes - search for a serviceable access to the parent ($C_{20}H_{20}$) hydrocarbon", Tetrahedron **53**, 10029 (1997).

[135]J. M. Vásquez-Pérez, G. U. G. Martínez, A. M. Köster, and P. Calaminici, "The discovery of unexpected isomers in sodium heptamers by Born–Oppenheimer molecular dynamics", The Journal of Chemical Physics **131**, 124126 (2009).

[136]S. E. Pérez-Figueroa, "Estructura y estabilidad de fullerenos endohedrales que contienen lantánidos y actínidos", PhD thesis (Cinvestav, Ciudad de México, 2019).

[137]*Matrix market: A visual repository of test data for use in comparative studies of algorithms for numerical linear algebra, featuring nearly 500 sparse matrices from a variety of applications, as well as matrix generation tools and services*, `https://math.nist.gov/MatrixMarket/index.html`.

[138]*Wolfram research, Inc., Mathematica, version 12.2*, Champaign, IL, 2020.

[139]D. Mejía-Rodríguez and A. M. Köster, "Robust and efficient variational fitting of Fock exchange", J. Chem. Phys. **141**, 124114 (2014).

[140]T. H. Dunning, "Gaussian basis sets for use in correlated molecular calculations. I. The atoms boron through neon and hydrogen", J. Chem. Phys. **90**, 1007 (1989).

[141]B. P. Pritchard, D. Altarawy, B. Didier, T. D. Gibson, and T. L. Windus, "New basis set exchange: An open, up-to-date resource for the molecular sciences community", J. Chem. Inf. Model. **59**, 4814 (2019).

[142]H. Iikura, T. Takao, Y. Takeshi, and H. Kimihiko, "A long-range correction scheme for generalized-gradient-approximation exchange functionals", J. Chem. Phys. **115**, 3540 (2001).

[143]A. V. Krukau, O. A. Vydrov, A. F. Izmaylov, and G. E. Scuseria, "Influence of the exchange screening parameter on the performance of screened hybrid functionals", J. Chem. Phys. **125**, 224106 (2006).

[144]P. M. W. Gill, B. G. Johnson, and J. A. Pople, "A standard grid for density functional calculations", Chem. Phys. Lett. **209**, 506 (1993).

[145]J. N. Pedroza-Montero, "Iterative density fitting for ab-initio nanoscale simulations", PhD thesis (Cinvestav, Mexico city, 2020).

[146]R. R. Zope, T. Baruah, M. R. Pederson, and B. I. Dunlap, "Static dielectric response of icosahedral fullerenes from C_{60} to C_{2160} characterized by an all-electron density functional theory", Phys. Rev. B **77**, 115452 (2008).

[147]W. Küchle, M. Dolg, H. Stoll, and H. Preuss, "Energy-adjusted pseudopotentials for the actinides. Parameter sets and test calculations for thorium and thorium monoxide", J. Chem. Phys. **100**, 7535 (1994).

[148]*The stuttgart pseudopotentials and valence basis sets*, `http://www.tc.uni-koeln.de/PP/clickpse.en.html`.

[149]L. N. Gorokhov, A. M. Emelyanov, and Y. S. Khodeev, "Mass-spectroscopic investigation of stability of gaseous U_2O_2 and U_2", High Temp. **12**, 1156 (1974).

[150]M. E. Casida, "Time-dependent density functional response theory for molecules", in *Recent advances in density functional methods*, edited by D. P. Chong (World scientific, Singapore, 1995).

[151]J. Carmona-Espíndola, "Time-dependent auxiliary density perturbation theory: Method, implementation and applications", PhD thesis (Cinvestav, Mexico City, 2012).

[152]E. R. Davidson, "Use of double cosets in constructing integrals over symmetry orbitals", J. Chem. Phys. **62**, 400 (1975).

[153]J. D. Dixon, "High speed computation of group characters", Num. Math. **10**, 446 (1967).

[154]M. Johansson and V. Veryazov, "Automatic procedure for generating symmetry adapted wavefunctions", J. Cheminformatics **9**, 8 (2017).

[155]E. Blokker, "A theory for the construction of the irreducible representations of finite groups. II", Int. J. Quantum Chem. **7**, 1091 (1973).

[156]F. Janetzko, A. M. Köster, and D. R. Salahub, "Development of the cyclic cluster model formalism for Kohn-Sham auxiliary density functional theory methods", J. Chem. Phys. **128**, 024102 (2008).

[157]M. L. Ellzey, "Using group theory to obtain eigenvalues of nonsymmetric systems by symmetry averaging", Symmetry **1**, 10 (2009).